

**Investigations Towards
New Multidentate Ligands
As
Potential Multimodal Imaging Agents**

Cuhananthan Wijayanayagam Sathiyajith

A thesis submitted to the University of Wales in accordance with the requirements for the degree of Doctor of Philosophy in the Faculty of Science, Department of Chemistry, University of Wales, Cardiff.

OCT 2010

UMI Number: U585433

All rights reserved

INFORMATION TO ALL USERS

The quality of this reproduction is dependent upon the quality of the copy submitted.

In the unlikely event that the author did not send a complete manuscript and there are missing pages, these will be noted. Also, if material had to be removed, a note will indicate the deletion.



UMI U585433

Published by ProQuest LLC 2013. Copyright in the Dissertation held by the Author.
Microform Edition © ProQuest LLC.

All rights reserved. This work is protected against
unauthorized copying under Title 17, United States Code.



ProQuest LLC
789 East Eisenhower Parkway
P.O. Box 1346
Ann Arbor, MI 48106-1346

DECLARATION

This work has not previously been accepted in substance for any degree and is not concurrently submitted in candidature for any degree.

Signed...*C.W. Sathiyagat*..... (Candidate) Date...*25.10.2010*.....

STATEMENT 1

This thesis is being submitted in partial fulfilment of the requirements for the degree of PhD.

Signed...*C.W. Sathiyagat*..... (Candidate) Date...*25.10.2010*.....

STATEMENT 2

This thesis is the result of my own independent work, except where otherwise stated. Other sources are acknowledged by explicit references.

Signed...*C.W. Sathiyagat*..... (Candidate) Date...*25.10.2010*.....

STATEMENT 3

I hereby give consent for my thesis, if accepted, to be available for photocopying and for inter-library loan, and for the title and summary to be made available to outside organisations.

Signed...*C.W. Sathiyagat*..... (Candidate) Date...*25.10.2010*.....

Acknowledgements.....

I simply could not believe myself, that I am writing this section of my PhD thesis. When the yearning for success becomes an unquenchable thirst, it will simply be granted to the deserved person. Yet, to confront the difficulties, disappointments and discouragements and the opposition within; during the process, requires inevitable, loving and kind support. Tears roll down my eyes, when I reflect the support extended by Angelo to make myself totally independent. I very much regret that I could not find a proper word in the dictionary, as I believe 'thanks' is not the word to express the gratitude. Pete, without your earnest support and timely guidance, I would not have realised my ambition to become an Inorganic Biochemical Scientist. The positivity instilled by Pete and the ever burning urge created for perfection by Angelo, cannot be expressed in simple words. Thanks a lot for providing me a fully funded studentship to embark on this most fascinating project which I value next to my heart. I am simply blessed! Dr. Newman your moral support and guidance throughout my project is highly valued. Especially, with strict time constraints to produce a thesis of this nature would not have been a reality without you. Thanks Dr. Morley, for mentoring myself on and off during the project. Also like to recall, Mike's and Ian's passion for chemistry and Simon's passion for luminescence as well.

In the most memorable three years, I was fortunate to deal with many loving and caring friends. May I take this opportunity to value the affection extended by Praba, Fawaz, Tom, Mat, Dan, Jen, Lucy, Floroa, Tim, Lenali, Steve, Wixey, James and Thusit (not in a particular order). James inspired myself through his passion for Medical Imaging, which we shared together. Apart from this, thanks James for being the light house to help me travel through the twilight zone with inspiring emails and conversations!! Thanks Fawaz for providing a good company and the inspiration through your devotion and organizing capabilities throughout my stay. Thanks Abdul for reinforcing my faith from time to time. Ben, I truly admire your leadership and the kind support extended during difficult times...Stacey and Hue, shall never forget the affection extended. Also its time to extend my heart felt gratitude to Rob, Robin, Garry, Jemie, Mal, Alun, Alan, Terrie, Trish, Sham and all the skilled and semi/unskilled staff at Cardiff Universtiy, who provided support throughout my stay in Cardiff University. Garry and Jemie your support in the stores is truly valued.

I would like to extend my love towards my Parents and my Brothers; Ajit, Maju and my sister- in- law Shivi, who were backing me constantly towards my goal.

I also would like to extend my heartfelt gratitude to all my relatives. Especially to my cousin, Gana and his wife Jana without whom, I would not have been able to travel through. To My both Uncles, every encouragement is highly valued and great fully remembered. To Periyammah-Periyappah, and Joe-Shamini, for their immense support and encouragement throughout; To Mami, Chittah-Chitappah and my dearest sister Uma, the most loving kind full guidance is cherished forever; To Ganga Aunty, Thavam Aunty, Selva Uncle and Nalliah uncle for their timely guidance. To my college friends, especially, Parthipan, Vatsan, Mat, Bahi, Vasanthan, thanks for encouraging myself throughout and also to my Sai brothers and sisters at Cardiff and Leicester Sai Centres, for their encouragement.

Last but not least, I wish to acknowledge the support and guidance extended by, Prof.S. Liyanaghe for introducing Pete and Angelo, paving way forward, towards my mission to become an Inorganic Biochemical Scientist. This thesis is a dedication to the dearest lord and to you all guys.

Summary

A Coordination chemistry based historical perspective of contrast agents which are utilised in various imaging modalities, forms the basis of **Chapter 1**. Chapter 1 also highlights the various latest advancements and the challenges confronted therein. **Chapter 1** culminates in highlighting the need for dual purpose contrast agents.

Chapter 2 and **Chapter 3** deals with polyamino poly carboxylate derivatives based on EDTA and DTPA respectively. **Chapter 2** sheds light upon Teslascan and other related manganese based potential contrast agents. It also highlights the emergence of Mn (II) as the direct competitor for Gd (III) in the face of Nephrogenic Systemic Fibrosis (NSF) reported for Gd based contrast agents. The chapter culminates in describing the synthesis of a library of EDTA bisamides, including four new EDTA bisamides. **Chapter 3** in turn takes a detailed look at a series of DTPA analogues and DTPA bisamides synthesized by scientists all over the world. It also highlights the various synthetic methodologies undertaken by the able scientists. The chapter culminates in describing four new multidentate ligands synthesized in this project, namely two new DTPA analogues and two new DTPA Bisamides. It has been shown that the synthetic methodology utilised to synthesize symmetric naphtha derivative **L⁵** is fairly unique.

Chapter 4 and **Chapter 5** report the investigations carried out on these new multidentate ligands in terms of relaxometry, potentiometry and luminescence. Interesting results were obtained from relaxometric and luminescence measurements. For instance, symmetric naphtha derivative, reported a relaxivity of $8.8 \text{ mM}^{-1}\text{s}^{-1}$, relaxivity obtained for Mn (II) complex of EDTA bisamide of 4-aminomethylpyridine is also highly commendable.

Investigations on the optical properties of the multidentate ligands require a separate chapter. Thus it is has been allotted **Chapter 5**. DTPA bisamide of N, N-Bis[(tert-butoxycarbonyl)methyl-2-bromoethylamine was found to quench the fluorescence upon binding with Cu (II), indicating its application as luminescent sensor for Cu (II).

Abbreviations

Å	Angstrom
Ar	Aromatic
ATP	Adenosine tri phosphate
ACN	Acetonitrile
K	Equilibrium constant
BOLD	Blood oxygen level dependence
BFC	Bi functional chelates
BFCA	Bi functional chelating Agents
BLEDTA	Bleomycin derivative
Bipy	2,2'-bipyridine
br	Broad
BSA	Blood serum albumin
¹³ C	Carbon 13 isotope
°C	degrees centigrade
cm ⁻¹	Reciprocal centimetres/wave number
CDTA	Trans-1,2-diaminocyclohexane tetra acetate
CT	Computerized tomography
Cyclen	1,4,7,10-tetraazacyclododecane
δ	NMR chemical shift
Δ	Crystal field splitting
DCC	Di isopropyl carbodiimide
DDP	Carboxy-decylamidomethyl-N-2,3-dihydroxypropyl)- ethylenediamine-N,N'-diacetate
DPA	Dipicolylamine
DFB	Deferrioxamine
DCM	Dichloromethane
DMF	N,N-dimethylformamide
DTPA	Diethylene triamine penta acetic acid
DTPAA	DTPA-bisanhydride
DMSO	Dimethylsulfoxide
DMAP	4-Dimethyl amino pyridine
DNA	Deoxy ribo nucleic Acid
d	Doublet
DOTA	1,4,7,10-tetraazacyclododecane-1,4,7,10-tetraacetic acid
DO3A	1,4,7,10-tetraazacyclododecane-1,4,7-triacetic acid
DPA	Dipicolylamine
DPDP	N, N'-Dipyridoxylethylenediamine-N,N'-diaceticacid- 5,5',- Bis(phosphate)
DVB	DiVinyl Benzene
dd	Double doublet
EBAME	Ethylenedimainetetraacetic acid bis-(5-aminosalicylic acid methyl ester
EDDADA	N,N-(bisacetic)-N'N-(bisacetanilide)ethylenediamine
EDAC	1-Ethyl-3-(3-dimethylaminopropyl)carbodiimide hydrochloride
EDTA	Ethylene diamine tetra acetic acid pyridylacetamido)acid
EET	Exited energy transfer
EDTAA	EDTA bis anhydride
ε	Extinction coefficient
EPR	Electron paramagnetic resonance
EHPG	N, N'-ethylenebis [2-(o-hydroxyphenyl)glycine]

Potential Multimodal Imaging Agents

ESMS	Electro spray ionisation mass spectrometry
Eq	Equivalent
FFC	Fast field cycling relaxometry
eV	Electron volt
FAB	Fast atom bombardment
FDG	Fluorodeoxyglucose(¹⁸F)
g	Grams
GIT	Gastro intestinal tract
h	Hour
¹H	Proton
HBED	N, N'-bis (hydroxybenzyl)ethylenediamine-N, N'-diacetic acid
HMPA	Hexamethyl phosphoric triamide
HOMO	Highest occupied molecular orbital
HPLC	High performance liquid chromatography
HRMS	High resolution mass spectrometry
Hz	Hertz
IR	Infrared
ICT	Internal charge transfer
IDA	Imino diacetic acid
IO	Iron oxide particles
J	Coupling constant
kJ	Kilojoule
λ	Light wavelength
λ_{max}	Wavelength of the band at maximum absorption
L	Litre/ligand
LDP	N,N'-Bis-(Carboxy-laurylamidomethyl-N-2,3-dihydroxypropyl)-ethylenediamine-N,N'-diacetate
LDA	Lithium diisopropyl amine
LUMO	Lowest unoccupied molecular orbital
M	Metal/molar concentration
m	Multiplet
Mr	Molecular weight
Me	Methyl
MEA	Methoxyethylamide
MMEA	Methylmethoxyethylamide
mg	Milligram
MHz	Mega hertz
mL	Millilitre
Mol	Mole
mmol	Millimole
MRI	Magnetic resonance imaging
NBS	N-Bromo succinimide
NIRF	Near infra red fluorescence
NMR	Nuclear magnetic resonance
NMG	N-Methyl glucaamine
N-BOC	1,2-diaminoethane, tert-Butyl N-(2-aminoethyl)carbamate
ODDA	1,4,10,13-tetraoxa-7,16-diazacyclooctadecane-7,16-diacetate
ODP	N,N'-Bis(carboxy-octadecylamidomethylene-N-1,2-dihydroxypropyl)-ethylenediamine-N,N'- diacetate
Ppm	Parts per million
PBS	Phosphate Buffer Solution
PCT	Photo induced charge transfer

Potential Multimodal Imaging Agents

PLP	Pyridoxal-5-phosphate
PET	Positron emission tomography
PET	Photo induced electron transfer
PDTA	1,3-propylenediamine tetra acetic acid
PLED	N,"-dipyridoxylethylenediamine-N, N'-diacetic acid
PRE	Proton relaxation enhancement
RNA	Ribo nucleic acid
RF	Radio frequency
SCA	Smart contrast agent
SPECT	Single photon emission computerized tomography.
SPIO	Superoxide Iron Oxide Particles
SOD	Superoxide dismutase
TFA	Trifluoro acetic Acid
TREE	Targeted relaxation enhancement agent
TREN	Tris-(2aminoethyl)amine
TRIEN	Triethylene tetra amine

CONTENTS**CHAPTER 1 -----2****CONTRAST AGENTS FOR MEDICAL IMAGING-----2**

1.0	INTRODUCTION TO MOLECULAR IMAGING	2
1.1	HISTORY OF MEDICAL IMAGING: AN OUTLOOK	3
1.1.1	<i>X-ray</i>	3
1.1.1.1	Origin of Tomography	4
1.1.1.2	Positron Emission Tomography (PET)	6
1.1.1.3	Single photon emission computerized tomography (SPECT)	7
1.1.2	<i>Magnetic Resonance Imaging (MRI), How it has originated</i>	7
1.1.2.1	Principles of Magnetic Resonance Imaging (MRI)	8
1.2	NEED FOR CONTRAST ENHANCEMENT	8
1.2.1	<i>Improving Image Quality of MRI – Need & Solutions</i>	8
1.2.2	<i>Need for contrast enhancement- Brief History</i>	9
1.3	IMAGE ENHANCEMENT THROUGH MRI CONTRAST AGENTS.	10
1.3.1	<i>Lanthanide metal ions in contrast agents</i>	12
1.3.1.1	Gadolinium (III) complexes	13
1.3.1.2	Comparison of Acyclic and Macrocyclic complexes of Gadolinium	15
1.3.1.3	Dysprosium Complexes as MRI contrast agents	17
1.3.2	<i>Metalloporphyrins of Iron (III) and Manganese (III)</i>	19
1.3.3	<i>Native Proteins Acting as Contrast Agents</i>	19
1.3.4	<i>Gastrointestinal Contrast Agents</i>	20
1.3.5	<i>Stable nitroxide Radicals as MRI contrast agents</i>	20
1.3.6	<i>Super Paramagnetic Iron oxide Particles (IO)</i>	21
1.4	LATEST DEVELOPMENTS & MODIFICATIONS IN CONTRAST AGENTS.	23
1.4.1	<i>Smart Contrast Agents</i>	23
1.4.2	<i>pH-activated Contrast Agents</i>	24
1.4.3	<i>Metal ion Concentration Activated Contrast Agents</i>	25
1.4.4	<i>Enzyme-activated Contrast Agents</i>	25
1.4.5	<i>Site specific Agents</i>	25
1.5	EMERGING TRENDS IN IMAGING TECHNOLOGY	28
1.5.1	<i>EPR (Electron Paramagnetic Resonance)</i>	28
1.5.2	<i>Optical Imaging (Optical Tomography)</i>	28
1.5.3	<i>Overcoming Challenges with NIRF Imaging Agents</i>	30
1.5.4	<i>Functional Imaging</i>	30

CHAPTER 2 -----38**EDTA BASED DERIVATIVES -----38**

2.1	INTRODUCTION TO EDTA BASED DERIVATIVES	38
2.1.1	<i>EDTA</i>	38
2.1.2	<i>Detoxification of Metal Ions</i>	38
2.1.3	<i>Salts of Transition Metals as MRI Contrast Agents and Their Early History</i>	39
2.1.4	<i>Mn (II) emerging as the immediate competitor for Gd (III)</i>	44
2.1.5	<i>Subsequent research into Mn (II) complexes as MRI CAs</i>	44
2.1.5.1	Story of Tesla Scan and the challenges faced at the outset	44
2.1.5.2	Complexation of Mn (II) with acyclic amino poly carboxylates	47
2.1.5.2.1	PDTA	47
2.1.5.2.2	Backbone substituted EDTA analogues	47
2.1.5.2.3	Synthesis of EDTA bisamides	50
2.1.5.2.4	Intrinsic stability of Manganese complexes	54
2.1.5.3	Utilising Bifunctional Chelates	57
2.2	RESULTS AND DISCUSSION	58
2.2.1	<i>Ligand Design and Synthesis</i>	58
2.2.1.1	Synthesis of EDTA bis amide of N-(2-Aminoethyl)-1, 8-naphthalimide (L ¹)	59

Potential Multimodal Imaging Agents

2.2.1.2	Synthesis of EDTA bisamide of sulphonamide (L ²)	60
2.2.1.3	Synthesis of EDTA bisamide of Para Aminophenol (L ³)	60
2.2.1.4	Preparation of four new EDTA bis amides and some challenges faced therein	61
2.2.1.5	Attempted Synthesis of some Chromophore bearing EDTA bisamides	65
2.2.2	Complexation with Transition Metal Ions	68
2.2.2.1	Characterisation of EDTA bisamides	68
2.2.2.2	Complexation with Transition metal cations.	69
2.3	EXPERIMENTAL SECTION	70
2.3.1	Synthesis of EDTA bisamides	71
2.3.1.1	Synthesis of EDTA bisamide of N-(2-Aminoethyl)-1,8-naphthalimide (L ¹)	71
2.3.1.1.1	Complexation of L ¹ with MnCl ₂ (MnL ¹)	71
2.3.1.2	Synthesis of EDTA bisamide of Sulfonamide (L ²)	72
2.3.1.2.1	Complexation of L ² with ZnCl ₂ (ZnL ²)	73
2.3.1.2.2	Complexation of L ² with MnCl ₂ (MnL ²)	73
2.3.1.3	Synthesis of EDTA bisamide of Aminophenol (L ³)	73
2.3.1.3.1	Complexation of L ³ with ZnCl ₂ (ZnL ³)	74
2.3.1.4	Synthesis of EDTA bisamide of 4-aminomethyl pyridine (L ⁴)	74
2.3.1.4.1	Complexation of L ⁴ with MnCl ₂ (MnL ⁴)	75
2.3.1.5	Synthesis of EDTA bisamide of AminoAnthraquinone (L ⁵)	76
2.3.1.5.1	Complexation of L ⁵ with MnCl ₂ (MnL ⁵)	76
2.3.1.6	Synthesis of EDTA bisamide of Aminomethylsulphonic acid (L ⁶)	77
2.3.1.6.1	Complexation of L ⁶ with MnCl ₂ (MnL ⁶)	77
2.3.1.7	Synthesis of EDTA bisamide of the amino acridine (L ⁷)	78
2.3.1.7.1	Complexation of L ⁷ with ZnCl ₂ (ZnL ⁷)	79
2.3.1.8	Attempted Synthesis of EDTA bisamide of Trien naphthaderivative	79
2.3.1.9	Attempted synthesis of EDTA bisamides of 5-aminonaphthalene -2 sulphonicacid (L ⁸)	80
2.3.2	Attempted Synthesis of EDTA bisamide of taurine (L ⁹)	80
2.4	CONCLUSION	81

CHAPTER 3 ————— 86

DTPA ANALOGUES AND DTPA BIS AMIDES ————— 86

3.1	INTRODUCTION TO DTPA DERIVATIVES	86
3.1.1	DTPA	86
3.1.2	DTPA as a complexing agent- Historical View	86
3.1.2.1	Complexation with Transition metal cations.	87
3.1.3	Incorporation of reagents to DTPA based transition metal complexes	87
3.1.4	Introducing Lanthanides to DTPA	88
3.1.5	Gadolinium with DTPA	89
3.1.6	Synthetic methodologies for introducing functionality to DTPA	93
3.1.7	Creating DTPA functionality- A Retro synthetic approach	109
3.1.7.1	DTPA analogue through backbone substitution	110
3.1.7.1.1	Substitution in the Central Nitrogen	110
3.1.7.1.2	Substituted Terminal nitrogen	114
3.1.7.1.3	Direct substitution ethylene carbon in the backbone	121
3.1.7.1.4	DTPA analogues based on conformationally constrained structures	123
3.1.8	DTPA based amide derivatives bearing chromophores:	126
3.2	RESULTS AND DISCUSSION	127
3.2.1	Ligand design and Synthesis of DTPA analogues	127
3.2.1.1	Symmetric Naphtha derivative	127
3.2.1.1.1	Ligand Design	127
3.2.1.1.2	Ligand Synthesis	129
3.2.1.2	Asymmetric Naphtha	137
3.2.1.2.1	Ligand Design	137
3.2.1.2.2	Ligand Synthesis	137
3.2.2	Novel synthesis of DTPA based bisamides	140
3.2.2.1	DTPA based bis amide of N-(2-Aminoethyl)-1, 8-naphthalimide	140
3.2.2.1.1	Ligand design & Synthesis	140
3.2.2.2	DTPA based bis amide of 4-amino methyl pyridine	141
3.2.2.2.1	Ligand design & Synthesis	141
3.3	EXPERIMENTAL SECTION	142
3.3.1	Synthesis of Naphthalinic anhydride derivatives	142
3.3.1.1	Synthesis of N, N -Bis (tert-butoxycarbonyl) methyl -2-ethanolamine (4)	142
Alkylation ⁷⁴		142
3.3.1.2	Synthesis of N,N-Bis[(tert-butoxycarbonyl) methyl-2-bromoethylamine (1) ⁷⁵	143

Potential Multimodal Imaging Agents

3.3.1.3	Synthesis of N-(2-Aminoethyl)-1, 8-naphthalimide (6)	144
3.3.1.4	Alkylation of Naphthalic anhydride derivative with N,N-Bis[(tert-butoxycarbonyl) methyl-2-bromoethylamine (L^{10})	144
3.3.1.5	Hydrolysis of Alkylated Naphthalic Anhydride derivative (L^{11})	145
3.3.1.5.1	Complexation reaction of L^5 with Gd (III) Chloride	145
3.3.1.6	Reaction with Naphthalic anhydride and Triethylenetetraamine (7)	146
3.3.1.7	Alkylation of Naphthalic anhydride derivative (L^{12})	147
3.3.1.8	Hydrolysis of Alkylated Naphthalic Anhydride derivative (L^{13})	147
3.3.1.8.1	Complexation reaction of L^{13} with Gd (III) Chloride	148
3.3.2	Synthesis of DTBA Bismaides	148
3.3.2.1	Synthesis of DTPAbisamide of Amine functionalized naphtha derivative (L^{14})	148
3.3.2.2	Synthesis of DTPAbisamide of aminomethyl pyridine (L^{15})	149
3.4	CONCLUSION	150

CHAPTER 4: PART A 156

RELAXIVITY MEASUREMENTS 156

A.4.1	What is Relaxivity? Or Why is it Important?	156
A.4.1.1	The factors defining relaxivity	156
A.4.1.2	Influence of Temperature and Field strength in the measurement of Relaxivity	163
A.4.1.3	Principles of NMR spectroscopy underlying the Magnetic	163
A.4.1.4	Fast Field-Cycling Relaxometry	167
A.4.1.4.1	General Aspects of Practical Application of FFC	167
A.4.1.4.2	Basic principles of FFC	168
A.4.2	Results and Discussion	171
A.4.2.1	Manganese and Copper complexes of EDTA bis amino methyl pyridine ($Mn-L^4$ and $Cu-L^4$)	171
A.4.2.2	Manganese and Iron complexes of EDTA bis amino methyl	176
A.4.2.3	Collective overview	181
A.4.2.4	Symmetric naphtha derivative of N-(2-Aminoethyl)-1,8-naphthalimide (L^{11})	183

CHAPTER 4: PART B 186

POTENTIOMETRIC MEASUREMENTS 186

B.4.1	Evaluation of Potential Contrast Agents	186
B.4.1.1	Need for evaluation of contrast agents	186
B.4.1.2	Protonation Constants and Stability Constants	186
B.4.1.2.1	What is meant by 'Stability Constants'?	187
B.4.1.3	Complex formation and Chelate Effect	191
B.4.1.3.1	Hard-Soft Acid-Base Classification (HSAB)	192
B.4.1.4	Methods available for determining stability constants	193
B.4.1.4.1	Potentiometry	193
B.4.1.4.2	Spectrophotometry	194
B.4.1.4.3	NMR spectroscopy	194
B.4.1.4.4	Conductimetry	194
B.4.1.5	Some Theoretical Aspects relevant to Potentiometric Measurements	195
	Electrode Calibration Theory	195
	Common Sources of Errors and their minimisation: Ensuring Precision and Accuracy	197
B.4.2	Results and Discussion	198
B.4.2.1	Evaluation of EDTA based Ligands	199
B.4.2.1.1	Protonation Constants and Deprotonation Curves of EDTA bisamides	199
B.4.2.1.1.1	Assignment of Protonation Constants	200
B.4.2.1.1.2	Analysis of Deprotonation Curves	203
B.4.2.1.2	Formation constants and Complexation Curves	204
B.4.2.1.2.1	Formation constants	204
B.4.2.1.2.2	Analysis of Titration Curves	206
B.4.2.2.1	Protonation Constants and Deprotonation Curves of L^{15} and L^{11}	209
B.4.2.2.1.1	Protonation Constants	209
B.4.2.2.1.2	Analysis of Deprotonation Curves	210
B.4.3	Experimental Section	211

CHAPTER 5 -----218**LUMINESCENCE MEASUREMENTS -----218**

5.1	LUMINESCENCE: AN INTRODUCTION -----	218
5.1.1	<i>What is luminescence?</i> -----	218
5.1.2	<i>Lifetime (of luminescence)</i> -----	222
5.1.3	<i>Luminescent Sensors</i> -----	223
5.1.3.1	Understanding PET -----	224
5.1.3.2	Kinds of PET sensors on the basis of modulating factor -----	226
5.1.3.3	Cation sensors; Targeting main group Elements -----	228
5.1.3.4	Targeting Alkaline Earth metal ions as analytes -----	230
5.1.3.5	Targeting Transition Metal ions -----	231
5.1.3.6	Targeting Lanthanide Ions -----	239
5.2	RESULTS AND DISCUSSION -----	240
5.2.1	<i>Importance of Fluorimetric Evaluation</i> -----	240
5.2.1.1	Spectrofluorimetric Evaluation of the EDTA Bisamides -----	243
5.2.1.2	Spectrofluorometric Evaluation of DTPA Analogues -----	246
	Fluorescence on binding with Lanthanides -----	246
5.2.1.3	Spectrofluorometric Evaluation of DTPA based bisamides -----	250
5.3	EXPERIMENTAL SECTION -----	256
5.4	CONCLUSION -----	256

To My,

*Dearest Ever Loving Lord,
Ever Loving Mum, Dad and Brothers,
Ever so Caring Relatives,
Most Caring Supervisors
All my encouraging friends
Prestigious Cardiff University
All who belong to USJP and I.Chem.Ceylon
All Scientists dedicated to Molecular Imaging
This is a Dedication!!!*

Chapter 1

Contrast Agents for Medical Imaging

1.0 Introduction to Molecular Imaging

Imaging science is always progressing, with the advancement of various imaging modalities.

Among the number of available imaging modalities used in the 1950-1960s and, magnetic

resonance imaging has proved its significance over past few decades. This field's growth is

attributed to its application in various fields of medicine.

With the advancement of imaging technology, the role of contrast agents in medical

imaging has become more prominent. The use of contrast agents in medical imaging has a

long history, dating back to the early days of radiography. The use of contrast agents in

radiography was initially limited to the use of barium sulfate as a contrast agent. This is

possible through a combination of chemical and physical properties of the contrast

agents.

The use of contrast agents in medical imaging has evolved significantly over the years.

Today, contrast agents are used in a wide range of imaging modalities, including

radiography, computed tomography (CT), magnetic resonance imaging (MRI), and

ultrasound. The use of contrast agents in medical imaging has become an essential

part of many diagnostic procedures. The use of contrast agents in medical imaging has

also led to the development of new imaging techniques, such as positron emission

tomography (PET) and single-photon emission computed tomography (SPECT).

The use of contrast agents in medical imaging has also led to the development of new

imaging modalities, such as molecular imaging. Molecular imaging is a branch of

imaging that focuses on the use of contrast agents to visualize specific molecules in

the body. This type of imaging is used to study the function of specific molecules and

to identify potential drug targets. The use of contrast agents in molecular imaging has

Chapter 1

Contrast Agents for Medical Imaging

1.0 Introduction to Molecular Imaging

Imaging science is gaining momentum, with the advancement of various imaging modalities. Among the number of available imaging modalities (such as CT, PET etc), magnetic resonance imaging has proved its significance over past three decades. This could mainly be attributed to its spatial resolution and specificity, which are great advantages in medical imaging.

Molecular medicine is the future of patient management and health care.¹ Imaging has a key role to play in achieving this objective. Significant advancement could be realised through the translation, from a dominant *in-vitro* technology to an *in-vivo* one. This is possible through a combination of chemical synthesis, molecular biology and imaging hardware.

The in-depth study of the inside of the human body has been a persistent challenge to medical doctors, scientists and also the designers of commercial devices. In fact, when X-rays were discovered at the end of nineteenth century, it brought about a powerful impact and was considered the ultimate instrument of such study. With time it became evident that X-ray radiography could hardly be called a non-invasive technique due to destructive effect on the tissues caused by ionizing radiation. Even with modern advancements in X-ray techniques, though considered as much more safe and sophisticated than it was in the earlier stages, it still employs the same kind of radiation and therefore contributes to the same kind of health risks as years ago.

So, as it could be seen, there was need of better technique, capable of eliminating or having negligible impact on health. It so happened that the technique known as Nuclear Magnetic Resonance, which was discovered in the mid-nineteen forties did not seem to be of

much importance initially. After a short period of time, however, it was realized that it had tremendous potential for a great variety of applications, including its contribution to Imaging Science. Actually, the thought of making use of it to study the human body was conceived in sixties. It, however, nearly took a decade alongside advancements in computer technology before these thoughts were put into practice.

Nuclear Magnetic Resonance involves radiofrequency electromagnetic waves with low intensity. This helps in the study of substances placed in a strong magnetic field. The interesting thing to note here is that neither the radiation employed, nor the strong magnetic field have been proven to be harmful to living organisms in any way so far. Remarkable progress has been achieved using this non-invasive technique during the last decade, yet more new dimensions of this worthy invention are in rapid progress.

The very significant place attained by today's imaging modalities, has not taken place overnight. What follows is a brief historical account on the developments of imaging technology, specifically related to Medicine/Healthcare. The following section describes the parallel development of appropriate contrast agents for the modalities discussed. While doing so, we shall focus our attention mostly on contrast agents for MRI and/or PET.

1.1 History of Medical Imaging: An Outlook

1.1.1 X-ray

In fact Philip Leonard observed that electrons are generated in a glass vacuum tube, when a voltage is applied between a cathode and an anode. When these electrons strike the glass, they cause it to glow - and this can be seen in a darkened room. He named this phenomenon as 'Cathode Rays'. In 1895, Nov 8th, Wilhelm Rontgen first discovered a fascinating phenomenon.²

He had acknowledged the fascinating finding of a high energy emission, which could be able to pass through the material that was opaque to light. Rontgen had sealed up a tube, such that light emission is prevented from the glass. When he tested the device to make sure it was

completely light sealed, however, he noticed a glow from a table at some distance- a distance far too great to be reached with cathode rays. On the table was a sheet of cardboard painted with the barium platinocyanide. Since the origin of the rays could not be understood by Roentgen, he called it as “X”rays. Finally he submitted a publication that depicted a photograph of a skeletal hand in 28th of December in 1895. He was the first to receive Nobel Prize for Physics in 1901.

Presently, X-rays are known to be electromagnetic radiation emitted by electrons that have relatively higher energy and far shorter wavelengths in comparison to photons. Formerly, X-rays were distinguished from gamma rays based on the relatively higher energy and relatively shorter wavelength possessed by gamma rays. The origin of the latter, however, is now attributed to the nucleus.

1.1.1.1 Origin of Tomography

The driving motive behind the history of Tomography was to get a better look inside the chest. Thereby the heart, lungs, and any tuberculosis or tumours could be better seen, without the interference of the rib cage in front and behind. To accomplish this, a Topographic system was developed with the following principle.

X-ray source to the left while the image plate is moved to the right. The axis of rotation of a line from the source to the plate must be on a plane of interest inside the body; structures in the middle of the patient would remain relatively clear while those in back and front will be blurred. Many patents based on purely mechanical devices followed. In 1937, however, William Watson filed a patent application for the first important system that made a series of axial topographic images (slices). The patient sat on a stool that was rotated through a full circle as the image was being made along with the simultaneous movement of the the X-ray plate. The seat of the stool was mounted on a telescoping column that could be raised or lowered to get axial sections at various locations in the body. This device actually achieved considerable commercial success.

The birth of Computerised Axial Tomography

Following Watson, there were several developments on this area of technology. “None blurring” is one such method. Although these worked, they involved a truly enormous amount of X-ray exposure. Therefore Gabriel Frank *et al.*^{3,4} discovered a fascinating principle, namely “Back Projection” technology.

Hounsfield’s Computerized Tomography (CT/CAT)

In the early 1960’s, four entirely independent researchers (Oldendorf at UCLA, Kiev in Russia, Brownell and Chesler from Massachusetts) took advantage of recent advances in computers at that time. They tried their best to utilise this advantage to develop, computer based, back projection, axial tomography system. Their efforts, however, were not so fruitful. It was in 1973, the British scientist, Hounsfield, was awarded a patent for discovering the first, computerised axial tomography system.

On the other hand, ‘Allan Cormack’, a South African scientist, independently discovered the solution of the problem of “line integrals”^{5, 6} a mathematical technique that is used in most modern CT scan computation. In honour of this great work, both, Hounsfield and Allan Comrack received the coveted Nobel Prize in Medicine in 1979.

Advances of CT Scanning include dramatic achievement in the speed of scanning and the utilisation of simultaneous acquisition to obtain as many as 128 image slices. All these have impacted CT’s capabilities to prevent motion similar to a fast camera.

Along with the advancement of improved intravenous contrast agents, the quality of CT angiography targeted for coronary and cerebral vessels continues to improve. In fact, in the recent past, there were developments for real time CT scanning with ‘O’-arm units. Contrast agents used in CT, are iodine based and are absorbed by abnormal tissues. Though one may say resolution is lower in CT, it has extremely good low contrast resolution, which enables the detection of very small changes in tissue type. CT gives accurate diagnostic information about the distribution of structures inside the body.

1.1.1.2 Positron Emission Tomography (PET)

This imaging technique also has 40 years of history since the initial attempt to obtain an image using positron emitters as a clinically useful tool. This long period of time could be justified by the fact that several elements had to be merged to produce the imaging modality of today. There were attempts in the history to demonstrate the advantages of positron imaging, using coincidence-counting technique. In fact, the first, clinically useful positron camera was developed in 1960s. The image produced by the camera mainly of planar tomographic nature. Kuhl and Edwards⁷ successfully accomplished 'Transaxial emission tomography' thereafter advancements in PET were fairly slow until CT became powerful. In the 1970's, a more modern version of positron emission CT refer to dual-modality imaging, was introduced by Phelps *et al.*⁷ Thereafter many more developments took place, culminating in a very sensitive modality.

With regard to in-vivo imaging, PET is considered to be the current solution where sensitivity is concerned. It is this sensitivity (femto or nano molar biological concentrations), which makes PET suitable for imaging molecular events. The use of PET is limited by access to hardware as it requires ready access to a Cyclotron, since commonly used isotopes (¹³N (10 min), ¹¹C (20.3 min), ¹⁵O (2.07 min), ¹⁸F (1.83 h)) can have prohibitively short half lives. PET is quantitative in the sense it does provide the ability to characterize receptors and ligands at molecular concentrations.⁸ In fact the great contribution in drug development comes from its ability to label a compound with radio nuclide isotope thus maintaining its physiochemical properties. PET radio nuclides based on ¹⁸F particularly, fluorodeoxyglucose (glycolysis marker) have been useful in probing neoplastic processes and has been widely used.

Transcription (the process of transcribing DNA to RNA), which dominates the manufacture of cellular proteins, often considered to be the focal point in investigating cancer. PET is found to be really useful in imaging the regulation of transcription.

1.1.1.3 Single photon emission computerized tomography (SPECT)

SPECT is another powerful technique that has been used to image several molecular processes and is comparatively cheaper than PET. SPECT acts by detecting γ -emitting radionuclides.

1.1.2 Magnetic Resonance Imaging (MRI), How it has originated

Tracing back the history of MRI, one may discover that there were three major phases. Firstly, the discovery of the fundamental physics and biological properties of nuclear magnetic resonance, secondly, the emergence of designs to accomplish imaging with MRI, and finally the emergence of neurologically optimized methods such as functional MRI. It is necessary to have a detailed outlook on each phase. To begin with, let us consider the emergence of Nuclear Magnetic Resonance.

Olfgang Pauli (1900-1958) initially proposed the existence of the physical basis of magnetic resonance. After which, Isidor Rabi (1898-1988) conducted the first experiment that proved the existence of magnetic resonance. Felix Bloch (1905-1983) and Edward Purcell (1912-1997) independently established the presence of nuclear magnetic resonance in solids. Erwin Hahn (born 1921) fully explained the refocusing pulse/spin echo concept that greatly enhances the utility of measurement of T_2 relaxation in most biological situations. Most importantly for MRI, noticing some irregularities in some spectra he was evaluating, he made the suggestion in 1924 that atomic nuclei should have magnetically related spins. He was indeed correct. In fact it has laid the foundation for the physical basis of magnetic resonance upon which everything else in this field is built up.

Having understood the background of various dimensions of this medical imaging science we are now in a position to appreciate the comparative importance of MRI. The necessity of dual modalities and the role of MRI in that area also need to be discussed. In order to do this, we should try to understand the principles underlying MRI.

1.1.2.1 Principles of Magnetic Resonance Imaging (MRI)

Very similar to X-Ray, Computerized Axial Tomography (CAT), MRI is a method of obtaining images of the body in thin slices. The method measures the characteristics of hydrogen nuclei of water and nuclei with similar chemical shifts, altered by chemical environment across the slice.

This is the major difference of MRI from proton coupling constants.⁹ MRI gives spatial distribution of the intensity of water proton signal in the volume of the body under investigation. This signal intensity depends on the amount of water in the given place and on the magnetic relaxation times T_1 and T_2 which in turn are influenced by a range of factors.^{10, 11} Deducing these factors in each case are the ultimate goal of the radiologist, who is attempting to diagnose the problem by way of examining the MR images. In many cases MRI is the only way to do unambiguous diagnosis, especially in detection of cerebral abnormalities, multiple sclerosis and lesions in sites often obscured by bone artefact on CT scans.

In comparison to CT, MRI has inherently superior contrast scale, because of that, despite of relatively high cost of equipment and maintenance; it has established its presence in most hospitals, clinics and research institutes in developed countries. Its increasing influence in the third world countries also commendable.

1.2 Need for contrast enhancement

1.2.1 Improving Image Quality of MRI – Need & Solutions

Plain MRI also has a few disadvantages when compared to contrast-enhanced computed tomography. The difficulty in reliably distinguishing the tumours from the surrounds in head examinations, difficulty in identify loops of small bowel, thus creating problems in diagnosis of lesions in abdominal images are good examples to cite a few. Undoubtedly these short comings have prompted the significant amount of effort that has been put up to improve the image quality. Since the signal intensity in MRI depends not only on the amount of water in a

given place, but also on the magnetic relaxation times T_1 and T_2 , the chances are more to change the resolution of the picture. It is not easy, however, to effect changes in the proton density of the tissue. Therefore, the ideality of the solution for the problem lies on changing T_1 and T_2 relaxivities of water protons *in vivo*.¹²

Spin-lattice relaxation time T_1 and Spin-Spin relaxation time T_2 (see Chapter 4) could be shortened considerably in the presence of paramagnetic species. While T_1 shortening results in increase in signal intensity, shortening T_2 gives the opposite results. The concentration of the paramagnetic species is inversely proportional to signal intensity. This could be further interpreted as follows. In the low concentrations, increase in the concentration of the contrast agent leads to enhanced signal intensity due to T_1 . This will continue until an optimum value for the concentration is achieved. Further increase in concentration results in decrease in signal intensity due to the effect of T_2 . It has proved in clinical practise that less than optimal contrast or negative contrast is achievable. This phenomenon justifies the more frequent usage of T_1 contrast agents than T_2 contrast agents.

1.2.2 Need for contrast enhancement- Brief History

Contrast agents have been used in diagnostic radiology since 1905 when Voelcker and Von Lichtenberg used colloidal silver for retrograde pyelography.¹³ Radio opaque iodinated contrast agents are in widespread clinical use and for each new imaging modality; radiologists have sought potential contrast agents.¹⁴⁻³⁵ With some modalities contrast agents have brought major advances and are in everyday clinical use, for example X-ray computed tomography, whereas in ultrasound, contrast agents have failed to make an impact.

Following is a brief description of the history of contrast agents used in variety of modalities MRI, PET, PET /CT, PET /MRI with the attention mostly focused upon MRI and PET /MRI contrast agents.

1.3 Image Enhancement through MRI Contrast Agents.

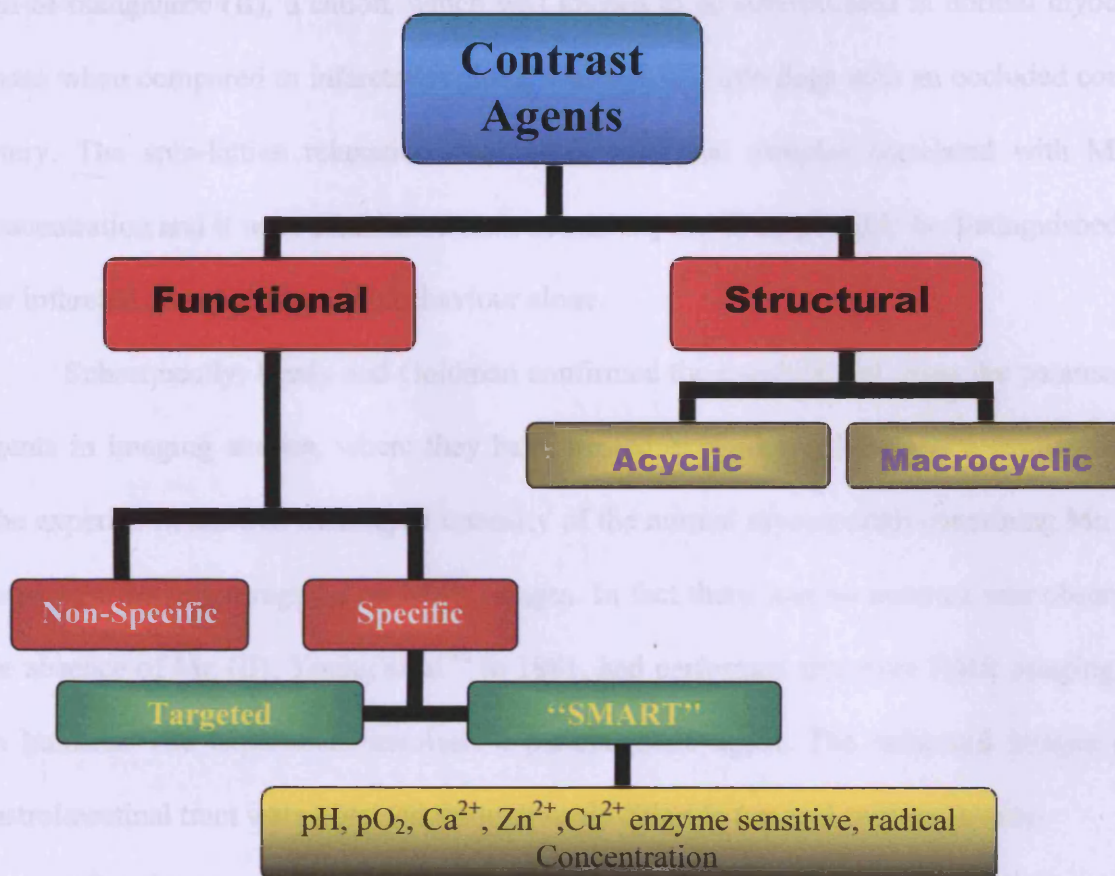


Figure 1:- Schematic representation of the types of modern contrast agents

Initial investigations leading on to the new area of contrast agents are being described here.

The fact that ferric nitrate (a paramagnetic salt) could be utilised in enhancing the relaxation rate of water protons was first described by Bloch *et al.*³⁶ Well acknowledged theory related to solvent nuclear relaxation rate in the presence of paramagnetic chelates was first developed by Bloembergen, Solomon, Eisinger, Schulman, and Blumberg. They have demonstrated that binding of a paramagnetic metal ion to a macromolecule, (in their case DNA), enhances the water proton relaxation efficiency via lengthening of the rotational correlation time.³⁷⁻³⁹

This phenomenon, which came to be known as proton relaxation enhancement (PRE), has been utilised extensively to study hydration and structure of metalloenzymes.⁴⁰

The pioneering 1973 work of Lauterbur *et al.*⁴¹ towards imaging with NMR were extended to human imaging in 1977. Lauterbur, Mendoca-Dias, and Rudin were first to demonstrate the ability of paramagnetic chelates in the identification of tissues, this was

Potential Multimodal Imaging Agents

postulated on the basis of different water proton relaxation times. They have investigated a salt of manganese (II), a cation, which was known to be concentrated in normal myocardial tissue when compared to infarcted regions, was injected into dogs with an occluded coronary artery. The spin-lattice relaxation rates ($1/T_1$) of tissue samples correlated with Mn (II) concentration and it were established that, normal myocardium possibly be distinguished from the infarcted zone by relaxation behaviour alone.

Subsequently, Brady and Goldman confirmed the capability of using the paramagnetic agents in imaging studies, where they have treated excised dog hearts in a similar fashion. The experiment showed that signal intensity of the normal myocardium containing Mn (II) is better than infarcted regions on NMR images. In fact there was no contrast was observed in the absence of Mn (II). Young *et al.*⁴² in 1981, had performed first ever NMR imaging study on humans. The experiment involved a paramagnetic agent. The enhanced images of the gastrointestinal tract were obtained through ferric chloride (an oral contrast agent).

After three years, the first ever demonstration of diagnostic potential of paramagnetic agents was pronounced by Carr *et al.*⁴³ In 1985, Burnett *et al.*⁴⁴ described the use of Gd_2O_3 particles as a prototype MR contrast agent shown to reduce liver and spleen T_1 by 50% at relatively low doses. Due to toxicity issues, however, it was also dropped in to low profile.

The prominent problem with paramagnetic naked heavy metal ions is their toxicity. Investigation has directed on the development of stable paramagnetic ion complexes. Both the metal ion and the ligand usually exhibit substantial toxicity in the unbound state. Together, however, they may create a thermodynamically and kinetically stable compound which is much less toxic.

Complexation of the metal ion with an organic ligand, while considerably decreasing toxicity, may alter paramagnetic properties of the metal. Cr-EDTA complex was the first of such agent attempted, however constraints with synthesis and long-term stability prevented its clinical application (see **Chapter 2**). After which comes the famous Gd (III) diethylenetriaminepentaacetate $[Gd(DTPA)(H_2O)]^{2-}$ it was administered intravenously to

patients with cerebral tumours, providing enhancement of the lesion in the region of cerebral capillary breakdown. Gd(DTPA)²⁻ complex, a renally excreted chelate with a very high formation constant (**Table-1**), had sufficiently favourable properties to be approved by Food and Drug Administration of USA for use in cranial disease diagnostics in mid-1988. Thereafter Bayer.Plc took its commercial production and brought out the brand name ‘Magnevist’.

Stability constant of Gd-DTPA: 10²³

Half-life in urine 21.0 min after intravenous injection
 in blood 19.6 min

Table 1:

Compound	LD ₅₀ (with intravenous dose in rats)
Gd-DTPA	10.0
Gd-EDTA	0.3
Gd-Cl ₃	0.4
Meglucamine diatrizoate (Common X-ray contrast agent)	18.0

1.3.1 Lanthanide metal ions in contrast agents

Although some iron-and manganese-containing materials are commercially important, the predominant contrast agents in commercial use today is still the “*Magnevist*” and its DOTA analogue “*Dotarem*”. The interesting story of Magnevist is reserved for **Chapter 3**.

“*Dotarem*” are comprised of a Gd (III) ion within chelating ligands based on a polyaminocarboxylate motif (linear DTPA and cyclic DOTA respectively).⁴⁵ As acyclic poly amino carboxylates are being dealt in detail in **Chapter 2**, we shall focus the attention mostly towards cyclic poly amino carboxylates in this section.

The tetra-aza cycle of DOTA is capable to adopt its most stable conformation. Thus DOTA forms highly stable lanthanide chelates. The solid state X-ray structure of Gd(DOTA)⁻ indicates that the Gd (III) situated in the centre of a capped square anti prismatic cage, with the water molecule in an axial position.⁴⁶ When in solution, it exists as a pair of interchangeable isomers; the major square anti prismatic and the minor twisted square anti prismatic (see **Fig-2**).⁴⁷

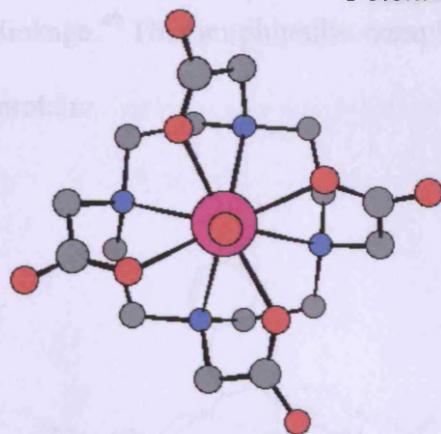


Figure 2:- Gd (III) complex of DOTA⁴⁷

1.3.1.1 Gadolinium (III) complexes

As **Chapter 3**, describes in detail Gd (III) and its chelate's unique properties, this section will be looking at its application possibilities as targeted contrast agents.

Targeted contrast agents contribute an additional layer of molecular specificity to the richness of anatomical and functional information already attainable by MRI. The major challenge, however, for molecular MR imaging is sensitivity: micro molar concentrations of Gd (III) are required to cause a detectable signal change, which makes detecting proteins by MRI a challenge. Most of the gadolinium chelates are bifunctional molecules comprising a protein-targeting moiety and typically one or more gadolinium chelates for detection by MRI.

Relaxivity of contrast agent depends on protein binding itself. As in other imaging modalities, binding with proteins enables the contrast agent to be concentrated at region of interest. This process is carried out through the facilitation of the relevant pharmacodynamic effects. One of the notable pharmacodynamic effects is the increasing the relaxivity of the contrast agent. This in turn will increase MR signal.⁴⁸ In designing new agents, optimization of both the targeting function and the relaxivity is crucial. In the past, there were many acyclic and cyclic and macrocyclic chelates of Gadolinium that had been tested and verified for this purpose (See **Fig-4**).

MS-325 is one such agent. It has been approved as serum-albumin-targeted contrast agent. This was specifically designed for blood vessel imaging. In MS-325, the Gd(DTPA)(H₂O) ligand core (DTPA) had been modified to attach a biphenylcyclohexyl

moiety via a phosphodiester linkage.⁴⁹ This amphiphilic complex targets serum albumin: the most abundant blood plasma protein.

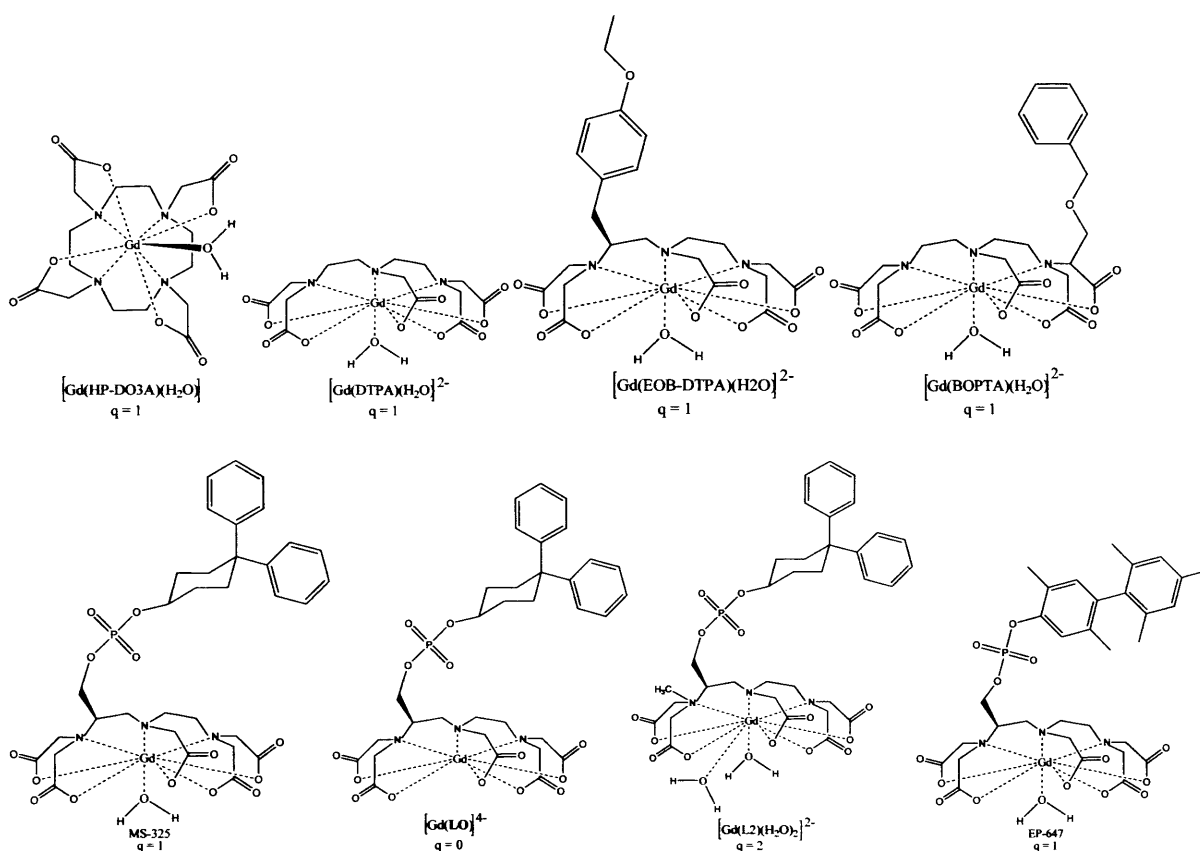


Figure 4:- Some functionalised Gd Chelates⁴⁸, q:- Number of water molecules in the inner coordination sphere of the complex (Hydration number)

The complexes, whose participation in *in vivo* transmetallation reactions, much slower than renal excretion rates, will have significant increase in their toxicities (compared to prediction based on thermodynamics). In short, the delay in clearance of any Gd (III) complexes will result in significant increase in toxicity. The following **Fig-5** shows other ligands often used in gadolinium studies.

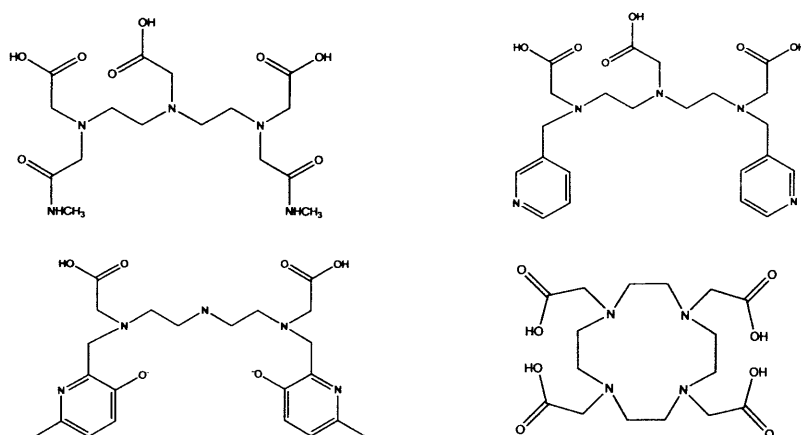


Figure 5:- A representation of the Chelates typically used for Gd complexation

Gd (III) has been shown to inhibit Ca (II) binding to mammalian cardiac sarcoplasmic reticulum. The mechanism of toxicity could involve hemodynamic disruption. An example⁵⁰ of two another perspective ligands is shown on **Figure 6**.

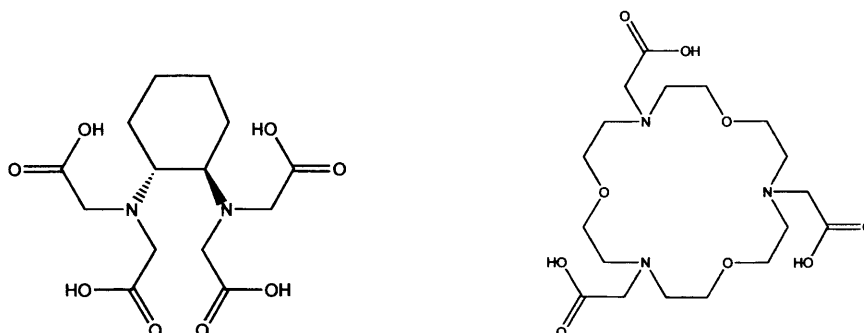


Figure 6:- Cyclic and Acyclic Chelating agents some more examples

Gadolinium Chelates – Pros and Cons

Potential improvement also lies in the idea of covalently coupling the ligand to protein to generate tissue-specific contrast agents.⁵¹ Understandably, search for new potential ligands for Gd (III) complexation is still a hot area of investigation. Gd-DTPA²⁻ (also known as “Gado” among medics) now serves as a bench mark for new contrast agents that are being synthesized and evaluated. The criteria include thermodynamic stability, rates of excretion, toxicity, lipophilicity, bio distribution and percent change in MR signal intensity. Some of the complexes are slightly better than Gd-DTPA in particular tests, others are a little worse. Neither of them, however, has received much attention as Gd-DTPA itself.⁵²

This complex is by far not the best choice as of today, but it is relatively well-known choice, widely used in many MRI facilities on a daily basis. Accumulated experience paves the way forward to offset the shortcomings of Gd-DTPA²⁻ in many cases. Therefore the agent continues to play indispensable role in modern MR imaging.

1.3.1.2 Comparison of Acyclic and Macrocyclic complexes of Gadolinium

There are six clinically approved contrast agents used worldwide for intravenous administration. Among them, four are gadolinium based with a polyaminocarboxylate ligand forming highly stable complexes.

The other two are mangafodipir trisodium.⁵³ (also known as Teslascan) and ferumoxides^{54, 55} which are super paramagnetic iron oxide nanoparticles often coated with dextrans.

The anionic complexes of $\text{Gd}(\text{DTPA})^{2-}$ (Magnevist) and $\text{Gd}(\text{DOTA})^-$ (Dotarem) were the first complexes used in clinical practice. The $\text{Gd}(\text{DTPA-BMA})$ (Omniscan) and $\text{Gd}(\text{HPDO3A})$ (Prohance) are neutral compounds based on the structures of the anionic complexes. $\text{Gd}(\text{DTPA})^{2-}$ forms a stable octa dentate, similarly to $\text{Gd}(\text{DOTA})^-$, but their formation is very different. Preparation of DTPA is relatively easier than preparation of DOTA, further DOTA requires the synthesis of 1, 4, 7, 10-tetra-azacyclododecane, which is time consuming.⁵⁶ The DTPA ligand forms stable chelates based on a distorted tricapped trigonal prism with the three nitrogens, five carboxylic oxygens, and the necessary water molecule coordinating to the gadolinium centre.⁵⁷ Lanthanide chelates produced with DOTA exhibits excellent stability, owing to its tetra-aza cycle, which could adapt the most stable confirmation. Through the X-ray crystallography of $\text{Gd}(\text{DOTA})^-$, it was evident that Gd (III) is situated in the centre of a capped square antiprismatic cage, while the water molecule occupies the axial position.⁵⁸ In solution, however, it exists as a pair of interchangeable isomers; the major square antiprismatic and the minor twisted square anti prismatic.

Thermodynamically stable, neutral gadolinium complexes are formed with DTPA-BMA and HP-DO3A complexes.⁵⁸ Kinetically stronger complexes are formed with HP-DO3A. It is because of its rigid ring structure of the macrocycle (minimum five coordination sites need to break down simultaneously), which prevents release of the metal. In the case of DTPA-BMA, however, sequential breaking of the coordination sites could be seen.^{59,60}

These first generation contrast agents are very useful, and have accounted for the rise in MRI scans being used in diagnosis. They distribute mainly into the intravascular and interstitial space, and although they are deemed to be nonspecific, they can accumulate within the kidneys due to glomerular filtration.⁶¹ The next generation of contrast agents are designed to be more specific and more efficient, with remarkably very high relaxivity,⁶² higher thermodynamic stability and a more favourable rate of excretion. As will be seen in some

Potential Multimodal Imaging Agents

examples discussed later, this can be achieved by attaching the contrast agent to larger structures such as dendrimers⁶³ or micelles.⁶⁴ In efficiency terms, the new reagents are usually compared to the DOTA and DTPA complexes due to their prior clinical approval.^{65, 66}

There were other elements in lanthanide series of the periodic table that were also considered to produce contrast agents.

Table 2: Physiochemical characteristics of commercially available, extra cellular, predominantly renally excreted gadolinium-based commercially available MR contrast agents-Safety Profile⁶⁷

Characteristics	<i>Magnevist</i> gadopentetate dimeglumine (0.5 mol/L)	<i>Dotarem</i> gadoterate meeglumine (0.5 mol/L)	<i>Prohance</i> gadoteridol (0.5 mol/L)	<i>Omniscan</i> gadodiamide (0.5 mol/L)	<i>Multihance</i> gadobenate dimeglumine (0.5 mol/L)	<i>Gadovist</i> Gadobutrol (1.0 mol/L)	<i>Optimark</i> gadoversetamide (0.5 mol/L)
Molecular Structure	Linear, ionic	Cyclic, ionic	Cyclic, non ionic	Linear, non ionic	Linear, ionic	Cyclic, non ionic	Linear, non ionic
Thermodynamic Stability Constant (log K _{st})	22.1	25.8	23.8	16.9	22.6	21.8	16.6
Conditional Stability Constant at pH 7.4	18.1	18.8	17.1	14.9	18.4		15.0
Acid dissociation rate (k(obs)s ⁻¹)	1.2 x 10 ⁻³	2.1 x 10 ⁻⁵	6.3 x 10 ⁻⁵	> 2 x 10 ⁻²			
Osmolality (Osm/Kg)	1.96	1.35	0.63	0.65	1.97	1.6	1.11
Viscosity (mPa at 37 °C)	2.9	2.0	1.3	1.4	5.3	4.96	2.0
T ₁ relaxivity (L/mmol s ⁻¹)1.5 T, plasma	4.1	3.6	4.1	4.3	8.3	4.7	4.7
T ₁ relaxivity (L/mmol s ⁻¹)3.0 T, plasma	3.7	3.5	3.7	4.0	6.2	3.6	4.5
Metal Chelate (mg/ml)	469	278.3	279.3	287	334	605	330.9
Excess Chelate (mg/ml)	0.4	0	0.23	12	0	0.5	28.4

1.3.1.3 Dysprosium Complexes as MRI contrast agents

Dysprosium (III) is one such lanthanide ion that has been used in MRI. It has been classified as negative contrast agent. As the clinical MRI is moving towards the utilisation of higher magnetic fields, where the commercial contrast agents based on Gd (III) shows poor relaxation times. One way of overcoming this shortcoming is the increasing attention on dysprosium-based complexes, due to their relatively slow water exchange rates. Thereby these complexes increase the residence time thus having an impact on optimising the r₂ relaxivity. Also dysprosium-based complexes, owing to their high magnetic susceptibility, which creates local field gradients resulting in lowering of T₂.⁶⁸

The magnetic field dependence of $1/T_1$ and $1/T_2$ of solvent protons in water has been examined in numerous accounts using some Dy (III) analogues of clinically used Gd (III) agents.⁶⁸⁻⁷⁰

In essence, dysprosium complexes in which the water molecules have a long mean water residence time hold the potential application as negative contrast agents at high magnetic fields due to their efficient transverse relaxivity.

Muller *et al.* have demonstrated, *via* Dy(DOTA)⁻, that lengthening the residence time of water can actually be detrimental, because the transverse relaxivity can then be limiting.⁷¹ Experiments have shown that the transverse relaxivity of complexes with fast exchange of water protons increases with the square of the magnetic field and the residence time (t_M).⁷²

At high magnetic fields, mean water residence time, which is greater than 1 ms imposes limitations on the relaxivity for dysprosium complexes, whereas mean water residence times, greater than 100 ns imposes limitations on the relaxivity at both high and low magnetic fields. Therefore, optimisation of mean water residence time (in between 0.1 and 1 ms) will result in obtaining r_2 , at the required high magnetic fields. Therefore it can be concluded that structural design of a molecule is inevitable to optimising r_2 , due to its balancing factors required. Further fine tuning of these mean water residence times and thereby the relaxivities, may result in promising contrast agents, which can be of use in high field MRI.⁷¹

The use of Dysprosium (III) compounds as negative contrast agents is still fairly new, and it will be interesting to look at their development over the next decade. On the other hand, analogues of Eu (II) which are isoelectronic to Gd (III) had been proposed as alternative to Gd (III) chelates. Further, it was thought to be a good choice as a spectroscopic probe for Ca (II). It is because its ionic radius lies between those of Ca (II) and Sr (II) (i.e. 125 pm Vs 112 and 126 pm).⁷³ Moreover its chemical properties are similar to those of the alkaline earth metal ion Merbach *et al.*^{74,75} investigated the water exchange kinetics and electronic relaxation of the following Eu (II) complexes: $[\text{Eu}(\text{DTPA})(\text{H}_2\text{O})]^{3-}$, $[\text{Eu}(\text{ODDM})]^{2-}$ and

[Eu(ODDA)(H₂O)], ligands in the latter two complexes are ODDMH₄ and ODDAH₂ respectively.

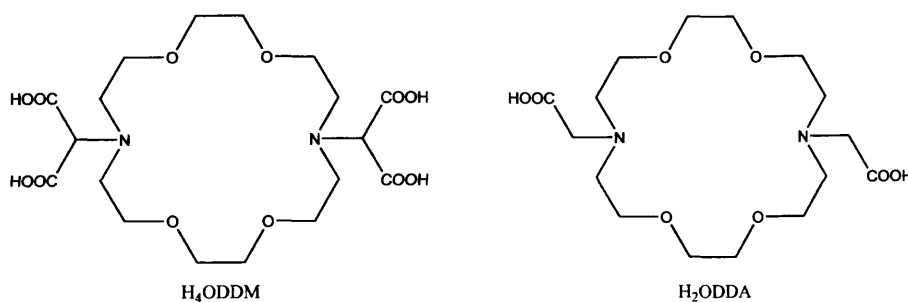


Figure 7:- Cyclic ligands as chelates for Eu

1.3.2 Metalloporphyrins of Iron (III) and Manganese (III)

Porphyrins have been known for decades as indicators of various metabolic disorders and disease states.^{76, 77} They are used in photodynamic therapy of tumors,⁷⁸ the low toxicity of metalloporphyrins and their selective retention in tumours has led recently to their study as MRI contrast agents.⁷⁹⁻⁸¹

Theoretical treatment of relaxivity of some of the metalloporphyrins is relatively new area of development. Metalloporphyrins of Mn (III) and Fe (III), however, show favourable properties as MRI contrast agents for tumour detection. They are strongly influencing MRI contrast agent research and should lead to interesting discoveries in the near future.

1.3.3 Native Proteins Acting as Contrast Agents

Heme-containing proteins could be considered as "natural" contrast agents, similar to previously discussed iron (III) porphyrins. Hematomas are easily identified by MRI. Paramagnetic deoxyhemoglobin within intact blood cells causes a local region of high magnetic field.⁸² This results in rapid dephasing of water protons diffusing in the region of acute hematoma with shortening of T₂, which results in low signal.

A similar observation was made when magnetically susceptible ferritin is deposited in macrophages in hemochromatosis. Even though, these are not site specific contrast agents, they could be put to successful use in certain diagnostics.

1.3.4 Gastrointestinal Contrast Agents

So far, the only clinically approved agents employed in gastrointestinal imaging are soluble iron compounds (Ferrous gluconate, ferric ammonium citrate) and $\text{Gd}(\text{DTPA})^{2-}$. There is a shortcoming with dosage of iron salts, which may not exceed the levels above those, when iron supplementation is used. The usage of iron oxide nano particles as oral contrast agent is yet to be discovered.

1.3.5 Stable nitroxide Radicals as MRI contrast agents

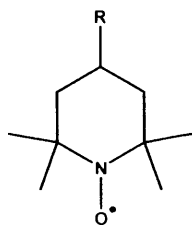


Figure 8:- Stable Nitroxide Radical

Radicals generally cause damage to the living tissues, the cyclic nitroxides, however, are a diverse range of stable free radicals that have unique antioxidant properties. It is because of their ability to interact with free radicals⁸³ they had been used as biophysical tools for many years.

Protection against radiation-induced radicals, cell signalling, functional imaging, chemoprevention and anticancer activity are a few of the numerous applications of these nitroxide radicals. Recently with the advent of EPR imaging (a concept which will be dealt in detail in the later sections), there was a new dimension of its usage had emerged.

In order to utilize nitroxides as MRI contrast agents, their reduction in a variety of normal tissues must be documented. The distribution and reduction of the nitroxides Tempol, 3CP, and carboxy-Proxyl were examined in MRI experiments⁸⁴.

Using MRI, it was possible to monitor the distribution and reduction of all three nitroxides. The reduction rates in normal tissue and tumour were calculated from these experiments.

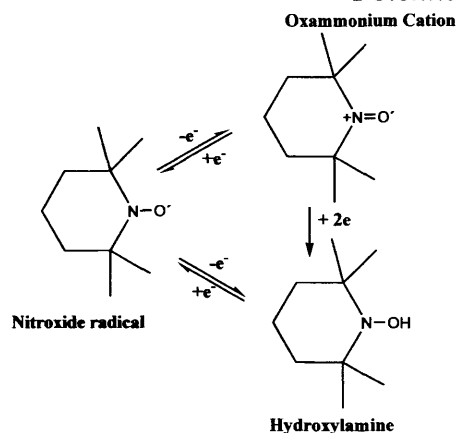


Figure 9:- A typical *in vivo* equilibria of the nitroxide compounds between the EPR detectable form (Nitroxide radicals) and that of EPR-non detectable form (hydroxylamine)

Even though, the paramagnetic effect of oxygen has been proved, its introduction as contrast agents is far from trivial.

1.3.6 Super Paramagnetic Iron oxide Particles (IO)

This is a relatively new type of contrast agents, which is advancing rapidly in the contrast agent research. They are made out of nonstoichiometric microcrystalline magnetite cores, on to which dextrans or siloxanes are coated. These colloids are now widely used in the pharmaceutical development, especially as tissue –specific contrast agents.^{85, 86}

Use of these colloids as tissue-specific contrast agents is now a well-established area of pharmaceutical development.^{85, 86} Today, by injecting iron oxide based nano particles as MRI contrast agents, it is possible to study lymphatic system and some specific tumours and their metastasis.⁸⁷

In particular, the type of surface coating, and the coating characteristics of nano particles are significant factors for the biological properties of nano particles and their destination target. Dextran coated iron oxides have been used for a long time.

They have been shown to decrease signal intensity in brain to mural regions on T₂ weighted images. Comparative evaluation of IO particles coated with Starch and Dextran was also carried out in the past.⁸⁸

In an alternative comparative study, effect of different amine and hydroxyl groups on the surface was evaluated in rat liver.⁸⁹ Surface modification of super paramagnetic nano

Potential Multimodal Imaging Agents

particles using different coating materials was also investigated by other workers for *in vivo* bio-medical applications and MR imaging, surface modification of superparamagnetic nano particles using different coating materials were also attempted.⁹⁰ Uptake of anionic IO particles (AMNP) was also shown.⁹¹

The light absorption ability is considerably high. The characteristic magnetic hysteresis observed in most of the super paramagnetic materials is not to be seen.

Utilisation of Mossbauer spectra, experimentally proved that there is no covalent bonding between the ion surface and that of coated dextran.^{92,93}

Apart from Mossbauer Spectroscopy there was and still is much interest in studying these non stoichiometric compounds with all the other vast array of modern physical-chemical methods: single crystal X-ray diffraction, powder X-ray diffraction, transmission electron microscopy, dynamic light scattering, atomic absorption spectroscopy, spectrophotometry, electron microscopy, superconducting quantum interference devices etc.^{92,94}

The compositions and physiochemical properties of nonstoichiometric magnetites are continuously variable between those of Fe_3O_4 and Fe_2O_3 .

Conceptually, these cation-deficient, inverse-spine phases are formed by partial oxidation of Fe (II) in stoichiometric magnetite. The Fe (II) content is typically 8-15 mol%. The lattice parameters of these colloids also fall between those of Fe_3O_4 and Fe_2O_3 .

Versatility of SPIO compounds, owing to their fine tunable properties for specific applications, put them as promising contrast agents. Furthermore, their toxicity levels are low and that it could be cleared from the organism rapidly. Site specific experiments (receptor-specific) SPIO delivery has been proved to be successful. Feridex I.VTM, EndoremTM, Gastro markTM, LumiremTM, SineremTM and much more are on the waiting list to be patented.

1.4 Latest developments & Modifications in Contrast Agents.

It is imperative to design systems with enhanced relaxivity, responsiveness and specific targeting abilities, to combat the challenges faced by molecular imaging.

1.4.1 Smart Contrast Agents

This is one of the rapidly advancing areas in MRI contrast agent research, where design and utilisation of “smart” contrast agents are on the rise. These are also known as responsive contrast agents. It is because their relaxivity is susceptible to changes in physiological surroundings. These changes could be in terms of pH, partial pressure of oxygen (this was well noted in Eu (II)/Eu (III) redox pairs) metal ion concentration or enzyme activity. There are several reviews published on this important area of MRI research. For instance, review published by Lowe *et al.*⁹⁵ in 2002 was a commendable one. It will be appropriate however, to look in to some important advancement in the area. Lowe⁹⁵ mentions that, the drive behind this area of smart contrast agents is supported by the fact that healthy tissue has a pH of 7.4, whereas tumour tissue is more acidic (6.8). This could be utilised to produce contrast agents that can be used to map tumours. Fullerene based, pH responsive contrast agents have been published by Toth *et al.*⁹⁶. In this agent, metallo fullerenes encapsulate metal ions in to their interior space. This has paved the way for potential medicinal applications as the fullerene cage protects the metal ion from being released in to the body. This in turn potentially increases the mean water residence time *in vivo*.⁹⁷ In fact Toth *et al.*⁹⁶ were not the first to bring up the idea of introducing gadofullerene derivatives as MRI agents.^{98, 99} The general trend is that the values are high side, (up to $81 \text{ mM}^{-1}\text{s}^{-1}$), but also very varied.

The availability of water-soluble gadofullerenes however, enabled further developments in this area, even though initially the relaxivities of these compounds was on lower side (when compared to commercial contrast agents). Therefore, Toth *et al* have attempted to understand the underlying mechanism for relaxivity in these compounds. They have synthesized fully characterised water soluble gadofullerene derivatives $\text{GdC}_{60}(\text{OH})_x$ and $\text{GdC}_{60}[\text{C}(\text{COOH})_2]$.

The measured relaxivities $\text{GdC}_{60}(\text{OH})_x$ were approximately ten times those of the commercial contrast agents. The high field maxima were discovered to be at approximately 40 MHz and the relaxivities were measured at 60 MHz as a function of pH.

They have discovered that with the decrease of pH, the relaxivities increased for compounds $\text{GdC}_{60}(\text{OH})_x$ and $\text{GdC}_{60}[\text{C}(\text{COOH})_2]$ by a factor 2.6 and 3.8 respectively. This could be explained in terms of proton exchange rate influenced by pH and also the temperature. Temperature effect was evident from the studies of static and dynamic light scattering (SLS and DLS) which showed aggregation. This in turn will affect the tumbling rate thereby the proton relaxivity.

These contrast agents were subsequently used for more specific biological applications, such as to track DNA delivery to specific cells, detect gene expression, and to monitor the changes in the activity of enzymes beyond their value in basic research; all of these procedures have potential applications in clinical work in the area of gene therapy, etc.

In theory, the relaxivity of these designer switchable contrast agents can tailor made to be conditionally dependent on certain variables like enzymatic activities, signalling messenger, calcium ion concentration, ion channel functions, receptors systems, degree of glycation of proteins, temperature, pH, pO_2 , gene expression and molecular recognition involved.

1.4.2 pH-activated Contrast Agents

This is one of most important factor in designing SCAs. While the extracellular pH is maintained slightly basic, the opposite scenario could be observed in tumour tissues. On the other hand, intracellular pH for both normal and tumour cells remain the same.

This was attributed to homeostatic mechanism. Stimulating MRI contrast agents by pH variation seems to be a promising way to high light tumours. Comparatively, an increase in the glycolytic activity could result in pH decrease in the intracellular region of tumours than its surrounding healthy tissues. This also forms the basis for pH related MRI contrast agents.

1.4.3 Metal ion Concentration Activated Contrast Agents

Sufficient concentration of metal ions (eg calcium, magnesium, iron, copper etc.) is vital to healthy living. Their deficiency may result in serious diseases. Therefore, monitoring their distribution *in vivo*, is highly desirable. Thus, several potential SCAs are being developed, which are sensitive to concentration variation of metal ions.

1.4.4 Enzyme-activated Contrast Agents

These agents potentially provide means for measuring enzyme activity and also their localization. The sensitivity of these agents depends upon their interaction with specific enzymes. If the interaction is sufficiently strong to increase the rotational correlation time of adducts, significantly higher relaxivities could be observed. Li *et al.* reported the first such contrast agent based on macrocyclic ligands.

1.4.5 Site specific Agents

MRI contrast media contributes to diagnostic imaging through its biophysical dimension. That has resulted upon the introduction of this novel type of contrast agent. These agents are also known as targeted relaxation enhancement agent (TREE) or a site specific agent (as it is commonly known).

The major advantage of these agents is that, their response will depend not on only on cellular or organ uptake (mass transfer events – as governing CT or scintigraphic images) but also on the fraction of the agent bound to macro molecules at any given time in the tissue of interest.¹⁰⁰ As shown in **Fig-18**, intelligent use of this binding-enhancement effect can considerably increase target-to-nontarget ratios in terms of relaxation rate changes.

In essence, the relaxation enhancement effect is designed to work synergistically with optimal bio distribution properties, permitting the highest contrast on the MRI image with the lowest possible dose of contrast media.

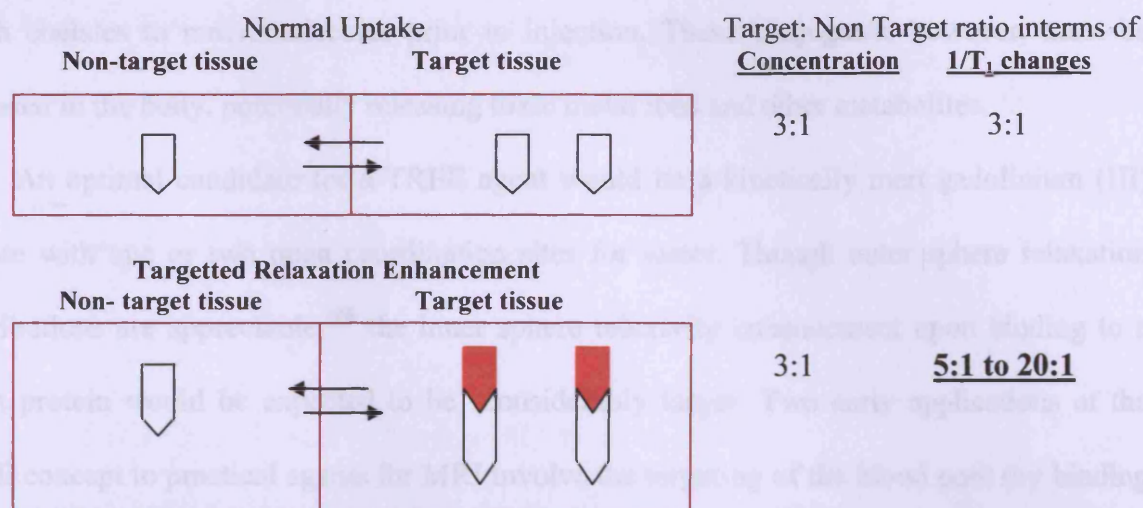


Figure 10:- The enhancement of MRI contrasts with targeted relaxation agents. The binding of a fraction of the agent molecules (triangles) to target macromolecules can increase relaxivity and tissue contrasts above that possible with "normal" uptake processes. The increase in the $1/T_1$ target: nontarget ratio is calculated based on the assumption that relaxivities increase by 2- to 10-fold upon binding.¹⁰⁰

The blood pool contrast agents in present use are not specific to a type of tissue. They however, preferably distributed within the blood stream, owing to their hypophilicity.¹⁰¹ Since it is a rapidly advancing area, it is worthy to mention a few examples which could indicate the versatility of these contrast agents. DOTA analogues are extensively used in MRI derivatives of this basic cyclen macrocycle, such as phosphonate esters,¹⁰² and methylene phosphonates.¹⁰³⁻¹⁰⁵ are of interest as well. In fact, it was proposed by Luke *et al.* that bisphosphonate monoamide analogue of DOTA could be utilised as potential bone imaging contrast agent. Nearly two decades, geminal bisphosphonates have been in usage for treatment of bone diseases.¹⁰⁶ due to their high attraction for the bone surface.¹⁰⁷ The presence of phosphorus acid moieties on cyclen macrocycles has been shown to lead to faster water exchange.

The optimal application of the TREE concept will involve *reversible*, non covalent binding of the metal chelate to the target protein or macromolecule of interest. The importance of this is largely toxicological: the unbound chelate molecules in equilibrium with the bound will be continuously excreted from the body by normal (and presumably safe) pathways such as the renal and hepatobiliary routes.

An alternative approach to take advantage of the binding-enhancement effect is to covalently attach chelates to macromolecules prior to injection. These conjugates, however, must be degraded in the body, potentially releasing toxic metal ions and other metabolites.

An optimal candidate for a TREE agent would be a kinetically inert gadolinium (III) chelate with one or two open coordination sites for water. Though outer sphere relaxation contributions are appreciable,¹⁰⁸ the inner sphere relaxivity enhancement upon binding to a target protein would be expected to be considerably larger. Two early applications of the TREE concept to practical agents for MRI involve the targeting of the blood pool (by binding to human serum albumin) and the hepatocytes of the liver (by binding to certain cytosolic proteins). Gadolinium(III) chelates suitable for these applications have been patented^{109,110}

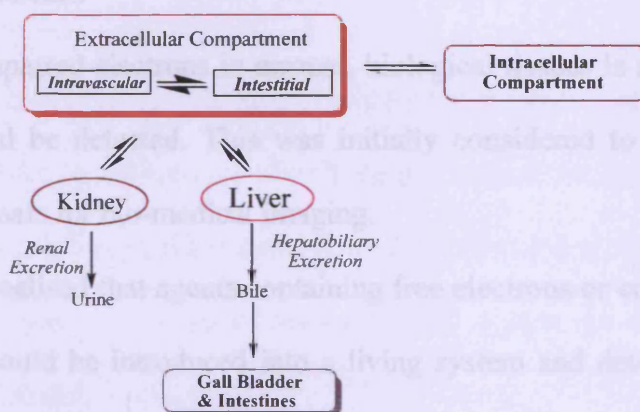


Figure 11: Distribution sites and excretion pathways for intravenously administered soluble metal complexes

Other Contrast Agents

Other than these paramagnetic agents mentioned so far, there are other materials and methods that could also act as MRI contrast agents. These agents are quite similar to one used in X-ray methods. One recent example is the utilisation of vegetable oils for rectal imaging through MRI.^{111, 112}

1.5 Emerging Trends in Imaging Technology

Apart from the Bio-Medical Imaging techniques, it is worth mentioning its various advanced dimensions. In this 'Era of Information', advancement of technology to unimaginable heights is frequently encountered and the imaging science is no exception to this.

We shall now direct our attention to more advanced facets of imaging technology within the context of chemistry.

1.5.1 EPR (Electron Paramagnetic Resonance)

An extension of this MRI is the use of techniques previously reserved for the laboratory such as EPR imaging, which detects unpaired electrons in such species as transition metal complexes and free radicals.¹¹³⁻¹¹⁵

The availability of unpaired electrons in normal, biological tissues is scarce to an extent that any EPR signal could be detected. This was initially considered to be a limitation to the utilisation of EPR signals for bio-medical imaging.

It was rapidly realised that agents containing free electrons or compounds converted to such agents *in-vivo* could be introduced into a living system and detected. The detection is possible in terms of frequencies similar to those used in MRI.¹¹⁵ After their administration *in-vivo*, nitroxide compounds are found in an equilibrium between the nitroxide radical form, which is detected by EPR, and the reduced hydroxylamine form, which is not detected by EPR because of its diamagnetic nature.¹¹⁶ It is because cellular redox processes convert the compound.

1.5.2 Optical Imaging (Optical Tomography)

There are techniques having an optical basis (such as bio luminescence, fluorescence), are rising as powerful alternative imaging modalities. Their contribution especially, to molecular imaging in disease and therapy becoming more commendable in recent times. This was achieved through the combination of innovative molecular biology and innovative chemistry.

Potential Multimodal Imaging Agents

The researchers have recently developed optical methods, which are capable of imaging a range of cellular and molecular processes *in-vivo* (protein interaction, degradation of proteins and activity of protease enzymes to name a few). Although optical imaging was introduced initially for researching small animals, its scope has been extended to clinical medicine.¹¹⁷

The *in vivo* fluorescence and bioluminescence imaging have enacted a vital role of interrogating biological systems, especially in rodent models for human diseases. Through the utilisation of integrated light distributions that are being emitted from the surface of the animal, most of the systems to date produce 2-D images only. This will in turn severely compromise the ability to quantify and also localizing the signals accurately, which is attributed to their strong dependence on optical properties of the tissue on depth. This has a significant impact on.

There is great interest in extending the in-vivo fluorescence and bioluminescence imaging modalities to the reconstruction of volumetric images that accurately localize signals and enable quantitative studies of fluorescent contrast agents and proteins. This is significant, as potentially higher temporal and spatial resolution than competing modalities like PET can be achieved at a considerably low cost.

In fluorescence imaging, an external light of appropriate wavelength is used to excite a target fluorescent molecule, followed almost immediately by release of longer-wavelength, lower-energy light for imaging. Targets for fluorescence imaging may be endogenous molecules (such as collagen or haemoglobin), fluorescent proteins (green fluorescent protein [GFP] and related molecules), or optical contrast agents with fluorescent molecules.

Although each of these sources of fluorescence can be used for cellular and molecular imaging in small-animal models, optical contrast agents have the potential to extend from preclinical research to patient care.

1.5.3 Overcoming Challenges with NIRF Imaging Agents

The most pressing challenge faced by optical imaging probes and instrumentation, targeted toward eventual clinical applications, is overcoming attenuation and scattering of light by tissues. For light in the visible spectrum, absorption by haemoglobin and other molecules may decrease optical signals by approximately 10-fold per centimetre of tissue. Therefore to image fluorescence in deeper tissues, investigators have devised strategies for imaging near-infrared fluorescence (NIRF) with emission wavelengths between 650 and 900 nm.

Further, within these wavelengths, absorption of light by haemoglobin, lipids, and water is lowest, and a dramatic reduction in the tissue auto fluorescence also observed. As a result, the sensitivity of NIRF imaging agents is greatly enhanced, potentially enhancing the chances of tomographic optical imaging signals to be detected at depths of 7–14 cm.

1.5.4 Functional Imaging

This is an area of Medical Imaging and which is also an extension of MRI technique. In the horizons it is expected to revolutionize the whole area. For more than 20 years, magnetic resonance imaging (MRI) has been an important tool for studying the brain. Application of MRI to problems in neuroscience blossomed in the early 1990s with the development of functional MRI (fMRI) methods to map spatio temporal patterns of brain activity in human subjects.¹¹⁸⁻¹²⁰ The basis of most current fMRI experiments in humans and animals is the blood oxygen-level dependence (BOLD) effect,^{121, 123} a combination of changes in local blood oxygenation, flow and volume that in healthy individuals are reflexively triggered by elevated neural activity. It is because, hemodynamic changes can be monitored directly by MRI, the BOLD effect offers a non-invasive, although indirect, readout of regional brain activity. Temporal characteristics of the BOLD effect were established by correlating defined patterns of sensory stimulation with time series of evoked fMRI signal changes¹¹⁸

References

1. R. Y. Tsien, *Nat Rev Mol Cell Biol: Suppl.*, 2003, 16.
2. B. Kevles, in *Naked to the bone: medical imaging in the twentieth century*, Rutgers University Press, New Brunswick, New Jersey, 1997.
3. S. Webb, in *From the watching of shadows : the origins of radiological tomography*, A. Hilger, New York, 1990.
4. G. Frank, *DE. Pat.*, 693,374, 1940.
5. A. Cormack, *J. Appl. Phys.*, 1963, **34**, 2722.
6. A. Cormack, *J. Appl. Phys.*, 1964, **35**, 2908.
7. D. J. Schlyer, *Ann. Acad. Med. Singapore.*, 2004, **33**, 146.
8. K. D. Jurasz, *Cancer Imaging.*, 2004, **4**, 162.
9. N. E. Bolus, R. George, J. Washington and B. R. Newcomer, *J. Nucl. Med. Technol.*, 2009, **37**, 63.
10. W. G. Bradley, in *Non-invasive Medical Imaging*, 1984, vol. 1, pp. 193-204.
11. F. W. Wehrli, J. Macfall, T. H. Newton and G. Potts, in *Advanced Imaging Techniques*, Clavadel Press, San Francisco, 1983.
12. F. A. Mettler, L. R. Muroff and M. V. Kulkarm, in *Magnetic Resonance Imaging and Spectroscopy*, Churchill Livingstone, New York, 1986.
13. D. H. Carr, *Magn. Reson. Imaging.*, 1985, **3**, 11.
14. S. B. Yu and A. D. Watson, *Chem. Rev.*, 1999, **99**, 2353.
15. J. Skucas, in *Radiographic Contrast Agents*, Aspen Publishers, Rockville, 1989.
16. E. D. Osborne, C. G. Sutherland, A.J. Scholl and L. G. Rowntree, *J. Am. Med. Assoc.*, 1923, **80**, 368.
17. A. J. Binz, *Urology*, 1931, **25**, 297.
18. T. Rumpel, *Muenchen Med. Wschr.*, 1897, **44**, 420.
19. W. B. Cannon, *Am. J. Physiol.*, 1898, **1**, 359.
20. P. Dawson, *Brit. J. Urol.*, **66**, 561.
21. D. Muller, M. Foulon, B. Bonnemain and F. Vandamme, *J. Microencapsulation.*, 2000, **17**, 227.
22. E. Moniz, A. Pinto and A.Lima, *Rev. Neurol.*, 1931, **32**, 646.

23. P. Radt, *Med. Klin.*, 1930, **26**, 1889.
24. Council on Pharmacy and Chemistry of the American Medical Association. *J. Am. Med. Assoc.*, 1932, **99**, 2193.
25. J. A. Nadel, W. G. Wolfe, P. D. Graf, J. E. Youker, N. Zamel, H. M. Austin, W. A. Hinchcliffe, R. H. Greenspan and R. R. Wright, *N. Engl. J. Med.*, 1970, **283**, 281.
26. R. Shapiro, *Radiology*, 1955, **65**, 429.
27. S. B. Yu and A. D. Watson, *Chem. Rev.*, 1999, **99**, 2353.
28. J. Novak and J. Podlaha, *J. Inorg. Nucl. Chem*, 1974, **36**, 1061.
29. L. Miersch, T. Ruffer, H. Lang, S. Schulze, M. Hietschold, D. Zahn and M. Mehring, *Eur. J. Inorg. Chem.*, 2010, 4763.
30. S. B. Yu, M. Droege, B. Segal, S. Downey, T. Sanderson, J. Fellmann and A. Watson, *Inorg. Chim. Acta.*, 1997, **263**, 61.
31. T. Vehmas and P. Tervahartiala, *Acta. Radiol.*, 1996, **37**, 804.
32. R. M. Nalbandian, W.T. Rice and W. O. Nickel, *Ann. N.Y. Acad. Sci.*, 1959, **78**, 779.
33. P. L. Roberts, N. Chuang and H. C. Roberts, *Eur. J. Radiol.*, 2000, **34**, 166.
34. F. Calliada, R. Campani, O. Bottinelli, A. Bozzini and M. G. Sommaruga, *Eur. J. Radiol.*, 1998, **27**, S157–S160.
35. J. M. Correias and S. D. Quay, *Clin. Radiol.*, 1996, **51**, 15.
36. F. Bloch and H. W. Packard, *M. Phys. Rev.*, 1948, **70**, 474.
37. N. Bloembergen, E. M. Purcell and R.V.Pound, *Phys. Rev.*, 1948, **73**, 678.
38. T. R. Kibo and K. Tomita, *J. Phys. Soc. Jpn.*, 1954, **9**, 888.
39. I. Solomon, *Phys. Rev.*, 1955, **99**, 559.
40. R. A. Dwek, *Nuclear Magnetic Resonance in Biochemistry : Applications to Enzyme Systems*, Clarendon, Oxford, 1973.
41. W.S. Hinshaw, P. A. Bottomley and G. N. Holland, *Nature (London)*, 1977, **270**, 272.
42. I. R. Young, G. J. Clarke and D. R. Gales, *Comput. Tomogr.*, 1981, **5**, 534.
43. D. H. Carr, J. Brown and G. M. Bydder, *J. Lancet.*, 1984, 484.
44. K. L. Watkin and M. A. McDonald, *Acad. Radiol.*, 2002, **9**, S285.
45. M. Bottrill, L. Kwok and N. J. Long, *Chem. Soc. Rev.*, 2006, **35**, 557.

46. L. A. Chang, L. C. Francesconi, M. F. Malley, K. Kumar, Z. Gougoutas, M. F. Tweedle, D. W. Lee and L. J. Wilson, *Inorg. Chem.*, 1993, **32**, 3501.
47. G. Bombieri and R. Artali, *J. Alloys and Comp.*, 2002, **344**, 9.
48. P. Caravan, *Acc. Chem. Res.*, 2009, **42**, 851.
49. Z. C. Tyeklar, S. S. Dumas, P. Bernard, S. Nadler, K. M. Midelfort, M. Greenfield, J. Troughto and R. B. Lauffer, *J. Med. Chem.*, 2002, **45**, 3465.
50. C. B. Wiegers, *Magn. Resonan. Imaging.*, 1992, **10**, 903-911.
51. M. Spanoghe, *Magn. Resonan. Imaging.*, 1992, **10**, 913-917.
52. B. Carollo, *Magn. Reson. Imaging.*, 1990, **8**, 381-393.
53. C. S. Zuo, P. R. Seoane, J. Hu, P. P. Harnish and N. M. Rofsky, *Radiology*, 2004, **232**, 160.
54. L. F. Gamarra, E. S. Brito, W. M. Pontuschka, E. Amaro, H. C. Parma and G. F. Goya, *J. Magn. Magn. Mater.*, 2005, **289**, 439.
55. D. K. Kim, M. Mikhaylova, F. H. Wang, J. Kehr, B. Bjelke, Y. Zhang, T. Tsakalagos and M. Muhammed, *Chem. Mater.*, 2003
56. G. R. Weisman and D. P. Reed, *J. Org. Chem.*, 1996, **61**, 5186.
57. J. J. Stezokowski and J. L. Hoard, *Isr. J. Chem.*, 1984, **24**, 323.
58. L. A. Chang, L. C. Francesconi, M. F. Malley, K. Kumar, Z. Gougoutas, M. F. Tweedle, D. W. Lee and L. J. Wilson, *Inorg. Chem.*, 1993, **32**, 3501.
59. M. F. Tweedle, P. Wedeking and K. Kumar, *Invest. Radiol.*, 1995, **99**.
60. K. A. Gibby and W. A. Gibby, *Invest. Radiol.*, 2004, **39**, 138.
61. W. P. Cacherris, S. C. Quay and S. M. Rocklage, *Magn. Reson. Imaging.*, 1990, **8**, 467.
62. H. J. Weinmann, W. Ebert, B. Misselwitz and H. S. Willich, *Eur. J. Radiol.*, 2003, **46**, 33.
63. T. N. Fatin-Rouge, R. Meuli and C. G. Bunzli, *J. Alloys Compd.*, 2004, **374**, 298.
64. G. M. Nicolle, E. Toth, H. Schmitt-Willich, B. Raduchel and A. E. Merbach, *Chem. Eur. J.*, 2002, **8**, 1040.
65. G. M. Nicolle, E. Toth, K. P. Eisenwiener, H. R. Macke and A. E. Merbach, *J. Biol. Inorg. Chem.*, 2002, **7**, 757.
66. J. Feng, G. Sun, F. Pei and M. Liu, *Bioorg. Med. Chem.*, 2003, **11**, 3359.
67. V. M. Runge and M. A. Kirchin, *Top. Magn. Reson. Imaging.*, 2003, **14**, 426.

68. L. V. Elst, A. Roch, P. Gillis, S. Laurent, F. Botteman, W. M. Bulte and R. N. Muller, *Magn. Reson. Med.*, 2002, **47**, 1121.
69. J. Vymazal, W. M. Bulte, J. A. Frank, G. D. Chiro and R. A. Brooks, *J. Magn. Reson. Imaging.*, 1993, **3**, 637.
70. W. M. Bulte, C. Wu, M. W. Brechbiel, R. A. Brooks, J. Vymazal, M. Holla and J. A. Frank, *Invest. Radiol.*, 1998, **33**, 841.
71. K. E. Keller, S. Fossheim and S. H. Koenig, *Invest. Radiol.*, 1998, **33**, 835.
72. L.V. Elst, S. Zhang, A. D. Sherry, S. Laurent, F. Botteman and R. N. Muller, *Acad. Radiol.*, 2002, **9**, S297.
73. L. V. Elst, A. D. Sherry, S. Laurent, F. Botteman and R. N. Muller, *Proc. Int. Soc. Magn. Reson. Med.*, 2000, **8**, 2057.
74. E. Toth, L. Burai and A. E. Merbach, *Coord. Chem. Rev.*, 2001, **363**, 216.
75. L. Burai, E. Toth, S. Seibig, R. Scopelliti and A. E. Merbach, *Chem. Eur. J.*, 2000, **6**, 3761.
76. R. D. Shannon, *Acta Crystallogr Sect. A: Cryst. Phys. Diffr. Theor. Gen. Cryst.*, 1976, **32**, 751.
77. A. Policard, *Comp. Rend. Soc. Biol.*, 1924, **91**, 1423.
78. F. Figge, *Proc. Soc. Exp. Biol. Med.*, 1948, **68**, 640.
79. M. W. Berns, *Lasers. Surg. Med.*, 1984, **4**, 1.
80. N. J. Patronas, *Cancer Treat. Reports.*, 1986, **70**, 391.
81. S. K. Saini, *Magn. Reson. Imaging.*, 1995, **13**, 985.
82. G. A. Mercier, *Magn. Reson. Imaging.*, 1995, **13**, 807.
83. J. M. Gomori, *Radiology*, 1985, **157**, 87.
84. B. P. Soule, F. Hyodo, K. Matsumoto, N. L. Simone, J. A. Cook, M. C. Krishna and J. B. Mitchell, *Free Radical Biol. Med.*, 2007, **42**, 1632.
85. F. Hyodo, K. Matsumoto, A. Matsumoto, J. B. Mitchell and M. C. Krishna, *Cancer Res.*, 2006, **66**, 9921.
86. J. T. Ferrucci and D. D. Stark, *Am. J. Roentgenol.*, 1990, **155**, 943.
87. P. F. Hahn, *Am. J. Roentgenol.*, 1991, **156**, 252.
88. D. K. Kim, M. Mikhaylova, F. H. Wang, J. Kehr, B. Bjelke, Y. Zhang, T. Tsakalacos and M. Muhammed, *Chem. Mater.*, 2003, **15**, 4343.
89. O. Mykhaylyk, A. Cherchenko and A. Ilkin, *J. Magn. Magn. Mater.*, 2001, **225**, 173.

90. D. Portet, B. Denizot and E. Rump, *Drug Dev. Res.*, 2001, **54**, 173.
91. D. K. Kim, M. Toprak and M. Mikhailova, *Mat. Res. Soc. Symp Proc.*, 2002, **704**, 201.
92. C. Wilhelm, C. Billotey and J. Roger, *Biomaterials*, 2003, **24**, 1001.
93. C. W. Jung and P. Jacobs, *Magn. Reson. Imaging.*, 1995, **13**, 661.
94. C. W. Jung, *Magn. Reson. Imaging.*, 1995, **13**, 675.
95. E. Murad, J. H. Johnson and G. L. Long, in *Mossbauer spectroscopy applied to inorganic chemistry*, Plenum Press, New York, 1984.
96. M. P. Lowe, *Aust. J. Chem.*, 2002, **55**, 551.
97. H. Shinohara, *Rep. Prog. Phys.*, 2000, **63**, 843.
98. E. Toth, R. D. Bolskar, A. Borel, G. Gonzalez, L. Helm, A. E. Merbach, B. Sitharaman and L. J. Wilson, *J. Am. Chem. Soc.*, 2005, **127**, 799.
99. S. Zhang, D. Sun, X. Li, F. Lei and S. Liu, *Fullerene Sci. Technol.*, 1997, **5**, 1635.
100. H. K. M. Mikawa, M. Okumura, M. Narazaki, Y. Kanazawa, N. Miwa and H. Shinohara, *Bioconjugate Chem.*, 2001, **12**, 510.
101. R. B. Lauffer, *Magn. Reson. Med.*, 1991 **22**, 339.
102. V. Jacques and J. F. Desreux, *Top. Curr. Chem.*, 2002, **221**, 123.
103. I. Lazar, A. D. Sherry, R. Ramasay, E. Brucher and R. Kiraly, *Inorg. Chem.*, 1991, **30**, 5016.
104. A. D. Sherry, G. C. Geraldles and W. P. Cacheris, *Inorg. Chim. Acta.*, 1987, **139**, 137.
105. G. C. Geraldles, A. D. Sherry and W. P. Cacheris, *Inorg. Chem.*, 1989, **28**, 3336.
106. A. D. Sherry, *J. Alloys Compd.*, 1997, **249**, 153.
107. J. R. V. Kubicek, J. Kotek, P. Hermann, L. V. Elst, R. N. Muller, Z. I. Kolar, H. T. Wolterbeek, J. A. Peters and I. Lukes, *J. Am. Chem. Soc.*, 2005, **127**, 16477.
108. H. Fleisch, in *Bisphosphonates in Bone Disease*, Academic Press, London and California, 2000.
109. R. B. Lauffer, *Chem. Rev.*, 1987, **87**, 901.
110. R. B. Lauffer and T. J. Brady, *US Pat.*, 4,899,755, 1990.
111. R. B. Lauffer, *US Pat.*, 4,880,008, 1989.
112. P. Pokieser, *Magn. Reson. Imaging.*, 1995, **13**, 979.

113. R. Butch, *Am. J. Roentgenol.*, 1986, **146**, 1155.
114. H. J. Halpern, D. P. Spencer and J. V. Polen, *Rev. Sci. Instrum.*, 1989, **60**, 1040.
115. P. Kuppusamy, M. Chzhan, K. Vij, M. Shteynbuk, D. J. Lefer, E. Giannella and J. L. Zweier, *Proc. Natl. Acad. Sci. USA.*, 1994, **91**, 3388.
116. K. J. Liu, P. Gast, M. Moussavi, S. W. Norby, N. Vahidi, T. Walczak, M. Wu and H. M. Swartz, *Proc. Natl. Acad. Sci. USA.*, 1993, **90**, 5438.
117. A. Samuni, C. M. Krishna, J. B. Mitchell, C. R. Collins and A. Russo, *Free Radic. Res. Commun.*, 1990, **9**, 241.
118. Luker and Luker, *J. Nucl. Med.*, 2008, **49**, 1.
119. K. K. Kwong, *Proc. Natl. Acad. Sci. U S A.*, 1992, **89**, 5675.
120. S. Ogawa, *Proc. Natl. Acad. Sci. USA.*, 1992, **89**, 5951.
121. J. W. Belliveau, *Science*, 1991, **254**, 716.
122. S. Ogawa, *Magn. Reson. Med.*, 1990, **14**, 68.
123. S. Ogawa and T. M. Lee, *Magn. Reson. Med.*, 1990, **16**, 9.

CHAPTER 2

EDTA Based Derivatives

2.1 Introduction to EDTA based derivatives

2.1.1 - EDTA

EDTA is a hexadentate ligand, where the ethylene chains between the four carboxylic acid groups and has been classified as a "conformational" ligand by definition, are also by carboxylic acids, in which several carboxylic acid groups have to be

CHAPTER 2

EDTA

Based

Derivatives

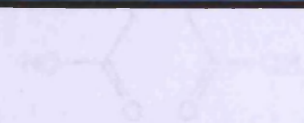


Figure 1: Chemical structure of EDTA (Ethylenediaminetetraacetic acid)

2.1.2 Detoxification of Metal Ions

Studies investigating the chelating ability of EDTA and its ability to remove toxic substances from metal ions was initiated as early as 1950s,¹ because these studies were not directed towards synthesizing a contrast agent. With regard to MRI contrast agents, one of a key question is if the ligand can 'detoxify' the aluminum (Al³⁺) ion.

The literature has an interesting account about the ratio of aluminum [Al-EDTA] (which has ED_{0.5} 4.3 mg/kg by day) have been shown to be more toxic than CuCl₂.

CHAPTER 2

EDTA Based Derivatives

2.1 Introduction to EDTA based derivatives

2.1.1 EDTA

EDTA is a hexadentate ligand, where the ethylene diamine backbone has been modified by four carboxy methyl groups and has been classified as a ‘complexone’. Complexones by definition are aminopoly carboxylic acids, in which several carboxy alkyl groups bind to one or more nitrogen atoms. As a result, coordination of a single metal ion establishes several chelate rings. The practical value of EDTA lies in its ability to form stable, water-soluble complexes with many metal ions. In 1946, Schwarzenbach utilised this property to determine hardness of water. Since then it has found application in areas such as biology, phytochemistry,¹ sequestration of metal ions,² extraction and separation of metals³ to name a few.

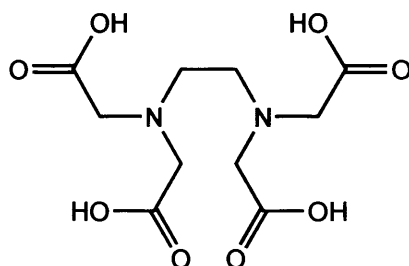


Figure 1:- Ethylene Diamine Tetra acetic Acid (EDTAH₄)

2.1.2 Detoxification of Metal Ions

Studies investigating the chelating ability of EDTA to detoxify (removal of toxic substances) metal ions was initiated as early as 1950s,⁴ though these studies were not directed towards synthesizing a contrast agent. With regard to MRI contrast agents, however, a key question is if the ligand can ‘detoxify’ the ubiquitous Gd (III) ion.

The literature has an interesting account about this piece of research.¹ [Gd-EDTA]⁻ (which has LD₅₀, 0.3 mmol/kg in rats) have been shown to be more toxic than GdCl₃

Potential Multimodal Imaging Agents

(which has LD₅₀ 0.5 mmol/kg in rats¹, because, it is able to labilize gadolinium (log K_{stab} 17) for distribution to a wide variety of sites *in vivo* (mainly skeletal bones). Also, the gadolinium complex of EDTA has a net charge of -1, and is generally administered as soluble salts (sodium and N-methylglucamine). Unfortunately, these salts can cause localized disturbances in osmolality, which in turn, lead to edema and other undesirable effects within the body.

For the above and other reasons, Gd-EDTA and related complexes are generally considered too toxic for clinical use. In fact, there is literature evidence which states that attempts to coordinate Y³⁺ with EDTA⁴⁻ yielded both positive and negative results; that is Y[EDTA]⁻ dissociated *in vivo*¹ and it was discovered later on that this complex was an excellent reagent for selective delivery of yttrium to bone surfaces.

2.1.3 Salts of Transition Metals as MRI Contrast Agents and Their Early History

“Nephrogenic Systemic Fibrosis” (NSF) is a fibrotic disorder generally observed in renal failure patients. It was recently discovered that some (for eg:- Gadoversetamide) extracellular gadolinium based contrast agents (Gd-CAs) trigger the development of NSF.⁵ As reported by FDA in the recent past, the delayed adverse reactions caused by NSF is the worst among the other side effects (such as Contrast induced nephropathy (CIN), anaphylactoid reactions) created by other Gd-CAs.⁶ Therefore NSF, prompting the scientists to look for non gadolinium based contrast agents. Tracing back the history of contrast agents indicates that the pioneering attempts to produce viable contrast agents for MRI, has involved the usage of two of the transition metal ions (Mn (II) and Cr (III)).

Among the potential transition metal ions bearing a maximum five unpaired electrons ((Mn (II), Fe (III), Cr(III), Co (III), Tc (III) and Ru (II)), three of them have played a significant role as potential MRI contrast agents throughout the history. Therefore it is essential for the scope of the thesis to have a brief historical outlook on these most potential transition metal ions.

Manganese (II): This transition metal ion has five unpaired electrons and the longest electron spin relaxation time among the transition elements. In fact the first true MRI contrast enhancing agent examined *in vivo* was MnCl_2 . Perhaps because of its abundance in the pancreas, liver, kidney and heart,¹ it was used to demonstrate contrast enhancement of canine myocardial tissues. Later it was used as a gastrointestinal tract (GIT) imaging agent, (commercially known as 'LumenHance'). The utilisation of 'LumenHance' as a GIT agent was possible due to uptake of the paramagnetic manganese ion (Mn (II)) by hepatocytes (chief functional cells of the liver and liver is a part of GIT). It was found that 30-35% of the manganese existing in the portal vein is being absorbed by the liver, thus contributing to reduced toxicity. Further it has exhibited good relaxivities. The r_1 value of the 'LumenHance' solution (where the major component is MnCl_2) is $20.9 \text{ mM}^{-1}\text{s}^{-1}$ at 10 MHz, 37 °C and the r_2 is $35.0 \text{ mM}^{-1}\text{s}^{-1}$ at 10 MHz, 37 °C.⁷ Since it has high r_1 and r_2 values, it has been utilised both as a T_1 contrast agent (by increasing the signal intensity of the T_1 weighted images as well as a T_2 agent (by reducing the signal intensity of T_2 weighted images). This has undergone its Phase III clinical trials in 1999. It was discovered in the clinical trials that large volumes needs to be consumed, this was a major short coming (In the clinical trials carried out, it was discovered that 14% of the patients were not able to consume at least 800 ml of the 'Lumenhance' solution)

Iron (III): Another transition element which needs to be considered is the ferric ion (Fe^{3+}). This high spin d^5 ion may also potentially have 5 unpaired electrons and may be of interest on the basis of its biological importance. There is a very large volume of literature available on the biochemistry of iron. It is also interesting to note, Fe (III) has an r_1 of $6.8 \text{ mM}^{-1}\text{s}^{-1}$ at 20 MHz and 37 °C. These factors make it stand as a candidate for potential MRI contrast agent. The free Fe (III), however, is toxic (LD_{50} 0.42 mmol/Kg). Iron poisoning leads to increased respiration rate and pulse rates. Also it was found to cause congestion in blood vessels.

Potential Multimodal Imaging Agents

Further, Fe (III) was found to act as a Lewis acid catalyst for the hydrolysis of phosphates. Therefore, the complete complexation of Fe (III) with potential ligands will lead to the reduction in toxicity, through the reduction in oxidative cell damage. Moreover, by eliminating the excess coordination sites, due to coordination, will minimize its Lewis acid character. Thereby it contributes to the reduction in toxicity.

Therefore investigations for suitable ligand systems were carried out. One such ligand is the ammonium citrate, which has afforded Ferric Ammonium Citrate. This is the major ingredient in Gerritol and has been considered as oral contrast agent. The r_1 value discovered to be $1.60 \text{ mM}^{-1}\text{s}^{-1}$ (at 16 MHz). Gerritol, however, came across two shortcomings. Firstly it went through inhomogeneous distribution in small bowel. Secondly it contained 12% ethanol, which had prevented its use in large volumes. Complexation with N, N'- Ethylenebis-[2-(o-hydroxyphenyl) glycine] (EHPG) was also investigated. Fe-EHPG exhibited r_1 value of $0.9 \text{ mM}^{-1}\text{s}^{-1}$ at 10.70 MHz and 37 °C. Further several derivatives of EHPG also been complexed with Fe (III) towards the investigation as MRI contrast agent. A complex of Fe (III) with N,N'-bis (2-hydroxybenzyl)ethylene diamine-N,N'-diacetate (HBED) was also investigated as an MRI contrast agent. The r_1 value obtained was $1.10 \text{ mM}^{-1}\text{s}^{-1}$ at 10.7 MHz and 37 °C.⁸

Chromium (III): The Cr- EDTA complex was prepared by McDonald and Downes by direct reaction of chromium (III) chloride with EDTA bisanhydride under aqueous conditions at pH 10. The alkaline condition was used as chromium (III) Hydroxide has a low solubility product, ($K_{sp} = 10^{-30}$), meaning that the amount of free chromium ion is negligible when compared to Cr-EDTA, making its contribution to proton relaxation insignificant. Cr-EDTA was found to decrease the T_1 value significantly (See Table 1). The Cr- EDTA was found to be useful in the observation of tissue muscularity, breakdown of the blood – brain barrier and renal function.⁹

Table 1: T₁ and T₂ values of Cr-EDTA complex prepared by Runge *et al.*⁹

Variation in T ₁ and T ₂ with changes in concentration of Cr-EDTA (sterile water, in-vitro at 2.5 MHz)		
Concentration of Cr-EDTA (mg/ml)	T ₁ (milliseconds)	T ₂ (milliseconds)
0.016	1,016 ± 3	230 ± 70
0.080	941 ± 4	230 ± 60
0.400	584 ± 3	190 ± 70
2.000	159 ± 1	120 ± 30
10.000	30 ± 10	40 ± 90

Cu (II) Complexes of copper have received little attention as contrast agents for MRI. Cu (II) ions have unfavourable electronic relaxation times and have only one unpaired electron, therefore they have a significantly lower relaxivity than ions of manganese and iron. In the past Cu(II)EDTA was studied by Vymazal *et al.*¹⁰ and had been compared with other paramagnetic ion chelates (see Table 2).

Table 2:- Depicting the comparison of relaxivities of paramagnetic chelates (Based on transition and lanthanide metal ions)¹⁰

Longitudinal Relaxivity (L.mol ⁻¹ .sec ⁻¹) of chelated Paramagnetic Ions at Five different Field Strengths					
Chelate	Frequency at 37 °C (MHz)				
	2.13	10.00	21.29	42.57	63.86
Gd(III)-DTPA	6.2	4.8	3.6	3.2	3.2
Gd(III)-EDTA	11.7	7.6	6.4	5.2	4.9
Fe (III)-EDTA	2.8	2.1	1.4
Mn (II)-EDTA	4.2	3.3	2.2	2.2
Cu (II)-EDTA	0.4	0.3	0.2	0.2	0.2

They have reported comparatively low relaxivities. On the other hand, free Cu (II) ion is relatively non toxic (i.e. LD₅₀ in mice is 55 mmol kg⁻¹) in comparison with Mn (II) and Fe (III) ions (LD₅₀ in mice is 0.3 mmol/Kg in mice and 0.88 mmol/Kg in mice respectively). This fact invokes the possibility to use higher concentrations of copper complexes. This in turn could help to compensate its low relaxivity.

Potential Multimodal Imaging Agents

Further Cu-EDTA was examined to be a potential contrast agent for MR Microscopy cartilage in comparison with Cu (II) chloride. It was found however, that interaction with anionic proteoglycan molecules slows the relative rate of diffusion of Cu (II) ions when compared with EDTA. This was experimentally proved. The neutralization of the anionic groups on the proteoglycans by either acid or enzymatic digestion led to a decrease in the relaxivity of local protons. Cu(EDTA-doped polyacrylamide gels) were spotted with sulphuric acid, and thereby the change in the relaxivity of the copper (II) solution was visualised, while the acid diffused throughout the gel (non GD). A series of derivatives of tetramic acid (TA) were synthesized and then complexed with copper (II) (Cu-TA). The ability of the Cu-TA derivatives to cross membranes was measured using deflocculated oocytes cells. The T_2 time value for intracellular water of an oocyte is very short and does not qualify for analysis of the membrane permeation of a contrast agent, whereas the T_1 values of the water signal of the oocytes, are a parameter well suited for this purpose as reported. Copper clusters formed by the reaction of D-penicillamine with copper (II) chloride had been attached with antibodies or other biotinylated proteins via linker molecule and been used as imaging agents.

Cu- EDTA

Finally organic polymers of Cu-EDTA were tested as potential contrast agents. Similarly copper complexes of mercaptosuccinic acid and carboxymethylcellulose were tested as potential contrast agents. It is worth noting that the relaxivities reported for these contrast agents lies on the lower side. For instance, Cu (II)-mercaptosuccinic acid-dextran conjugate exhibited an r_1 value of $0.6 \text{ mM}^{-1}\text{s}^{-1}$ (at 10 MHz, 37 °C), in a 1: 2.13 glycerol-water solvent mixture. Further Cu (II)-carboxymethylcellulose complex exhibited r_1 value of $2 \text{ mM}^{-1}\text{s}^{-1}$ under the same conditions. The relaxation properties of the Glycerol-water solution are similar to those of body fluids. Therefore it has been selected instead of water.¹¹

2.1.4 Mn (II) emerging as the immediate competitor for Gd (III)

Contrary to the Gd (III) (the most widely used MRI contrast agent of choice), manganese is an essential trace element present in all mammal cells: this is undoubtedly a major advantage. The widespread abundance has facilitated studies on the biochemical significance of Mn (II). The biochemistry of manganese is well established. It is essential for glucose and lipid metabolism and also plays an important role in oxidative phosphorylation along with a number of other important biochemical processes.¹²

Yet, the manganese ion can cause toxicity when released from the corresponding chelates *in vivo*; this mainly applies when the manganese ion is administered intravascularly, as in this case the natural regulation of its adsorption by the intestine fails. Further, the chronic exposure to manganese resulted in neurological disorders similar to that of Parkinson disease.¹³ In an acute condition, it could result in hepatic failure,¹⁴ sometimes may lead to cardiac failure.¹⁵

2.1.5 Subsequent research into Mn (II) complexes as MRI CAs

Therefore it is necessary for Mn (II) to be administered as a stable complex, in order to prevent any toxicity due to the free metal ion and also improve its elimination from the body. There now exists a significant body of research into the co-ordination chemistry of Mn (II), targeted towards identifying new potential contrast agents:

2.1.5.1 Story of Tesla Scan and the challenges faced at the outset

Investigation with N,N'-dipyridoxylethylenediamine-N,N'-diacetic acid (PLED)

Initially Taliaferro *et al.*¹⁶ have investigated the solution properties of the N,N'-dipyridoxylethylenediamine-N,N'-diacetic acid (PLED). PLED contains six donor groups as does N,N'-Bis(hydroxybenzyl)ethylenediamine-N,N'-diacetic acid (HBED) and N,N'-ethylenebis [2-(o-hydroxyphenyl) glycine] (EHPG). With respect to steric effects, however, geometries and basicities of the respected ligands, contribute to the variation of the overall stabilities of these chelates. For instance, aliphatic nitrogens contribute to reduction in the

Mn (II) forms stable complexes with DPDP. The complexes were further developed to afford the commercially available ‘Tesla Scan’.

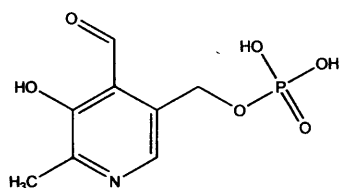
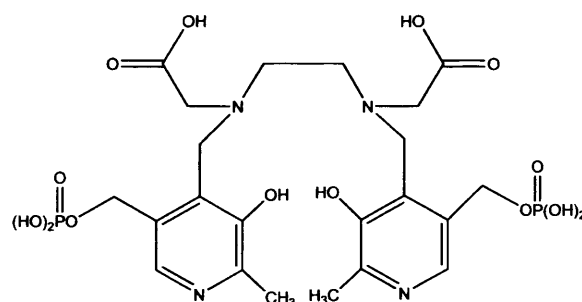


Figure 3:-Pyridoxal-5'-phosphate (PLP), co-enzyme for vitamin B₆

Mn–DPDP complex: Tesla Scan

The commercially available manganese based MRI contrast agent, Teslascan, is actually the manganese complex of DPDP, saltified with Na (I) (1:3). This is also known as mangafodipir trisodium. ‘Teslascan’ was considered useful for MRI diagnosis of pancreas, adenocarcinoma and pancreatitis¹. Mn-DPDP has a safety factor of **360** at the recommended clinical dosage (**0.005 mmol/kg**). Also the r_1 and r_2 relaxivities measured were $1.88 \text{ mM}^{-1}\text{s}^{-1}$ and $3.7 \text{ mM}^{-1}\text{s}^{-1}$ respectively (at 20 MHz and 37 °C). Mn-DPDP uptake preferentially been carried out by normal hepatocytes. Therefore the uptake mechanism was attributed to pyridoxine transporters in the early stages of investigation.¹⁸ It was later discovered however, that uptake of individual components of Mn-DPDP takes place through two different mechanisms. Further it was pointed out that uptake mechanism involved the release of manganese from the complex due to transmetallation with Zn (II). This is further justified by the stability constants of Mn-DPDP and Zn-DPDP ($10^{15.1}$ and $10^{18.95}$ respectively).



DPDP

Figure 4:- N, N'-Dipyridoxyethylenediamine-N, N'-diaceticacid-5,5'-Bis(phosphate), synthesized by Rocklage et al.

Challenges faced by Teslascan

Mn-DPDP, however, shows some instability *in vivo*. A recent biodistribution study proved that this complex dissociates and releases manganese which accumulates in liver, pancreas and kidneys, whereas the undissociated chelate is removed through glomerular filtration. The MRI properties of Mn-DPDP would therefore be ascribable mainly to the manganese ion released by the complex, which accumulates in the liver and pancreas. While Mn-DPDP is successful in imaging focal liver lesions, it has a limited ability to differentiate these lesions.

2.1.5.2 Complexation of Mn (II) with acyclic amino poly carboxylates

2.1.5.2.1 PDTA

There is one paper which states¹⁹ the longitudinal proton relaxation times in rabbit tissues after intravenous administration of MnCl₂ and of Mn-PDTA (1,3-propylenediamino-N, N', N'', N'''-tetraacetate) have been evaluated. They have observed a peak relaxivity of around 45 mM⁻¹s⁻¹ at 10 MHz and 37 °C for a low dosage (80 pmol/Kg) of MnCl₂. They have reported the similar values for Mn-PDTA for spleen (for the minimal up take of Mn (II)).

2.1.5.2.2 Backbone substituted EDTA analogues

Later the investigations were diverted towards EDTA, specifically EDTA bisamides. The investigations of EDTA analogues, however, preceded EDTA bisamides even though they were not precisely targeted towards MRI contrast agents. Following is the brief introduction to the synthesis of such EDTA analogues.

EDTA analogue from, 1-phenylglycinonitrile hydrochloride

The efforts have been concentrated in making analogues of EDTA as well. Sundberg *et al.*²⁰ described the synthesis of 1-(p-benzenediazonium)ethylenediaminetetraaceticacid, the coupling of this compound to proteins and the binding of radioactive metal ions to the protein-bound chelating groups. In their synthesis, 1-phenylglycinonitrile hydrochloride was converted to N,N'-diacetyl-1-phenylethylenediamine by catalytic hydrogenation. The aromatic ring of diamine was nitrated.

Potential Multimodal Imaging Agents

The resulting product was refluxed in mixed acetic acid-hydrochloric acid to yield diamine-4 and the Compound 4 was reacted with aminopolycarboxylic acid to yield 5, and the aromatic nitro group of 5 then was reduced to yield 6 (see Fig-5).

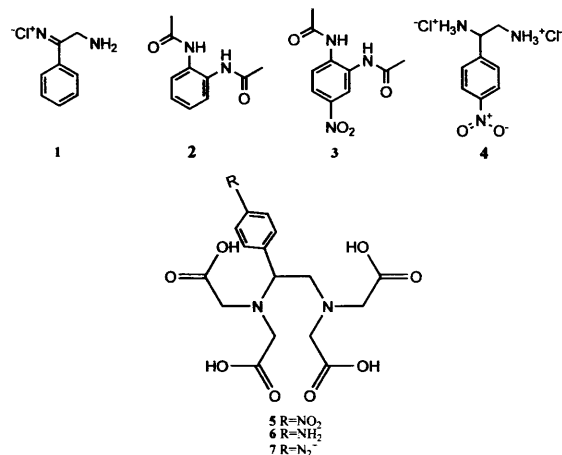


Figure 5:- Depicting the conversion of Product 4 to the EDTA analogue Synthesized by Sundberg *et al*

Bleomycin derivative: Another EDTA analogue

De Reimer *et al.*²¹ in 1979 along with his colleagues, utilised this strategy of making analogues of EDTA to produce bleomycin derivative (BLEDTA) containing a powerful metal-chelating group, which was radio labelled with In -111 to study its *in-vivo* distribution. Co(III)-bleomycin converted to its active form and alkylated with 1-(p-bromoacetamidophenyl) ethylenedinitrilotetraacetic acid. Upon fractionation BLEDTA was isolated (see Fig-6). In this approach they have ensured that the EDTA moiety in BLEDTA is free to coordinate with other metal ions.

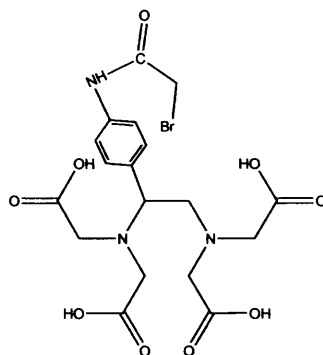


Figure 6:-1-(p-bromoacetamidophenyl) ethylenedinitrilotetraacetic acid specifically synthesized by De Reimer *et al.* to produce thermodynamically stable Bleomycin derivative.

EDTA analogue of IDAPr (3,4-HP)₂

M.A.Santos *et al.*²² reports the synthesis of Bis(3-hydroxy-4-pyridinone) - EDTA derivative which was targeted to chelate Al (III) to produce potential therapeutic Al- chelating agent.

In order to find a substitute for Desferrioxamine(DFB), which is commonly used as aluminium-decorating agent in the chelation therapy, Santos and his colleagues sort the help of bidentate ligands containing an alpha- hydroxy-acetone group, having high affinity for trivalent hard metal ions (eg- Fe (III) and Al (III)). They have initially found that 3-hydroxy-4-pyridinones (3,4HP) is the suitable candidate. Moreover unlike DFB, the compound found to possess very high stability under extreme biological conditions. The fact that, bidentate mono-hydroxy pyridinones, however, needs high clinical doses lead to the development of multidentate ligands, which could potentially increase the chelating efficacy and thus minimizing drug induced toxicity. Therefore they have produced a tetradentate derivative of Imino diacetic acid (IDA) by condensing two equivalents of 1-(3-aminopropyl)-3-benzyloxy-2-methyl-4-pyridinone with N-benzyliminodiacetic acid(activated via ethylchloroformate in THF), which was then flash chromatographed to afford the bis-hydroxypyridinone N,O-protected intermediate, IDABzPr(3,4-HPBz)₂. Upon deprotection imino-bis(acetyl(1-(3-aminopropyl)-3-hydroxy-2-methyl-4-pyridinone (IDAPr(3,4-HP)₂) was yielded.

Later in the following year, as they have found that the, hydrophilicity of the aforementioned derivative was not sufficient enough, Santos *et al.*²³ have prepared the ethylenediaminodiacetic acid analogue (see Fig-7). This was thought to possess higher potential for metal-complexation and eventual derivatization because of the two extra methyl carboxylic groups.

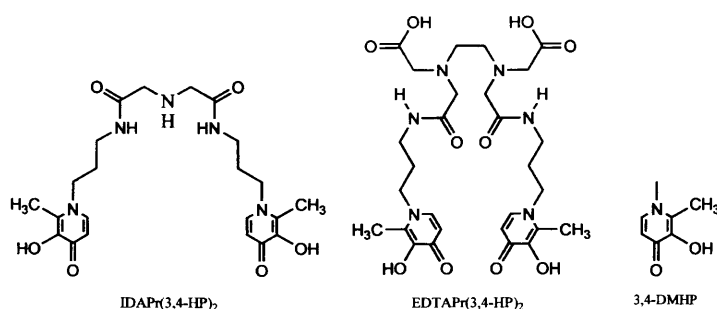


Figure 7:- Ethylenediaminodiacetic acid analogue of IDAPr (3, 4-HP)₂, synthesized by Santos *et al.*

2.1.5.2.3 *Synthesis of EDTA bisamides*

Among the acyclic poly amino carboxylates mentioned so far, EDTA stands out. This could be justified by the fact that it undergoes biodegradation readily when compared to PDTA. Further it has the most suitable chelating properties.²⁴ As such, combining these two (i.e. Mn and EDTA) to produce a synergistic effect, seems to be quite logical and this is exactly what the scientists carried out.

Moreover, efforts have been directed to design new ionic and neutral paramagnetic metal complexes which avoid or minimize the aforementioned disadvantages. In general, this goal can be achieved by converting one or more of the free carboxylic acid groups of the complexing agent to neutral, non-ionizable groups. Thus in the case of EDTA, one such approach is to synthesize derivatives of EDTA through amide formation. Talking about amide formation with EDTA, again various accounts of various methods of preparation of EDTA bisamides could be seen in the literature. What follows is a brief account of the literature review on various ways and means of synthesizing EDTA bisamides and their complexation with transition metal cations, specifically with Mn (II).

EDTA amides of X – Amine naphthalene sulfonic acid derivatives

A series of derivatives of *x*-Aminonaphthalene-*y*-sulfonic acid as EDTA bisamides have been prepared. Further their fluorescence behaviour towards transition metals has also been investigated, in which naphthalene moiety acted the role of fluorophore. Ortega *et al.*²⁵ had combined the advantageous aspects of both fluorosensing along with selective metal immobilization (via exploring the metal binding properties of EDTA). Initially, the four different resins (Argopore, Merrifield (4% DVB), Merrifield (1% DVB), and Wang-OH) were chlorinated to give each of their respected chlorinated forms. Subsequently these chlorinated resins were attached with corresponding alkyldiamines. After which these resins were reacted with EDTA bisanhydride in dimethylformamide. These resin derivatives were then treated with corresponding amine derivatives of naphthalene sulphonic acid.

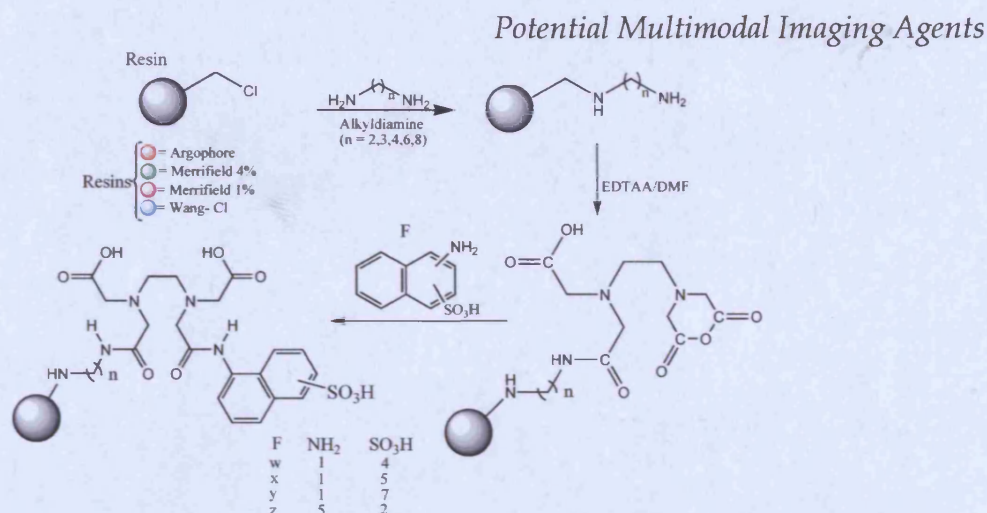


Figure 8:- Synthetic scheme for EDTA bisamides as resin derivatives, to be used as sensor material for the recognition, detection and measurement of different metal ions

EDTA bisamides of 5-Amino salicylic acid

Bagley *et al.*²⁶ have utilised 5-Aminosalicylic acid to prepare EDTA based bisamide. The conjugated ethylenediminetetraacetic acid bis-(5-aminosalicylic acid methyl ester) (5-EBAME) showed similar activity to super oxide dismutase (SOD). The synthetic procedure adapted to synthesize EBAME as follows. The EDTAA suspended in THF was refluxed with 5-amionsalicylic acid methyl ester and pyridine. The resulted precipitate was washed with ethanol. Precipitate was dissolved in hot water. The product was isolated after hot filtration and subsequent wash with acetone. Similar procedure was adapted to synthesize 4- EBAME as well.

EDTA based bisamides of aliphatic and aromatic amines

a) EDTA Based bisamides of aliphatic amine derivatives

A review of the literature indicated a few examples of preparation of EDTA bisamides. Although there are many examples for chelation of EDTA with lanthanides, relatively a few examples could be discovered on the coordination chemistry of EDTA functionalised derivatives. There were instances in the literature which indicates the incorporation of propyl amine²⁷, iso-propylamine, tert-butylamine,²⁸ and hydroxypropyl groups to EDTA backbone. In all of these, EDTA bisamides are produced by the amide groups which are both N-substituted by the respected alkyl amines. These alkyl amines were reacted with EDTAA in 1:2 stoichiometric ratios. These EDTA bisamides were subsequently complexed with suitable metal cations (such as Zn (II), Cu (II), etc).

b) EDTA based bisamides of aromatic amine derivatives

Literature review also revealed the synthesis of EDTA bisamides, prepared by the incorporation of 2 amino pyridine, aniline (EDTAPA and EDDADA respectively), through the reaction with EDTA bisanhydride (1:2 stoichiometric ratio) in 4-dimethyl amino pyridine (DMAP). Formic acid was used as a catalyst. Tanaka *et al.*²⁹ synthesized the aforementioned bisamides to investigate the thermodynamic properties (specifically enthalpy and entropy changes) of the EDTA derivatives. The observed differences between first and second protonation constants of the EDTAPA was mainly attributed to enthalpic term. They also observed that unlike EDTA, EDTAPA do not show any selective properties towards Co (II), Zn (II), Ni (II), Cd (II), Cu (II), and Pb (II) in water due to complete enthalpy – entropy compensation effect.

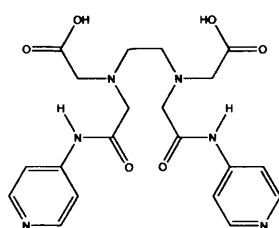


Figure 9:- Ethylenedinitrilo-N,N-diacetic-N,N-bis(2-pyridylacetamido) EDTAPA

Rami *et al.*³⁰ describes the synthesis of EDTA bisulfonamides through the incorporation of amino sulphonamides such as sulphanilamide **8**, metanilamide **9**, homosulfanilamide **10**, 4-aminoethyl-benzenesulfonamide **11** and 5-amino-1,3,4-thiadiazole-2-sulfonamide benzenesulfonamide **12** (see Fig-10) towards producing carbonic anhydrase inhibitors of the tumour-associated isoforms, through the complexation with Cu (II).

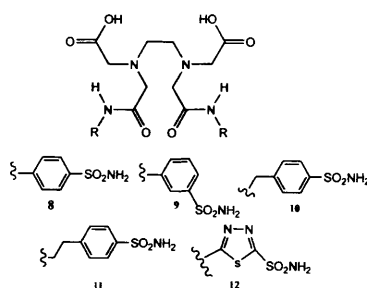


Figure 10:- Amino sulphonamides used in Carbonic anhydrase inhibitors

EDTA based bisamides of sulfathiazole, aniline and naphthalic acid

Guiry *et al.*³¹ prepared EDTA based bisamides of Sulfathiazole, 5-Amino naphthalic acid and 4-Hydroxyaniline EDTA bisamide, through more or less, similar procedure described by Rami *et al.* when conducting studies on polymorphism of paracetamol. The synthetic procedure undertaken as follows. EDTAA was reacted with 5-amionisothalic acid, triethylamine in DMF at room temperature. The crude product was stirred overnight in excess isopropyl alcohol. The removal of the solvents yielded the product. A similar procedure was adapted for the synthesis of other amides (see Fig-11).

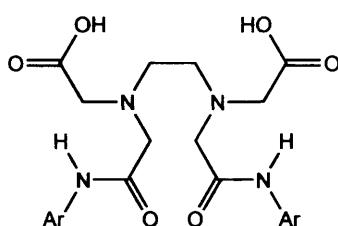


Figure 11:- Schematic representation of EDTA bisamides prepared by Guiry *et al.*,
ArNH₂: Sulfathiazole, 5-Amino naphthalic acid and 4-Hydroxyaniline

Macrocyclic EDTA based bisamides

Ki-young Choi *et al.*³² studied the metal ion binding properties of the macrocyclic EDTA based bisamide. The preparation of 4,10,13-Tris(carboxymethyl)-8,15-dioxo-1,4,7,10,13-pentacyclopentadecane (EDTA-DAM) was achieved first synthesizing 10,13-Bis(carboxymethyl)-8,15-dioxo-1,4,7,10,13-pentaazacyclopentadecane(EDTA-DET) through the cyclization of EDTA bis(anhydride) and diethylenetriamine in DMSO/1,5-diazobicyclo[4.3.0]nonene(DBN) solvent medium. This was then alkylated with t-butyl bromoacetate in diisopropylethylamine, thereafter it was deprotected to yield EDTA-DAM. They have discovered that the copper complexes of EDTA bisamides possess higher stability constants than their lanthanide counter parts, owing to the matching capabilities of the ligand cavity size and also could be the result of ionic radi of Cu (II).

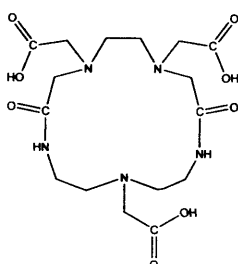


Figure 12:- Macro cyclic EDTA bisamide prepared by Choi *et al.*

2.1.5.2.4 *Intrinsic stability of Manganese complexes*

Most of the manganese complexes known until now are relatively unstable *in-vivo*. There is an extensive research has been carried out in the past to understand the extent and the vigour of toxicological effects of manganese complexes *in-vivo*, which revealed the potential harm caused by these manganese complexes.³³ The intrinsic stability of manganese complexes is on the lower side, when compared to lanthanides. This in fact predominantly contributes to the challenges faced by the manganese complex, on its way towards a successful contrast agent.

These challenges could be viewed from two perspectives. Firstly, from the manganese perspective, it is the challenge about the transmetallation. So as to say it could be displaced from the complex by other divalent cations like Ca (II), Mg (II), and Zn (II). From the ligand perspective, unlike gadolinium, manganese is an essential nutrient for mammals and some organisms have developed special carrier systems and cellular uptake mechanisms,³⁴ indicating the potential competitor threat, which could be faced by the ligand (when it's dissociates from the complex due to low stability of the complex) by the endogenous chelators. As a result there is a great concern about the potential harmful effects for the human body has been widely studied, The study reveals that the free Manganese could cause tetragenic effects, which in fact had been proved in the case of Mn-DPDP.³⁵⁻³⁶ Further problems relating to chronic exposure to manganese are well documented. The severe disorder caused in the central nervous system has also been accounted. A recent study reveals the accumulation of free manganese from the potential contrast agent in the brain of mice and the harmful effects incurred.

Mn complex of the EDTA based derivative bearing diphenylcyclohexyl moiety (MnL1)

In contrast, Lauffer *et al.*³⁷ had stated in his research in 1987, that Mn (II) bound to proteins could produce extremely large relaxivities (for eg 275mM-1s-1) and for Mn(II)-pyruvate kinase; 96mM⁻¹s⁻¹ for Mn (II)-concanavlin A, which are slow tumbling compounds.

In the very recent past, the details obtained from the fact that $[\text{Mn}(\text{EDTA})(\text{H}_2\text{O})]^{2-}$ could be a good starting point to synthesize a contrast agent, attracted Troughton and colleagues to synthesize a high relaxivity manganese based contrast agent.

Starting from L-serinamide hydrochloride, through a five step synthesis they have obtained the protected form of the (R)-({2-(Bis-*tert*-butoxycarbonylmethyl-amino)-1-[(4,4-diphenyl-cyclohexyloxy)-hydroxy-phosphoryloxymethyl]-ethyl-*tert*-butoxycarbonylmethyl-amino)-acetic acid *tert*-butylester *t*-butyl protection was removed by using the mixture of HCl/MeCN to obtain the pure ligand, which then complexed with manganese chloride under acidic condition.

A diphenylcyclohexyl moiety, as used in the MS-325 was then linked to the EDTA derivative through a phosphodiester bond which is then conjugated to serum albumin in the blood (see Fig-13).

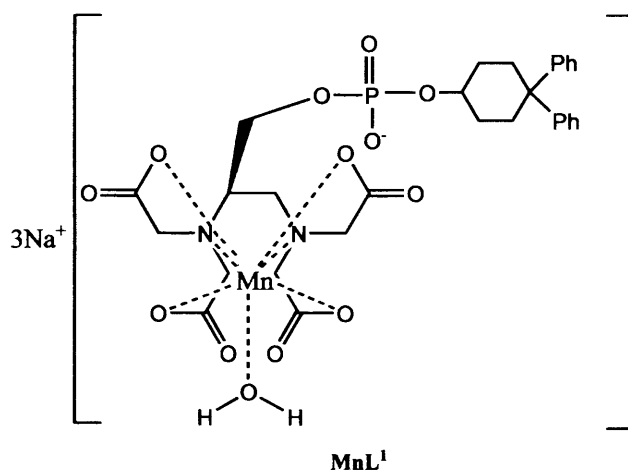


Figure 13:- Mn complex of the EDTA based derivative synthesized by Troughton *et al.*

The usage of a binding group has the advantage to provide means for targeting blood vessels, which will reduce T_1 due to the reduction in the tumbling rate. This will significantly enhance relaxativity.³⁸

Mn-EDTA-DDP

Although Mn-EDTA and some of its derivatives acted as good liver imaging agents, they could not be considered as blood pool imaging agents or, to image bone marrow and spleen. Under these circumstances Mn derivatives of liposome proved to be successful MR contrast agents and are effective in imaging the blood pool, liver, spleen and bone marrow and also it

has been proved that when they are smaller in size (i.e <50nm) they responded more effectively.

In a recent study, MRI contrast agents were evaluated consisting of Mn-EDTA lipophilic derivatives (for example, Mn-EDTA-DDP) bound to the membranes of small unilamellar liposomes ("memosomes"), which are potentially valuable for hepatic and cardiac perfusion imaging. Taking these facts into consideration Unger *et al.*^{39,40} in their patented research reports the synthesis of Mn-EDTA-DDP, Mn-EDTA-LDP, Mn-EDTA-ODP ((DDP: Carboxy-decylamidomethyl-N-2,3-dihydroxypropyl)-ethylenediamine-N,N'-diacetate, LDP: N,N'-Bis-(Carboxy-laurylamidomethyl-N-2,3-dihydroxypropyl)-ethylenediamine-N,N'-diacetate, ODP: N,N'-Bis(Carboxy-octadecylamidomethylene-N-1,2-dihydroxypropyl)-ethylenediamine-N,N'- diacetate. The synthetic procedure involved in Mn-EDTA-DDP as follows. They initially synthesized DDP, by refluxing decylamine with glycidol in methanol. Product was purified by recrystallisation. Purified DDP was then reacted with EDTAA in methanol, applying slight heat. The removal of solvent yielded the product. A similar procedure was adapted to synthesize EDTA derivatives of LDP and ODP. These ligands were subsequently complexed with Mn (II).

These chelates or, more preferably, in combination with lipids or liposomes, are reportedly particularly useful. These kind of chelated complexes have been reported in number of other patents as well. Interruption of alkylene chain by one or more substituents selected from O, S, CHOH, CHSH, are stated to be particularly useful for imaging of liver, kidneys, pancreas and gastrointestinal tract.

EDTA based bisamides from blood proteins

Differing from the above approaches, Lauffer *et al.* prepared EDTA amides through the conjugation of proteins such as Bovine Immunoglobulin (IgG) and Bovine Serum Albumin in an attempt to produce enhanced paramagnetic based contrast agent which could have enhanced relaxivity.⁴¹ Bovine Immunoglobulin (IgG) and Bovine Serum Albumin were multiply labelled with EDTA. Mn (II) was inserted in to the binary conjugate to form ternary

conjugate (i.e. protein-ligand-metal ion). Measured relaxivities revealed the dramatic difference in relaxivity of ternary conjugates from that of binary conjugate (5-10 fold increase in relaxivity in the 10-40 MHz field range). Synthetic procedure adapted could be briefed as follows. Protein was reacted with large excess of EDTAA according the procedure of Hnatowich *et al.* Thereafter reaction mixture was dialyzed.

2.1.5.3 Utilising Bifunctional Chelates

Ligands that were bearing a second functional group, which will enable the ligand to covalently attach to a targeting moiety is becoming more popular. These are known as 'bifunctional chelates'.⁴² The functional groups commonly found in the chelates are electrophiles, which will react with nucleophilic groups of the targeting vector.

Further this takes place under mild conditions. The pioneers of bifunctional chelates are the polyamino poly carboxylates or complexones. In 'complexones' one or more of the carboxylate group is activated to react with an amine group. More over, in the case of amides they only coordinate quite readily with transition metal cations (such as Mn^{2+} , Cu^{2+} , Zn^{2+} , Cr^{2+} and/or lanthanide metal ions (such as Gd^{3+} , Eu^{3+} , Yb^{3+}). This coordination will not result in the change of denticity (i.e. EDTA based bisamides remains as Hexadentate and most commonly for DTPA based bisamides as Octadentate), It does affect, however, the overall charge of the complex and the electron density on the metal ion.⁴³ Depending upon application, these features may or may not be detrimental. Although there were extensive physical studies undertaken to investigate the physical properties of the parent EDTA and DTPA complexes, the bifunctional ligands have been put up in low profile.

So far the investigations have clearly outlined that small variations in the structure could result in widely differing properties. This thesis is concerned about the synthesis of contrast agents, which will have the fluorescence capability; a special attention has been given to incorporate precursors having both amine functional group and the chromophoric moieties, with the EDTA bisanhydride. We have successfully incorporated precursors, such as amino

anthraquinone and amine functionalised naphtha derivative, which will be dealt in detail in the proceeding sections.

2.2 Results and Discussion

2.2.1 Ligand Design and Synthesis

It may be obvious from Section 2.1, in order to produce a novel dual purpose contrast agent which could be utilised in MRI and/or PET requires a chromophore to be part of the desired bifunctional ligand.⁴⁴ Therefore our first objective is to find the precursor which has an inherent chromophore in itself.

Since naphthalene moiety has the inherent conjugation, it was thought to incorporate N-(2-aminoethyl)-1,8-naphthalimide. This is because 1,8-naphthalimides are well known for their strong absorption and remarkable fluorescence yields.⁴⁵ They are also known for their anticancer activity.

Synthesis of N-(2-Aminoethyl)-1, 8-naphthalimide

The procedure reported by Licchelli *et al.*⁴⁶ was employed with slight modification. 1,8 naphthalic anhydride was added portion wise, to a stirring large excess (10 times) of ethylene diamine. The reaction mixture was refluxed overnight. Thereafter, excess ethylene diamine was removed by distillation. The crude product was washed several times with diethyl ether. To yield the product as pale yellow precipitate.

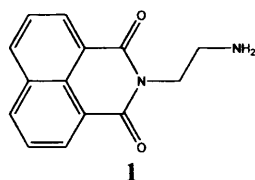


Figure 1:- N-(2-Aminoethyl)-1, 8-naphthalimide

The product was sufficiently pure enough (a trace amount of dimer was also visible in the proton NMR spectrum) to be carried on to the next step.

Having identified and synthesized the chromophoric moiety for a hexa coordinate ligand, our next objective is to synthesize the EDTA bisanhydride, which is then prepared according to a literature procedure⁴⁶ (see Fig-2).

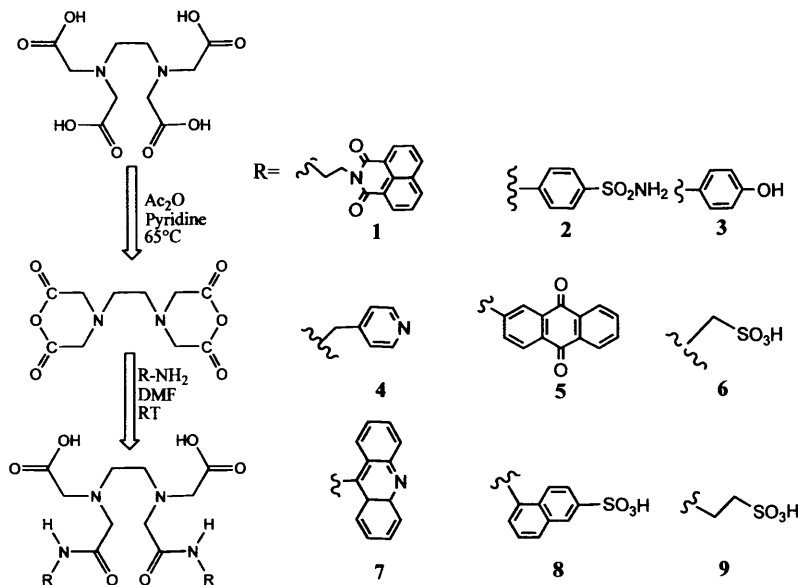


Figure 2:- depicting the synthetic pathway for the synthesis of EDTA bisamides

2.2.1.1 Synthesis of EDTA bis amide of N-(2-Aminoethyl)-1, 8-naphthalimide (L¹)

Initially it was decided to synthesize L¹ (see Fig-3) in dichloromethane by reacting EDTAA with **1** in 1:2 stoichiometric ratio. The ¹H NMR spectrum of the crude product, however, indicated the presence of mixture of mono and bis amides. Therefore it was decided to change the reaction media to acetonitrile.

Once again the reaction ended up in a mixture of amides rather than the expected pure bisamide. Purification through recrystallisation in methanol, toluene, and ethanol also failed. Further, thin layer chromatography also proved futile (in spite of the usage of various combinations of DCM/Methanol). This has prevented the possibility for column chromatography.

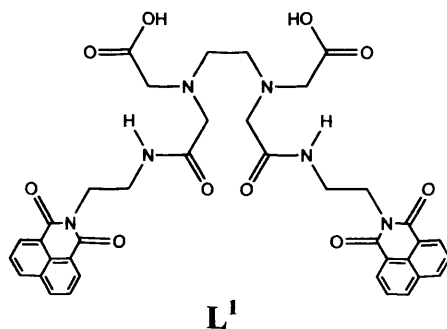


Figure 3:- EDTA bisamide of N-(2-Aminoethyl)-1, 8-naphthalimide

2.2.1.2 Synthesis of EDTA bisamide of sulphonamide (L^2)

This continuous failure prompted us to investigate other procedures highlighted by our literature search. At this point, we came across the procedure of making EDTA bisamides reported by Rami *et al.*³⁰ We were not successful in synthesizing L^2 according to the procedure. The method was modified by mixing solutions of the EDTA bisanhydride and the respective sulphonamide precursor in a small amount of DMF, at room temperature giving rise to a mixture of mono and bis amides (determined by ^1H NMR spectroscopy).

A successful outcome was achieved by slow (dropwise) addition of the sulphonamide solution to a solution of the EDTAA. The product was obtained as an off white, free flowing powder. Yield was 35%. The crude product was further washed with acetone and subsequently with acetonitrile. In the ^1H NMR spectrum, a singlet resonance was observed for the methylene protons indicating the two fold symmetry of the desired bisamide.

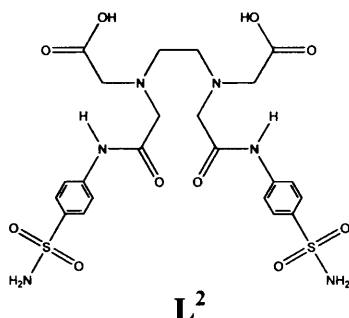


Figure 4:- EDTA bisulphonamide

2.2.1.3 Synthesis of EDTA bisamide of Para Aminophenol (L^3)

This was prepared according to a synthetic procedure reported by Guiry *et al.*² the procedure could be summarised as follows. To a mixture comprising of EDTAA and triethylamine in DMF was added 4-amino phenol portion wise. The reaction was then allowed to stir for 24 h at room temperature. Then the solvent was removed. Thereafter isopropyl alcohol was added to the dark brown crude product and allowed to stir for 72 h. After which, the product was obtained by filtration and the precipitate was dried.

It was discovered that by allowing the reaction mixture to stir for more than 72 h in IPA (96 h), noticeable improvement was observed in the purity of the final product. This could be

attributed to the complete removal of impurities from the ligand by the IPA. The hydroxyl group in the L^3 (see Fig-5) could provide the site for conjugation with micro spheres.⁴⁷

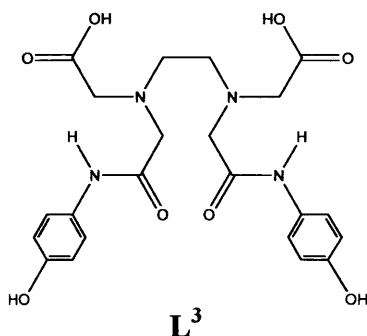


Figure 5:- EDTA bisamide of 4-amino phenol

2.2.1.4 Preparation of four new EDTA bis amides and some challenges faced therein

EDTA bisamides of N-(2-Aminoethyl)-1, 8-naphthalimide (L^6) and amino methyl pyridine (L^4)

The above described modified procedure was used to prepare EDTA bisamide of N-(2-Aminoethyl)-1, 8-naphthalimide (L^1) (see Fig-2) and EDTA bisamides of amino methyl pyridine (L^4). It is interesting to note, similar to our ligand L^4 , Tanaka *et al.* reports a synthesis of ethylenedinitrilo-N, N'-diacetic-N, N'-bis (2-pyridylacetamido) acid (EDTAPA) (see Fig-6) through the incorporation of 2-aminopyridine to EDTA bisanhydride in 1:2 molar ratio. They have used dichloromethane as a solvent instead of DMF. Additionally they have used DMAP (as base) and formic acid (as catalyst). Further, it was noted that EDTAPA is sparingly soluble in cold water and is readily recrystallised from hot water, whereas L^4 is more freely water soluble.

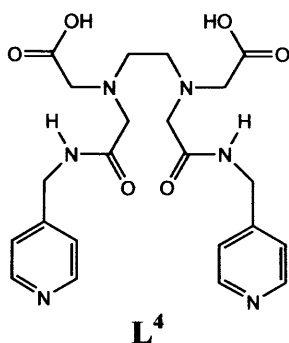


Figure 6:- EDTA bisamide of 4-amino methyl pyridine

NMR Spectroscopy (^1H and ^{13}C)

In L^1 , due to the symmetric nature of the ligand, one would expect 6 peaks to be visible in the ^1H NMR spectrum, which was clearly visible in the spectrum, except for two solvent peaks, a broad singlet in 4.7 ppm, which was assigned as water peak. Other than this there is only one peak visible which could not be assigned to any protons in the structure of L^1 , as this appears in 1.9ppm with the negligible integral, it has been assigned as methyl proton of acetone, which normally appears around 2 ppm in D_2O , and except for these two solvent peaks the proton NMR spectrum indicated a very pure ligand. ^{13}C NMR spectrum of the same ligand indicated 8 peaks which were assigned to the carbons in the structure.

EDTA bisamide of Amino Anthraquinone (L^5)

In the case of L^5 (see Fig-7) also, the modified procedure described for L^4 was followed. At the work up, however, addition of dichloromethane did not yield the precipitate. Therefore it was decided to evaporate the filtrate and analyse the crude product. The proton NMR spectrum indicated the presence of the product along with excess starting material, namely 2-aminoanthraquinone.

Further, purification was attempted with methanol and ethanol wash; however impure product was still observed. At this point it was decided to wash the crude product with dichloromethane. The proton NMR spectrum of the washings indicated the presence of 2-aminoanthraquinone, while the proton NMR spectrum of the undissolved solid indicated the presence of the product along with small amount of starting material. Repeated washings with dichloromethane yielded a substantially pure product, good enough for characterisation and further use. The product (dark brown glassy material) was characterised by proton NMR spectrum. In the ^1H NMR spectrum a trace amount of starting material was visible. The broad singlets at 6.7 ppm, 6.9 ppm & 7.3 ppm were assigned to protons of aminoanthraquinone, while the proton NMR spectrum of the washings indicated the 2 amino anthraquinone, the starting material.

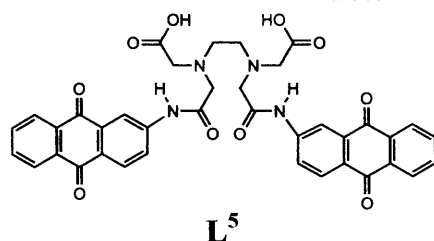


Figure 7:- EDTA bisamide of 2-amino anthraquinone

EDTA bisamide of Amino Methyl Sulphonic Acid (L⁶)

The modified procedure of **L⁴** was attempted for **L⁶** (see Fig-8) EDTAA was mixed with Amino methyl sulphonic acid **2** (see Figure-9). The reaction mixture was allowed to stir overnight. A distinct colour change was observed (dark brown solution turned to dark ash coloured solution).

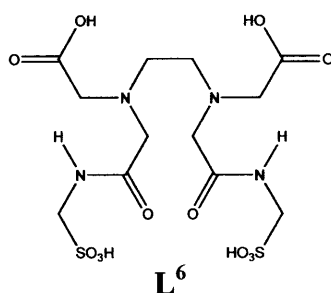


Figure 8:- EDTA bisamide of amino methyl sulphonic acid

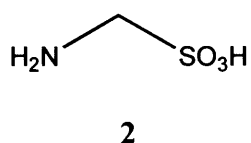


Figure 9:- Amino methyl sulphonic acid

The ¹H NMR spectrum of the crude product exhibited peaks of EDTA as well as peaks due to excess amino methyl sulphonic acid. Failure of this attempt diverted our attention towards an alternate approach. Inonue *et al.*⁴⁸ reported a procedure to synthesize diester derivatives from dioxotetraazacycloalkane diacetic acid. The procedure is summarised as follows.

The 12edtaen **3** (see Fig-10) was suspended in DMF. To which added pulverized KHCO₃ and subsequently added ethyl iodide. The reaction mixture was stirred for 20 h at room temperature. To the resulting solution, water was added and the product was extracted, initially with dichloromethane and subsequently washed with sodium sulphite and water. The removal of the solvent yielded the product as colourless solid.

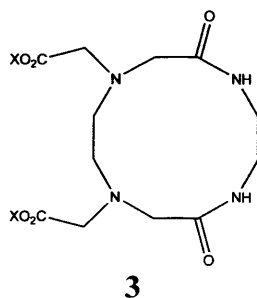


Figure 10:- X:H -12edtaen-H₂ and X-C₂H₅ : 12edtaen-des

It was expected that adapting the procedure of long chain alkylation to alkylate the L⁶ will enable the alkylated product to be extracted into the organic layer during solvent extraction, while retaining the impurity in the aqueous layer facilitating removal of the starting materials (Amino methyl sulphonic acid).

We have adapted this procedure and used iodoheptane instead of iodoethane, (See Fig-6). After the work up, ¹H NMR spectrum of the final product indicated a prominent peak corresponding to methine proton of the amino methyl sulphonic acid and the peak related to heptyl group was not visible. Thereafter the same reaction was carried out with iodobutane, in order to facilitate alkylation with less steric hindrance. ¹H NMR spectrum once again revealed the attempt was futile, as a huge peak corresponding to methine proton of the amino methyl sulphonic acid is visible. Reaction was repeated from potassium carbonate to cesium carbonate. The cesium carbonate was powdered in order to effectively neutralise the HI formed in the reaction. Expected improvement could not be observed in the proton NMR spectrum.

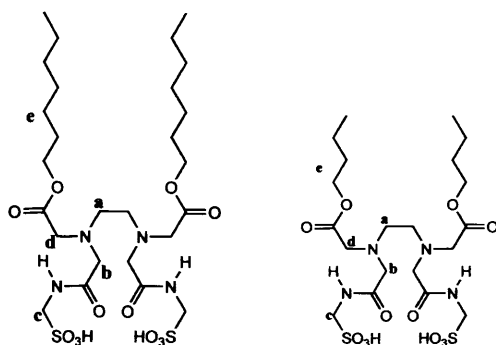


Figure 11:- Depicting the expected, esterified EDTA mono spacer

At this point we came across a synthetic procedure for DTPA bisamide of para amino benzoic acid, reported by Liu *et al.*⁴⁹ They mixed DTPAA with para amino benzoic acid in water at 273 K for 4 h and then allowed the reaction to stir for a further 24 h at room temperature.

Thereafter, when the pH was adjusted to 3-4, a great deal of precipitate appeared. The precipitate was filtered and recrystallised with hot methanol.

The aforementioned procedure was adapted to synthesize EDTA bisamide of amino methyl sulphonic acid. Upon adjustment of pH, however, only a negligible amount of precipitate was formed. It was then decided to evaporate the reaction mixture to dryness. The proton NMR spectrum was obtained. The proton NMR spectrum indicated the presence of expected product along with large excess of starting material (i.e. amino methyl sulphonic acid). After which the solid was dissolved in hot methanol. The proton NMR spectrum of the undissolved solid indicated the presence of substantially pure product, which could be utilised in subsequent synthetic steps.

Although we were successful in making the reaction to go to completion, however, the purity of the ligand and the yield was comparatively low in comparison to other aforementioned bisamides. It was found that the purity and yield of the reaction was highly dependent on the quality of the EDTAA starting material.

Despite a similar melting point and NMR data, when the EDTAA was prepared using distilled acetic anhydride and distilled diethyl ether under nitrogen atmosphere throughout the preparation, a better yield (95%) could be obtained with substantial increase in purity (compared to the previous yield of 80%).

2.2.1.5 Attempted Synthesis of some Chromophore bearing EDTA bisamides

EDTA bisamide of Amino Acridine (L⁷)

In line with the modified procedure used to prepare L¹, L⁴ and L⁵, initially decided to react 9-amino acridine with EDTAA. As the reagent was supplied as the HCl salt, first the ligand was deprotonated. The supplied reagent (9-amino acridine hydrochloride) was initially suspended in water, after which 2-3 pellets of NaOH was added and observed the formation of deprotonated aminoacridine as precipitate in the solution. The solution was extracted with dichloromethane (the problem of partial insolubility of the precipitate in dichloromethane was overcome by the addition of small amount of toluene and acetone). The deprotonation yielded

a pure activated form of 9-amino acridine (see Fig-12). The proton NMR spectrum clearly indicated the proton of the free amine along with the expected peaks.

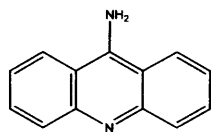


Figure 12:- Deprotonated Amino acridine

This deprotonated 9-amino acridine had been utilised to produce the EDTA bisamide of 9-amino acridine (see Fig-13). In the proton NMR spectrum of L^7 , one would expect to see 7 peaks comprising, four peaks related to aromatic hydrogens (two triplets and two doublets) and three peaks contributed by the aliphatic hydrogens (three singlets belong to the acid, amide protons and methylene protons of the ethylene diamine backbone). While the expected peaks were present and the integrals related to aromatic peaks and the NH peak indicated 4H each, integrals of the two aliphatic peaks also related to 4H each. The integral of the peak, however, assigned to methylene proton of ethylene diamine backbone indicated an unusual 8H. This has made the purity of the ligand in question.

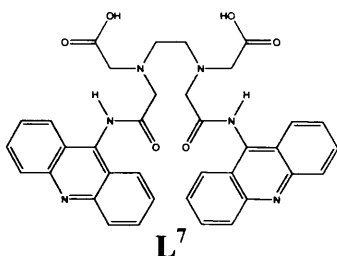


Figure 13: - EDTA bisamide of deprotonated 9-amino acridine

Solubility problems of 5-aminonaphthalene-2-sulphonic acid (L^8)

The modified procedure used for L^4 was employed in the synthesis of L^8 as well. It was observed, however, that 5-amino naphthalene-2-sulphonic acid was sparingly soluble in DMF. This has resulted in incomplete transfer (both via cannula and syringe transfers) of the 5-amino naphthalene-2-sulphonic acid to EDTAA. The proton NMR spectrum of the precipitate indicated the presence of a mixture of mono and bis amides.

Therefore, in order to facilitate solubility, the partially dissolved 5-amino naphthalene-2-sulphonic acid was slightly heated and then subsequently it was transferred effectively to the EDTAA. The proton NMR spectrum of the purified precipitate indicated the product;

however the peaks could not be assigned properly. All of the six peaks belong to the naphthalene sulphonic acid was identified with the considerable down field shift in the proton NMR, when compared to the starting material (i.e 5-amino-naphthalene sulphonic acid). The three singlets related to methylene hydrogen of ethylene diamine backbone, methylene hydrogens attached to the amide arm and methylene hydrogen attach to carboxylic arm also identified (with the help of the correlating the integrals of the respected peaks along with the aromatic peaks). There were extra three singlets, however, noted in the region of 3.5 ppm - 3.65 ppm, which could not be assigned reasonably to any protons. The amide stretching vibration, however, was noted in the IR (1645 cm^{-1}).

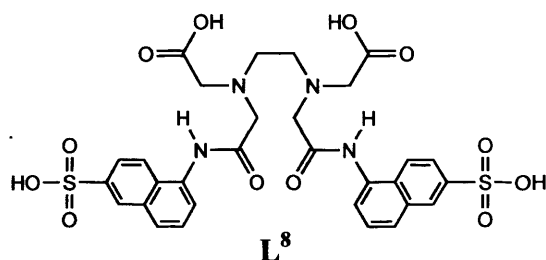


Figure 14: - EDTA bisamide of 5-amino naphthalene-2-sulphonic acid

Attempted synthesis of the EDTA bisamide of Taurine (L⁹)

Following the successful synthesis of **L⁶**, the Taurine derivative of EDTA was synthesized. Initially the same procedure described for **L⁶** was carried out. The proton NMR spectrum, however, indicated the presence of EDTA and excess taurine along with the expected product. Recrystallisation in methanol and ethanol failed. Thereafter the reaction was repeated with the addition of 2.5 times of base (to activate taurine). The solvent was removed. The proton NMR spectrum of the solid indicated the presence of product along with excess taurine as well as EDTA.

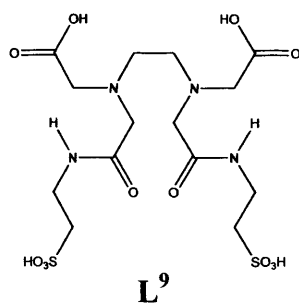


Figure 15:- EDTA bisamide of taurine

2.2.2 Complexation with Transition Metal Ions

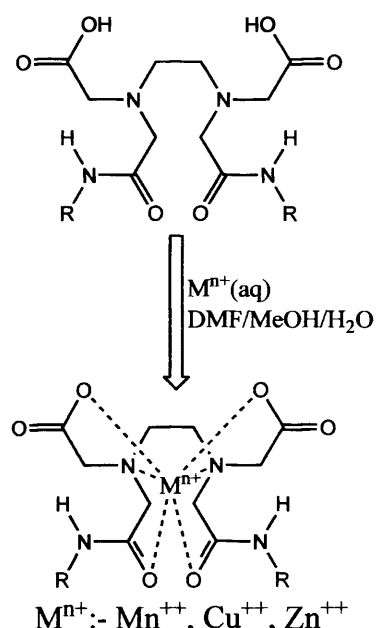


Figure 16:- Schematic representation of the complex formation of Bisamides, where R: auxiliary groups

2.2.2.1 Characterisation of EDTA bisamides

The initial ^1H NMR spectrum exhibited solvent peaks for L^2 and L^3 , which was attributed to solvent peaks related to DMF, triethylamine and water and acetone respectively. ^{13}C NMR spectra were not obtained as they are known ligands.

IR Spectroscopy

Tabulated values exhibited in Table 1 indicate the common trend of amide stretching vibrations exhibited by these amides. It could be seen that values lies in the range of $1633\text{-}1674\text{ cm}^{-1}$ which lies within commonly observed range of $1630\text{-}1695\text{ cm}^{-1}$, indicating the validity of the findings.⁵⁰

Table 1: IR Stretching Frequencies of EDTA bisamides and their complexes

Compound	$\nu(\text{C}=\text{O})$ Amide	$\nu(\text{O}-\text{H})$	$\nu(\text{C}=\text{O})$ -Acid	$\nu(\text{C}=\text{O})$ amide of EDTA bis amide complexes		
				Mn(II)	Zn (II)	Cu(II)
L^1	1674(s)	3435(br)	-	1607(vs)	1632(s)	1625(s)
L^2	1672(s)	3411(br)	-	1634(s)	1635(s)	-
L^3	1633(s)	3272(br)	-	-	-	-
L^4	1666(s)	3438(br)	1712(w)	1638(br)	1632(vs)	1638(s)
L^5	1673(s)	3440(br)	1710(w)	1653(w)	1624(w)	1618(w)
L^6	1636(s)	3443(br)	-	1641(s)	1640(s)	-
L^7	1643(s)	3423(br)	-	-	1638(s)	-
L^8	1645(s)	3441(br)	1722(m)	1636(s)	1636(s)	-

^a IR spectra measured using KBr discs.

2.2.2.2 Complexation with Transition metal cations.

For the purpose of complexation along with the targeted Mn (II) ion, two more cations, specifically Cu (II) and Zn (II) ions were selected. Each of these selections was on accord of two fold objectives. Firstly, Cu (II) and Zn (II) are endogenous cations, thus representing the physiological environment. Secondly, Cu (II) also has the potential to be used in PET imaging (as its isotope- ^{64}Cu) and Zn (II) also could facilitate characterisation through proton NMR spectroscopy, due to its diamagnetism.

^1H NMR spectroscopic characterisation

^1H NMR spectrum of the Zn complexes of L^1 - L^7 , all exhibited the expected down field shift in their proton NMR spectra. It was also observed a characteristic duplication of peaks. This may be attributed to the isomers produced in the NMR solution due to donor exchange by the metal. The ^1H NMR spectra of the Cu (II) complexes of L^1 and L^4 (CuL^1 and CuL^4) and also the Mn (II) complexes of L^3 (MnL^3) and L^5 (MnL^5) could not be obtained as these metal ions exhibit paramagnetism due to unpaired electron(s) in their d orbital.

Infrared spectroscopic characterisation

It could be observed from Table 1 (see Figure-17), carbonyl stretching vibrations of the amide group shifting to lower values. For instance, amide stretching vibration of the EDTA bisulphonamide (L^2) has shifted from 1672 cm^{-1} to 1635 cm^{-1} in ZnL^3 . This kind of significant red shift could be attributed to the weakening of C=O bond upon complexation, indicating the amide oxygen coordination to the transition metal ion. Similar to Zn (II) complexes, the shifting of amide stretching vibrations to lower values for CuL^1 and CuL^5 could be observed. MnL^3 also exhibited a similar shift to the lower value. Shifting to lower energy, however was not observed in the case of MnL^6 and ZnL^6 , this may be attributed to the weakly coordinating amide oxygen. Further, IR spectra of complexes, specifically, MnL^3 , ZnL^3 , CuL^1 and CuL^6 exhibited broad peak around 3200 cm^{-1} - 3400 cm^{-1} . This could be attributed to the presence of water in complexes.⁵¹

Characterisation through Mass Spectrometry

High resolution mass spectra were obtained for L¹, L⁴ and L⁵. In the case of L⁶ only low resolution mass spectral data could be obtained. Data for L² and L³ were not obtained as they are known ligands. All the ligands exhibited protonated molecular ion.

2.3 Experimental Section

Experimental

General Experimental:

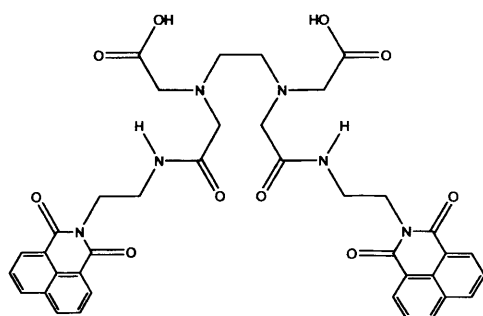
Reagents were obtained from commercial sources and used as received unless otherwise noted. Solvents were dried and purified under N₂ by using standard methods and were distilled immediately before use, specifically dimethylformamide and pyridine was distilled using anhydrous calcium hydride. All compounds were prepared under N₂ unless otherwise mentioned. The NMR spectra were obtained using a Bruker ARX 400 at 20 °C in CDCl₃ unless otherwise noted. Mass spectra were performed on a micro mass Platform II system operating in Flow Injection Analysis mode with the electro spray method. Infrared spectra were recorded with a JASCO FTIR-410 spectrometer between 4000 and 250 cm⁻¹ as KBr pellets. UV/Vis spectra were recorded with a JASCO V-570 spectrometer.

Synthesis of EDTA bisanhydride

EDTA (5.0 g, 17 mmol) was suspended in pyridine (8 mL) and acetic anhydride (7.0 g, 68 mmol) was added dropwise to the stirring solution. The reaction mixture was allowed to stir for 24 h at 65 °C. The resulting anhydride was filtered off and washed thoroughly with freshly distilled acetic anhydride and dry diethylether. The white-cream powder was then dried under vacuum until constant weight was obtained. The product was characterised by infrared spectroscopy and measuring its melting point. Yield 4.2 g, 96%. IR (KBr disc) (cm⁻¹): 3445(br), 1810(vs), 1760(s), 1130(s); Melting point: 189-191 °C.

2.3.1 Synthesis of EDTA bisamides

2.3.1.1 Synthesis of EDTA bisamide of N-(2-Aminoethyl)-1,8-naphthalimide (L^1)



The procedure was similar to that of L^1 . To EDTA bisanhydride (0.308 g, 1.20 mmol) dissolved in dimethylformamide (10 ml) was added N-(2-Aminoethyl)-1,8-naphthalimide **1** (0.579 g, 2.40 mmol) dissolved in dimethylformamide (10 ml) dropwise. After the complete addition, the reaction mixture was allowed to stir over night at room temperature. Thereafter dichloromethane (50 ml) was added to the reaction mixture, upon which the precipitate was formed. The precipitate was filtered and washed initially with acetone and subsequently with acetonitrile. Yield 0.38 g, 45%; ^1H NMR (400 MHz, d_6 -DMSO: Me_4Si): δ_{H} (ppm) 10.00 (s, 2H, NH), 8.35 (dd, 4H, $J = 7.75, 14.16$ Hz, ArH), 8.15 (s, 1H, NH), 7.75 (t, 2H, $J = 7.71$ Hz, ArH), 7.50 (m, 2H, NCH_2), 3.4 (s, 2H, NCH_2COOH), 3.3 (m, 2H, NCH_2CH_2), 3.1 (s, 2H, NCH_2CONH), 2.6 (s, 2H, $\text{NCH}_2\text{CH}_2\text{N}$); ^{13}C NMR (400 MHz, D_2O): δ_{C} 173.00, 171.23, 163.95, 134.40, 131.47, 130.85, 127.67, 127.38, 122.36, 57.63, 55.35, 52.26, 37.08; IR (KBr disc) (cm^{-1}): 3435(br), 1674(s), 1590(s).

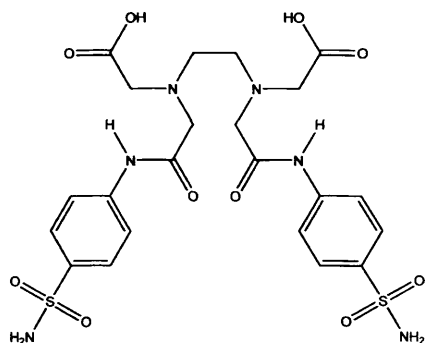
2.3.1.1.1 Complexation of L^1 with MnCl_2 (MnL^1)

L^1 (0.0736 g, 0.1 mmol) was dissolved in dimethylformamide and MnCl_2 (0.01258 g, 0.1 mmol) was dissolved in minimum amount of distilled water. The solution of the ligand was added drop wise to the solution of the salt and allowed to stir for 20 min. Then the solvent was removed under vacuum, and the residue was washed with acetone and chloroform several times.

Complexation of L^1 with ZnCl_2 (ZnL^1), Complexation of L^1 with CuCl_2 (CuL^1), was also carried out as per the procedure outlined for MnL^1 . In the preparation of CuL^1 , however,

the ligand was dissolved in ethanol instead of dimethylformamide. $[\text{Zn}^{\text{II}}(\text{L}^1)]\text{Cl}_2$: Yellow precipitate (90% yield). ^1H NMR (400 MHz; D_2O): 8.45 (m, 4H), 8.00 (m, 4H), 7.80 (m, 4H), 3.55 (s, 2H), 3.40 (s, 2H), 3.15 (s, 2H), 3.05 (s, 2H), 3.00 (s, 4H), 2.90 (s, 2H), 2.70 (s, 2H); IR (KBr pellet, cm^{-1}): 3434(br), 1632(br), 1262(w), 1437(w), 1384(m), 1104(w), 1032(br). $[\text{Mn}^{\text{II}}(\text{L}^1)]\text{Cl}_2$: Dark brown precipitate (88% yield). IR (KBr pellet, cm^{-1}): 3545(br), 1686(w), 1616(s), 1594(w), 1443(m), 1378(m), 1261(s), 1099(br). $[\text{Cu}^{\text{II}}(\text{L}^1)]\text{Cl}_2$: Dark green precipitate (85% yield). IR (KBr pellet, cm^{-1}): 3448(br), 1625(br), 1384(w), 1344(w), 1261(s), 1096(s), 1027(m), 803(s).

2.3.1.2 Synthesis of EDTA bisamide of Sulfonamide (L^2)



The reaction was carried out according to a slightly modified procedure than what was reported by Rami *et al.*³⁰ This is as follows. To EDTA bisanhydride (1.6 g, 6.24 mmol) dissolved in dimethylformamide (20 ml) was added completely dissolved solution p-aminosulfonamide (2.151 g, 12.48 mmol) dropwise. After the complete addition of sulphonamide, the reaction mixture was allowed to stir overnight at room temperature. Thereafter, dichloromethane was added in two portions (50 ml), upon which precipitate was formed. The precipitate was filtered and washed initially with acetone and subsequently with acetonitrile. Yield 1.2 g, 37%; ^1H NMR (400 MHz, D_2O with K_2CO_3 : Me_4Si): δ_{H} (ppm) 7.55 (d, 4H, $J = 8.4$ Hz, ArH_a), 7.35 (d, 4H, $J = 8.6$ Hz, ArH_b), 3.50 (s, 4H, NCH_2COOH), 3.30 (s, 4H, NCH_2CONH), 2.95 (s, 4H, $\text{NCH}_2\text{CH}_2\text{N}$); IR (KBr disc) (cm^{-1}): 3411(br), 1672(vs), 1595(vs), 1548(vs), 1521(s), 1316(w), 832(vs).

^{13}C NMR and Accurate Masspec spectral data were not obtained as this is a known compound.

2.3.1.2.1 Complexation of L^2 with $ZnCl_2$ (ZnL^2)

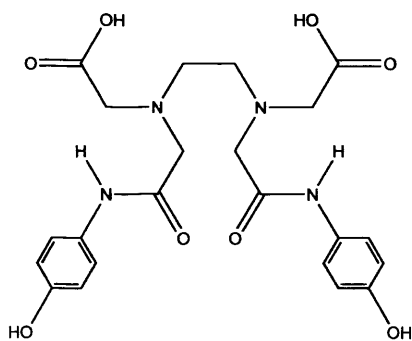
L^2 (0.06 g, 0.1 mmol) was completely dissolved in MeOH and $ZnCl_2$ (0.136 g, 1.0 mmol) was dissolved in minimum amount of distilled water. The solution of the ligand was added dropwise to the solution of the salt and allowed to stir for 20 min. The solvents were removed on the rotaevaporator and then high vacuum, and then the crude product was washed with acetone and chloroform, to obtain the complex. $[Zn^{II}(L^2)][Cl]_2$: Black precipitate (95% yield). 1H NMR (400 MHz; D_2O): 7.75 (d, 2H, $J = 8.6$ Hz), 7.60 (dd, 4H, $J = 6.0, 6.5$ Hz), 7.50 (d, 2H, $J = 8.9$ Hz), 3.75 (s, 2H), 3.70 (s, 2H), 3.40(s, 2H), 3.35 (s, 2H), 3.05 (s, 2H), 2.75 (s, 2H); IR (KBr pellet, cm^{-1}): 3414(br), 3079(m), 1632(s), 1366(s), 1262(w), 1029(s); ESIMS(-ion): found m/z 661.0388, Calc 661.0365 for $[(ZnL^2-3H)]^-$.

2.3.1.2.2 Complexation of L^2 with $MnCl_2$ (MnL^2)

L^2 (0.06 g, 0.1 mmol) was completely dissolved in MeOH and $MnCl_2$ (0.0629 g, 0.5 mmol) was dissolved in minimum amount of distilled water. The solution of the ligand was added dropwise to the solution of the salt and allowed to stir for 20 min. The solvents were removed on the rotaevaporator and then high vacuum, and then the crude product was washed with acetone and chloroform, to obtain the complex. $[Mn^{II}(L^2)][Cl]_2$: Pale white precipitate (95% yield). IR (KBr pellet, cm^{-1}): 3446(br), 1634(s), 1592(w), 1549(w), 1405(m), 1324(m), 1261(s), 1097(s), 1024(w), 801(s), 699(w); ESIMS(-ion): found m/z 652.0486, Calc 652.0454 for $[(MnL^2-3H)]^-$.

Complexation of L^2 with Cu (II) was not carried out as it was done in the past.³⁰

2.3.1.3 Synthesis of EDTA bisamide of Aminophenol (L^3)



Potential Multimodal Imaging Agents

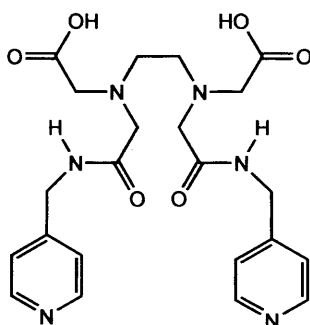
To EDTA bisanhydride (1.0 g, 3.90 mmol) was dissolved in dimethylformamide (16 ml) and was added triethylamine (0.79 g, 7.80 mmol) followed by portion wise addition of 4-amino phenol (0.85 g, 7.80 mmol). Then reaction mixture was allowed to stir for 48 h at room temperature. After which, the solvent was removed under reduced pressure. Thereafter isopropyl alcohol was added to the dark brown oily crude product and allowed to stir for 72 h. The product was filtered and dried in high vacuum. Yield 0.38 g, 43 %; ^1H NMR (400 MHz, $\text{d}_6\text{-DMSO: Me}_4\text{Si}$): δ_{H} (ppm) 10.00 (s, 2H, NH), 7.50 (d, 4H, $J = 7.8$ Hz, ArCHa), 6.70 (d, 4H, $J = 7.9$ Hz, ArCHb), 3.45 (s, 8H, NCH_2CONH , NCH_2COOH), 2.85 (s, 4H, $\text{NCH}_2\text{CH}_2\text{N}$); IR (KBr disc) (cm^{-1}): 3272(br), 2970(w), 1633(s), 1515(vs), 699(s).

^{13}C NMR and MASS Spectral data were not obtained as it is a known compound.²

2.3.1.3.1 Complexation of L^3 with $\text{ZnCl}_2\text{-ZnL}^3$

L^3 (0.079 g, 0.1 mmol) was dissolved in dimethylformamide and ZnCl_2 (0.023 g, 0.1 mmol) was dissolved in minimum amount of H_2O . The solution of the ligand was added dropwise to the solution of the salt and allowed to stir for 20 min. Then the solvent was removed under vacuum and the residue was washed with acetone and chloroform several times. $[\text{Zn}^{\text{II}}(\text{L}^3)][\text{Cl}]_2$: Pale brown precipitate (95% yield). ^1H NMR (400 MHz; D_2O): 6.65-6.60 (m, 4H), 6.40-6.35 (m, 4H), 3.65- 2.70 (m, 12H); IR (KBr pellet, cm^{-1}): 3434(br), 1635(s), 1515(m), 1448(w), 1384(s), 1262(s), 1102(br).

2.3.1.4 2.3.1.4 Synthesis of EDTA bisamide of 4-aminomethyl pyridine (L^4)



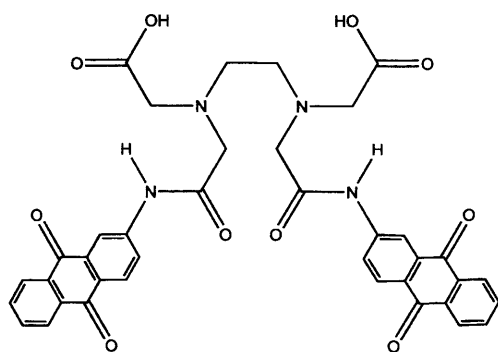
To EDTA bisanhydride (0.867 g, 3.38 mmol) completely dissolved in dimethylformamide (10 ml) was added 4-aminomethyl pyridine (0.73 g, 6.76 mmol) dissolved in dimethylformamide (10 ml), dropwise. The reaction mixture was allowed to stir overnight at room temperature.

Thereafter, dichloromethane was added to the reaction mixture, upon which precipitate was formed. The precipitate was filtered and washed initially with acetone and subsequently with acetonitrile. Yield 1.4 g, 88 %; ^1H NMR (400 MHz, D_2O with K_2CO_3 : Me_4Si): δ_{H} (ppm) 8.30 (d, 2H, $J = 5.8$ Hz, ArCH_6), 7.20 (d, 2H, $J = 5.6$ Hz, ArCH_2), 4.35 (s, 2H, NHCH_2), 3.30 (s, 2H, NCH_2COOH), 3.15 (s, 2H, $\text{NCH}_2\text{CH}_2\text{CONH}$), 2.70 (s, 2H, $\text{NCH}_2\text{CH}_2\text{N}$); ^{13}C NMR (400 MHz, D_2O with K_2CO_3): 179.26, 175.30, 148.99, 148.78, 122.63, 59.36, 58.69, 53.46, 41.98; IR (KBr disc) (cm^{-1}): 3438(br), 1712(cm^{-1} (w)), 1666(vs), 1561(w); ESIMS(+ion): found m/z 473.2131, Calc 473.2149 for $[(\text{L}^4)\text{H}]^+$.

2.3.1.4.1 Complexation of L^4 with $\text{MnCl}_2(\text{MnL}^4)$

L^4 (0.079 g, 0.1 mmol) was dissolved in dimethylformamide and MnCl_2 (0.021 g, 0.1 mmol) was dissolved in minimum amount of H_2O . The solution of the ligand was added dropwise to the solution of the salt and allowed to stir for 20 minutes. Then the solvent was removed under high vacuum and the residue was washed several times with acetone and chloroform.

Complexes ZnL^4 , CuL^4 was also prepared as per the procedure outlined for MnL^4 , with 1:1, ligand to metal ratio, using their respective chlorides. $[\text{Zn}^{\text{II}}(\text{L}^4)][\text{Cl}]_2$: Pale yellow precipitate (91% yield). ^1H NMR (400 MHz; D_2O): 8.25 (d, 2H, $J = 6.5$ Hz), 8.10 (m, 2H), 7.10 (d, 2H, $J = 7.1$ Hz), 6.95 (m, 2H), 4.25(s, 2H), 3.55(s, 2H), 3.45(s, 2H), 3.35(s, 2H), 3.30 (s, 2H), 3.25(s, 2H), 2.85(s, 2H); IR (KBr pellet, cm^{-1}): 3414(br), 3079(m), 1632(s), 1366(s), 1262(w), 1029(s). UV/Vis [λ_{max} , nm (ϵ_{M} , $\text{M}^{-1}\text{cm}^{-1}$)] in H_2O : 234(21,197), 333(10,013), 350(8, 831). $[\text{Mn}^{\text{II}}(\text{L}^4)][\text{Cl}]_2$: Pale yellow precipitate (77% yield). IR (KBr pellet, cm^{-1}): 3230(br) 1638(br), 1459(w), 1384(s), 1118(s), 1064(s), 1025(s). $[\text{Cu}^{\text{II}}(\text{L}^4)][\text{Cl}]_2$: Pale green precipitate (93% yield). IR (KBr pellet, cm^{-1}): 3427(br), 1638(s), 1379(s), 1261(m), 1011(s), 1027(s). ESIMS(-ion): found m/z 534.1306, Calc 534.1288 for $[(\text{CuL}^4\text{-H})]^+$.

2.3.1.5 Synthesis of EDTA bisamide of AminoAnthraquinone (L^5)

To EDTA bisanhydride (0.926 g, 3.62 mmol), completely dissolved in dimethylformamide (15 ml), was added 2-aminoanthraquinone (1.614 g, 7.23 mmol) dissolved in dimethylformamide (15 ml), dropwise. After the complete addition, the reaction mixture was allowed to stir overnight at room temperature. Then the reaction mixture was filtered, the filtrate was then evaporated to dryness. The crude product was washed with dichloromethane several times to obtain the product as dark brown glassy material. Yield 1.6 g, 72%; ^1H NMR (400 MHz, d_6 -DMSO: Me_4Si) δ_{H} (ppm) 10.6 (s, 1H, CH_2COOH), 8.25 (s, 1H, NH), 7.95 (m, 5H, Ar_{H}), 7.75 (s, 2H, Ar_{H}), 3.6 (s, 2H, NCH_2COOH), 3.5 (s, 2H, NCH_2CONH), 2.85 (s, 2H, NCH_2); ^{13}C NMR (DMSO, 400 MHz): δ_{C} 182.32, 181.20, 173.05, 170.96, 144.31, 134.62, 134.31, 133.99, 133.06, 128.90, 127.90, 126.81, 126.74, 123.94, 116.00, 58.71, 55.77, 53.08, 48.96; IR (KBr disc) (cm^{-1}): 3440(br), 1673(vs), 1624(s), 1591(vs), 1379(w), 1328(s), 1296(m), 1261(vs); ESIMS(+ion): found m/z 725.1837, Calc 725.1860 for $[(L^5) \text{Na}]$.

2.3.1.5.1 Complexation of L^5 with $\text{MnCl}_2 - \text{MnL}^5$

L^5 (0.07 g, 0.1 mmol) was dissolved in dimethylformamide and MnCl_2 (0.014 g, 0.11 mmol) was dissolved in minimum amount of distilled water. The solution of the ligand was added dropwise to the solution of the salt and allowed to stir for 2 h. The solvent was removed under high vacuum, and the residue was washed several times with acetone and chloroform.

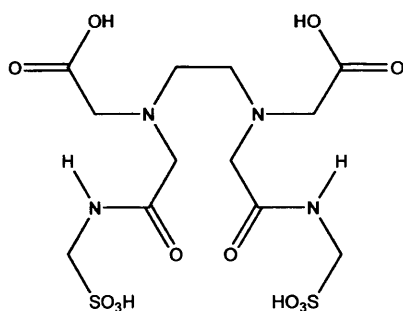
Complexation of L^5 with ZnCl_2 (ZnL^5) and Complexation of L^5 with CuCl_2 (CuL^5) was also carried out as per the procedure outlined for MnL^5 . $[\text{Zn}^{\text{II}}(\text{L}^5)][\text{Cl}]_2$: Dark brown precipitate (94% yield). ^1H NMR (400 MHz; DMSO): 10.51 (m, 2H), 8.40 (s, 1H), 8.35 (s, 1H), 8.10-8.00 (m, 10H), 7.90 (m, 2H), 7.85 (m, 2H); IR (KBr pellet, cm^{-1}): 3435(br), 1674(m),

Potential Multimodal Imaging Agents

1624(w), 1590(s), 1550(w), 1456(w), 1384(s), 1330(s), 1294(s), 1104(br), 930(m).

$[\text{Mn}^{\text{II}}(\text{L}^5)][\text{Cl}]_2$: Dark brown precipitate (94% yield). IR (KBr pellet, cm^{-1}): 3793(br), 1674(s), 1589(s), 1559(w), 1549(w), 1419(m), 1095(w). UV/Vis [λ_{max} , nm (ϵ_{M} , $\text{M}^{-1}\text{cm}^{-1}$)] in DMF: 270(75, 143), 243(53,450), 210(42, 643), 339(14, 820). $[\text{Cu}^{\text{II}}(\text{L}^5)][\text{Cl}]_2$: Pale green precipitate (94% yield); IR (KBr pellet, cm^{-1}): 3431(br), 1618(w), 1590(s), 1542(s), 1492(m), 1459(m), 1379(s), 1384(s), 1330(s), 1294(s), 1262(s), 1098(s), 1021(s).

2.3.1.6 Synthesis of EDTA bisamide of Aminomethylsulphonic acid (L^6)



2-Aminomethanesulfonic acid (1.56 g, 14 mmol) and NaHCO_3 (0.456 g, 5.43 mmol) was dissolved in water (30 ml), and was added EDTA bisanhydride (1.8 g, 7.025 mmol) portion wise, the reaction mixture was then cooled down to 0 °C and allowed to stir for 4 h. After 4 h the ice bath was removed and allowed the reaction mixture to stir at room temperature for 24 h. Then the reaction mixture was filtered and the filtrate was evaporated to dryness. The crude product was washed with hot methanol. Yield 0.8 g, 53%; ^1H NMR (400 MHz, D_2O : Me_4Si): δ_{H} (ppm) 4.40 (s, 2H, $\text{NHCH}_2\text{SO}_3\text{H}$), 3.80 (s, 4H, NCH_2COOH & NCH_2CONH), 3.50 (s, 2H, $\text{NCH}_2\text{CH}_2\text{N}$); ^{13}C NMR (D_2O , 400 MHz) δ_{C} 173.95, 169.56, 68.89, 67.53, 64.58, 49.13; IR (KBr disc) (cm^{-1}): 3443(br), 3240(br), 3079(br), 1636(s), 1409(s), 1209(s), 1041(vs); ES(+ion): found m/z 478.11, calc 478.12 for $[(\text{L}^6)\text{H}]^+$.

2.3.1.6.1 Complexation of L^6 with MnCl_2 (MnL^6)

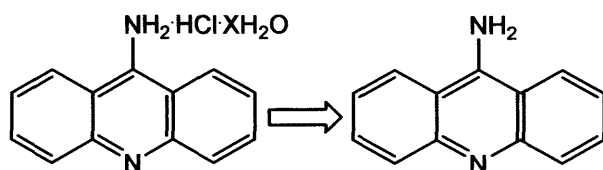
Ligand L^6 (0.096 g, mmol) was dissolved in water and MnCl_2 (0.024 g, mmol) was dissolved in minimum amount of distilled water. The solution of the ligand was added drop wise to the solution of the salt and the reaction mixture was allowed to stir for 20 minutes. Then the

solvent was removed under high vacuum, and the residue was washed with acetone and chloroform several times.

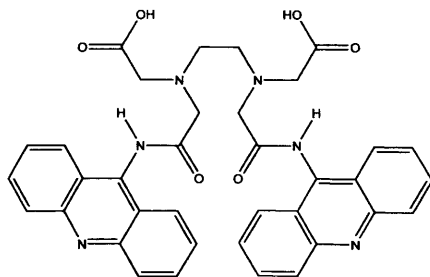
The complexation of L^6 with $ZnCl_2$ (ZnL^6) was also carried out as per the procedure outlined for MnL^6 . The complexation of L^6 with $CuCl_2$ was not carried out. $[Zn^{II}(L^6)][Cl]_2$: Yellow precipitate (48% yield). IR (KBr pellet, cm^{-1}): 3443(br), 1640(br), 1605(w), 1504(w), 1445(m), 1187(m), 1313(w), 1261(s), 1043(s). $[Mn^{II}(L^6)][Cl]_2$: White precipitate (62% yield). IR (KBr pellet, cm^{-1}): 3443(br), 1641(m), 1590(w), 1402(s), 1336(m), 1048(s).

2.3.1.7 Synthesis of EDTA bisamide of the amino acridine (L^7)

(a) Deprotonation of Aminoacridine hydrochloride (L^{7a})



The commercially obtained, 9-amino acridine hydrochloride was dissolved in distilled water (with occasional heating). Thereafter, 2-3 pellets of NaOH was added, no sooner, it was added the formation of the precipitate was observed (indicating the deprotonation of aminoacridine hydrochloride). This was then extracted in to dichloromethane (the problem of partial insolubility of the precipitate in dichloromethane was overcome by the addition of small amount of toluene and acetone). The organic layer was dried with $MgSO_4$. The removal of the solvents under reduced pressure yielded the pure deprotonated amino acridine as yellow powdered solid. Yield 0.3 g, 93%; 1H NMR (400 MHz, d_6 -DMSO: Me_4Si): δ_H (ppm) 8.45 (d, 2H, $J = 8.8$ Hz, $ArCH_2$), 7.85 (d, 4H, $J = 8.4$ Hz, $ArCH_5$), 7.70 (t, 4H, $J = 8.0$ Hz, $ArCH_4$), 7.35 (t, 2H, $J = 7.6$ Hz, $ArCH_3$); IR (KBr disc) (cm^{-1}): 3423(br), 3139(br), 1659(s), 1644(m), 1592(s), 1542(s), 1372(m), 1267(s), 1163(s), 755(s).

(b) Synthesis of EDTA bisamides of the deprotonated aminoacridine (L^{7b})

To EDTA bisanhydride (0.145 g, 0.564 mmol) dissolved in dimethylformamide (5 ml) was added 9-amino acridine (0.220 g, 1.133 mmol) dissolved in dimethylformamide (5 ml), dropwise. The reaction mixture was allowed to stir over night at room temperature. Thereafter, dichloromethane (50 ml) was poured in to the reaction mixture and stirred for 5 min. The precipitate was washed thoroughly with acetone and subsequently with acetonitrile. Yield 0.2 g, 55%; $^1\text{H NMR}$ (400 MHz, D_2O with K_2CO_3 ; Me_4Si): δ_{H} (ppm) 7.93 (d, 2H, $J = 8.7$ Hz, ArCH_2), 7.77 (d, 2H, $J = 9.0$ Hz, ArCH_5), 7.59 (t, 2H, $J = 8.8$ Hz, ArCH_4), 7.27 (t, 2H, $J = 7.6$ Hz, ArCH_3), 3.25 (s, 2H, NCH_2COOH), 3.08 (s, 2H, NCH_2CONH), 2.74 (s, 2H, $\text{NCH}_2\text{CH}_2\text{N}$); IR (KBr disc) (cm^{-1}): 3423(br), 2963(s), 1643(s), 1593(m), 1482(s), 1387(m), 1262(s), 1164(m), 1095(s), 801(s).

2.3.1.7.1 Complexation of L^7 with ZnCl_2 (ZnL^{7b})

L^7 (0.064 g, 0.1 mmol) was dissolved in dimethylformamide and ZnCl_2 (0.014 g, 0.1 mmol) was dissolved in minimum amount of distilled water. The solution of the ligand was added dropwise to the solution of the salt and allowed to stir for 20 min. Then the solvent was removed under vacuum, and the residue was washed with acetone and chloroform several times. Product was obtained as glassy material. $[\text{Zn}^{\text{II}}(\text{L}^7)]_2[\text{Cl}]_2$: Dark yellow precipitate (96% yield). IR (KBr pellet, cm^{-1}): 3413(br), 1638(s), 1592(s), 1504(m), 1478(m), 1379(m), 1373(m), 1265(w), 1165(s), 1032(m), 859(s).

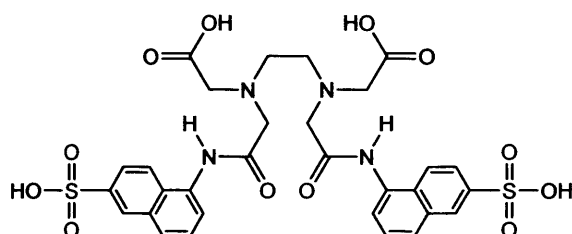
2.3.1.8 Attempted Synthesis of EDTA bisamide of Trien naphthaderivative

To EDTA bisanhydride (0.198 g, 0.774 mmol), dissolved in dimethylformamide (7 ml), and was added Trien naphtha derivative (0.505 g, 1.548 mmol) dissolved in dimethyl formamide

Potential Multimodal Imaging Agents

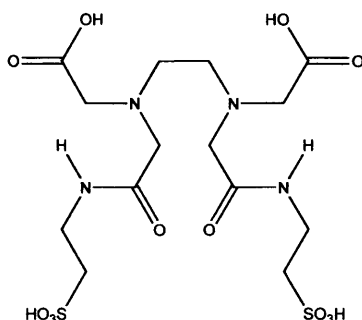
(7 ml), dropwise. The reaction was then allowed to stir over night. Then dichloromethane (50 ml) was poured in to the reaction mixture and stirred for 5 minutes, mixture was filtered, half way through filtration, added another portion of dichloromethane (50 ml) and filtered again. The precipitate was washed thoroughly with acetone and then acetonitrile subsequently. The proton NMR spectrum of the product indicated that the reaction is not successful.

2.3.1.9 Attempted synthesis of EDTA bisamides of 5-aminonaphthalene-2-sulphonic acid (L^8)



To EDTA bisanhydride (0.308 g, 1.20 mmol) dissolved in dimethylformamide (5 ml), was added 5-aminonaphthalene-2-sulphonic acid (0.538 g, 2.40 mmol) dissolved in dimethylformamide (5 ml) dropwise. The reaction mixture was allowed to stir over night at room temperature. Thereafter, dichloromethane (50 ml) was poured in to the reaction mixture and stirred for 5 min. The reaction mixture was filtered; half way through the filtration added another portion of dichloromethane (50 ml) was added and filtered again. The precipitate was washed thoroughly with acetone and subsequently with acetonitrile. ^1H NMR spectrum indicated the presence of starting material along with the desired product.

2.3.2 Attempted Synthesis of EDTA bisamide of taurine (L^9)



Attempt I

Accurately weighed EDTA bisanhydride (0.36 g, 1.405 mmol) was dissolved in water, and NaHCO₃ (0.59 g, 7.02 mmol) added slowly and then Taurine (0.352 g, 2.812 mmol) was added at 0 °C. The reaction mixture was allowed to stir at 0 °C for 4 h. After that the reaction mixture was allowed to stand in room temperature.

Attempt II

EDTA bisanhydride (0.36 g, 1.405 mmol) was dissolved in dimethylformamide (5 ml), similarly Taurine (0.352 g, 2.81 mmol) was also dissolved in dimethylformamide (5 ml). After ensuring the complete dissolution of taurine, excess NaHCO₃ (0.59 g, 7.02 mmol) was added. The reaction mixture was transferred to the completely dissolved EDTA bisanhydride solution dropwise. The reaction was then allowed to stir over night at the room temperature. Then dichloromethane (50 ml) was poured in to the reaction mixture and stirred for 5 minutes. The reaction mixture was filtered and half way through filtration added another portion of dichloromethane (50 ml) was added and filtered again. The precipitate was washed thoroughly with acetone and subsequently with acetonitrile. The ¹H NMR spectrum was not promising enough.

2.4 Conclusion

The synthesis of 9 new EDTA based bisamides was attempted, of which 6 ligands were successfully prepared and 4 of them have never been made before. These ligands represent the first attempt to provide an EDTA based bifunctionalised ligands bearing a chromophoric moiety, to act as potential multimodal diagnostic tools/probes.

References

1. A. D. Vassil, Y. Kapulnik, I. Raskin and D. E. Salt, *Plant Physiol.*, 1998, **117**, 447.
2. P. W. Jones and D. R. Williams, *Inorg. Chim. Acta.*, 2002, **339**, 41.
3. N. Manouchehri, S. Besancon and A. Bermond, *Anal. Chim. Acta.*, 2006, **559**, 105.
4. P. Wood, in *MRI for technologists*, McGraw-Hill Medical; 2nd edition, 2000.
5. H. S. Thomsen and P. Marckmann, *Eur. J. Radiol.*, 2008, **66**, 153.

6. T. Grobner, *Nephrol Dial Transplant.*, 2006, **21**, 1104.
7. D. D. Schwer, J. A. Davies and N. Richardson, *Contrast Agents*, Springer, Berlin, Heidelberg, 2002.
8. S. K. Larsen, B. G. Jenkins, N. G. Memon and R. B. Lauffer, *Inorg. Chem.*, 1990, **29**, 1147.
9. V. M. Runge, M. A. Foster, J. A. Clanton, M. M. Jones, C. M. Lukehart, M. S. Hutchison, J. R. Mallard, F. W. Smith, L. Partain and A. E. James, *Radiology.*, 1984, **152**, 123.
10. J. Vymazal, W. M. Bulte, J. A. Frank, G. D. Chiro and R. A. Brooks, *J. Magn. Reson. Imaging.*, 1993, **3**, 637.
11. P. Rongved and J. Klaveness, *Carbohydr. Res.*, 1991, **214**, 315.
12. H. A. Shroeder and A. P. Nason, *Clin. Chem.*, 1971, **17**, 461.
13. C. W. Olanow, *Ann. N.Y. Acad. Sci.*, 2004, **1012**, 209.
14. S. V. Chandra and G. S. Shukla, *Arch. Toxicol.*, 1976, **35**, 319.
15. L. Wolf and L. Baum, *Am. J. Roentgenol.*, 1983, **141**, 193.
16. C. H. Taliaferro, R. J. Motekaitis and A. E. Martell, *Inorg. Chem.*, 1984, **23**, 1188.
17. S. M. Rocklage, W. P. Cacheris, S. C. Quay, F. E. Hahn and K. N. Raymond, *Inorg. Chem.*, 1989, **28**, 477.
18. B. Gallez, C. Baudalet, J. Adline, V. Charbon and D. M. Lambert, *Magn. Reson. Imaging.*, 1996, **14**, 1191.
19. M. Spiller, R. D. Brown, S. H. Koenig and G. L. Wolf, *Magn. Reson. Med.*, 1988, **8**, 293.
20. M. W. Sundberg, C. F. Meares, D. A. Goodwin and C. I. Diamanti, *J. Med. Chem.*, 1974, **17**, 1304.
21. L. H. DeRiemer, C. F. Meares, D. A. Goodwin and C. I. Diamanti, *Journal of Medicinal Chemistry.*, 1979, **22**, 1019.
22. M. A. Santos, G. L. Gano, G. Cantinho and E. Farkas, *Dalton Trans.*, 2004, 3772.
23. M. A. Santos, S. Gama, L. Gano and E. Farkas, *J. Inorg. Biochem.*, 2005, **99**, 1845.
24. B. Nortemann, ACS symposium series 910, Braunschweig, Germany, 2005; p 151.
25. H. S. Ortega, G. P. Luis, S. K. Lopez and I. A. Rivero, *J. Comb. Chem.*, 2009, **11**, 1030.

26. M. A. Bailey, M. J. Ingram, D. P. Naughton, K. J. Rutt and H. T. Dodd, *Transition Met. Chem.*, 2008, **33**, 195.
27. C. P. Iglesias, D. M. Corsi, L. V. Elst, R. N. Muller, D. Imbert, G. Bünzli, É. Tóth, T. Maschmeyer and J. A. Peters, *Dalton Trans.*, 2003, 727.
28. Y. M. Wang, Y. J. Wang and Y. L. Wu, *Polyhedron.*, 1999, **18**, 109.
29. D. Namor and A. P. Tanaka, *J. Chem. Soc., Faraday Trans.*, 1998, **94**, 3105.
30. M. Rami, J. Y. Winum, A. Innocenti, J. L. Montero, A. Scozzafava and C. T. Supuran, *Bioorg. Med. Chem. Lett.*, 2008, **18**, 836.
31. K. P. Guiry, J. M. Kelleher, S. E. Lawrence, M. T. McAuliffe, A. Moynihan and A. L. Ryan, *J. Enzyme Inhib. Med. Chem.*, 2007, **22**, 550.
32. K. Y. Choi, K. S. Kim and J. C. Kim, *Polyhedron.*, 1994, **13**, 567.
33. B. Gallez, C. Baudalet, J. Adline, M. Geurts and N. Delzenne, *Chem. Res. Toxicol.*, 1997, **10**, 360.
34. (a) B. Gallez, G. Bacic and H. M. Swartz, *Magn. Reson. Med.*, 1996, **35**, 14;
(b) D. Grant, K. Zech and E. Holtz, *Invest. Radiol.*, 1994, **29**, 5249.
35. S. O. Hustvedt, D. Grant, T. E. Southon and K. Zech, *Acta Radiol.*, 1997, **38**, 690.
36. (a) B. Gallez, G. B. Harold, M. Swartz, *Magn. Reson. Med.*, 2005, **35**, 14;
(b) B. Misselwitz, A. Muhler and H. J. Weinmann, *Invest. Radiol.*, 1995, **30**, 611.
37. R. B. Lauffer, *Chem. Rev.*, 1987, **87**, 901.
38. J. S. Troughton, M. T. Greenfield, J. M. Greenwood, S. Dumas, A. J. Wiethoff, J. Wang, M. Spiller, T. J. McMurry and P. Caravan, *Inorg. Chem.*, 2004, **43**, 6313.
39. E. C. Unger, *US Pat.*, 5,312,617, 1994.
40. T. Fritz, G. Wu, D. Shen, B. Kulik, T. New, M. Crowell, N. Wilke and E. Unger, *J. Liposome. Res.*, 1994, **4**, 811.
41. R. B. Lauffer, J. S. Thomas, T. R. Brady, O. Brown, C. Baglin and S. H. Koenig, *Magn. Reson. Med.*, 1986, **3**, 541.
42. M. Woods, Z. Kovacs and A. D. Sherry, *J. Supramol. Chem.*, 2002, **2**, 1.
43. (a) S. Aime, A. Barge, J. I. Bruce, M. Botta, A. K. Howard, J. M. Moloney, D. Parker, A. S. de Sousa and M. Woods, *J. Am. Chem. Soc.*, 1999, **121**, 5762.
(b) D. D. Dischino, E. J. Delaney, J. E. Emswiler, G. T. Gaughan, J. S. Prasad, S. K. Srivastava and M. F. Tweedle, *Inorg. Chem.*, 1991, **30**, 1265.
44. K. D. Jurasz, *Brit. J. Radiol.*, 2003, **76**, S98.
45. A. Pardo, E. Martin, L. Poyato, J. Camacho, M. Guerra, R. Weingand, F. Braña and M. Castellano, *J. Photochem. Photobiol., A.*, 1989, **48**, 259.

46. M. Licchelli, A. O. Biroli, A. Poggi, D. Sacchi, C. Sangermania and M. Zema, *Dalton Trans.*, 2003, 4537.
47. D. R. Breed, R. Thibault, F. Xie, Q. Wang, C. J. Hawker and D. J. Pine, *Langmuir.*, 2009, **25**, 4370.
48. M. B. Inoue, R. E. Navarro, I. O. Landin, D. M. Lopez, M. Inoue and Q. Fernando, *Inorg.Chim. Acta.*, 1998, **269**, 224.
49. Y. C. Liu, S. L. Ma, Q. L. Guo, J. Zhang, M. Q. Xu and W. X. Zhu, *Inorg. Chem. Commun.*, 2005, **8**, 574.
50. B.C. Smith, in *Infrared spectral interpretation: a systematic approach*, CRC Press, 1999.
51. D. W. Zhang, Z. Y. Yang, B. D. Wang, S. P. Zhang and R. D. Yang, *Chem. Pharm. Bull.*, 2006, **54**, 1203-206.

CHAPTER 3

DTPA Analogues and DTPA Bis Amides

3.1 Introduction to DTPA derivatives

3.1.1 DTPA

Throughout the history of radiopharmaceutical imaging, several chelating agents have been used.

As also known as diethylenetriamine pentaacetic acid (DTPA), it is a polyamine macrocyclic ligand. It contains five carboxylic acid groups and three secondary amine groups.

CHAPTER 3 ***DTPA Analogues*** **&** ***DTPA Bisamides***

Figure 3-1: Diethylenetriamine pentaacetic acid (DTPA)

3.1.2 DTPA as a complexing agent: Historical View

Though this chapter predominantly deals with functionalizing DTPA, it is necessary to take a short insight, about the history of radiopharmaceutical DTPA.

The following is a brief account of the coordination of DTPA with various transition & actinoid metal ions.

CHAPTER 3

DTPA Analogues and DTPA Bis Amides

3.1 Introduction to DTPA derivatives

3.1.1 DTPA

Throughout the history of synthesizing imaging agents, polyamino poly carboxylates (which are also known as “complexones”), play an important role. DTPA is a polyamino polycarboxylate ligand like EDTA. It could be viewed as an expanded version of EDTA. It contains the diethylene triamine backbone, which has been modified by five carboxymethyl groups.

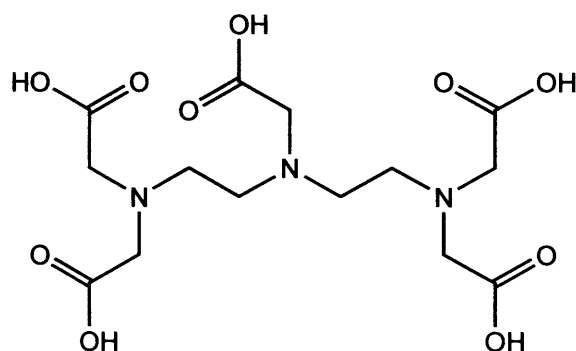


Figure 1:- Diethylene Triamine Penta Acetic acid (DTPA)

3.1.2 DTPA as a complexing agent- Historical View

Though this chapter predominantly deals with functionalising DTPA, it is necessary to have a clear insight, about the history of functionalising DTPA.

The following is a brief account of the complexation of DTPA with various transition & lanthanide metal ions

3.1.2.1 Complexation with Transition metal cations.

DTPA based transition metal complexes in chelation therapy

The initial field of complexones in biomedical applications was in chelation therapy.^{1,2} Ca-DTPA and Zn-DTPA have been used for over 40 years to speed up excretion of the radioactive transuranium elements (plutonium, americium and curium) from the body. In the study of 'Iron storage disease', the DTPA is used as a chelating agent to measure the iron content in urine³ in patients with excess iron stores. Alexander *et al.*⁴ reported studies on the effectiveness of Co (II)-DTPA and Zn (II)-DTPA in preventing the retention of radio cerium and radio yttrium in a rat. This was found to be insignificantly diminished, when compared with Ca (II)-DTPA.

Ruthenium complex as Imaging Agent

In an attempt to develop enhanced, cerebrospinal fluid imaging agent, ⁹⁷Ru-DTPA was evaluated.⁵ It was found that upon electrophoresis on cellulose acetate in borate buffer (pH 8); the unbound ruthenium stays at the point of origin, whereas ⁹⁷Ru-DTPA moves toward the anode. Thin layer chromatography also indicated 97-99 % chelation of the radiotracer. It was shown that the kinetics and excretion of ⁹⁷Ru-DTPA is similar to those of ¹¹¹In- DTPA.

Above are the few examples to indicate the efforts on complexation with transition metals and its impact to the field of health care. One may, however, find many such examples in the literature.

3.1.3 Incorporation of reagents to DTPA based transition metal complexes

This could be more effectively done by a brief comparison between its counterpart namely, EDTA. EDTA is a hexadentate ligand, whereas DTPA is an octadentate ligand. This feature seems to be useful, when complexing with transition metals (such as Zn²⁺, Cu²⁺ etc). Transition metals usually have a coordination number of six or less. Thus after forming a complex with a transition metal, DTPA still has the ability to bind to other reagents. For instance, in [CuDTPA]³⁻ DTPA binds in a hexadentate manner, utilizing the three amine

centres and three of the five carboxylates, leaving the rest, two of the carboxylates for coordination with other potential reagents. Incorporating these reagents, paves the way for transition metal complexes of DTPA to be used in variety of fields (specifically in medicine).

Incorporation into liposomes

Naoto *et al.*⁶ used ^{99m}Tc-DTPA in tumour imaging, and studied the bio distribution of ^{99m}Tc-DTPA-encapsulated liposomes in tumour bearing mice and reported a remarkable accumulation of the complex in the tumour tissue.

3.1.4 Introducing Lanthanides to DTPA

Atoms having larger radius in periods 5 & 6 of the periodic table favour higher coordination numbers, whereas bulky ligands favour lower coordination numbers. When we move across the d block, higher coordination numbers are more common on the left of the period and low coordination numbers are more common on the right of the period.

The stability of the complex, however, depends on the coordination number. Lanthanide favours higher coordination numbers and this has prompted scientists to explore complexation of DTPA with lanthanides. A review of the literature reveals a vast amount of information with regard to the synthesis of various Ln-DTPA complexes and their variety of uses. In respect of the relevancy to the thesis, some of the most important complexes are discussed.

La (III) and Tm (III): Daniele *et al.*⁷ have carried out studies on strong ion pair interactions between oppositely charged La(THP)³⁺ complex (THP = 1,4,7,10-tetrakis(2-hydroxypropyl)-1,4,7,10-tetraazacyclododecane) and that of Tm (III) complexes of DOTA , DTPA, TTHA and DOTP.

Through ¹³C NMR spectroscopy, they have examined the lanthanide induced chemical shifts of La (THP)³⁺ upon adduct formation with Tm (III) complexes. The selection of Tm (III) has been justified by its large chemical shifts and the enhancement of relaxation rates.

Dy (III): Luce Vander Elst *et al.*⁸ reported complexation studies of Dy complexes of DTPA and its derivatives as relaxation agents for very high field MRI. They have also reported its

beneficial effect on slow water exchange on the Transverse Relaxivities. Dy-complexes are localized in the extra cellular compartment of healthy tissues, and as a result of their relatively large magnetic susceptibility, they induce local field gradients that result in a decrease of T_2^* . This type of T_2^* effect, however, requires quite high concentrations of compound.

For lanthanide ions characterized by very short electronic relaxation times, such as Dy (III), Pr (III), Sm (III), Ho (III), Er (III), and Yb (III), a sizable contribution to longitudinal nuclear proton relaxation, resulting from the presence of a large static magnetic moment at high magnetic fields has been proposed by Bertini *et al.*⁹

This contribution, known as 'Curie relaxation', originates from the dipolar interaction between the water protons and a large static magnetic moment arising from the electrons. In their research, Elst *et al.*⁸ showed experimental evidence of the Curie longitudinal relaxation of different Dy-complexes of similar size and illustrated the influence of the magnetic field, and the residence time of the coordinated water molecule on the proton transverse relaxation rate.

Their finding on the complexes of Dy with DTPA derivatives shall be discussed later in the chapter. Likewise, there are many examples of lanthanide complexes of DTPA and their various applications could be found in a good amount of literature.

The importance of lanthanide complexation with DTPA and their significance in medical imaging, however, was not well realised until Gd-DTPA emerged as a successful contrast agent.

3.1.5 Gadolinium with DTPA

Gadolinium as a counter part

Gd has attracted the attention of scientists involved in coordination chemistry for several reasons. Gd (III) is the only lanthanide which has seven unpaired electrons. It is worth mentioning the fact, that two other lanthanides in the f-block, specifically dysprosium (III) and holmium (III) also enjoy higher magnetic momentum (due to orbital contributions to

electron angular momentum) than Gd (III). They, however, have very rapid electron spin relaxation due to the asymmetry of these electronic states. In contrast, Gd (III), possessing a symmetric “S” state creates an environment more advantageous to electron spins.

This will culminate in slower electronic relaxation rates. In comparison with Dy (III), Gd (III) is more closely in tune with the water protons frequency, during the process of water proton relaxation.¹⁰ Gd, being an obscure lanthanide element in the periodic table, has in the course of time, become a well known element in medical diagnostics as in the case of platinum in cancer therapeutics and technetium in cardiac scanning. With regard to research on contrast agents for MRI, gadolinium now appears to be the centre of such research.

The birth of Gd- DTPA

Gd (III) is a toxic ion. When injected intravenously, the lanthanides (rare earth elements) are bound to serum proteins and are readily displaced by weak complexing ions¹¹ (such as Ca (II)) from these proteins. Ionic solutions of the lanthanides will form colloids *in vivo* and undergo phagocytosis by the reticuloendothelial system, leading to accumulation in the liver, spleen and bone marrow.

They have long biological half lives (for weeks) with slow excretion in urine, bile and faeces. Therefore its toxicity needs to be eliminated or minimised, before it could be administered in the body. One of the ways of overcoming this problem is to chelate with ligands (since the atoms of the rare-earth elements do not form stable, covalent bonds with organic molecules, the paramagnetic Gd ion might be detoxified by complexation). Upon complexation, Gd will lose its toxicity (as the toxicity of the paramagnetic chelate is related to its stability, measurements on stability-especially on stability constants, will be dealt in great detail in chapter 4), but not the magnetic properties. This gives rise to the synthesis of Gadolinium chelates and among them Gd–DTPA has its place.

Invention of ‘Magnevist’

A brief account on the success story of Gd–DTPA (commercially known as ‘Magnevist’), is appropriate to this chapter. Owing to its success, ‘Magnevist’ serves as a bench mark contrast agent for past and future MRI contrast agents.

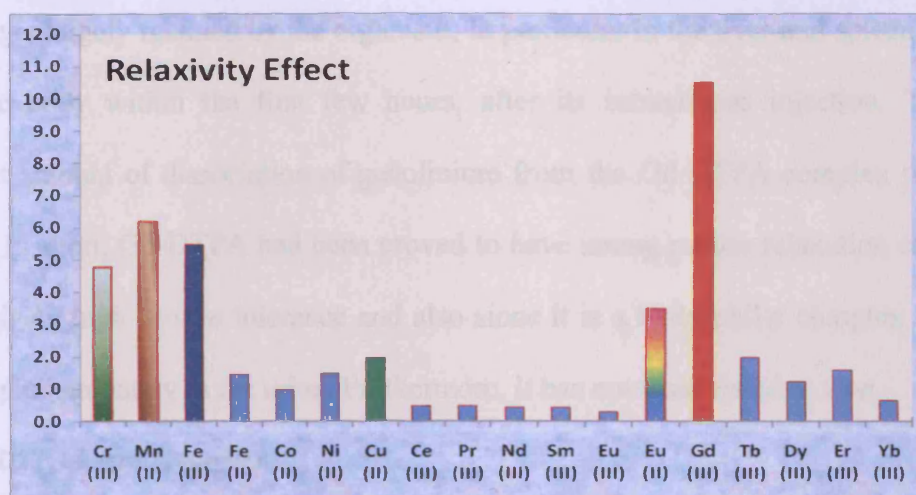


Fig 2:- Influence of paramagnetic ions on proton T_1 relaxation times, it becomes clear that comparatively, Gd possess high T_1 relaxation times of hydrogen protons

The powerful proton-relaxing effect of gadolinium can be attributed to a complex interplay of several factors, which includes a strong magnetic moment, long electron-spin-relaxation time, isotropy of g-tensors, rotational tumbling time, configuration and mobility of molecules of hydration and the proximity of hydrogen nuclei to the paramagnetic centre. Chelating gadolinium to EDTA or DTPA diminishes, but does not eliminate, gadolinium’s strong influence on proton T_1 and T_2 relaxation.

The coordination number of Gd (III) is estimated to be 9 or 10.¹² Therefore by using DTPA which has eight coordination sites as a chelating ligand, only eight of gadolinium’s 9 or 10 possible coordination sites could be filled. This leaves at least one or two sites open for fast-exchanging water protons to approach closely to the paramagnetic centre of the complex. The relaxivity enhancement of water protons is directly proportional to the number of available coordination water protons per paramagnetic ion. Therefore gadolinium complexes (Gd-DTPA and Gd-EDTA), compared with free gadolinium species, would be expected to have a reduced relaxation effects on water molecules. This expectation was perfectly supported by Weinmann’s results.¹³

Chelation effects and reduction in toxicity

The combination of Gd and DTPA minimises the toxicity, compared to the two components individually.¹⁴ This is reflected in the pharmacokinetic behaviour of Gd-DTPA when compared with gadolinium trichloride. Whereas the gadolinium ion from the gadolinium trichloride is largely retained by the organism; in particular in the liver and spleen, Gd-DTPA leaves the body within the first few hours, after its intravenous injection. There is no significant amount of dissociation of gadolinium from the Gd-DTPA complex noted within the body. In short, Gd-DTPA had been proved to have strong proton relaxation enhancement with relatively high *in-vivo* tolerance and also since it is a hydrophilic complex it is rapidly excreted, predominately in the urine. Furthermore, it has not dissociated *in vivo*.

Need for DTPA based bisamides

As for the above mentioned qualities, one would wonder, what is the need for further development and modifications of this unique contrast agent? The answer is quite straight forward. As mentioned earlier, the concentration of the gadolinium complex should be approximately twice as that of free gadolinium ion (this has been estimated as 0.01-0.05 mmol/kg body weight). Further, there are medical applications which require higher dosages up to 0.3 mmol/kg body weight. At the outset, one may assume, the problem is of an economical nature and that, it could be overcome easily. The subtlety of the problem, however, lies in osmolarity.

Osmolarity is influenced by the two residual negative charges of the Gd [DTPA]²⁻ and usually the osmolarity is regulated around 300 mmol /L. Raising this level with injected ions results in the collection of water within the unbalanced region, ultimately resulting in diluted ion concentration. This will lead to an osmotic shock to the red blood cells with consequent haemolysis.¹⁵ This has brought up the need for two balancing meglumine cations, a total of three particles, to contribute to osmolality. This was a powerful stimulus to the development of low osmolarity agents (both ionic and non ionic).

As with the iodinated agents, one way to reduce osmolality without reducing the concentration of the active agent is to make a non-ionic molecule.¹⁶ This very fact supports the discovery of DTPA based bisamides.

Having established the necessity for DTPA based bisamides let us now see how the requirement was fulfilled.

3.1.6 Synthetic methodologies for introducing functionality to DTPA

DTPA offers the advantage of incorporating a well-defined structural molecule, to a chosen biological molecule (which could be proteins in the blood, antibodies or similar biological macro molecules). To understand how this was made possible, it is necessary for us to know the various ways and means of incorporating functionality to DTPA ligands. This has been achieved in the past, through two major strategies.

Since we have utilised both these strategies, it will be appropriate to have a clearcut understanding of these strategies and how they had been utilised in the past.

First is to synthesize the anhydride of DTPA through condensation with the aid of acetic anhydride,¹⁷ then to react the DTPA bisanhydride thus synthesized with the appropriate amine functionalised reagents to produce DTPA based bisamides.¹⁸ These reagents could contain aliphatic or aromatic groups or both.

The second strategy was to use a retro synthetic approach to produce an analogue of DTPA, in which N,N-Bis[(tert-butoxycarbonyl)methyl]-2-bromoethylamine (see Fig-3) will dialkylate an amine containing reagent.

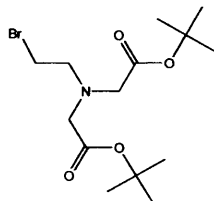


Figure 3:-N, N –Bis [(tert-butoxycarbonyl) methyl -2-bromoethylamine

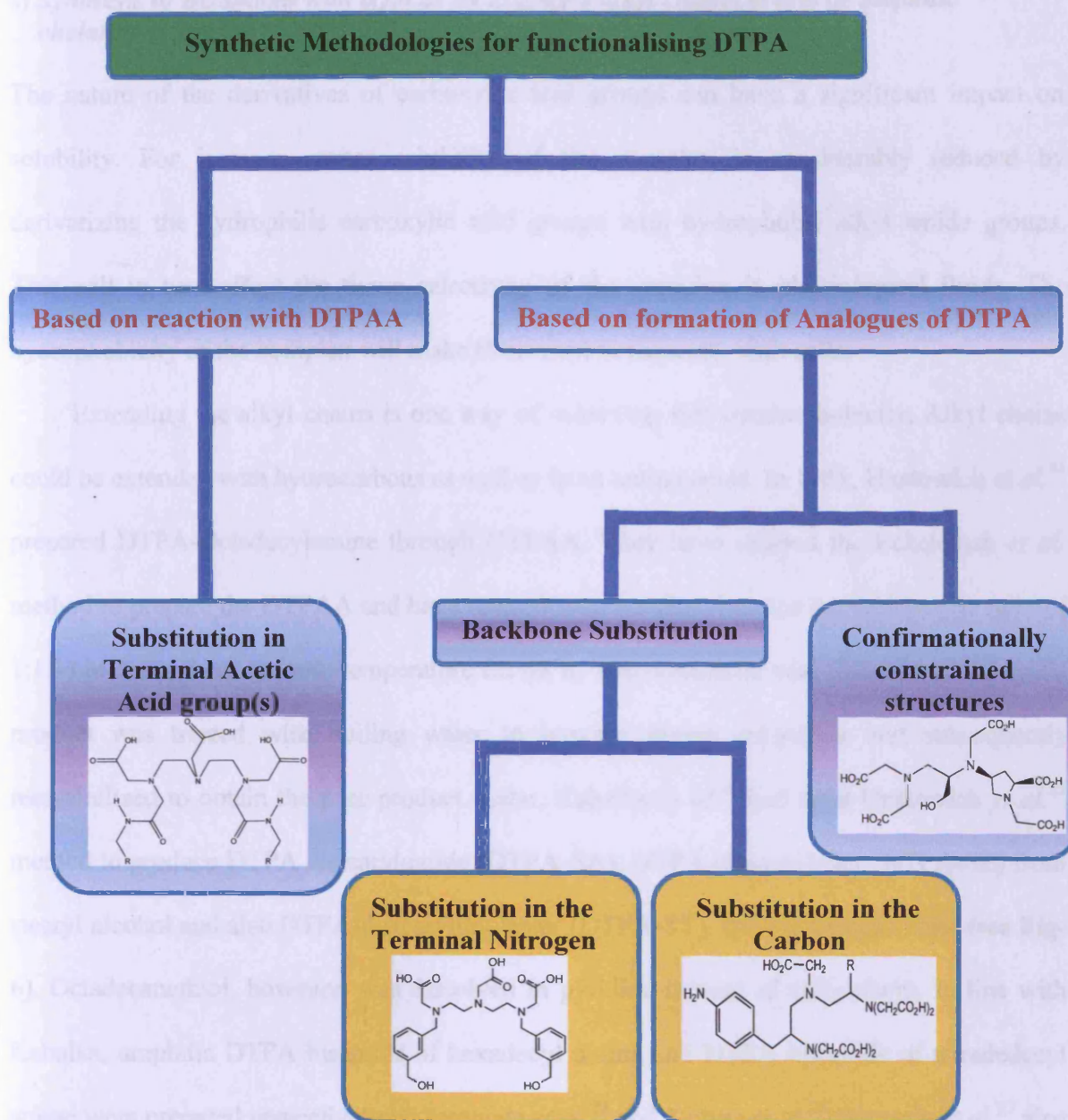


Figure 4:- Schematic representation of various strategies handled to functionalise DTPA

Eckleman's preparation of DTPA bisanhydride (DTPAA)

In 1975, Eckelman *et al.*¹⁹ synthesized DTPAA from DTPA in which DTPA was suspended in pyridine, acetic anhydride was added and the mixture was stirred at 65 °C for 24 hours.

This method is then referenced by many other papers.²⁰

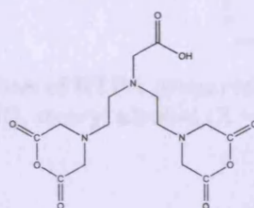


Figure 5:- bis anhydride form of DTPA synthesized by Eckelman *et al* (DTPAA)

a) **Synthesis of Bisamides with a focus on extended alkyl chains to acts as amphiphilic chelating agents**

The nature of the derivatives of carboxylic acid groups can have a significant impact on solubility. For instance, water solubility of the complex is considerably reduced by derivatizing the hydrophilic carboxylic acid groups with hydrophobic alkyl amide groups. This will in turn affect the tissue selectivity of the complex in physiological fluids. The hydrophobicity of the complex will make them tend to associate with cells.

Extending the alkyl chains is one way of achieving this hydrophobicity. Alkyl chains could be extended with hydrocarbons as well as from amino acids. In 1981, Hnatowich *et al.*²¹ prepared DTPA-Octadecylamine through DTPAA. They have utilised the Eckelman *et al.* method to prepare the DTPAA and have reacted with octadecyl amine (stoichiometric ratio of 1:1.1) in chloroform at room temperature for 48 h. The precipitate was filtered and the crude product was treated with boiling water to remove excess anhydride and subsequently recrystallized to obtain the pure product. Later, Kabalka *et al.*²² had used Hnatowich *et al.*²¹ method to produce DTPA distearylamine (DTPA-SA), DTPA distearylester (DTPA-SE) from stearyl alcohol and also DTPA-distearylthiolester (DTPA-ST), from octadecanethiol (see Fig-6). Octadecanethiol, however, was dissolved in pyridine instead of chloroform. In line with Kabalka, amphiphilic DTPA bisamide of hexadecyl amine and DTPA bisamide of tetradecyl amine were prepared respectively by Jasanada *et al.*²³ and Kimpe *et al.*²⁴ Jasanada *et al.*²³ also prepared DTPA-Octadecylamine (see Fig-7), while Kimpe *et al.*²⁴ also synthesized DTPA-BC14, DTPA-BC16 and DTPA-BC18 (see Fig-8).

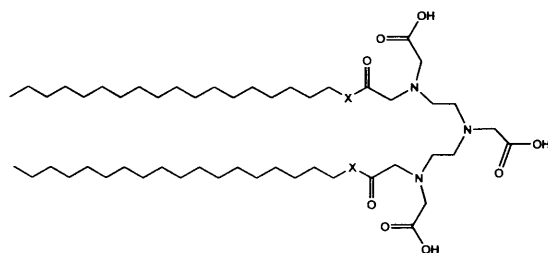


Figure 6:-Amphiphilic derivatives of DTPA prepared via the reaction of DTPAA with Stearylamine (X = NH), stearyl alcohol (X = O), and octadecanethiol (X = S)

Potential Multimodal Imaging Agents

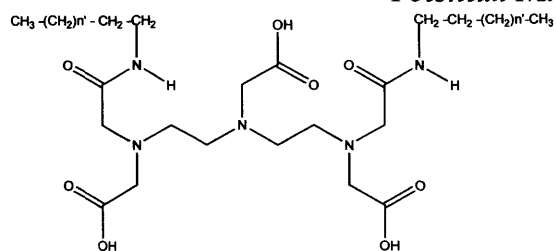
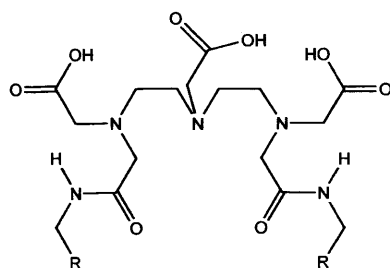


Figure 7:- Depicting DTPA-bis (hexadecylamido), $n'=13$ and DTPA-bis (octadecylamido), $n'=15$



DTPA-BC14, R= C₁₄H₂₉
 DTPA-BC16, R= C₁₆H₃₃
 DTPA-BC18, R= C₁₈H₃₇

Figure 8:- Amphiphilic chelating agents prepared by Kimpe *et al.*

X. Zhao *et al.*²⁵ synthesized amphiphilic ligands from alkyl ester of amino acids, namely tyrosine and phenyl alanine. The ligands diethylenetriamine-*N,N''*-di(acetyl-L-phenylalanine octadecylester)-*N,N,N''*-triacetic acid (DTPA-BPO) and diethylenetriamine-*N,N''*-di(acetyl-L-tyrosine octadecylester)-*N,N,N''*-triacetic acid (DTPA-BTO) were synthesized from DTPAA with L-phenylalanine octadecylester hydrochloride and L-tyrosine octadecylester hydrochloride respectively in pyridine (see Fig-9). Pyridine was used as solvent and as well as the scavenger of hydrochloric acid.

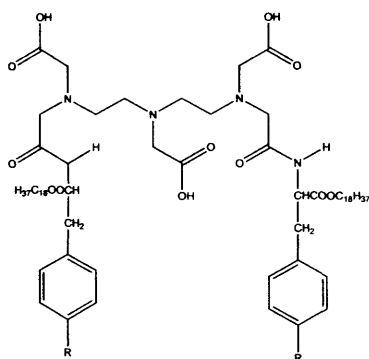


Figure 9:-DTPA based bisamides of L-phenylalanine octadecylester and L-tyrosine octadecyl ester
 Where R =H, DTPA-BPO; R =OH, DTPA-BTO

These long chain amphiphilic derivatives were mostly used to label liposomes. While, the alkyl chain anchors the molecule to the lipid bilayer, the lipophobic DTPA on the surface is exposed for chelation. Hnatowich *et al.*²¹ labelled with ⁶⁷Ga and conducted bio distribution studies, while Kabalka *et al.*²² labelled with Gd and utilised as MRI contrast agents for liver

imaging. Further, X. Zhao *et al.*²⁵ utilised the amphiphilic derivatives to produce lamellar membrane liposomes as drug carriers for the liver. On the other hand, Kimpe *et al.*²⁴ prepared Gd complexes and subsequently incorporated them into mixed micelles to produce supramolecular structures with decreased rotational motion.

c) DTPA based bisamides short chain alkyl amines

DTPA based bisamides of higher alkyl amines and complexation with Fe (III)

In 1987, Quay *et al.*²⁶ described the synthesis of DTPA bisamide (diamido acetyl diethylene triamine triacetic acid) and consequently complexed with Fe (III) chloride to produce, potential, low osmolality contrast agent. DTPAA was added in to 5 percent (v/v) ammonium hydroxide in water and the mixture was refluxed overnight to produce the amide derivative (diamido acetyl–diethylene triamine triacetic acid). The corresponding higher homologs of alkyl amines (dissolved in chloroform) were used to synthesize higher homologs of DTPA bisamides.

The paramagnetic complex has a prolonged circulation time due to its high stability (the stability constant not reported). They have pointed out that the amide contrast agent is less affected by enzymes degradation than simple ion-DTPA chelates (possibly due to increased molecular weight, which prevents immuno recognition²⁷). In addition, the higher homologues of DTPA bisamides tend to be less polar and to bind more to serum proteins, increasing their circulation time further. It was reported that these agents will be appropriate for imaging the hepatobiliary system.

DTPA-bis propylamide and DTPA-propylpolyester

Sherry *et al.*²⁸ synthesised DTPA-bispropylamide (DTPA-PA) (see Fig-10). Isobutylchloroformate and N-propylamine was added dropwise to a solution of dry acetonitrile, DTPAA and triethylamine. The product was obtained on an anion-exchange column. The same procedure was then used to prepare DTPA-propylester (DTPA-PE), except a large excess of n-propanol was added instead of n-propylamine.

Potential Multimodal Imaging Agents

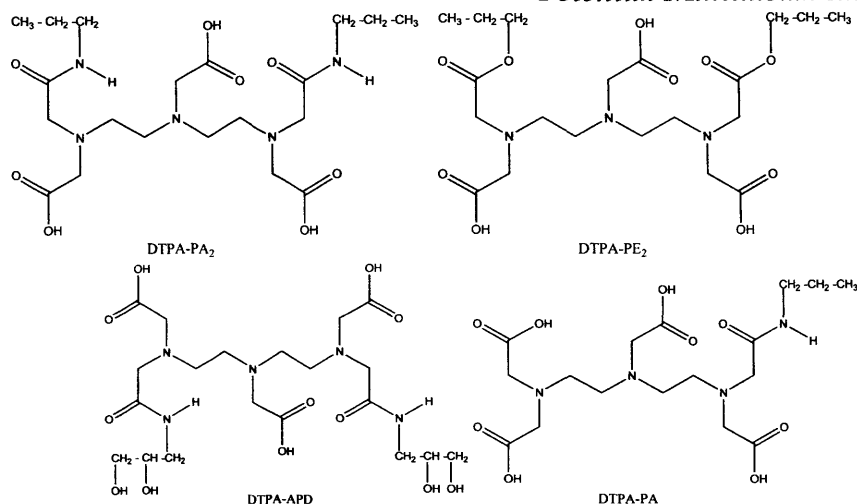


Figure 10:- DTPA based bisamides and esters prepared by Sherry *et al.* including DTPA-PA₂ DTPA-APD was purchased and purified through anion exchange chromatography.

Following Sherry, Konings *et al.*²⁹ synthesized DTPA-Bis(ethylamide) dihydrate (see Fig-11).

Instead of acetonitrile, they have used water as the solvent.

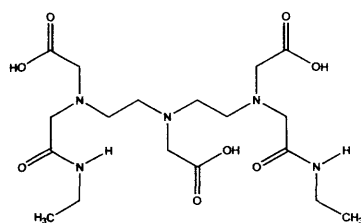


Figure 11:-Synthetic plan for DTPA based bisethylamide followed by Konings *et al.*

While Cacheris *et al.*³⁰ followed Quay *et al.*²⁶ procedure to prepare DTPA bisamide of methylamine, following year Geraldes *et al.*³¹ synthesized DTPA-bis (propylamide) as per the procedure mentioned by Sherry *et al.*²⁸ Vander Elst *et al.*³² synthesized a series of DTPA bisamides by adapting Konings *et al.*²⁹ procedure, reacting DTPAA with ammonia, ethylamine, n-butyl amine and bismethylamine (see Fig-12).

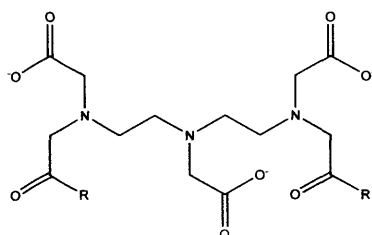


Figure 12:- DTPA bisamides prepared by Vander Elst *et al.*, where R=-NH₂, -NHCH₂CH₃, NH-(CH₂)₃-CH₃ and N(CH₃)₂

In 1995, Geraldes *et al.*³³ employed a slight modification to the procedure of Krejcarek and Tucker³⁴ thereby synthesized a library of DTPA bisamides of alkyl amines. Synthetic procedure undertaken as follows: DTPAA was added to an ice cold, vigorously stirred

Potential Multimodal Imaging Agents

solution of the amine. The reaction mixture was filtered and the crude product was recrystallized. The procedure was utilised to synthesize DTPA-PA, DTPA-MA, DTPA-EA, DTPA-BA, DTPA-HPA, DTPA-MEA, DTPA-NDMA, DTPA-MPEA, DTPA-BHEA and DTPA from their corresponding amines (see Fig-13).

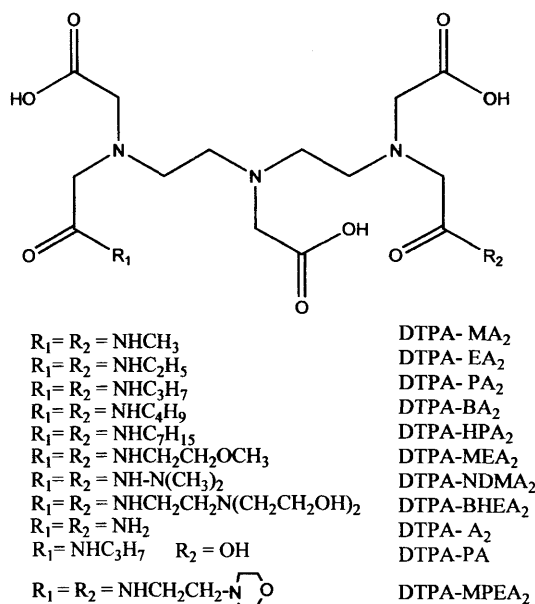


Figure 13:- Depicting various preparations of DTPA bisamides by Geraldès *et al.*³³

The aforementioned bisamides were complexed with lanthanide ions and their lanthanide complexes have been investigated for various purposes by these scientists. Konings *et al.*²⁹ reported that the studies on their Gd complexes have proved the amide carbonyl oxygens play a prominent role in the metal ion coordination. Cacheris *et al.*³⁰ have investigated the relationship between thermodynamics and the toxicity of Gadolinium complexes, while Geraldès *et al.*³¹ studied the structural dynamics of Ln (III) complexes. In a separate research project, Geraldès *et al.*³³ investigated the effects of replacement of the carboxylates with amide groups. They have determined the efficacy of the resulting Gd (III) complexes as contrast agents. The efficacy of these potential agents was studied through the determination of their stabilities and relaxivities. Vander Elst *et al.*³² prepared Dysprosium complexes of their bisamides and investigated the possibility to act as potential negative contrast agents, on the basis of high field effect on the water protons.

DTPA based mono and bis and Tris alkyl amides

In line with Gerald *et al.*³³, a decade later, Jaszberenyi *et al.*³⁵ also investigated the effect of replacement of a carboxylate with an amide group and its impact on the water exchange rate of the gadolinium complexes. Following the procedure of Gerald *et al.*³¹, they, however, have synthesized DTPA-N, N-bis [bis (n-butyl)]-N-methyl-tris (amide) (see Fig-14) instead of DTPA bisamide. Since the amide donor group does not bound to the metal as strongly as carboxylate, steric crowding becomes less prominent. This in turn leads to lowering the water exchange rate. In line with this, they have found that the gadolinium complex of the trisamide derivative have slower water exchange rate compared to gadolinium complex of the bisamide derivative. Investigations also revealed that the rate of water exchange of bis and tris amide derivatives are reduced in comparison to $[\text{Gd}(\text{DTPA})(\text{H}_2\text{O})]^{2-}$. Activation volumes justified a dissociative interchange and a limiting dissociative mechanism

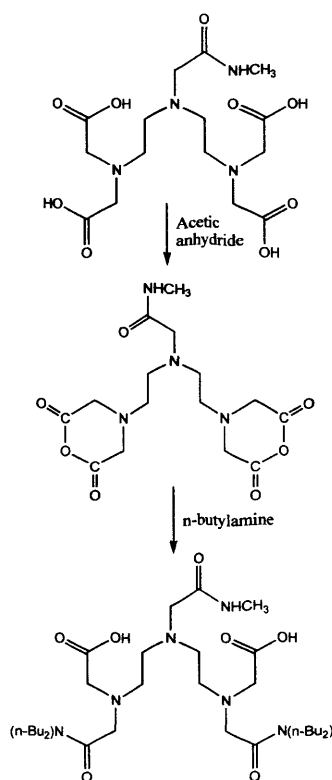


Figure 14:- Synthetic scheme depicting the synthesis of DTPA based Mono ethylamine propylamide

DTPA based bisamides bearing aromatic amines

Apart from aliphatic amines, aromatic amines also employed to produce DTPA based bisamides. In 1995, following the method of Konings, Bligh *et al.*³⁶ synthesized a series of

DTPA bisamide complexes containing, methylene phenyl, and ethylene phenyl side chains along with isopropyl and isobutyl. (see Fig-15).

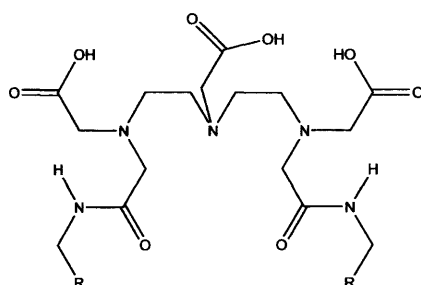


Figure 15:- A representative diagram to show the DTPA bisamides of iso propyl, methylenephenyl and ethylenephenyl. L¹; R-Prⁱ, L²; R-Buⁱ, L³; R-Bz, L⁴; R-Phenyl ethyl

Yun.Ming *et al.*³⁷ also followed the procedure of Konings *et al.*²⁹ and synthesized three DTPA bisamides derivatives of benzyl amine, isopropyl amine and tert-butyl amine (see Fig -16).

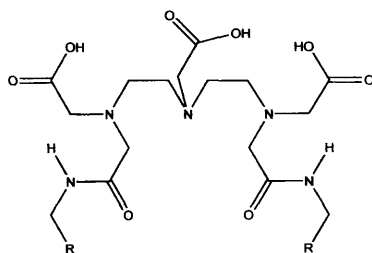
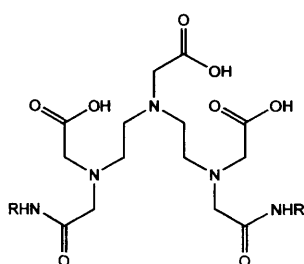


Figure 16:- Depicting DTPA based bisamides of isopropyl amine, tert-butyl amine, Benzyl amine R: CH (CH₃)₂, C (CH₃)₃, and CH₂C₆H₅

As aforementioned, Bligh *et al.* earlier published their work on non-ionic, bulky chelates. Four years later, in an extended series of preparation they have produced DTPA-bisamides containing isopropyl, isobutyl, cyclohexyl, 2-norbornyl, methylnephenyl, ethylene phenyl and 2-ethylhexyl side chains.³⁸ See Fig-17.

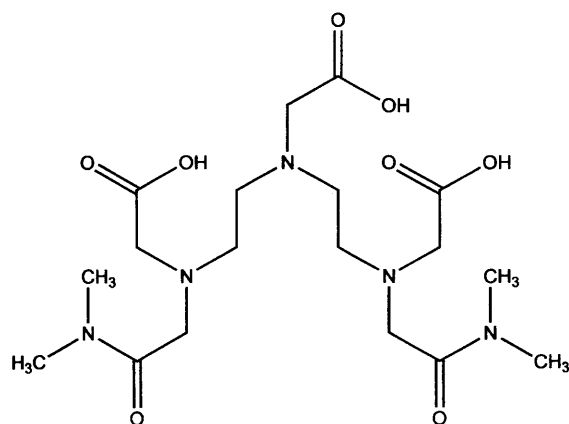


R	Abbreviated name
isopropyl	DTPA-B(iP)A
isobutyl	DTPA-B(iB)A
cyclohexyl	DTPA- B(iCH)A
2-norbornyl	DTPA- B(NB)A
methylenephenyl	DTPA-B(meP)A
ethylenephenyl	DTPA-B(etP)A
2-ethylhexyl	DTPA-B(etH)A

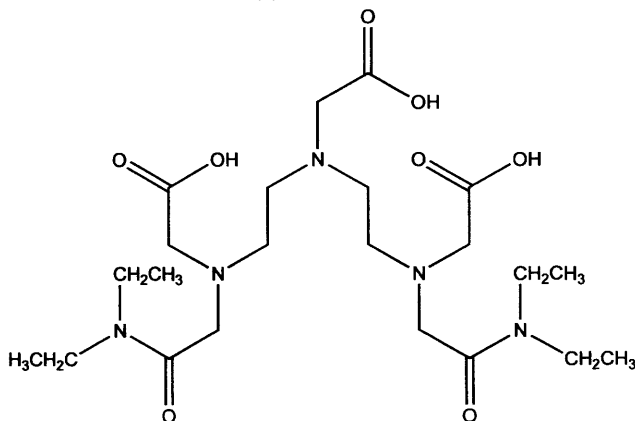
Figure 17:- Series of DTPA based bisamides synthesized by Annie Bligh *et al.*

Feng *et al.*³⁹ prepared a series of DTPA bisamides. Among these DTPA-BIN (see Fig-18)

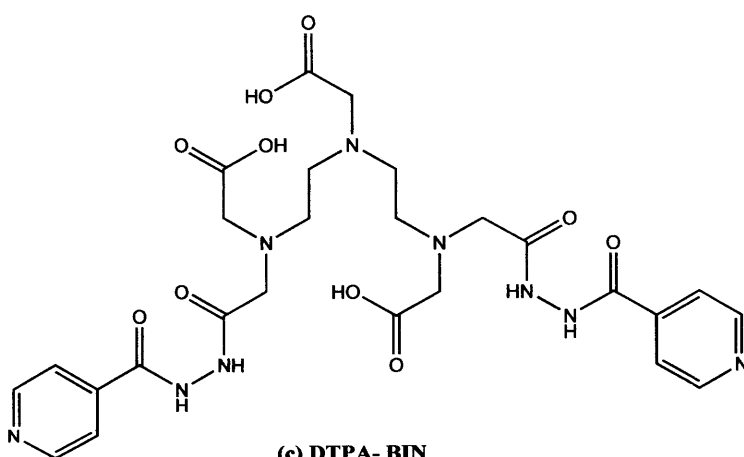
thought to be potential, low osmolality hepatic contrast agents.



(a) DTPA- BDMA



(b) DTPA- BDEA



(c) DTPA- BIN

Figure 18:- Depicting the DTPA bisamides of prepared by Feng *et al.*

Bligh *et al.* carried out a comparative study of the nuclear magnetic relaxation dispersion (NMRD) profiles for their Gd (III) complexes. Later, they have explored the chemistry of their Gd (III) chelates for their target specific ability and relaxation enhancement on water. On the other hand, Yun.Ming *et al.*³⁷ measured the stability and selectivity constants with metal

ions such as Gd (III), Zn (II), Ca (II), and Cu (II) to evaluate the possibility of using the complexes of their bisamides as potential MRI contrast agents.

c) DTPA based alkoxyalkylamides

Aliphatic and aromatic alkoxy alkyl amines was also employed to synthesize DTPA based alkoxyalkyl amides.

Based on aliphatic alkoxy amines

Webber *et al.*⁴⁰ in their patented research described the synthesis of DTPA based alkoxyalkylamides. "Bis[N-(2-methoxyethyl)-carbamoylmethyl] diethylenetriamine-N, N', N"-triacetic acid (see Fig -19) was prepared by a stirred suspension of DTPA-bisanhydride in isopropanol with 2-methoxyethylamine.

This method was also used to prepare other alkoxyalkylamides by reacting methoxy propylamine, methoxybutylamine, ethoxyethylamine, ethoxy propylamine, ethoxy butyl amine with DTPAA (in the stoichiometric ratio of 1:2).

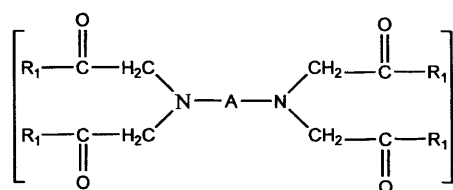


Figure 19:- Representative diagram of DTPA alkoxy amide prepared by Webber where R₁ represents the alkoxy amines.

In their patented research, Delaire *et al.*⁴¹ reported a similar synthesis of DTPA alkoxyalkyl amides but modifying the synthetic conditions. These modifications are suitable for large scale preparations of MRI contrast enhancement agents as claimed by Delaire *et al.*⁴¹ DTPAA was reacted with the primary or secondary amines; alkyl (mono, di and polyhydroxy) and alkoxy amines. Contrary to Webber's procedure they have added co-solvents to this reaction mixture (mostly they have used mixture of IPA /acetonitrile).

DTPA-bis(methoxyethylamide) (MEA), DTPA-bis(methylmethoxyethylamide) (MMEA) and DTPA-bis-(hydroxyethylmethoxyethylamide) (HEMEA) were synthesized by H.Imura *et al.*⁴² They have reacted DTPAA with appropriate amines according to the procedure described by Webber *et al.*⁴⁰ See Fig-20.

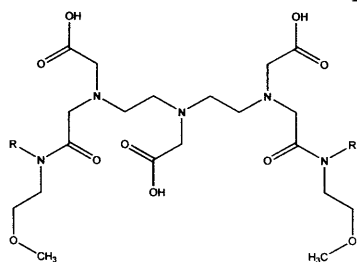


Figure 20:- DTPA based alkoxyalkyl amides prepared by H.Imura *et al.*, where R=H (MEA), R=CH₃ (MMEA), R= C₂H₄OH (HEMEA)

Webber *et al.*⁴⁰ measured the T₁ and T₂ relaxivities of the gadolinium complex of the DTPA bisamide, which were 4.69 and 4.40 mm⁻¹s⁻¹(at 10 MHz, 37 °C) respectively, while H.Imura *et al.*⁴² investigated the thermodynamic parameters. Thermodynamic parameters such as entropies and enthalpies are valuable information in understanding the role of ligand structure in paramagnetic complexes (especially, when investigating complexes useful for MRI). H.Imura *et al.*⁴² attributed the large, positive entropy changes to the bonding between the carboxylate groups and that of Ln (III). Negative enthalpy values have been attributed to the coordination of the nitrogen donors and the amide groups. They also found that two amide groups replace two water molecules upon complexation with Ln (III).

Based on aromatic alkoxy amines

Yun-Ming-Wang *et al.*⁴³ reported the synthesis of DTPA bis amide derivatives of adamantanamine, 2-methoxybenzylamine and 2-methoxyphenethylamine. They have once again used the procedure of Konings *et al.*²⁹ (with slight modification to that they have done in the previous year) (see Fig-21).

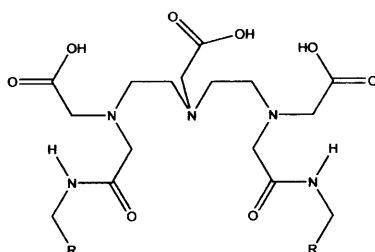


Figure 21:- DTPA based bisamides adamantanamine, methoxybenzylamine and 2-methoxyphenethylamine

Later, Yun-Ming Wang *et al.*⁴⁴ synthesized diethylenetriamine-N,N,N-triacetic-N,N-bis(2-methoxyphenethylamide) (see Fig-22). In fact they prepared DTPAA as described by Eckelman *et al.*¹⁹ and have reacted with 2-methoxyphenethylamine, according to the

procedure described by Konings. They have used DTPAA and amine in 1:3 stoichiometric molar ratios, instead of 1:2 used by Konings.

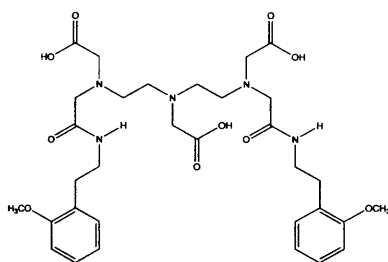


Figure 22:- DTPA based bisamide of diethylenetriamine-N, N, N-triacetic-N, N- bis (2-methoxyphenethylamide)

Yun-Ming-Wang *et al.*⁴³ in their previous project utilised their bisamides to study the interaction of those bisamides with metal ions such as Gd (III) and its competing endogenous cations (Zn (II), Ca (II), Cu (II)) towards producing a potential MRI contrast agent.

In the present project,⁴⁴ however, they have utilised their bisamide to prepare complexes of gadolinium and its interaction with bovine serum albumin (BSA). They suggested that the observed relaxivity increase may be assigned to the ability of the methoxy functional group to support network hydrogen bonded water molecules in the second coordination sphere of the Gd (III) ion, nearer to the surface of the BSA. This is further justified by the possibility to exclude the change in the coordination number of the metal ion (upon interaction of the complex with BSA). They also investigated the ¹⁷O NMR shifts of the dysprosium complexes

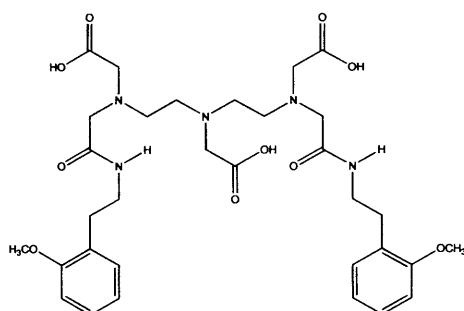


Figure 23:- DTPA based bisamide of diethylenetriamine-N, N, N-triacetic-N, N- bis (2-methoxyphenethylamide)

d) DTPA based Phenyl amides

DTPA based bisamide of benzyl amine as a chelating agent for MRI contrast agent

Aime *et al.*⁴⁵ attempted to produce a low osmolality paramagnetic contrast agent, which was reported in 1997. They synthesized bis (benzylamide) diethylenetriaminepentaacetic acid

(BBA-DTPA) and its Gd (III) and Lu (VI) complexes. DTPAA and benzyl amine was reacted together in DMSO at room temperature. Acetone was used to remove excess DMSO during the work up. Among the three factors (high relaxivity, thermodynamic stability and water solubility), water solubility is drastically reduced by the introduction of hydrophobic substituents. DTPA-Bisphenylmethyl amide was found to increase the water solubility of the paramagnetic chelate than DTPA-Bisphenylamide (i.e. from 0.049M-0.08M at 25 °C).

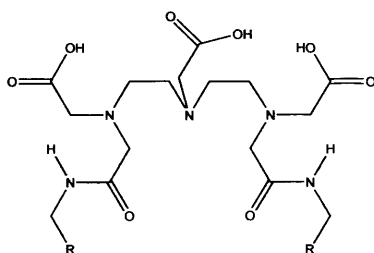


Figure 24:- DTPA bisamides of benzyl amines and methyl benzyl amine where R =CH₃, R=Phenyl, R=Phenyl methyl

DTPA-bis (benzylcarbamoylmethyl) amide derivative

The prominent role played by yttrium in the field of radio immunotherapy attracted the attention of David Parker⁴⁶ and his colleagues. Therefore in order to carry out investigations, they also synthesized N,N'-bis(benzylcarbamoylmethyl)-N,N,N''-diethylenetriaminetriacetic acid (see Fig-25). Synthetic procedure followed could be summarised as follows. DTPAA was reacted with benzyl amine, using pyridine as solvent. Precipitate obtained upon pH adjustment (3.5) was further washed with diluted hydrochloric acid. The obtained crystal structure of yttrium complex revealed the amide carbonyl ligation occurs in a distorted mono-capped square-antiprismatic structure. This also indicated only one water molecule bound to the metal.

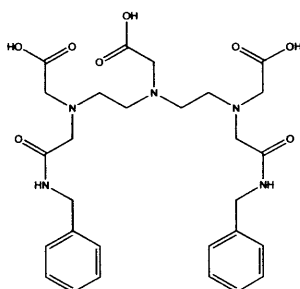


Figure 25: - DTPA bisamides of methyl benzene synthesized by David Parker *et al.*

DTPA based bisamide of (3-aminophenyl) boronic acid

Aime *et al.*⁴⁷ investigated paramagnetic probes with regard to their application in clinical chemistry (determination of analytes concentration). These paramagnetic probes could influence the relaxation properties of the solvent water protons. This in turn is dependent on the degree of interactions of these probes with the analytes. Therefore this interaction facilitates the determination of analytes concentration (10^{-4} - 10^{-5} M). They have synthesized a suitable functionalized derivative of the DTPA-gadolinium complex. They have prepared 6-(carboxymethyl)-3,9-bis((N-3-boroxylphenyl)carbamoyl)methyl)-3,6,9-triaundecanedioic acid. DTPAA was reacted with (3-aminophenyl) boronic acid sulphate in DMSO. Stability constant measured was $1.1 \times 10^{17} \text{ M}^{-1}$.

They measured the proton relaxation times of solutions of bisamide (0.56 mM) comprising variable concentrations of human serum albumin at various degrees of glycation (measured by fructosamine method).

A good linearity between the relaxivities and albumin fructosamine concentration also was reported. This in turn justifies the ability of the method to probe and determine glycosylated proteins.

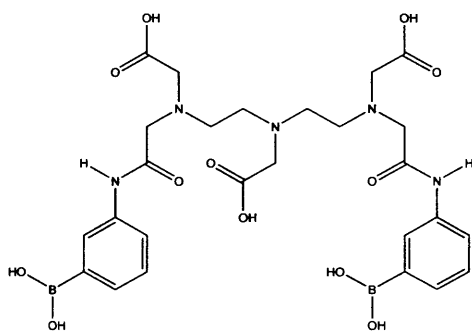


Figure 26:- DTPA based bisamide of (3-aminophenyl) boronic acid

The T_1 relaxivity reported by Aime *et al.* for the Gd complex of this DTPA based bisamide of (3-aminophenyl) boronic acid is slightly less than ($4.6 \text{ mM}^{-1}\text{S}^{-1}$ (at 20 MHz, 25 °C)) that of their previously reported gadolinium complex (Gd (III) DTPA-BBA), which has enjoyed $4.78 \text{ mM}^{-1}\text{S}^{-1}$ (at 20 MHz, 25 °C).

DTPA based bisamide of isoniazid

More recently, in an attempt to decrease the side effects associated with hyperosmolality and to improve the tissue- and/or organ-specificity of the paramagnetic chelates, Zhang *et al.*⁴⁸ prepared a novel DTPA based bisamide. Taking into consideration, that isoniazid is a very useful medicament to treat tuberculosis and its excellent solubility in water they have designed and synthesized a novel ligand from DTPA and isoniazid. DTPAA was reacted with isoniazid in pyridine. The novelty of the ligand was justified by its high T_1 relaxivity ($6.08 \text{ mM}^{-1}\text{S}^{-1}$ (at 20 MHz, 25 °C) high thermodynamic stability ($10^{20.84}$) and also by its high affinity for serum proteins (upon protein binding, T_1 relaxivity was $9.09 \text{ mM}^{-1}\text{S}^{-1}$ (at 20 MHz, 25 °C)).

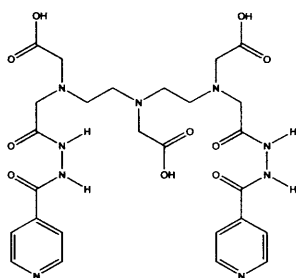


Figure 26:- Synthetic scheme of DTPA based bisamide of Isoniazids

DTPA based bissulphonamides

In 2000, Scozzafava *et al.*⁴⁹ had prepared a series of DTPA based bissulfonamides (see Fig-27). They have shown that the Zn complexes of these derivatives have topical antiglaucoma properties. The method used was as follows. DTPAA was added to a solution of 4-(2-aminoethyl)-benzene sulphonamide dissolved in anhydrous dimethylformamide. The mixture was stirred at room temperature for 4 h. Then it was poured in to large excess of dichloromethane and the solid obtained was filtered and washed with dichloromethane and acetone. The crude product was purified by HPLC.

Potential Multimodal Imaging Agents

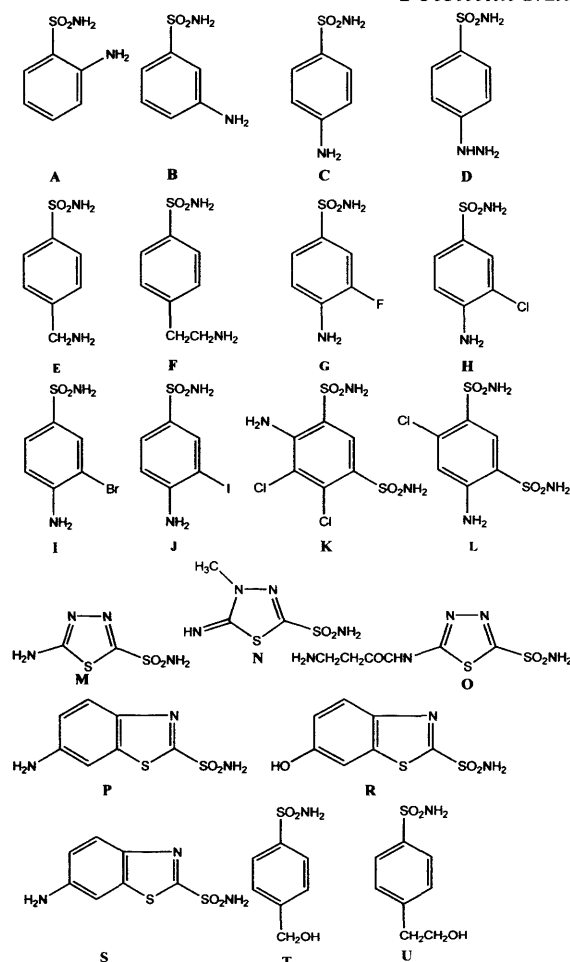


Figure 27:- A Library of DTPA based Sulphonamides

3.1.7 Creating DTPA functionality- A Retro synthetic approach

The most commonly used method for attaching DTPA chelates to other molecules involves the reaction between the cyclic bisanhydride and an amine residue on the target molecule. The stability constant, K , of the resulting carboxamide-derivatized metal chelate can be lower than that of the parent carboxylate by several orders of magnitude. For instance Gd(DTPA) is more stable than Gd(DTPA-BMA) by a factor of $10^{2.9}$ at pH 7.4. Another disadvantage of the carboxamide-derivatized metal chelate is their reactivity towards water in the aqueous solutions, in which the anhydride and bio molecule are frequently coupled. To circumvent this challenge, large excess of the anhydride must be used. More over, the bisanhydride contains two identical reactive groups and should be viewed as a potential cross-linking reagent⁵⁰ and also leads to denaturation of the antibody.

A plausible solution to these difficulties is a well-characterized metal chelate bearing a reactive functional group, such as an isothiocyanate, through which the chelate, with its full complement of carboxylates, may be attached to another molecule.

The potential utility of radioisotope conjugates (in both the detection and treatment of neoplastic disease) leads to the discovery of many synthetic approaches, specifically linking radionuclide to Immunoglobulin. Further this is best achieved by the use of “bifunctional” chelating agents (hence, molecules possessing both an array of metal binding groups (i.e., a chelating function) and an additional moiety through which the chelating portion of the molecule may be covalently linked to a protein (i.e., a protein-reactive function)). Most work to date has employed DTPA as the bifunctional chelator, methods having been developed; seek to use one of the five carboxymethyl groups in forming an amide bond to the antibody while the other four remain available for metal binding. Bifunctional chelating agents that incorporate a unique protein-reactive site should avoid a potential cross linking problems.

There are several such systems known to date. Tracing back the history of synthesizing analogues of DTPA, initially leads on to the work of Sunberg *et al.*⁵¹. They have synthesized EDTA derivative bearing a p-amino phenyl substituent, the details of which had been discussed in **Chapter 2**.

3.1.7.1 DTPA analogue through backbone substitution

Prior syntheses of functionalized DTPA analogues have two kinds of sub strategies. First is to place a p-nitro benzyl group at the methylene of a terminal acetic acid. Second is to have it on the diethylenetriamine backbone.

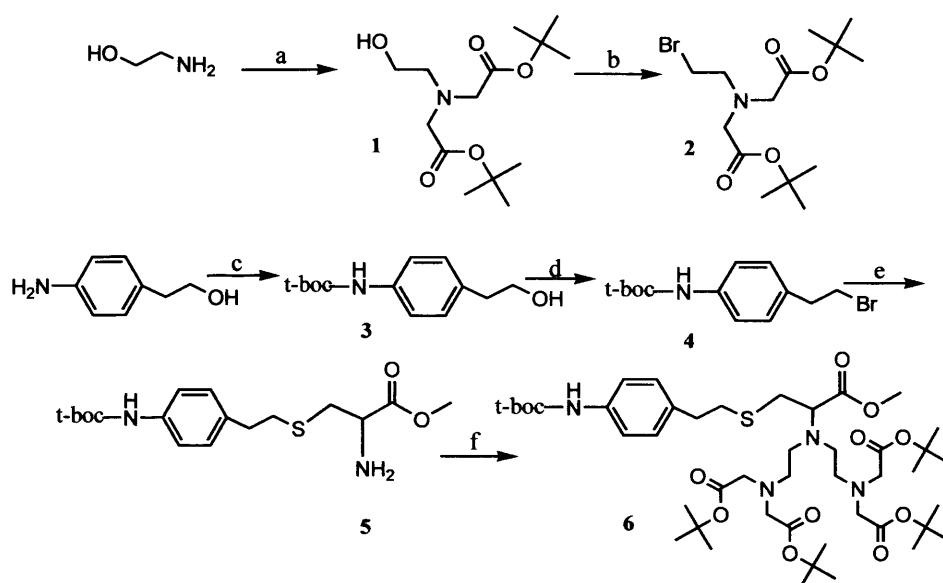
3.1.7.1.1 Substitution in the Central Nitrogen

1. Through central acetic acid arm with amino acids

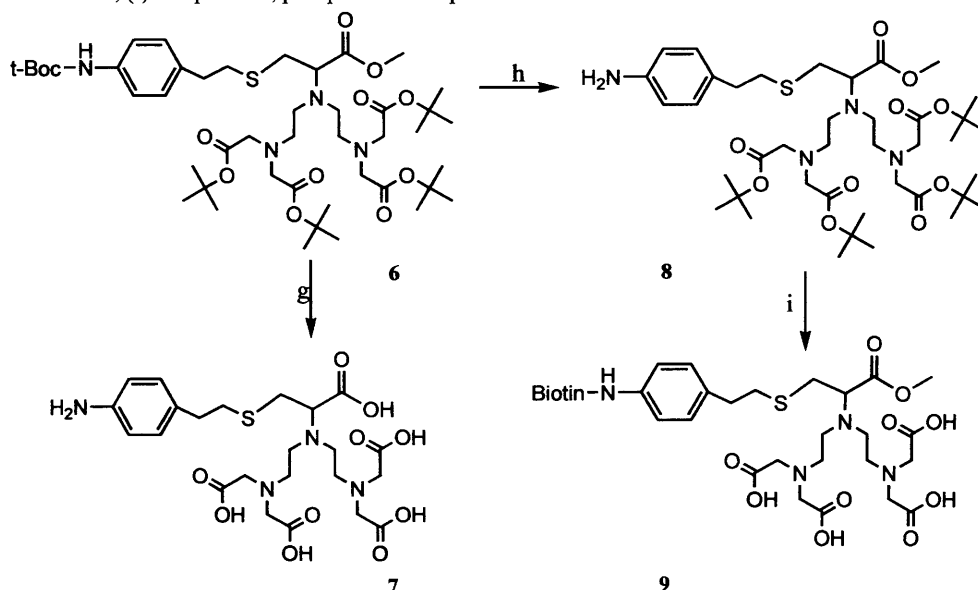
The central acetic acid group of the parent DTPA structure would bear the functional group. By placing the branching group on this central acetic acid, certain symmetry would be retained in the ligand arms. In addition, depending on the selection of amino acid, it is convenient to have various functionalities.

DTPA analogue from L- cysteine

For instance, Choi *et al.*⁵² synthesised a DTPA analogue which is derived from L-cysteine via N-dialkylation, using a bromide equivalent to **2**, with R = t-butyl groups. The reaction method was very long, and is shown in scheme 2(see Fig-28). Compound **6** was obtained as pale yellow oil. From **6**, the t-butyl and t-boc groups could be removed, or further functionality could be added. In this case it was attached to biotin.



Scheme 1: Reaction pathway of the cysteine based DTPA. Reagents and conditions; (a) $\text{BrCH}_2\text{COOtBu}/\text{K}_2\text{CO}_3/\text{DMF}/\text{RT}, 48 \text{ h}$; (b) $\text{NBS}/\text{PPh}_3/\text{CH}_2\text{Cl}_2/0^\circ\text{C}, 2 \text{ h}$; (c) $(\text{Boc})_2\text{O}/\text{TEA}/\text{CH}_3\text{OH}$; (d) $\text{NBS}/\text{PPh}_3/\text{CH}_2\text{Cl}_2/0^\circ\text{C}$; (e) Cysteine methyl ester/ $\text{NaOCH}_3/\text{CH}_3\text{OH}/\text{RT}$; (f) Compound **2**, phosphate buffer $\text{pH}=8/\text{RT}$.



Scheme 2: Hydrolysis and biotinylation of the DTPA derivatives. Reagents and conditions; (g) $\text{C}-\text{HCl}/70^\circ\text{C}/1 \text{ hr}$; (h) $3\text{M HCl}/\text{Ethylacetate}/\text{RT}, 30 \text{ h}$; (i) Biotin/TBTU/TEA/ $\text{CH}_2\text{Cl}_2/\text{RT}$ and $2.\text{C}-\text{HCl}/70^\circ\text{C}$.

Figure 28:- Synthetic scheme depicting the preparation of biotinylation of the DTPA Derivatives

DTPA analogue from L-phenylalanine

Syed *et al.*⁵³ have chosen a different strategy for backbone, by modification of DTPA. It was

Syed *et al.*⁵³ have chosen a different strategy for backbone, by modification of DTPA. It was based on the stereospecific displacement of triflate group of a 2-hydroxycarboxylic acid ethylester with amino group of p-nitro-L-phenylalanine methyl ester under complete inversion of configuration. Further these derivatives have not been prepared in enantiomerically pure form.

Therefore, Williams and Rapport⁵⁴ devised a strategy to produce DTPA analogues in pure forms, from amino acids. They have proposed the N-alkylation strategy as depicted in Fig-29 and Fig-30. The stepwise synthesis of 10, (see Fig-29) invokes the freedom of selection for carboxyl protecting groups. This will in turn facilitate deprotection and any further modifications. The position of this substituent can have important effects on confirmation and stability of the resulting metal chelate.

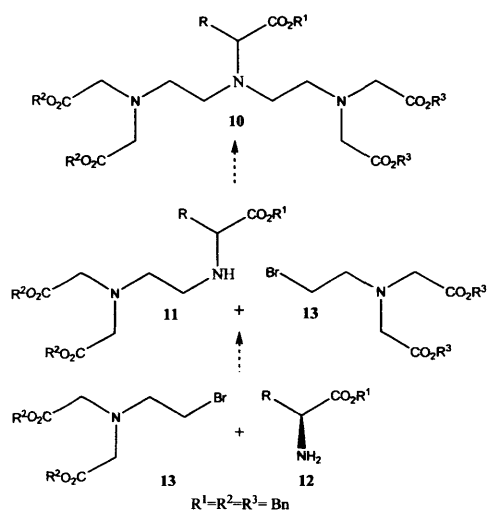


Figure 29:- Alkylation strategy devised by Williams and Rapport

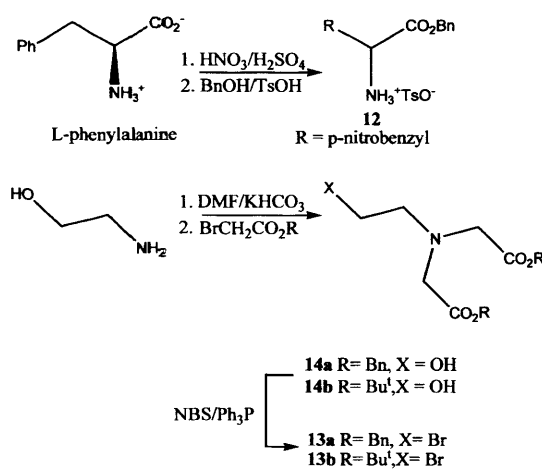


Figure 30:-Preparation of bromoderivative and alcohol derivative.

DTPA analogue from L-glutamic acid and L-lysine

Five years later, after Williams and Rapport, Anelli *et al.*⁵⁵ came up with an exciting approach. Anelli *et al.* synthesized DTPA analogue, starting from L-glutamic acid and L-lysine. They have discovered using such methodology, and suitable protections, conveniently yield DTPA Pentaesters. The following is a brief account of their methodology.

1-tert-Butyl 5-benzyl diester reacted with bromide 2 to afford hexaester. The isolation of 16 in fair yields is related to the easy lactamization of both 15 and the monoalkylated intermediate.

Potential Multimodal Imaging Agents

The dialkylation of **15** was carried out in homogenous phase, eliminating the need for two-phase conditions (as proposed by Rapport *et al.*) and proved to be the best. The cleavage of the benzyl ester protection of **16** by hydrogenolysis yielded the monoacid pentaester **17**. On the other hand, to obtain a DTPA pentaester with a free amino group, commercially available N6-Cbz L-lysine was esterified in tert-butyl acetate to afford **18**. Subsequent dialkylation with bromide **2** afforded protected pentaester **19**. Removal of Cbz moiety by hydrogenolysis yielded the amino pentaester **20** (see Fig-31). Pentaesters **17** and **20** can be easily reacted with substrates containing amino or carboxylic functionalities respectively and subsequently, the tertbutyl ester groups can be removed using routine methodologies. It was further established by Rapport, that there was no racemisation observed under the reaction conditions which they developed for the dialkylation of amino esters.

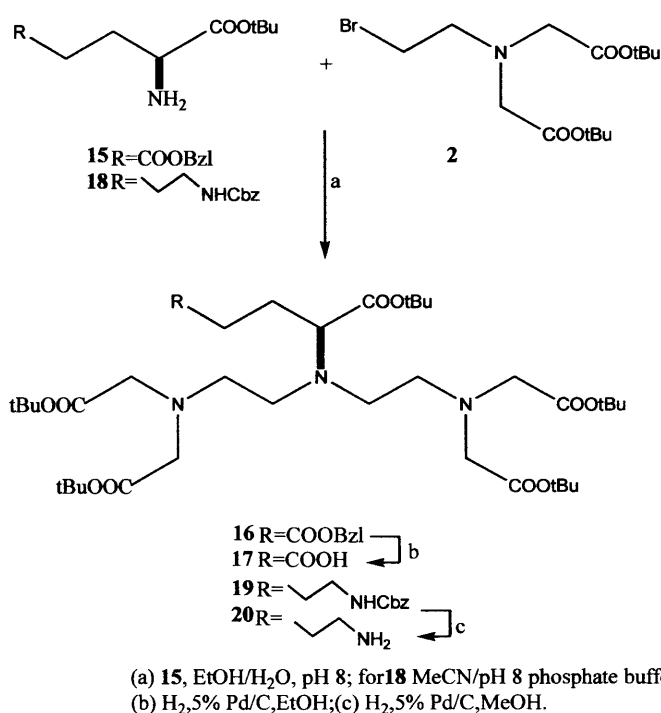


Figure 31:- DTPA analogue prepared by versatile bromoderivative.

II. Directly substituted central nitrogen in the backbone

In 2005, TimStorr *et al.*⁵⁶ had been attracted by the usage of NO scavengers in cancer treatment. As such, they have designed a DTPA analogue which could satisfy the above objective. Following a similar synthetic strategy to that developed by Williams and Rapport, they have synthesized a DTPA analogue bearing an ethyl group on the central amine. Two equivalents of compound **21** were reacted with ethylamine to afford the protected form of

DTPA analogue. The standard TFA hydrolysis of the tert-butyl ester groups afforded compound **24** (see Fig-32).

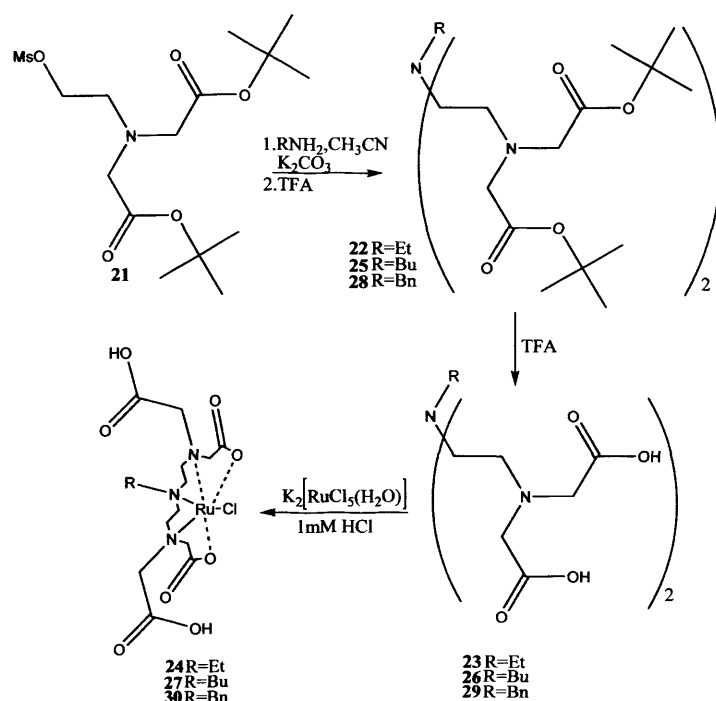


Figure 32:- Centrally functionalised DTPA analogue

3.1.7.1.2 Substituted Terminal nitrogen

I. Substitution through terminal acetic acid arm

Westerberg *et al.*⁵⁷ synthesized a p-isothiocyanatobenzyl moiety attached at the methylene carbon atom of one of the carboxymethyl arms. They have initially started with o-nitrophenyl pyruvic acid. The reductive alkylation and subsequent carboxymethylation steps, ended up in o-nitro benzyl analogue. Upon reduction of the nitro group, the product obtained as a six-membered lactam. Thereafter, to overcome this problem, they reinitiated the synthesis, starting with p-nitrophenyl pyruvic acid. This was obtained by acid hydrolysis of the azalactone, which was in turn obtained from the reaction of p-nitrobenzaldehyde with acetyl glycine. Intramolecular condensation during the carboxymethylation, leading to the formation of a lactam also proved to be a problem. In order to circumvent these problems, the secondary nitrogen atom of diethylenetriamine was first protected with a diethylacetamidemoiety which was eventually hydrolyzed to form the fifth carboxymethyl arm, through the alkylation and subsequent reduction steps. The reduction of the nitro benzyl

substituted chelators and the subsequent transformation into the ultimate protein-reactive forms were carried out according to a known procedure.⁵¹ (see Fig-33)

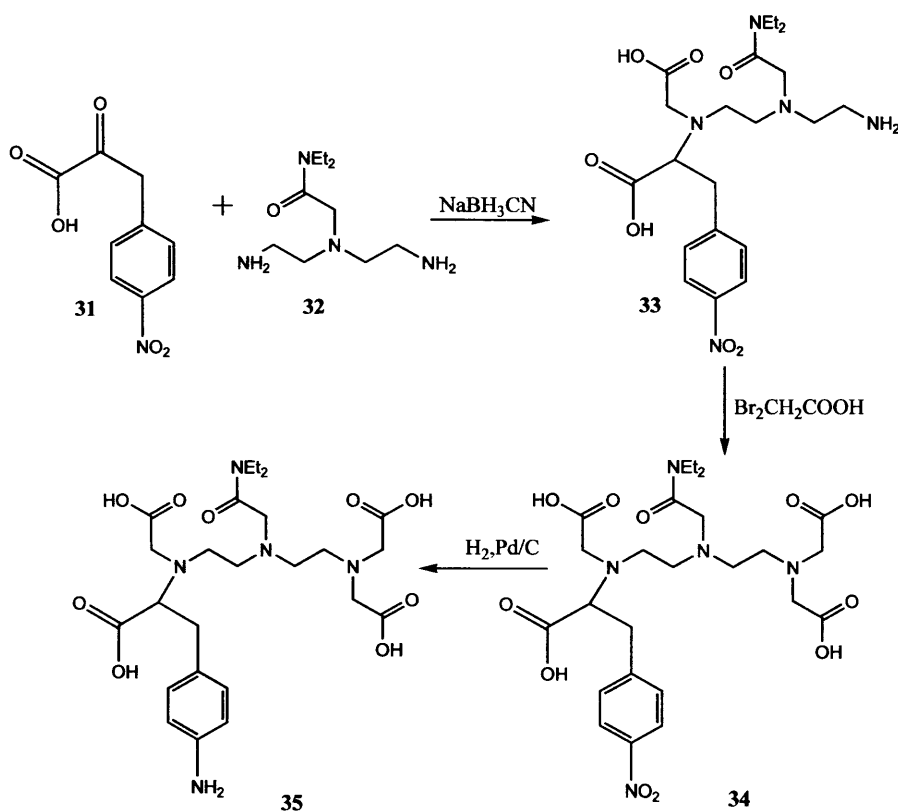


Figure 33: -P- iso thiocynato of benzyl group attached to terminal carboxyl arm of DTPA analogue

In the following year, Keana *et al.*⁵⁸ have investigated a more convenient route to synthesize DTPA analogue. They have synthesized this DTPA analogue to be utilised as a potential contrast agent. Initially, pentamethyl ester was prepared by reacting DTPA with SOCl_2 in methanol. To which aromatic moiety was introduced through the addition of lithium diisopropyl amide (LDA), benzyl bromide and HMPA. Thereafter, nitration and the subsequent conversion to aniline moiety were carried out along with the conversion of ester groups in to their lithium salts. After which amine group on the aromatic moiety was converted to isocyanate group (see Fig-34). Subsequent complexation with gadolinium trichloride yielded the derivative in the form of a sodium salt.

Potential Multimodal Imaging Agents

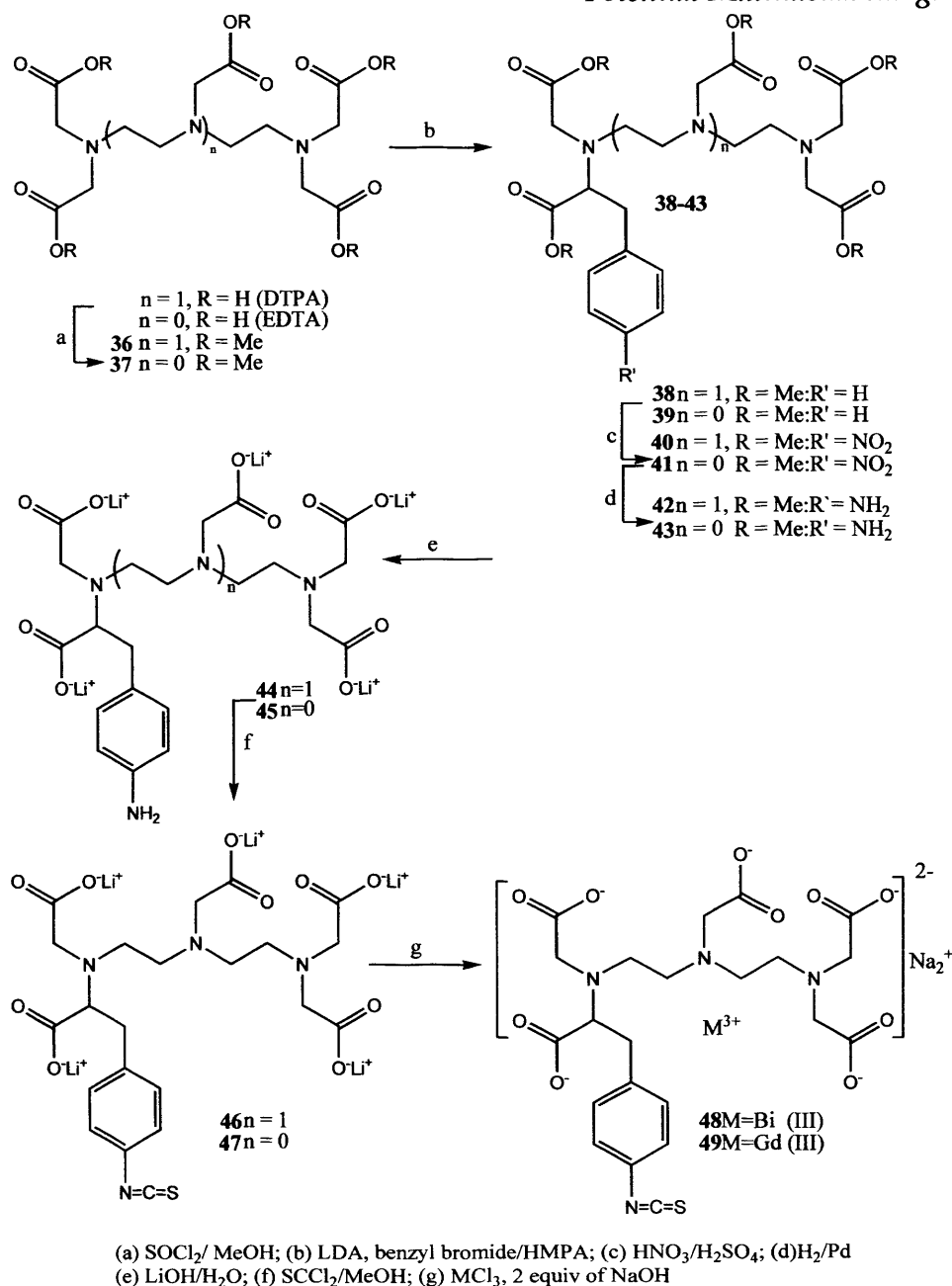


Figure 34:- DTPA analogues prepared by Keana *et al.*, P-isothiocyanatobenzyl terminal Carboxyl arm

Laurent *et al.*⁵⁹ discussed two methods for inserting a Bz group onto the 2-position of DTPA.

The first method involved reductive amination of a protected diethylenetriamine derivative with a α -keto acid and the second method is the mono-deprotection of protected DTPA, followed by alkylation. The first method involves producing the DTPA from a terminally Boc-protected diethylenetriamine. The central N atom of the DTPA backbone is alkylated and then reductive amination is carried out (see Fig-35a). The product is then alkylated with 2-bromoacetic acid and undergoes ester hydrolysis under alkaline conditions to give ligand 50. An issue found with this method was that the complex mixture of products, required

purification by HPLC. Therefore they have devised a second route which is similar to the method used by Keana *et al.* (see Fig-35b).

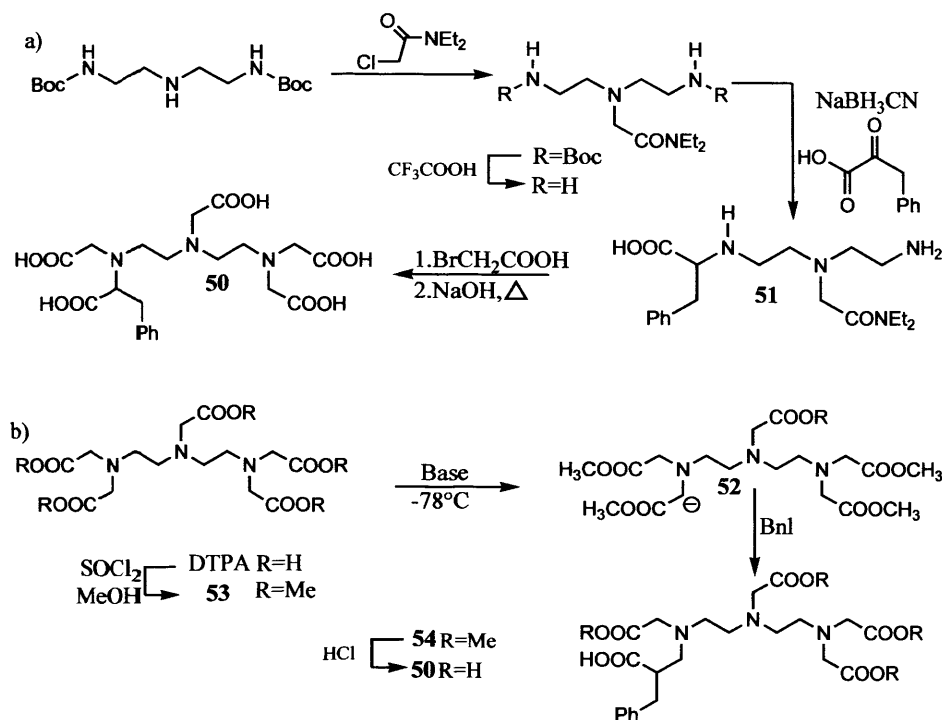
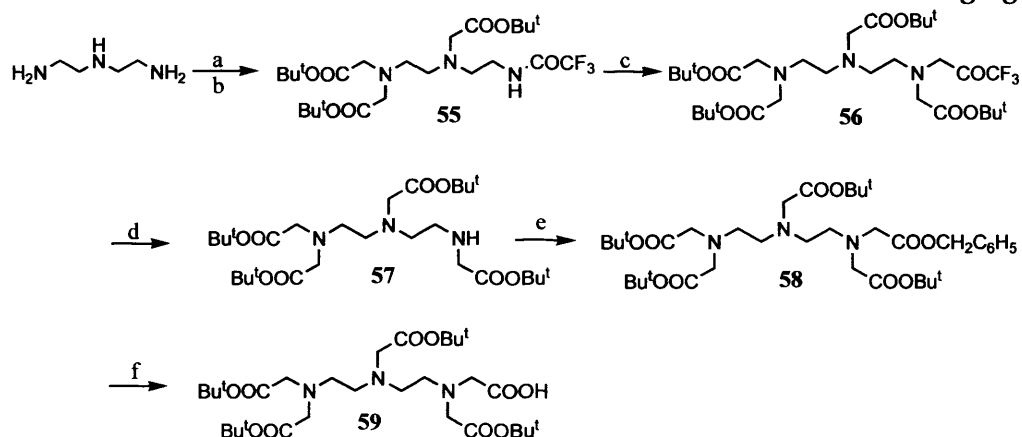


Figure 35: - Depicting two different approaches handled by Laurent *et al.* (a, b) for inserting Bn group in the 2- position of DTPA

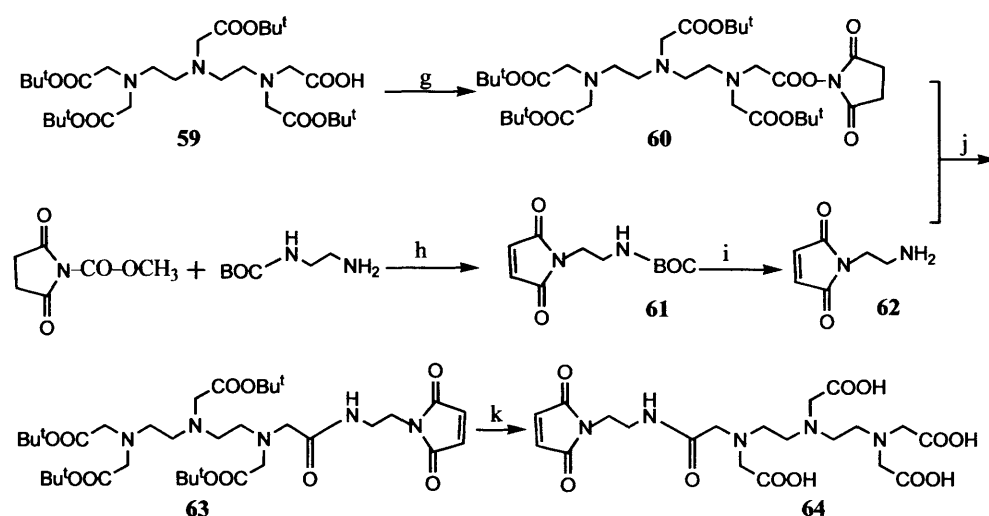
II. Substitution through Terminal carboxylic arm

Arano *et al.*⁶⁰ synthesized the monomaleimide derivative of DTPA (MDTPA, compound 64 in Fig-36) according to the procedure outlined in Fig-36. The synthesis of the compound requires the selective reactivity of only one of the five carboxylate groups.

Potential Multimodal Imaging Agents



Reagents:(a) $\text{CF}_3\text{COOC}_2\text{H}_5$; (b) $\text{BrCH}_2\text{COOBu}^t$, $i\text{Pr}_2\text{NEt}$;(c) $\text{BrCH}_2\text{COOBu}^t$, NaH ;(d) NH_2NH_2 , Bu^tOH ;(e) $\text{BrCH}_2\text{COOCH}_2\text{C}_6\text{H}_5$, $i\text{Pr}_2\text{NEt}$; (f) Pd/C , H_2 .



Reagents:(g) dicyclohexylcarbodiimide, N-hydroxysuccinimide;(h) NaHCO_3 ;(i) CF_3COOH ;
 (j) $i\text{Pr}_2\text{NEt}$;(k) CF_3COOH .

Figure 36:- Synthetic scheme depicting the synthesis of mono maleamide derivative

DTPA analogue bearing two identical groups targeted for sialic acid

Frullano *et al.*⁶¹ produced a potential contrast agent which could detect sialic acid. For which they have successfully synthesized the ligands **70** and **71** (see Fig-37), which are both composed of a central lanthanide-chelating unit flanked by two identical groups designed to interact with sialic acid. Ligand **70** was synthesized from tris-(2-aminoethyl) amine (TREN). Two of the three amine functions of this compound were protected with tert-butoxycarbonyl (Boc) groups by a known procedure⁶² which gave compound **65**. Treatment of **65** with 2-methylthio-2-imidazoline hydro iodide by refluxing in ethanol, followed by deprotection of **66** with HCl afforded **67**. The boronic acid function was introduced by reductive amination of **67** with 2-formylphenylboronic acid and sodium borohydride, which led to a mixture of mono and bis-substituted derivatives of **67**. The mixture was then separated by ion exchange

Potential Multimodal Imaging Agents

chromatography. **70** was obtained by condensation of **68** with DTPAA in ethanol. The bis-Boc-protected precursor of ligand **71** was synthesized by a published procedure.⁶³ Deprotection by treatment with TFA gave **69** almost quantitatively. Ligand **71** was obtained by reductive amination of **69** with excess 3-formylphenylboronic acid and sodium borohydride.

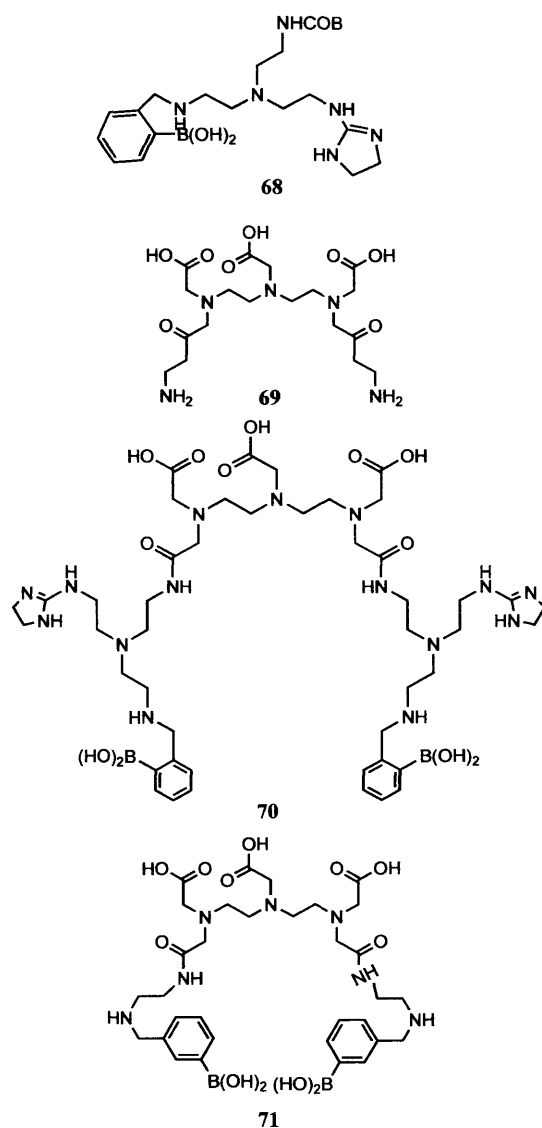
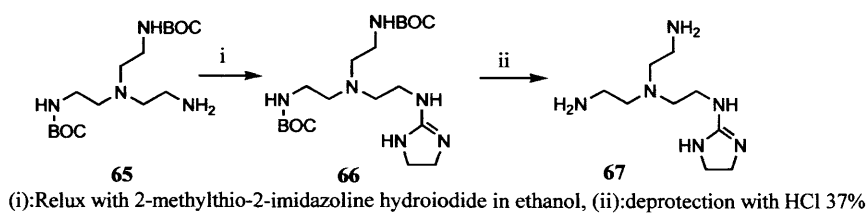


Figure 37:- DTPA prepared with boronic acid towards detecting sialic acid

III. Through direct substitution of the terminal nitrogen

DTPA analogue from Tren

In 2003, Couchet *et al.*⁶⁴ have synthesized a bifunctionalised DTPA analogue by means of a synthetic procedure containing three-step sequence. The reductive amination of diethylenetriamine with 2,2-bipyridine-5-carboxaldehyde was carried out. Thereafter trialkylation of the secondary triamine followed with deprotection of t-butyl ester groups, yielded the bifunctionalised ligand (see **Fig-38**). Alternatively, they have used the DTPAA to prepare the same ligand. They investigated the luminescence properties of the europium complex in aqueous media.

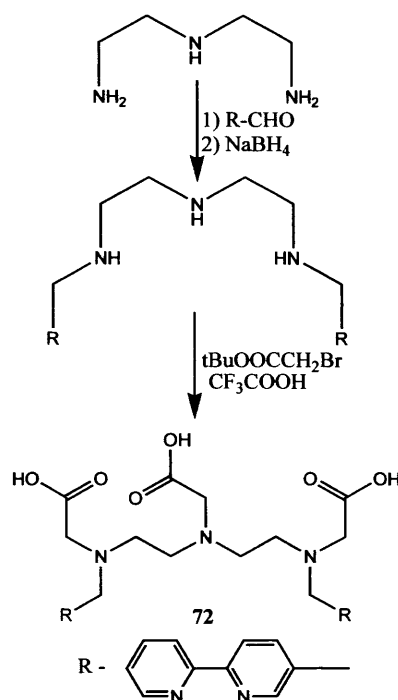


Figure 38:- Bipyridine functionalised DTPA analogue

DTPA analogue from 2, 6- di (hydroxymethyl) pyridine

Artali *et al.*⁶⁵ reported an alternative strategy to incorporate functionality to the terminal nitrogen of the diethylene triamine backbone, in that, 2,6-di(hydroxymethyl)pyridine was used to initiate the synthesis. The reaction pathway is shown in **Figure-39**. 2,6-di(hydroxymethyl)pyridine was monooxidised and reacted with 1, 4, 7-triazaheptane in dichloromethane to give a diimine **75**. This was reduced with NaBH₄ in refluxing ethanol, leading to the isolation of the derivative **76**, which was then alkylated with t-butyl bromoacetate under basic condition to produce **77**, and then **78** was produced with

trifluoroacetic acid, followed by evaporation in vacuum and treatment with diethyl ether to induce precipitation of the ligand.

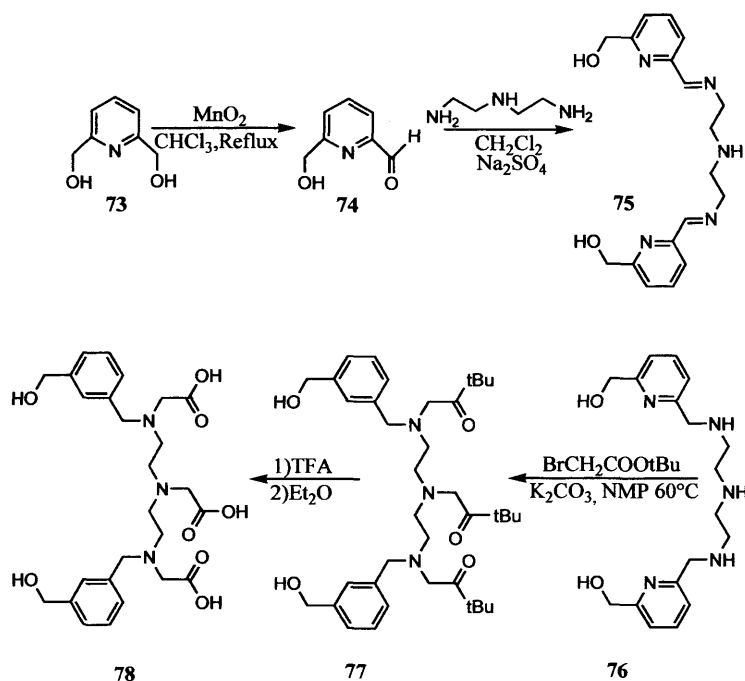


Figure 39:-Synthetic scheme depicting the preparation of 1, 4, 7-triazaheptane derivatives

3.1.7.1.3 Direct substitution ethylene carbon in the backbone

Despite the superiority of these bifunctional contrast agents (BFCAs) in terms of metal ion retention, their widespread use has been limited. This is more likely for reasons such as, complex separations involved in their synthesis and could be also because of the difficulties encountered in synthetic scale up. Under such circumstances, in 1991, Cummins *et al.*⁶⁶ proposed a synthetic route, which was not only convenient, but also yielded high yields of end product. They have claimed that this procedure could yield multigram quantities of the product. The procedure initially introduced for 1B-DTPA, later was extended to synthesize 1-(paminobenzyl)-4-methyl-DTPA (1 B4M-DTPA). It is recommended to have a closer look on the synthesis in Fig-40.

Potential Multimodal Imaging Agents

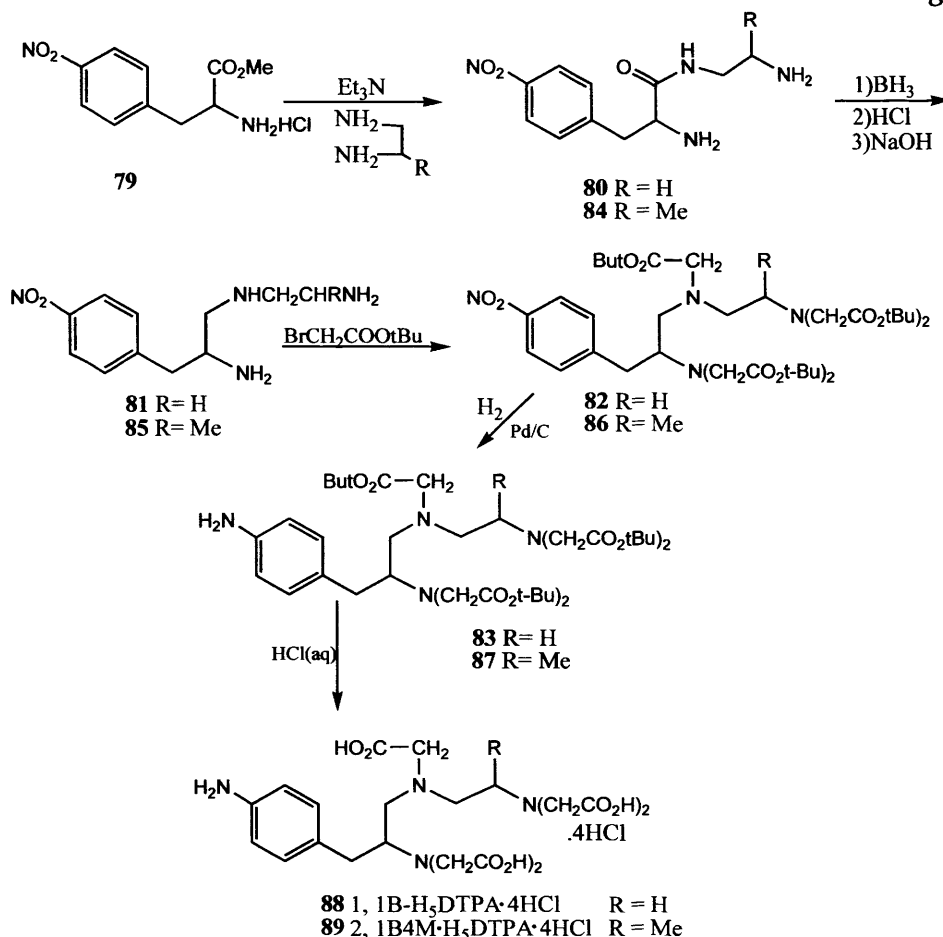
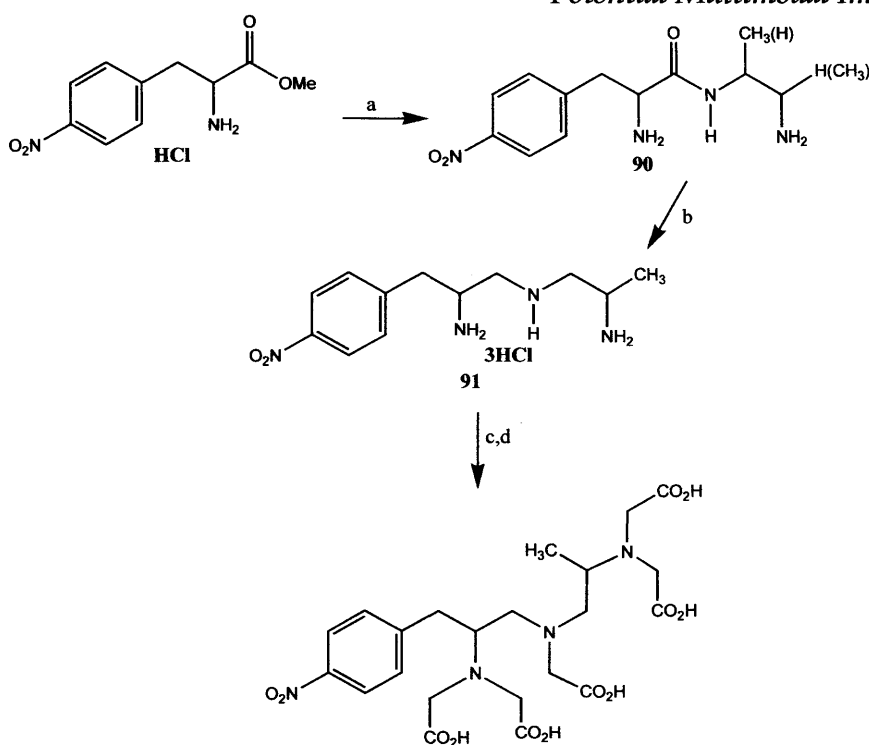


Figure 40:- Synthetic scheme for DTPA analogue synthesized by Cummins and co-workers

It has been a long-accepted tenet of coordination chemistry that the most stable complexes are formed when the coordination number of the metal is fully saturated by ligands. In line with this fact, Brechbiel *et al.*⁶⁷ in 1991 examined the importance of ligand structure features for retarding the release of yttrium *in-vivo*. They introduced the following modification to their previous ligand (see Fig-41). A methyl substituent was introduced to the carbon backbone, along with p-nitro benzyl group.

A notable aspect here is the substitution of 1,2-diaminopropane for 1,2-ethylenediamine in the aminolysis of methyl I-nitrophenylalaninate, followed by borane reduction of the resulting amino amide to give principally, precursor dien intermediates. The procedure is quite lengthy to be discussed. Fig-41 speaks for the procedure.

Potential Multimodal Imaging Agents



(a) Et₃N, 1,2-diaminopropane; (b) BH₃·THF, EtOH/HCl; (c) BrCH₂COOH, KOH; (d) H₂, Pd/C, Cl₂CS.

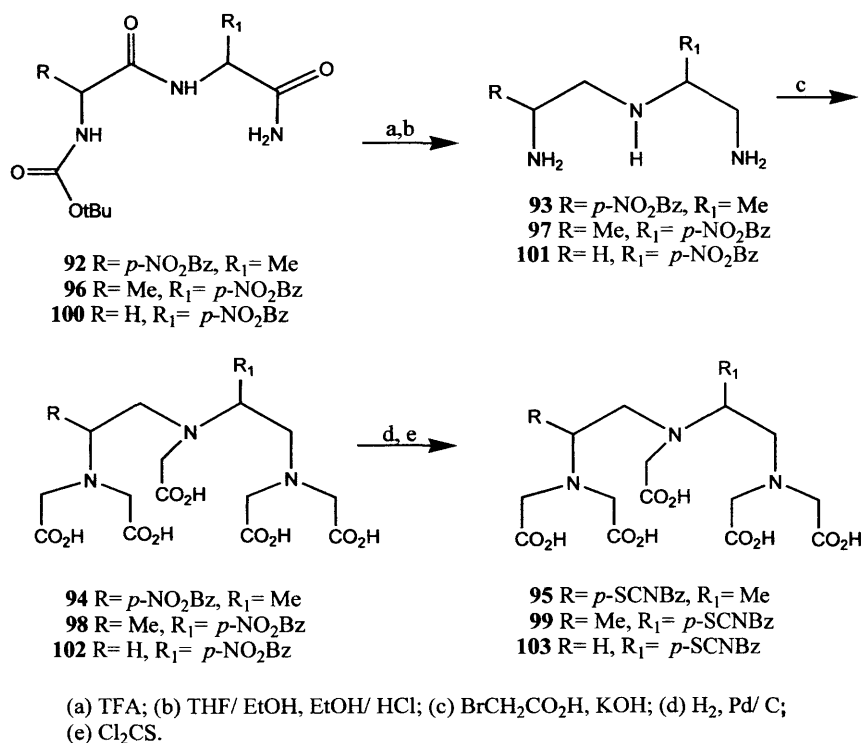


Fig 41:-Synthetic scheme depicting the lengthy procedure followed by Brechbiel *et al.*

3.1.7.1.4 DTPA analogues based on conformationally constrained structures

In an attempt to enhance the complex stability, the branching of the ethylene diamine backbone of DTPA could be effected through the introduction of rings in to the ligand. This in turn imposes conformational constraints on the specific portion of DTPA. These constraints

provide pre-organisation of the ligand's donor groups, such that it will reduce the entropy of formation of the metal complex. Further, constrain serves as a steric barrier to decomplexation. It may be expected that macrocyclic ligands could provide the greatest degree of conformational constraint. They, however, do not have structural flexibility to accommodate variety of metals as they possess a cavity of fixed dimension. This fact justifies the innovative approach taken by the scientists to produce conformationally constrained DTPA analogues.

I. Based on Amino Acids

DTPA analogue from *trans*-4-hydroxy-proline

It is also possible to produce functionality from 4-hydroxy-L-proline. Williams and Rapport⁶⁸ in 1994, prepared another DTPA analogue. This time they started with *trans*-4-hydroxy-proline. Through a series of synthetic steps they have produced **109** (see Fig- 42).

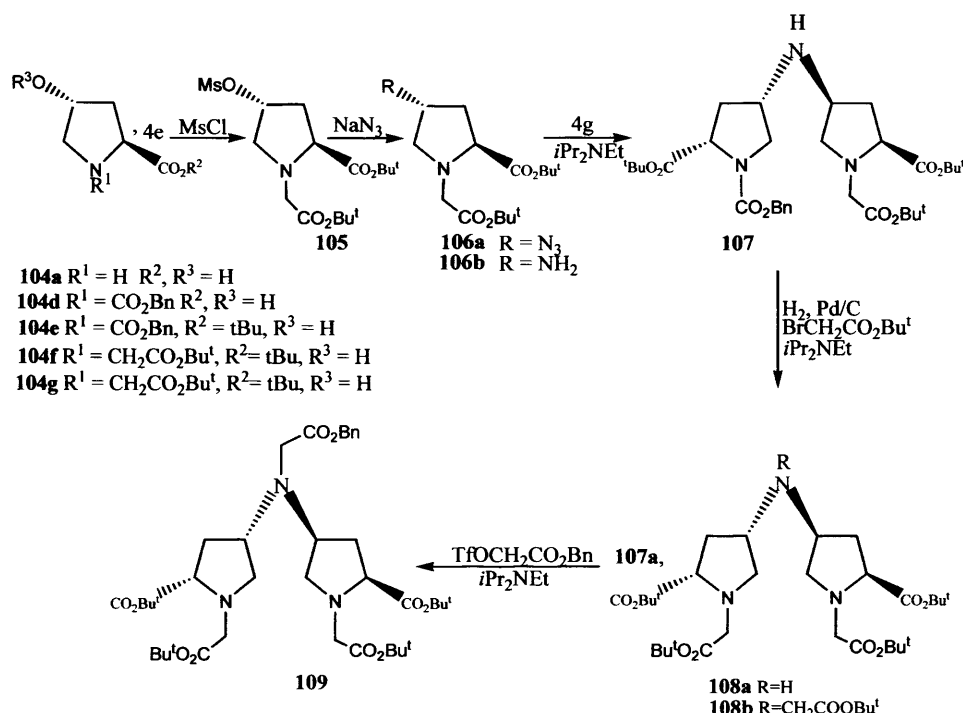


Figure 42:- Synthetic scheme depicting the preparation of DTPA analogue Starting from 4-hydroxy proline.

DTPA analogue from Serine and Proline towards conformationally constrained analogues

Pickersgill *et al.*⁶⁹ produced DTPA analogues. These differ from the pyridine containing DTPA ligands, as the smaller cyclic ring (5 carbons rather than 6) on the backbone leads to a more conformationally constrained ligand. The major synthetic steps involved in the synthesis

Potential Multimodal Imaging Agents

are; activation of triflate, low temperature alkylation with benzyl glycolate and finally the deprotection of the pentabenzyl esters (see Fig-43).

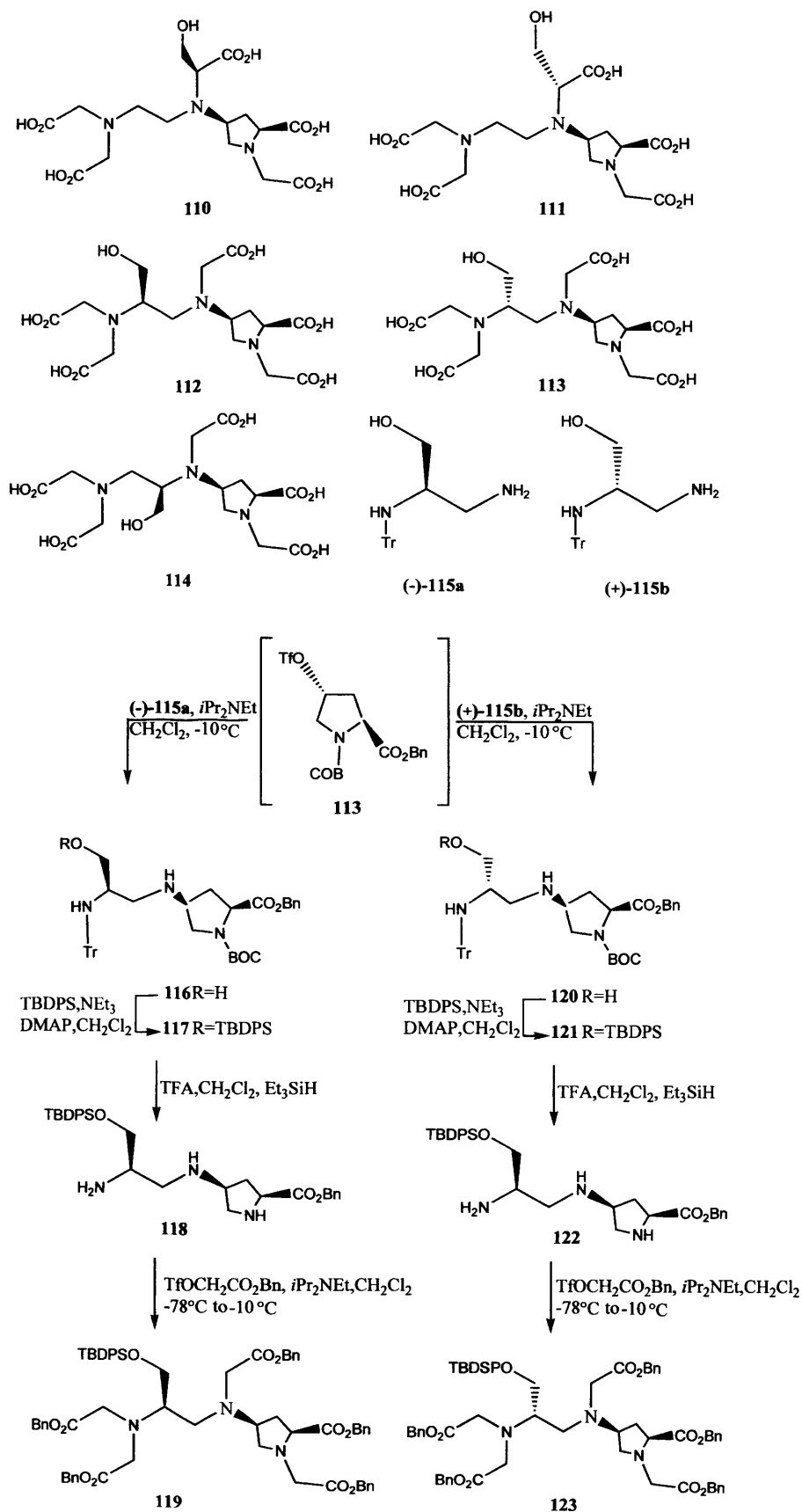


Figure 43:- Confirmationally constrained DTPA analogues synthesized by Pickers gill *et al.*

II. Based on Piperidine or Azepane ring

In the following year, Chong *et al.*⁷⁰ proved that conformationally restrained DTPA analogues could be achieved from piperidine ring or an azepane ring. Further, substitution of either the piperidine ring or an azepane ring with an amino group of the DTPA is expected to potentially increase complex stability and hepatobiliary clearance of the system. They have measured relaxivities of the gadolinium complexes as well. Initially 2,6-pyridinedicarboxylic acid was converted to *cis*-2,6-bis-(methoxycarbonyl)piperidine, this was then reacted with benzyl bromide under basic conditions to yield **124**, which then underwent base promoted reaction with LiBH₄ in THF to yield N-benzylated diol.

The hydroxyl groups of this diol were converted to their respective chloride by SOCl₂ to yield **125**. The treatment of **125** with NaN₃ in DMSO yielded the ring expanded diazide **126**, which was then through a series of conversions, converted to triamine derivative, which then was alkylated with t-butyl bromoacetate to provide **127**. Then **127** (**Fig-44**) was deprotected with HCl (g)/dioxane. A notable aspect in this synthesis is the ring expansion. This was attributed to the formation of aziridinium intermediate.

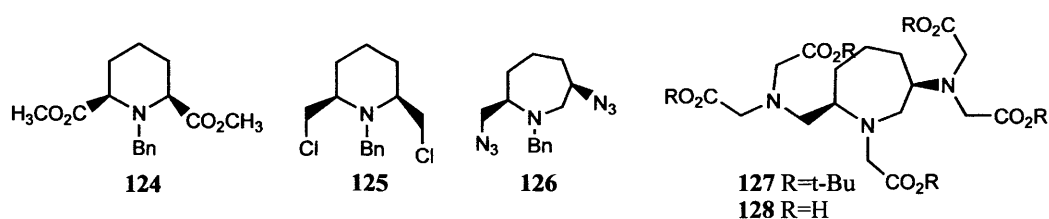


Figure 44:--Triamine derivative based on piperidine ring prepared by Chong *et al.*

3.1.8 DTPA based amide derivatives bearing chromophores:

A Novel Approach.

Keeping in line with the aforementioned BFCA's, we have successfully synthesized new BFCAs. These ligands have been synthesized by utilising both major strategies mentioned above. In making these ligands, we have paid special attention towards incorporating chromophores in to the diethylene triamine backbone. The chromophore was incorporated in the form of naphthalene moiety. The details will be discussed in the following sections.

3.2 Results and Discussion

3.2.1 Ligand design and Synthesis of DTPA analogues

3.2.1.1 Symmetric Naphtha derivative

3.2.1.1.1 Ligand Design

As part of satisfying our goal of producing dual purpose contrast agent, we intended to develop bifunctional chelating systems. These systems were developed such that they ensure high thermodynamic stability of the chelate which in turn will ensure very high tolerance under *in-vivo* conditions.

To meet these criteria, our initial attention was directed towards DTPA for reasons explained earlier in this chapter (see Section 3.1). It was then thought to synthesize, DTPA based mono amide by mixing DTPAA with ethylene diamine in 1:1 stoichiometric ratio.⁷¹ The approach is not as straight forward as it appears. As commonly encountered and widely reported⁷², all the attempts ended up with a mixture of mono and bis amides. Further, efforts to purify the mixture through column chromatography were not successful, as experienced and reported in aforementioned literature (however, a very recent publication,⁷³ claimed to solve this longterm difficulties).

The article published by Choi *et al.*⁷⁴ attracted our attention. They described the procedure of synthesizing DTPA analogue through N, N-Bis[(tert-butoxycarbonyl)methyl-2-bromoethylamine 1 (see Fig-1).

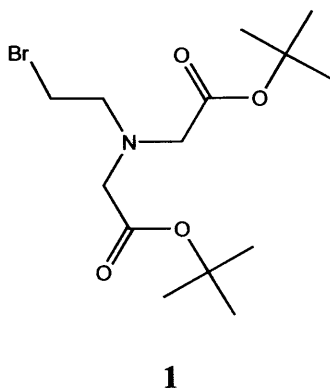


Figure 1:- N,N-Bis[(tert-butoxycarbonyl)methyl-2-bromoethylamine (Bromoderivative)

This has allowed us to synthesize new multidentate ligands. DTPA based monoamides could be prepared from DTPA analogues rather than through DTPAA. Therefore we have decided to utilise the strategy of synthesizing DTPA analogues from 'scratch' (see Section 3.5.2). This has triggered our synthesis to produce amine functionalised DTPA analogues, having the functionality in the central nitrogen of the ligand. Employing a retro synthetic approach and the stoichiometric ratio (1:2) commonly used, we found that by reacting one equivalent of amine functionalised precursor and two equivalents of bromoderivative could produce the desired analogue of DTPA (see Fig-2). The procedure reported by Anelli *et al.*⁷⁵ were employed to synthesize **2**. Yield was 28%. The shifting of the t-butyl peak and the doublets of para amino benzyl amine in the proton NMR spectrum, confirmed the success of the reaction. The estimated purity was 99%. The scaling up, however, was not successful. When the benzyl amine reactant was increased from 2.8 mmol to 3.7 mmol, the ¹H NMR spectrum of the crude product indicated the presence of excess para amino benzyl amine, which could not be removed by column chromatography.

Potential Multimodal Imaging Agents

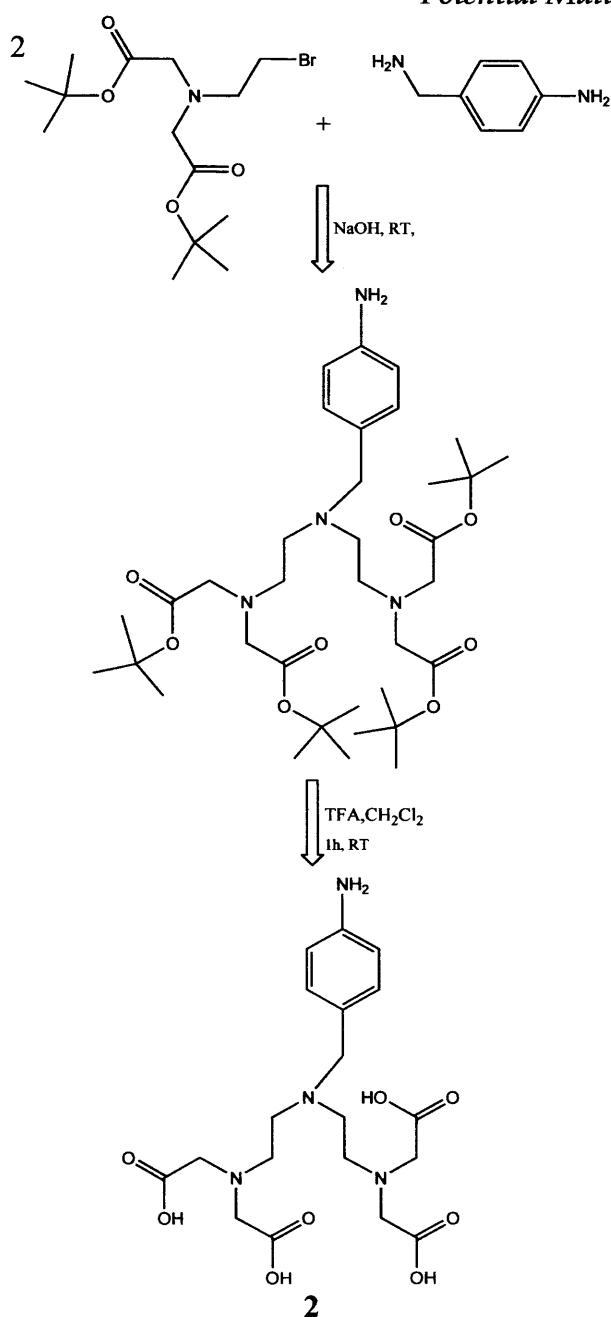


Figure 2: - Schematic representation of the successfully synthesized Centrally functionalized DTPA analogue

3.2.1.1.2 Ligand Synthesis

Synthesis of *N*-Boc protected amine functionalised DTPA analogue

It was then decided to synthesize centrally functionalised DTPA analogue with ethylene diamine (EDA). The need for protection of one of the amine groups of the EDA was realised, as there is a possibility for polymerisation. Since *N*-Boc protection is widely used in peptide chemistry, BOC protection with ethylene diamine was carried out (see Fig-3).

Synthesis of N-Boc-1,2-diaminoethane, tert-Butyl N-(2-aminoethyl)carbamate

The procedure employed could be summarised as follows. Di-tert butyl di carbonate dissolved in chloroform was added to the stirring ethylene diamine solution in chloroform, drop wise. After stirring for 2 h, the suspension was filtered and solvent removed. The residue was extracted with ethyl acetate and washed with brine. Upon drying over MgSO₄, the oily product was isolated. Yield was 38%. The distinct coupling of the triplets appeared on 2.75 and 3.1 ppm (J = 5.9 and J = 5.7 Hz respectively) in the ¹H NMR spectrum confirmed the success of synthesis coupled with a distinct peak for t-butyl group which was shifted to slightly upfield (1.54 ppm). These values were consistent with the chemical shifts reported by Essein *et al.*⁷⁶ Further, carbonyl stretching vibration of the ester at 1732 cm⁻¹ also supported the success of synthesis.

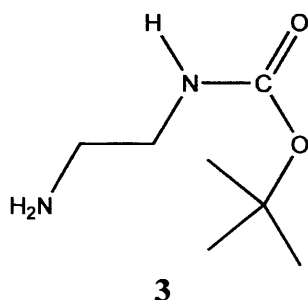


Figure 3:- N-Boc protected ethylene diamine

Challenges encountered in the synthesis of bromoderivative: Introducing a modified procedure

The procedure mentioned by Choi *et al.* was employed initially.⁷⁴ They first synthesized, N,N-Bis((tert-butoxycarbonyl)methyl)-2-ethanolamine (**alcohol derivative 4**, see Fig-4) through the alkylation of ethanolamine with tertiary butyl bromoacetate in DMF. This was then utilised as follows. N-bromosuccinimide (NBS) was added portion wise to the dissolved solution containing a mixture of **4** and triphenyl phosphine (PPh₃) in dichloromethane. After stirring for 2 h solvent was removed. Upon addition of diethyl ether, semisolid residue was formed. This was then triturated followed by flash chromatography to yield pure bromo derivative **1** (see Fig-1).

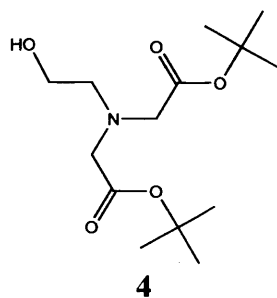
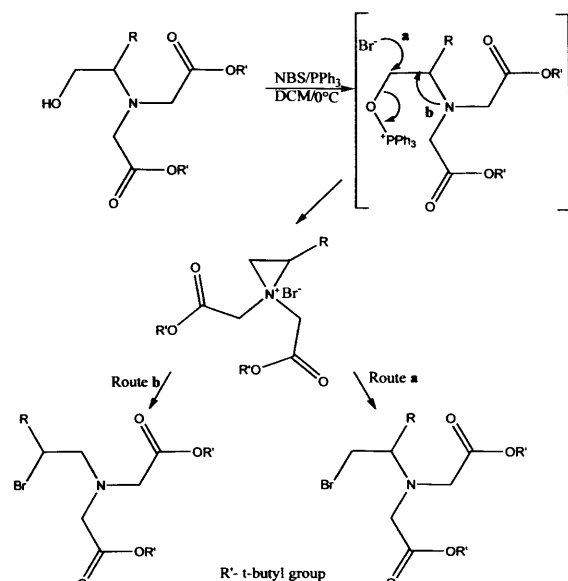


Figure 4:- N, N-Bis ((tert-butoxycarbonyl)methyl)-2-ethanolamine
(Alcohol derivative)

When the procedure was adapted to form **1**, however, it could not yield the desired results. The proton NMR spectrum of the crude product indicated no signs of bromination as the couplings of the triplets belong to the ethylene backbone were absent. Therefore, in a continuous search we came across the procedure reported by Williams and Rapport.⁵⁴ This was found to be, however, similar to that of Choi *et al.* When attempted, although the procedure helped to obtain the desired product, it could not be considered as a successful reaction. It is because of two reasons. Firstly, the product prepared as such, is not sufficiently pure. Secondly, the yield of the product was unacceptable (i.e.<10%). These observations prompted us to review the procedure being used. As a suitable initiative to solve the problem, we began our search for the mechanism of bromination utilising NBS/PPh₃. Song *et al.*⁷⁷ interesting findings on Aziridinium salts (see Fig-4) gave us an idea, yet it does not provide any information on the role of triphenyl phosphines (a recent publication outlines the role of PPh₃ in bromination⁷⁸).

They proposed that the β-amino alcohol reacts with the phosphonium salt (formed through the reaction between NBS and PPh₃) to yield an intermediate, this then subsequently undergoes rearrangement to form aziridinium cations, along with the removal of triphenylphosphine oxide. They have attributed the salt formation due to steric hindrance caused by the substitution in the backbone.

Potential Multimodal Imaging Agents



**Figure 5:- The proposed mechanism for bromination by Song *et al.*
Where R –benzyl, nitro benzyl, propyl groups**

It was thought, however, that, instead of allowing the bromination to take place *in situ*, it may be wise to prepare the phosphonium bromide first, by the portionwise addition of NBS to the dissolved solution of triphenyl phosphine in dichloromethane (successful preparation of the phosphonium bromide is indicated by the formation of sticky, semi solid-triphenylphosphine oxide). The prepared phosphonium bromide was then added in to the solution of alcohol derivative in dichloromethane dropwise. The rest of the procedure (see Fig-5) was followed as reported by Choi *et al.* The product was characterized by proton NMR spectroscopy which indicated the essential coupling of triplets ($J = 7.4$ Hz) belonging to the ethylene backbone.

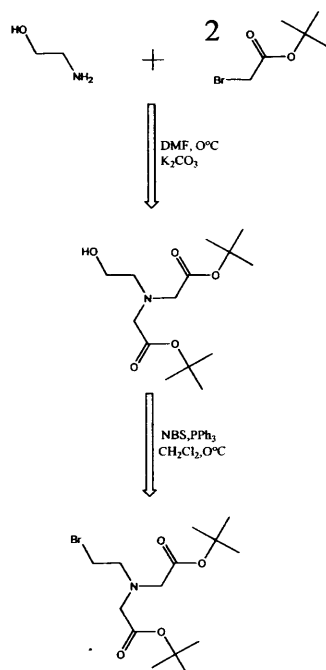


Figure 5:- Scheme representation of the modified procedure for bromide synthesis

Potential Multimodal Imaging Agents

The reaction was carried out according to a known procedure. 1,2-Diamino-N-tert-butylloxycarbonylethane was dissolved in 95% ethanol/water mixture. The pH was adjusted to 10 with NaOH. To which was added, Bromoderivative **1** dissolved in 95% ethanol dropwise. After 18 h of stirring, the ethanol was removed. Following acidification, the aqueous solution was extracted with dichloromethane. It was washed with water and dried over MgSO₄.

The crude product was purified by flash chromatography (diethyl ether: Hexane-1:5) and the pure protected ligand was isolated as a yellow oil. The yield, however, was less than 15%. As a matter of curiosity, it was deprotected with TFA/DCM to obtain the pure ligand and characterized by the ¹H NMR spectroscopy (see Fig-6). The NMR spectrum indicated the absence of t-butyl peak, and the other peaks were slightly shifted towards down field, while retaining the symmetry of the molecule.

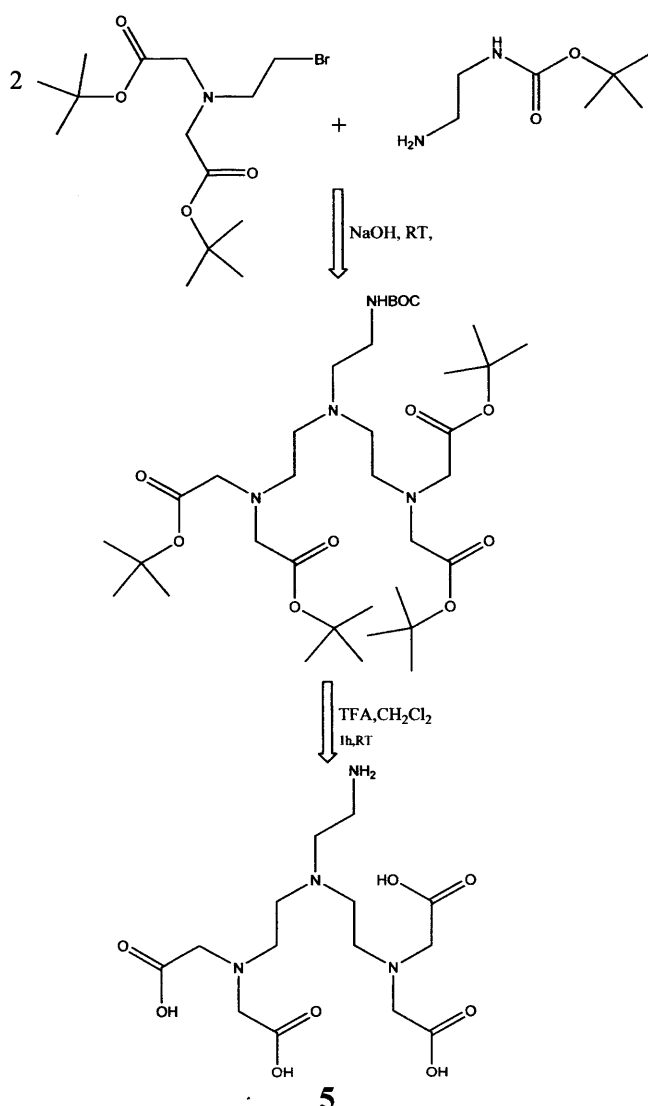


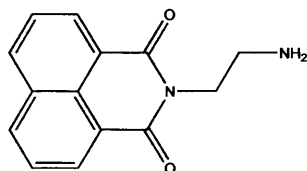
Figure 6:- Schematic representation of the attempted centrally substituted DTPA analogue

Introducing N-(2-Aminoethyl)-1, 8-naphthalimide as a suitable chromophore

Although, the product **5** obtained in high purity (99%), the yield was <25%. As a suitable alternative, it was thought to introduce N-(2-Aminoethyl)-1,8-naphthalimide **6** (see Fig-7), in to the diethylene triamine backbone. Moreover, naphthalimide moieties are considered to be good chromophores. Naturally, we thought this could be a good precursor to be reacted with **1**, which in turn would yield a functionalized DTPA analogue with strong chelating ability (through the provision of extra donor atoms).

It was also believed, through the nature of the synthesis, that the functionality will be positioned on the central nitrogen atom of the DTPA backbone. This will in turn support the stability of the chelate through the provision of extra donor atoms.⁷⁹ Therefore, all four carboxylate arms would be free to be involved in coordination. Hence we first synthesize, N-(2-Aminoethyl)-1,8-naphthalimide **6** as per the procedure reported by Licchelli *et al.*⁸⁰ (see Section 2.1.1)

The crude product was sufficiently pure for alkylation with bromoderivative **1**



6

Figure 7:- N-(2-Aminoethyl)-1, 8-naphthalimide

Overcoming challenges in alkylation

Alkylation proved to be challenging, in terms of selecting the right solvent and the relevant temperature. For the solvent, we have selected dimethylformamide (DMF) (after having unsuccessful attempts with chloroform). Two reasons dominated in the selection process. As the alkylation mechanism is expected to proceed through S_N2, it was thought a polar aprotic solvent could be the best selection, as it is known to facilitate S_N2. It was also found that reaction requires heating, in order to facilitate work up; DMF, which has a relatively low boiling point, was selected against the other alternative (DMSO).

Potential Multimodal Imaging Agents

Initially, N-(2-Aminoethyl)-1,8-naphthalimide was reacted with N-Bis[(tert-butoxycarbonyl)methyl-2-bromoethylamine **1** in the stoichiometric ratio of 1:2 in DMF. The ^1H NMR spectrum of the crude product, however, was not promising enough. Here we thought of the possibility of DMF being decomposed slightly. As such we thought to use a moderate temperature that was 65 °C. The compound **1** and amine functionalized naphthalic anhydride were dissolved in anhydrous DMF and heated to 65°C. The ^1H NMR spectrum of the crude product indicated the alkylation. It also indicated the need for further purification. We opted for column chromatography.

Thin layer chromatography carried out first, proved that 5% Dichloromethane /Methanol would be the ideal solvent mixture. The purified protected ligand (see Fig-8) thus obtained, subsequently underwent deprotection.

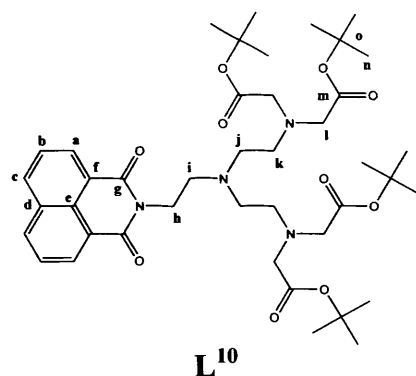


Figure 8: - t-butyl protected symmetric naphtha ligand

The protected ligand was characterized by NMR spectroscopy, IR spectroscopy and Mass spectrometry. Chemical shifts were assigned by comparison to previously published data.^{74, 79,}

⁸⁰ The deprotection was carried out by refluxing the protected ligand at 2M HCl for two hours as reported by Vogt *et al.*⁸¹ The deprotected ligand **L¹¹** (see Fig-9) was isolated in good yield (90%).

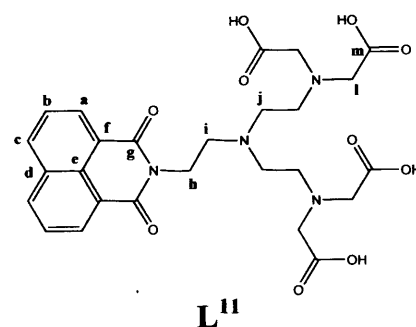


Figure 9-Symmetric deprotected ligand

The absence of peak related to t-butyl group, which has appeared on 1.40 ppm, indicated the success of deprotection, while the other protons give rise to only a negligible chemical shifts.

Characterisation through IR spectroscopy

Table 1, it is evident, that there is a significant frequency shift takes place towards the finger print region upon complexation with lanthanide metal ions (Gd (III) and Eu (III)). This could be attributed to the participation of amide oxygen in coordination.

As expected the magnitude of the shifts between the complexes of Gd (III) and Eu (III), however, is more or less the same. Further, it was rather surprising, no frequency shift was observed for Yb (III) complex, although the mass spectrum revealed the molecular ion.

Table 1:- A comparison of frequencies obtained for different vibrational modes of IR for the Symmetric naphtha ligand along with its starting materials and also complexed forms

vibration modes in IR	Frequencies observed for starting material and the protected unprotected forms of the ligand (cm ⁻¹)						
	Bromo derivative	Naphtha-EDA derivative	Protected Symmetric Ligand (L ¹⁰)	Deprotected Symmetric Ligand (L ¹¹)	Lanthanide complexes of Symmetric naphtha ligand		
					Gd	Eu	Yb
N(C=O) Amide	-	1662	1654	1655	1623	1622	1655
N(C=O)-Ester	1737	-	1739	-	-	-	-
N(C=O)-Acid	-	-	-	1695	1729	-	-
N(O-H)	-	-	-	3429	3424	3383	3401
N(N-H)	-	3346	3414	-	-	-	-

Characterisation through mass spectrometry

The molecular ions for the complexes of the symmetric ligand (L¹¹) of Gd (III), Yb (III), Eu (III) and Nd (III) were observed.

3.2.1.2 Asymmetric Naphtha

3.2.1.2.1 Ligand Design

Having succeeded in synthesizing a centrally functionalized DTPA analogue, our attention was directed towards the second sub strategy (see Section 3.5.2); to synthesize a DTPA analogue, functionalized in the terminal nitrogen of the diethylene triamine backbone.

In order to satisfy this purpose we have selected triethylene tetra amine (TRIEN). This was then reacted with 1,8 naphtha anhydride to produce Naphtha-TRIEN derivative (see Fig-10).

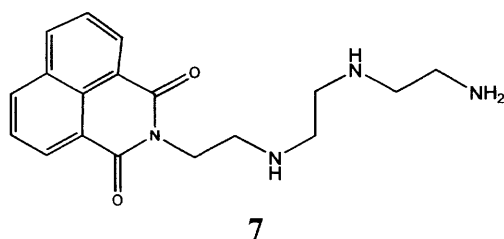


Figure 10:- Naphtha-TRIEN derivative synthesized in this project

3.2.1.2.2 Ligand Synthesis

Synthesis of Naphtha- TRIEN derivative

The same conditions were employed as that has been used for L¹ initially; the naphthalic anhydride was dissolved in excess triethylene tetra amine and refluxed. Solvent was removed through distillation. The ¹H NMR spectrum of the crude product, however, was not promising enough. We then opted for heating the reaction mixture to 120 °C. The ¹H NMR spectrum of the crude product was more promising (as the triplets of TRIEN relatively more visible in the latter, compared to the previous attempt). To purify further, we dissolved the crude product in dichloromethane. The mixture was filtered and the filtrate was evaporated. This was then dissolved in toluene. The toluene was decanted and the ¹H NMR spectrum was satisfactory.

Alkylation of naphtha derivative of TRIEN & Limitations

After the preparation of the precursor, it was decided to carry out the alkylation as per the conditions used for the symmetric naphtha derivative. The crude product suggested the need for further purification, as the excess naphthaderivative was visible in the ¹H NMR spectrum. Therefore, it was then decided to attempt the alkylation with 1:5 ratio rather than 1:4 (as we thought, excess tertiary butyl bromoacetate will ensure complete alkylation). The ¹H NMR

Potential Multimodal Imaging Agents

spectrum of the crude product suggested the success of the reaction. The need for further purification, however, was also felt from the proton NMR spectrum. The thin layer chromatography indicated the best solvent mixture (5% DCM/Methanol) for column chromatography. Unfortunately, the yield realised upon flash chromatography was very low ($\leq 20\%$). In spite of the low yield, the protected ligand was then deprotected (see Fig-11-13).

Resonances were assigned by comparison to previously published data.⁶⁶

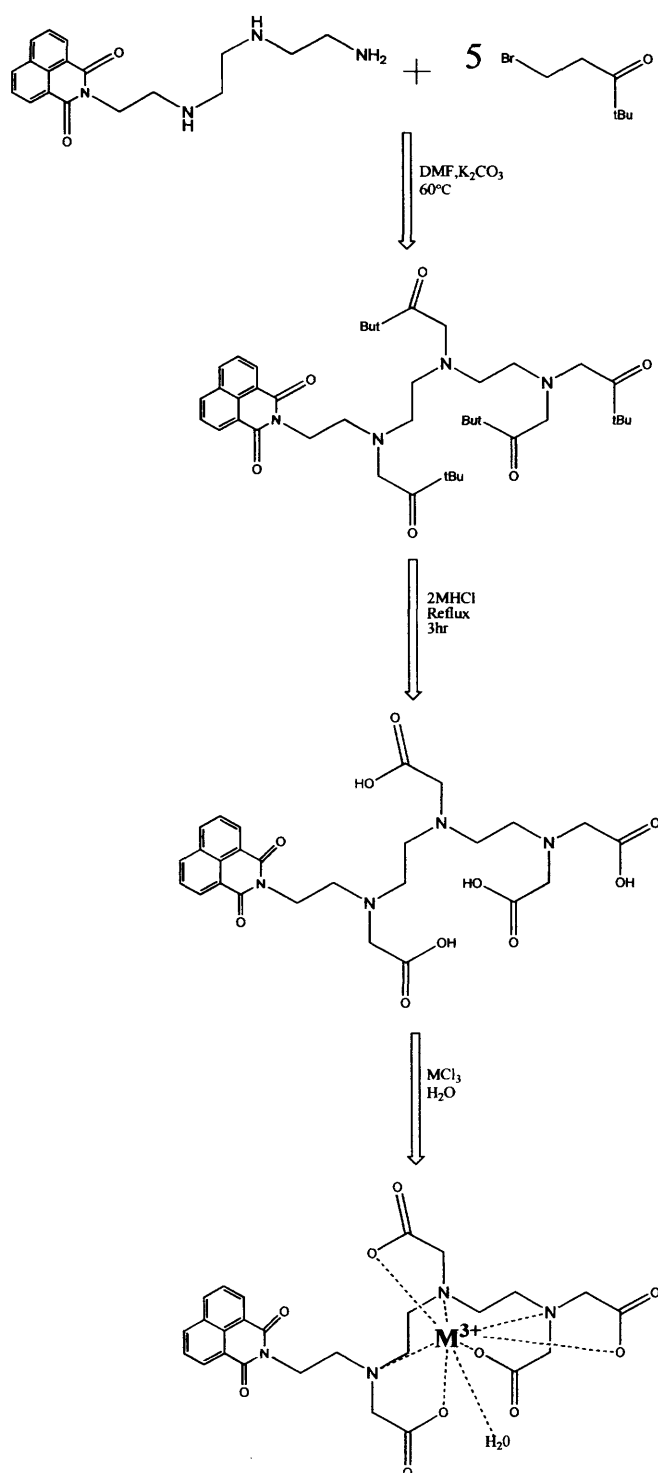
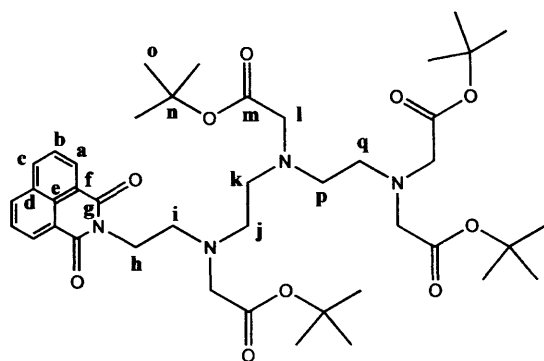
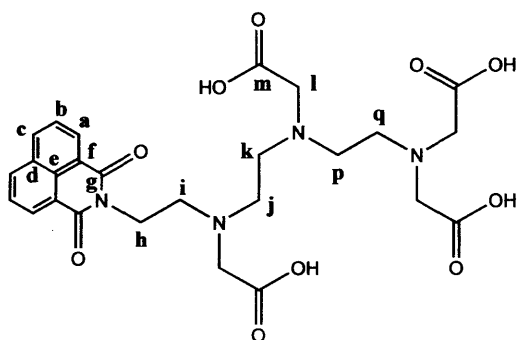


Figure 11:- Scheme representation of the synthesis of Asymmetric naphtha ligand



L¹²

Figure 12:- The synthesized protected asymmetric naphtha ligand



L¹³

Figure 13:- The synthesized Deprotected Asymmetric Naphtha ligand

Characterisation through IR spectroscopy

From Table 2, it is evident, that there is a significant shift in the frequency of amide stretching vibration occurs towards the finger print region upon complexation with Gd (III). Similar to symmetric ligand L¹¹, the amide oxygen coordination to the gadolinium ion could be reasoned for the above observation. The poor yield of the ligand as aforementioned has put up on limitations on investigation. Therefore only Gadolinium complex was prepared.

Table 2:- A comparison of frequencies obtained for different vibrational modes of IR for the Asymmetric naphtha ligand along with its starting materials and also its Gadolinium complexed form

Observed vibration modes of IR	Frequencies observed for starting material and the protected , unprotected forms and also the Gd complex of the ligand (cm ⁻¹)				
	Tertiary butyl bromo acetate	Naphtha-TRIEN derivative	Protected Asymmetric naphtha Ligand	Deprotected Asymmetric Naphtha Ligand	Gadolinium complex of the Asymmetric naphtha ligand
v(C=O) Amide	-	1659	1648	1654	1644
v(C=O)- Ester	1731	-	1732	-	-
v(C=O)- Acid	-	-	-	1738	1728
v(O-H)	-	-	-	3427	3403
v(N-H)	-	3416	3414	-	-

Characterisation through mass spectroscopy

The molecular ion of the complex of Gd (III) was visible in the mass spectrum.

3.2.2 Novel synthesis of DTPA based bisamides

3.2.2.1 DTPA based bis amide of N-(2-Aminoethyl)-1, 8-naphthalimide

3.2.2.1.1 Ligand design & Synthesis

Following the success of EDTA bisamides, it was thought to synthesize DTPA bisamides of selected precursors. Auxiliaries were selected such that they could act as luminescent sensors.

As such, naphthalimides is of great importance. This ligand will be dealt with in detail in

Chapter 4. The synthetic procedure was exactly the same modified procedure used to synthesize EDTA bisamides of 4-aminomethyl pyridine. Ligand was obtained in a good yield

(45%) (see Fig-14).

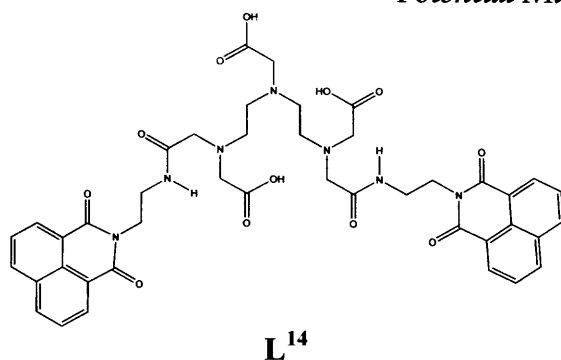


Figure 14:- DTPA bisamide of N-(2-Aminoethyl)-1, 8-naphthalimide

3.2.2.2 DTPA based bis amide of 4-amino methyl pyridine

3.2.2.2.1 Ligand design & Synthesis

Initially, the same synthetic procedure used to prepare EDTA bis amide of 4-aminomethyl pyridine was employed. The precipitate thus obtained, contained 25% of starting material (excess of 4-aminomethylpyridine). This was concluded from the proton NMR spectrum, which indicated the ratio of 1:4, between the doublet of L¹⁵ and that of the doublet of the amino methylpyridine. Recrystallisation with hot methanol and ethanol also failed, it was then thought to remove the material under very high vacuum.

The removal of starting material by high vacuum, however, yielded little success with removal of only 3% of excess 4-amino methylpyridine from the crude product. It was then thought to purify the ligand by continuous washing with acetone for a prolong period of time (7days). The method adapted for this purpose was soxhlet extraction. This has yielded substantial results, yielding a 92% pure ligand (see Fig-15). It should be noted, that despite the extended period used for Soxhlet extraction, purity of the ligand could not be improved further (as the trace amount of 4-amino methylpyridine could not be removed in its entirety).

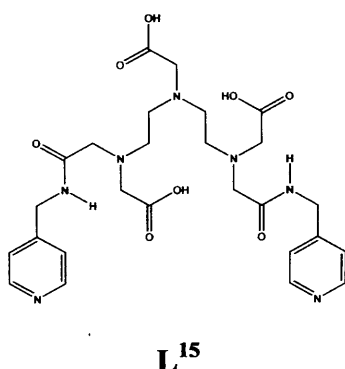


Figure 15:- DTPA bis amide of 4- amino methyl pyridine

3.3 Experimental Section

General Experimental: Reagents were obtained from commercial sources and used as received unless otherwise noted. Solvents were dried and purified under N₂ by using standard methods and were distilled immediately before use, specifically dimethylformamide, was distilled using anhydrous calcium hydride. All compounds were prepared under N₂ unless otherwise mentioned. The NMR spectra were obtained using a Bruker ARX 400 at 20 °C in CDCl₃ unless otherwise noted. Mass spectra were performed on a micro mass Platform II system, operating in Flow Injection Analysis mode, with the electrospray method. Infrared spectra were recorded with a JASCO FTIR-410 spectrometer, between 4000 and 250 cm⁻¹ as KBr pellets. UV/Vis spectra and measurements were recorded with a JASCO V-570 spectrometer.

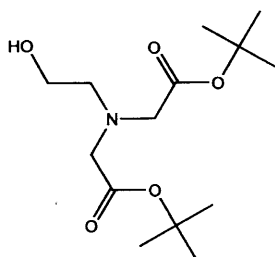
Synthesis of DTPA bisanhydride

DTPA (5.0 g, 12.72 mmol) was suspended in pyridine (8 mL) and acetic anhydride (7.0 g, 68 mmol) was added dropwise to the stirring solution. The reaction mixture was allowed to stir for 24 h at 65 °C. The resulting anhydride was filtered off and washed thoroughly with freshly distilled acetic anhydride and freshly distilled diethyl ether. The pale-cream powder was then dried under vacuum until constant weight was obtained. The product was characterised by infrared spectroscopy and measuring its melting point. Yield 4 g, 88%. IR (KBr disc) (cm⁻¹): 2940(br), 1820(vs), 1770(s), 1629(s); Melting point: 181-183°C.

3.3.1 Synthesis of Naphthalinic anhydride derivatives

3.3.1.1 Synthesis of N, N –Bis (tert-butoxycarbonyl) methyl -2-ethanolamine (4)

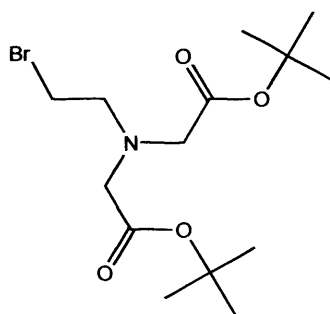
Alkylation⁷⁴



Potential Multimodal Imaging Agents

The procedure was used as reported by Choi *et al.*⁷⁴ except for slight modifications. To tert-butyl bromoacetate (17.02 ml, 116 mmol) dissolved in DMF (30 ml), potassium carbonate (12.514 g, 125 mmol) was added. The reaction mixture was cooled down to 0 °C and ethanolamine (2.98 ml, 49.4 mmol) added dropwise for 5 min. The reaction mixture was stirred at 0 °C for 30 min and then allowed to stir overnight at room temperature. After an addition of concentrated NaHCO₃ (100 ml) and diethyl ether (150 ml), the organic layer was separated and washed with concentrated NaHCO₃ (50 ml) and subsequently with brine (200 ml). The solvent was removed under reduced pressure to yield the product as pale yellow solid. Yield 14.2 g 42%; ¹H NMR (400 MHz; CDCl₃): δ_H 3.65 (t, 2H, J = 14.92 Hz, NCH₂OH), 3.40 (s, 4H, NCH₂COO), 2.85 (t, 2 H, J = 3.92 Hz, NCH₂), 1.46 (s, 18H, (CH₃)₃). ¹³C NMR spectrum and Mass spectrum were not obtained as it is a known compound.

3.3.1.2 Synthesis of N,N-Bis[(tert-butoxycarbonyl) methyl-2-bromoethylamine (1)⁷⁵

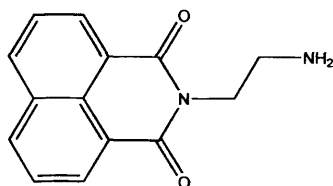


PPh₃ (4.3404 g, 16.53 mmol) was dissolved in dichloromethane (25 ml), subsequently added NBS (2.988 g, 16.78 mmol) portion wise and the mixture was allowed to stir at 0 °C (until the colour of the solution changes from yellow to light brown). The mixture was transferred to Alcohol derivative 4 (6 g, 20.74 mmol), dissolved in dichloromethane (25 ml), dropwise at 0 °C. After which, the reaction mixture was allowed to stir over night. The solvent was removed and to the resulting crude product was added diethyl ether. Upon which observed the formation of a sticky solid. The mixture was triturated and filtered. Filtrate was evaporated and the crude product was flash chromatographed (Hexane: Diethylether - 5:1). The product was obtained as colourless oil. Yield 2.0 g, 28 %; ¹H NMR (400 MHz; CDCl₃) δ_H (ppm) 3.45

(s, 4H, NCH₂COOC (CH₃)₃), 3.41 (t, 2H, J = 7.4 Hz, BrCH₂), 3.11 (t, 2H, J = 7.4 Hz, BrCH₂CH₂N), 1.44 (s, 18H, COOC (CH₃)₃).

¹³C NMR spectrum and Mass spectrum were not obtained as it is a known compound.⁷⁵

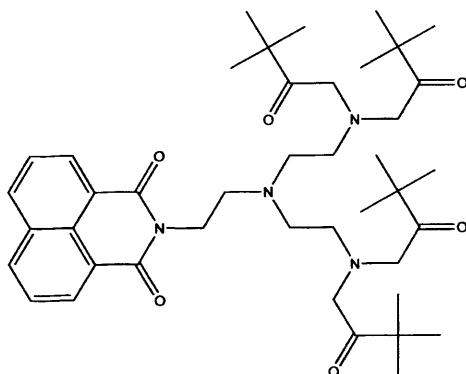
3.3.1.3 Synthesis of N-(2-Aminoethyl)-1, 8-naphthalimide (6)



To 1,8-Naphthalinic anhydride (2 g, 10.09 mmol), was added freshly distilled ethylene diamine (15 ml, 224.30 mmol) and allowed it to reflux overnight. Then the solvent was removed through distillation and high vacuum. Thereafter, the crude product was dissolved in dichloromethane and filtered. The precipitate was washed with diethyl ether. After washing it thrice, the product was obtained as pale yellow precipitate. Yield 1.4g, 58%; ¹H NMR (400 MHz; CDCl₃): δ_H (ppm) 8.60 (d, 2H, J = 8.00 Hz, ArH), 8.30 (d, 2H, J = 8.00 Hz, ArH), 7.70 (t, 2H, J = 8.11 Hz, ArH), 4.20 (t, 2H, J = 6 Hz, NCH₂CH₂), 3.00 (t, 2H, J = 6.65 Hz, NCH₂CH₂NH₂); ESI-MS (+ion): found m/z 241.0971, calc.241.0977 for [(6) H]⁺.

¹³C NMR spectrum and Mass spectrum were not obtained as it is a known compound.⁸⁰

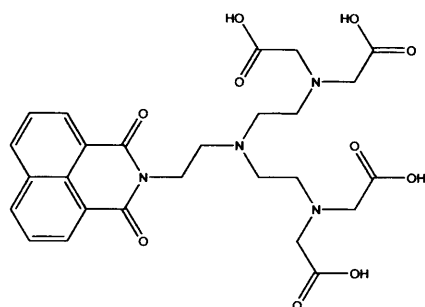
3.3.1.4 Alkylation of Naphthalic anhydride derivative with N,N-Bis[(tert-butoxycarbonyl) methyl-2-bromoethylamine (L¹⁰)



To N,N-bis[(tert-Butoxycarbonyl)methyl-2-bromoethylamine 1 (1 g, 2.84 mmol) was added K₂CO₃ (3.4 g, 87 mmol) and previously synthesized 6 (0.34 g, 1.42 mmol). Thereafter, DMF was added and the reaction mixture was gently heated up to 65 °C and allowed to stir

overnight. Then the solvent was removed. The ^1H NMR spectrum of the crude product indicated impurities. The crude product was flash chromatographed (5% MeOH: DCM mixture). The pure product was obtained as yellow oil. Yield 0.62 g, 54%; ^1H NMR (400 MHz, CDCl_3): δ_{H} (ppm) 8.50 (d, 2H, $J = 7.27$ Hz, Ar), 8.10 (d, 2H, $J = 8.13$ Hz), 7.70 (m, 2H), 4.30 (m, 2H), 3.40 (m, 8H), 2.85 (br s, 8H), 1.40 (s, 36H); ^{13}C NMR (400 MHz; D_2O): δ_{C} 170.70, 163.4, 133.22, 130.63, 127.19, 121.53, 80.88, 45.43, 52.45, 55.10, 27.10; IR (KBr disc) (cm^{-1}): 3440(br), 2977(s), 2931(w), 1736(s), 1702(w), 1661(vs), 1628(w), 1591(s); ESI-MS (+ion): found m/z 783.4578, calc 783.4544 for $[(\text{L}^{10}) \text{H}]^+$.

3.3.1.5 Hydrolysis of Alkylated Naphthalinic Anhydride derivative (L^{11})



To L^4 (0.12 g, 0.153 mmol) was added 2M HCl (10 ml, 323 mmol) and the reaction mixture was refluxed for 2 h. Then the solvent was removed under high vacuum and to give the product as pale yellow solid. Yield 0.072 g, 84%; ^1H NMR (400 MHz, D_2O) δ_{H} (ppm) 8.00 (d, 2H, $J = 6.79$ Hz), 7.92 (d, 2H, $J = 8.41$ Hz), 7.40 (t, 2H, $J = 6.94$ Hz), 3.7 (m, 4H), 3.40 (s, 8H), 2.90 (m, 4H), 2.80 (m, 4H); ^{13}C NMR (400 Hz, D_2O) δ_{C} 172.25, 168.72, 135.45, 135.65, 131.78, 131.59, 130.76, 127.09, 126.58, 119.92, 55.77, 55.34, 52.31, 50.81, 37.01; IR (KBr disc) (cm^{-1}): 3430(br), 2963(w), 1695(s), 1655(vs), 16259w), 1588(s); ESI-MS (+ion): Found m/z 557.16, calc 557.00 for $[(\text{L}^{11}) \text{H}]^-$.

3.3.1.5.1 Complexation reaction of L^5 with Gd (III) Chloride

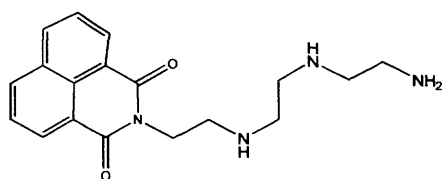
Initially two reactants, namely L^5 (28 mg, 0.05 mmol) and $\text{GdCl}_3 \cdot 6\text{H}_2\text{O}$ (18.0 mg 0.05 mmol) were added to two different vials. The ligand was dissolved in ethanol 10 ml, and heated slightly to ensure complete dissolution. Then GdCl_3 was dissolved in distilled H_2O , again heated to ensure complete dissolution. Thereafter the vial containing the metal salt solution

Potential Multimodal Imaging Agents

was kept over the mixer, and the ligand solution was added dropwise. The instantaneous formation of the precipitate was observed. After the complete addition of the ligand to the metal, the mixture was stirred for two days; care was taken to ensure to prevent any light interaction with the mixture, by covering the system with Allufoil. Then the solvent was evaporated via rotavaporator and high vacuum to give a yellow precipitate, which is the complex. Yield 84%; IR (KBr disc) (cm^{-1}): 3425(br), 1729(w), 1625(s), 1408(s); ESI-MS(-ion): found m/z 712.0898, calc 712.0890 for $[(L^5)\text{Gd}]$. UV/Vis [λ_{max} , nm (ϵ_M , $\text{M}^{-1}\text{cm}^{-1}$)] in H_2O : 235(17,658), 274(4128), 344(6279).

The complexation reaction of L^5 with Eu (III) chloride, Yb (III) chloride and Nd (III) chloride were carried out as described for complexation with Gadolinium. Except in the case of Nd (III) chloride it has to be dissolved in DMF, instead of water

3.3.1.6 Reaction with Naphthalinic anhydride and Triethylenetetraamine (7)

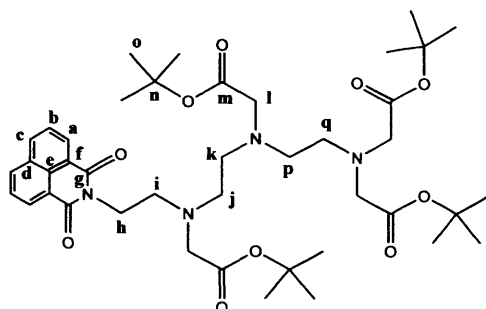


To 1,8-naphthalinic anhydride (1 g, 5.05 mmol) was added triethylene tetra amine (4.5 ml, 30 mmol) and allowed it to reflux overnight. Solvent was removed through distillation. Thereafter the crude product was dissolved in dichloromethane and filtered. The filtrate was evaporated and the ^1H NMR spectrum for the filtrate and that precipitate recorded. To purify further, it was decided to wash the precipitate in toluene and the toluene washings was evaporated to obtained the product as a dark brown sticky solid. Yield 0.7 g, 42%; ^1H NMR (D_2O , 400 Hz) δ_{H} (ppm) 8.5 (d, 2H, $J = 8.53$ Hz, ArH), 8.10 (d, 2H, $J = 8.14$ Hz, ArH), 7.70 (t, 2H, $J = 8.00$ Hz, ArH), 4.35 (t, 2H, $J = 5.8$ Hz, $\text{NCH}_2\text{CH}_2\text{NH}$), 2.95 (t, 4H, $J = 12$ Hz, $\text{NCH}_2\text{CH}_2\text{NH}$), 2.80 (t, 2H, $J = 8.00$ Hz, $\text{NHCH}_2\text{CH}_2\text{NH}$), 2.7 (t, 2H, $J = 10$ Hz, $\text{NHCH}_2\text{CH}_2\text{NH}_2$), 2.6 (m, 4H); IR (KBr disc) (cm^{-1}): 3416(br), 2964(s), 2822(w), 1699(s),

1660(vs), 1625(w), 1590(s), 1439(s); ESI-MS (+ion): found m/z 349.15, calc 349.17 for

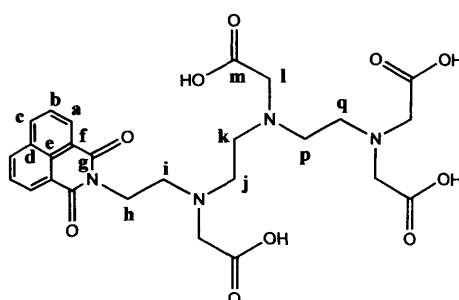
$[(7) H]^+$.

3.3.1.7 Alkylation of Naphthalinic anhydride derivative (L^{12})



To tertbutylbromoacetate (2.27 ml, 15.58 mmol) was added K_2CO_3 (10 g, 72.46 mmol) and previously synthesized **7** (1.011 g, 3.10 mmol). After the addition of DMF (20 ml), the reaction mixture was gently heated up to 65 °C and allowed to stir overnight. Then the solvent was removed. As it was discovered from the 1H NMR spectrum the crude product contains impurities, it was decided to flash chromatograph the material (Methanol: DCM). Product was obtained from eluents which were collected upon eluting with 10% MeOH: DCM solvent mixture. Solvents were removed through rotavaporation and high vacuum. Yield 0.25 g, 20%; 1H NMR ($CDCl_3$, 400 MHz) δ_H 8.50 (d, 2H, $J = 7.13$, ArH_a), 8.10 (d, 2H, $J = 7.98$, ArH_c), 7.70 (t, 2H, $J = 7.73$, ArH_b), 4.2 (m, 2H), 3.4 (s, 8H), 2.9 (m, 2H), 2.8 (m, 2H), 2.7 (m, 2H), 2.6 (m, 4H), 1.4 (s, 36H); ^{13}C NMR (400 MHz, $CDCl_3$): δ_c 169.03, 163.06, 132.84, 130.55, 130.15, 125.88, 121.66, 79.85, 55.02, 54.82, 51.92, 51.77, 50.92, 37.17, 27.08, 27.00, 27.14, 26.91; IR (KBr disc) (cm^{-1}): 3467(br), 2973(s), 2360(s), 1733(vs), 1648(s), 1595(s); ESI-MS(+ion): found m/z 783.45, calc 783.45 for $[(L^{12}) H]^+$.

3.3.1.8 Hydrolysis of Alkylated Naphthalinic Anhydride derivative (L^{13})



Potential Multimodal Imaging Agents

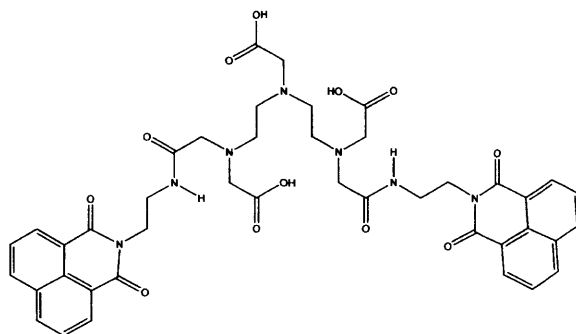
L^{12} (0.12 g, 0.15 mmol) was introduced to a round bottom flask and 2M HCl (10 ml, 324 mmol) added and the reaction mixture was refluxed for 2 h. After 2 h solvent was removed through rotavaporation and high vacuum. Yield 0.07 g, 58%; ^1H NMR (400 MHz, D_2O) δ_{H} (ppm) 8.00 (dd, 4H, $J = 8.8$ Hz, other constant not determined, $\text{ArH}_{\text{a,c}}$) 7.45 (t, 2H, $J = 26$ Hz, ArH_{b}), 3.00 - 4.25 (m, 18H); IR (KBr disc) (cm^{-1}): 3428(br), 29649(w), 2532(w), 1738(s), 1702(w), 1654(s), 1590(w); ESI-MS(+ion): found m/z 559.2057, calc 559.2040 for $[(L^{13})\text{H}]^+$.

3.3.1.8.1 Complexation reaction of L^{13} with Gd (III) Chloride

Complexation was carried out in a similar manner described for L^{11} . Yield 85%; IR (KBr disc) (cm^{-1}): 3404(br), 1728(w), 1644(s), 1408(s); ESI-MS(-ion): found m/z 714.23, calc 714.11 for $[(L^{13})\text{Gd}]$. UV/Vis [λ_{max} , nm (ϵ_{M} , $\text{M}^{-1}\text{cm}^{-1}$)] in H_2O : 235(6752), 267(1679), 345(2309).

3.3.2 Synthesis of DTBA Bismaides

3.3.2.1 Synthesis of DTPABisamide of Amine functionalized naphtha derivative (L^{14})

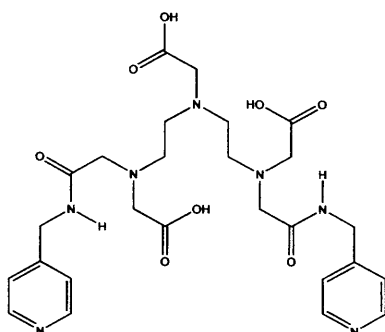


To DTPA bisanhydride (0.308 g, 0.816 mmol) dissolved in dimethylformamide (10 ml) was added N-(2-Aminoethyl)-1,8-naphthalimide **6** (0.413 g, 1.72 mmol) dissolved in dimethylformamide (10 ml), dropwise. After the complete addition, the reaction mixture was allowed to stir over night at room temperature. Then dichloromethane (50 ml) was added to the reaction mixture. The precipitate formed was filtered and was washed initially with acetone and subsequently with acetonitrile. Yield 0.38g, 45%; ^1H NMR (400 MHz; DMSO-d_6): δ (ppm) 8.4 (d, 2H, ArH_{a} , $J = \text{Hz}$), 8.35 (d, 2H, ArH_{c} , $J = \text{Hz}$), 8.15 (s, 1H, NH),

Potential Multimodal Imaging Agents

7.75 (t, 2H, ArHb, $J = 2.7$ Hz) 10.00 (s, 2H, NH), 7.50 (d, 4H, (m, 2H, NCH₂), 3.40 (m, 2H, NCH₂CH₂), 3.30 (s, 2H, NCH₂COOH), 3.1 (s, 2H, NCH₂COOH), 2.6 (s, 2H, NCH₂CH₂N); ¹³C NMR (400 MHz; D₂O) δ c: 173.00, 171.23, 163.95, 134.40, 131.4, 130.8, 127.67, 127.38, 122.36, 57.63, 55.35, 52.26, 37.08; IR (KBr disc)(cm⁻¹): 3436(br), 2963(s), 1699(s), 1660(vs), 1627(w), 1585(s).

3.3.2.2 Synthesis of DTPA bisamide of aminomethyl pyridine (L¹⁵)



DTPA bisanhydride (0.364 g, 1.018 mmol) was dissolved in dimethylformamide (7 ml) completely and was added 4-Aminomethyl pyridine (0.22 g, 2.036 mmol) completely dissolved in dimethylformamide (7 ml), drop wise. After the complete addition, the reaction mixture was allowed to stir at room temperature overnight. Then dichloromethane was added to the reaction mixture, a great deal of precipitate was formed, which was filtered and washed firstly with acetone and subsequently with acetonitrile. Yield 0.15g, 25%; ¹H NMR (400 MHz; D₂O with K₂CO₃, Me₄Si); 8.42 (d, ArCH₆, $J = 6.51$ Hz, 2H), 7.50 (d, ArCH₂, $J = 6.30$ Hz, 2H), 4.45 (s, NHCH₂, Ar 2H), 3.65 (s, 2H, NCH₂CH₂COOH), 3.30 (s, 2H, NCH₂COOH), 3.15 (s, 2H, NCH₂CH₂CONH), 2.70 (s, 2H, NCH₂CH₂N); ¹³C NMR (400 MHz; D₂O with K₂CO₃): 179.26 (CO), 175.30 (CO), 148.99, 148.78, 122.63, 59.36, 58.69, 53.46, 41.98; IR (KBr disc) (cm⁻¹): 3438(br), 1712(w), 1666(s); ESI MS⁺ion: found m/z 574.2645: calc. 574.2625 for [(L¹)H]⁺.

3.4 Conclusion

Utilising, retrosynthetic approach, two new DTPA analogues have been synthesized. Chromophore bearing, central nitrogen substituted, DTPA analogue has been synthesized for the first time. The Symmetric naphtha derivative of N-(2-Aminoethyl)-1,8-naphthalimide has four free carboxylic acid groups. This will favourably enhance the stability of the gadolinium chelate, while providing binding site for blood proteins (such as BSA). This will in turn potentially enhance the relaxivity. Two novel DTPA bisamides were synthesized.

It is also envisaged, that the pyridine N in the DTPA biamides of 4-aminomethylpyridine could act as donor atom for *fac*-Re(CO)₃(Bpy)Cl. This rhenium complex possess a very short emission life time (<10 ns).⁸² This has been attributed to the non radiated quenching of the excited state through the bound chloride ion. Interestingly, when the chloride was replaced with pyridine nitrogen, the life time is significantly enhanced (by two orders of magnitude).

These investigations clearly support the fact that the gadolinium complex of the DTPA bisamide of 4-aminomethyl pyridine could be a potential dual purpose contrast agent.

References

1. G. Andregg, F. A. Neu, R. Delgado, J. Felcman and K. Popov, *Pure Appl. Chem.*, 2005, **77**, 1445.
2. R. Byrne, T. Kiss, L. Lovgren, P. M. May, C. O. Onindo, L. D. Pettit, K. I. Popov, K. J. Powell, R. W. Ramette, S. Sjoberg and R. M. Town, "*Chelation therapy*" in *Interactive, problem-oriented softbook: Solution Equilibria: principles and applications*, Academic Software and K. J. Powell, UK, Release 1999.
3. L. W. Powell and M. J. Thomas, *J. Clin. Path.*, 1967, **20**, 896.
4. A. Cash, D. U. Khuong and D. Chambault, *Int. J. Radiat. Biol.*, 1964, **8**, 35.
5. Z. H. Oster, P. Som, M. C. Gil, R. G. Fairchild, A. G. Goldman, E. R. Schachner, D. F. Sacker, H. L. Atkins, G. E. Meinken, S. C. Srivastava, P. Richards and A. B. Brill, *J. Nucl. Med.*, 1981, **22**, 269.
6. N. Oku, Y. Namba, A. Takeda and S. Okada, *Nucl. Med. Biol.*, 1993, **20**, 407.

7. D. M. Corsi, H. V. Bekkum and J. A. Peters, *Inorg. Chem.*, 2000, **39**, 4802.
8. L. Vander Elst, A. Roch, P. Gillis, S. Laurent, F. Botteman, W. M. Bulte and R. N. Muller, *Magn. Reson. Med.*, 2002, **47**, 1121.
9. I. Bertini, F. Capozzi, C. Luchinat, G. Nicastro and Z. Xia, *J. Phys. Chem.*, 1993, **97**, 6351.
10. P. Caravan, J. J. Ellison, T. J. McMurry and R. B. Lauffer, *Chem. Rev.*, 1999, **99**, 2293.
11. G. Pintacuda, M. John, X. C. Su and G. Otting, *Acc. Chem. Res.*, 2007, **40**, 206.
12. J. Reuben, *Biochemistry*, 1971, **10**, 2834.
13. H. J. Weinmann, R. C. Brasch, W. R. Press and G. E. Wesbey, *Am. J. Roentgen.*, 1984, **142**, 619.
14. C. A. Zur and N. Schmiedebergs, *Arch. Pharmacol.*, 1964, **246**, 316.
15. (a) P. A. Rink and R. N. Muller, *Eur. Magn. Reson. Forum.*, 1992, **50**. (b) P. Dawson, *Clin. Radiol.*, 1994, **49**, 439.
16. P. Dawson, D. O. Cosgrove and R. G. Grainger, in *Text book of contrast media*, ISIS Medical Media Ltd, 1999.
17. M. Tulu and K. E. Geckeler, *Polym. Int.*, 1999, **48**, 909.
18. (a) Y. M. Wang, T. H. Cheng, G. C. Liub and R. S. Sheub, *J. Chem. Soc., Dalton Trans.*, 1997, 833; (b) J. F. Carvalho, S. H. Kim and C. A. Chang, *Inorg. Chem.*, 1992, **31**, 4065; (c) W. P. Cacheris, S. C. Quay and S. M. Rocklage, *Magn. Reson. Imaging.*, 1990, **8**, 467.
19. W. C. Eckelman, S. M. Karesh and R. C. Reba, *J. Pharm. Sci.*, 1975, **64**, 704.
20. S. Dutta, S. K. Kim, D. B. Patel, T. J. Kim and Y. M. Chang, *Polyhedron*, 2007, **26**, 3799.
21. D. J. Hnatowich, B. Friedman, B. Clancy and M. Novak, *J. Nucl. Med.*, 1981, **22**, 810.
22. G. W. Kabalka, M. A. Davis, T. H. Moss, E. Buonocore, K. Hubner, E. Holmberg, K. Maruyama and L. Huang, *Magn. Reson. Med.*, 1991, **19**, 406.
23. F. Jasanada and F. Nepveu, *Tetrahedron Lett.*, 1992, **33**, 5145.
24. K. Kimpe, T. N. Parac-Vogt, S. Laurent, C. Pierart, L. V. Elst, R. N. Muller and K. Binnemans, *Eur. J. Inorg. Chem.*, 2003, 3021.
25. X. Zhao, R. X. Zhuo, Z. G. Lu and W. Y. Liu, *Polyhedron*, 1997, **16**, 2755.
26. S. C. Quay, *US. Pat.*, 4,687,659, 1987.
27. J. M. Harris, N. E. Martin and M. Modi, *Drug Delivery Sys.*, 2001, **40**, 539.

28. A. D. Sherry, W. P. Cacheris and K. T. Kuan, *Magn. Reson. Med.*, 1988, **8**, 180.
29. M. S. Konings, W. C. Dow, D. B. Love, K. N. Raymond, S. C. Quay and S. M. Rocklage, *Inorg. Chem.*, 1990, **29**, 1488.
30. W. P. Cacheris, S. C. Quay and S. M. Rocklage, *Magn. Reson. Imaging.*, 1990, **8**, 467.
31. G. C. Geraldès, A. M. Urbano, M. C. Alpoim, M. A. Hoefnagel and J. A. Peters, *J. Chem. Soc. Chem. Comm.*, 1991, 656.
32. L. V. Elst, A. Roch, P. Gillis, S. Laurent, F. Botteman, W. M. Bulte and R. N. Muller, *Magn. Reson. Med.*, 2002, **47**, 1121.
33. G. C. Geraldès, A. M. Urbano, M. C. Alpoim, A. D. Sherry, K. T. Kuan, R. Rajagopalan, F. Maton and R. N. Muller, *Magn. Reson. Imaging.*, 1995, **13**, 401.
34. G. E. Krejcarek and K. L. Tucker, *Biochem. Biophys. Res. Commun.*, 1977, **77**, 581.
35. Z. Jaszberenyi, E. Toth, T. Kalai, R. Kiraly, L. Burai, E. Brucher, A. E. Merbach and K. Hideg, *Dalton Trans.*, 2005, 694.
36. W. A. Bligh, M. S. Chowdury, M. Mcpartlin and I. J. Scowen, *Polyhedron*, 1995, **14**, 567.
37. Y. M. Wang, T. H. Cheng, G. C. Liu and R. S. Sheu, *J. Chem. Soc. Dalton Trans.*, 1997, 833.
38. W. A. Bligh, M. S. Chowdhury, D. Kennedy, C. Luchinat and G. Parigi, *Magn. Reson. Med.*, 1999, **41**, 767.
39. J. Feng, G. Sun, F. Pei and M. Liub, *Bioorg. Med. Chem.*, 2003, **11**, 3359.
40. R. W. Weber, M. P. Periyasamy, *US. Pat.*, 5,137,711, 1992.
41. L. deLearie, W. H. Lin, D. A. Moore, D. H. White, *US. Pat.*, 5,508,388, 1996.
42. H. Imura, G. R. Choppin, W. P. Cacheris, L. A. de Learie, T. J. Dunn and D. H. White, *Inorg. Chim. Acta.*, 1997, **258**, 227.
43. Y. M Wang, S.T Lin, Y. J. Wang and R. S. Sheu, *Polyhedron*, 1998, **17**, 2021.
44. Y. M Wanga, Y. Ju Wanga, R. S Sheub, G. C Liub, W. C Linc and J. H. Lia, *Polyhedron*, 1999, **18**, 1147.
45. S. Aime, F. Benetollo, G. Bombieri, S. Colla, M. Fasan and S. Paoletti, *Inorg. Chim. Acta.*, 1997, **254**, 63.
46. D. Parker, K. P. Fiona, C. Smith, A. Batsanov and A. K. Howard, *J. Chem. Soc. Dalton Trans.*, 1994, 689.
47. S. Aime, M. Botta, W. Dastru, M. Fasano, M. Panero and A. Arnelli, *Inorg. Chem.*, 1993, **32**, 2068.

48. D. W. Zhang, Z. Y. Yang, B. D. Wang, S. P. Zhang and R. D. Yang, *Chem. Pharm. Bull.*, 2006, **54**, 1203.
49. A. Scozzafava, L. Menabuoni, F. Mincione, G. Mincione and C. T. Supuran, *Bioorg. Med. Chem. Lett.*, 2001, **11**, 575.
50. C. H. Paik, M. A. Ebbert, P. R. Murphy, C. R. Lassman, R. C. Reba, W. C. Eckelman, K. Y. Pak, J. Powe, Z. Steplewski and H. Koprowski, *J. Nucl. Med.*, 1983, **24**, 1158.
51. (a) M. W. Sundberg, C. F. Meares, D. A. Goodwin and C. I. Diamanti, *J. Med. Chem.*, 1974, **17**, 1304; (b) M. W. Sundberg, C. F. Meares, D. A. Goodwin and C. I. Diamanti, *Nature*, 1974, **250**, 587.
52. K. H. Choi, Y. D. Hong, M. S. Pyun and S. J. Choi, *Bull. Korean Chem. Soc.*, 2006, **27**, 1194.
53. S. M. Quadri and H. Mohammadpour, *Bioorg. Med. Chem. Lett.*, 1992, **2**, 1661.
54. M. A. Williams and H. Rapoport, *J. Org. Chem.*, 1993, **58**, 1151.
55. P. L. Anelli, F. Fedeli, O. Gazzotti, L. Lattuada, G. Lux and F. Rebasti, *Bioconjugate Chem.*, 1999, **10**, 137.
56. T. Storr, B. R. Cameron, R. A. Gossage, H. Yee, R. T. Skerlj, M. C. Darkes, S. P. Fricker, G. J. Bridger, N. A. Davies, M. T. Wilson, K. P. Maresca and J. Zubieta, *Eur. J. Inorg. Chem.*, 2005, 2685.
57. D. A. Westerberg, P. L. Carney, P. E. Rogers, S. J. Kline and D. K. Johnson, *J. Med. Chem.*, 1989, **32**, 236.
58. F. W. Keana and J. S. Mann, *J. Org. Chem.*, 1990, **55**, 2869.
59. S. Laurent, F. Botteman, L. V. Elst and R. N. Muller, *Helv. Chim. Acta.*, 2004, **87**, 1077.
60. Y. Arano, T. Uezono, H. Akizawa, M. Ono, K. Wakisaka, M. Nakayama, H. Sakahara, J. Konishi and A. Yokoyama, *J. Med. Chem.*, 1996, **39**, 3451.
61. L. Frullano, J. Rohovec, S. Aime, T. Maschmeyer, M. I. Prata, J. P. de Lima, G. C. Geraldes and J. A. Peters, *Chem. Eur. J.*, 2004, **10**, 5205.
62. B. Hamdaoui, G. Dewynter, F. Capony, J. L. Montero, C. Toiron, M. Hnach and H. Rochefort, *Bull. Soc. Chim. Fr.*, 1994, **131**, 854.
63. J. F. Carvalho, S. P. Crofts, S. M. Rocklage, *EP Pat.*, 91/00126, 1991.
64. J. M. Couchet, J. Azema, P. Tisnes and C. Picard, *Inorg. Chem. Commun.*, 2003, **6**, 978.
65. R. Artali, M. Botta, C. Cavallotti, G. B. Giovenzana, G. Palmisano and M. Sisti, *Org. Biomol. Chem.*, 2007, **5**, 2441.

66. C. H. Cummins, E. W. Rutter and W. A. Fordyce, *Bioconjugate Chem.*, 1991, **2**, 180.
67. M. W. Brechbiel and O. A. Gansow, *Bioconjugate Chem.*, 1991, **2**, 187.
68. M. A. Williams and H. Rapoport, *J. Org. Chem.*, 1994, **59**, 3616.
69. I. F. Pickersgill, H. Rapoport, *J. Org. Chem.*, 2000, **65**, 4048.
70. H. S. Chong, K. Garmestani, L. H. Bryant and M. W. Brechbiel, *J. Org. Chem.*, 2001 **66**, 7745.
71. G. Duarte, H. Gil, A. Peters, M. Colet, L. V. Elst, N. Muller and G. C. Geraldes, *Bioconjugate Chem.*, 2001, **12**, 170.
72. (a) M. Wolf, W. E. Hull, W. Mier, S. Heiland, U. B. Wust, R. Kinscherf, U. Haberkorn and M. Eisenhut, *J. Med. Chem.*, 2007, **50**, 139; (b) C. Muller, R. Schibli, E. P. Krenning and M. D. Jong, *J. Nucl. Med.*, 2008, **49**, 623; (c) C. J. Mathias, D. Hubers, P. S. Low and M. A. Green, *Bioconjug Chem.*, 2000, **11**, 253; (d) M. W. Brechbiel, O. A. Gansow, R. W. Atcher, J. Schlom, J. Esteban, D. Simpson and D. Colcher, *Inorg. Chem.*, 1986, **25**, 2772.
73. M. S. Ardestani, A. J. Arabzadeh, Z. Heidari, A. Hosseinzadeh, H. Ebrahimi, E. Hashemi, M. Mosayebnia, M. S. Alavidjeh, A. Alavi, M. H. Babaei, A. Rahmim, E.S. Ebrahimi and M. Amanlou, *J. Radioanal. Nucl. Chem.*, 2010, **283**, 447.
74. K. H. Choi, Y. D. Hong, M. S. Pyun and S. J. Choi, *Bull. Korean Chem. Soc.*, 2006, **27**, 1194.
75. P. L. Anelli, F. Fedeli, O. Gazzotti, L. Lattuada, G. Lux and F. Rebasti, *Bioconjugate Chem.*, 1999, **10**, 137.
76. H. Essien, J. Y. Lai and K. J. Hwang, *J. Med. Chem.*, 1988, **31**, 898.
77. H. A. Song, M. Dadwal, Y. Lee, E. Mick and H. S. Chong, *Angew. Chem.*, 2009, **121**, 1354.
78. X. Du, Y. Dai, R. He, S. Lu and M. Bao, *Syn. Commun.*, 2009, **39**, 3940.
79. M. A. Williams and H. Rapoport, *J. Org. Chem.*, 1993, **58**, 1151.
80. M. Licchelli, A. O. Biroli, A. Poggi, D. Sacchi, C. Sangermania and M. Zema, *Dalton Trans.*, 2003, 4537.
81. T. N. Parac-Vogt, K. Kimpe, S. Laurent, C. Pierart, L. V. Elst, R. N. Muller and K. Binnemans, *Eur. J. Inorg. Chem.*, 2004, 3538.
82. T. Koullourou, L. S. Natrajan, H. Bhavsar, J.A. Pope, J. Feng, J. Narvaine, R. Shaw, E. Scales, R. Kauppinen, A. M. Kenwright and S. Faulkner, *J. Am. Chem. Soc.*, 2008, **130**, 2178.

Chapter 4: PART A
Relaxivity Measurements

A.4.1 What is Relaxivity? Or Why is it Important?

The relaxation of a paramagnetic contrast agent could be defined as the ability of a paramagnetic agent to enhance the relaxation rate of surrounding water protons. The factors responsible for the relaxivity and their effects are not to be understood fully. Theoretical models, however, describe a long way to probe the factors affecting relaxivity.

A.4.1.1 Introduction of paramagnetic contrast agents

Most of the paramagnetic contrast agents are administered in high concentrations (0.1 mM) in which the relaxivity is not linearly related to higher dosages, see Fig-1). Usually, relaxivity of an agent is an issue. Paramagnetic contrast agents with high relaxivity could be used in lower doses or reduced contrast is equivalent dose in solution. The relaxivity of an agent is determined according to the standard theory of Solomon-Bloembergen. It should be possible to produce contrast agents with relaxivities more than 10 times higher than those that exist in current usage.

CHAPTER 4
Evaluation
of
Potential
Contrast Agents

Chapter 4: PART A

Relaxivity Measurements

A.4.1 What is Relaxivity? Or Why is it Important?

The relaxivity of a paramagnetic contrast agent could be defined as the ability of a paramagnetic chelate of 1mM concentration in solution, to enhance the relaxation rate of surrounding water protons. The factors contribute to the relaxivity and their effects are yet to be uncovered fully. Throughout history, however, scientists have travelled a long way to probe the factors affecting relaxivity.¹

A.4.1.1 The factors defining relaxivity

Optimisation of parameters of the relaxivity

Most of the commercially available contrast agents are efficacious only at high concentrations; 0.1 mM (with the exception of gadobutrol, which could be administered in higher dosages, see Fig-1). Naturally, enhancement of sensitivity is an issue. Paramagnetic chelates with high relaxivities could be detected in lower doses or enhance contrast at equivalent doses in relation to compounds with lower relaxivity. According to the standard theory of ‘Solomon-Bloembergen-Morgan’, it was predicted that it should be possible to produce contrast agents with relaxivities, more than 50 times higher than those that exist in current usage.²

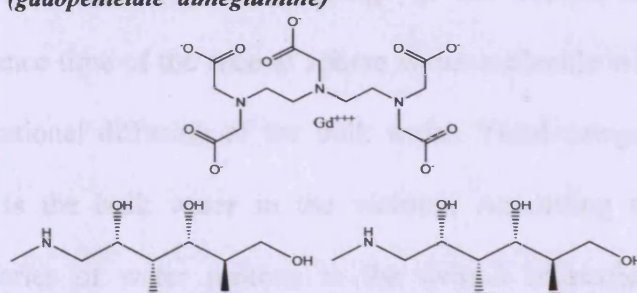
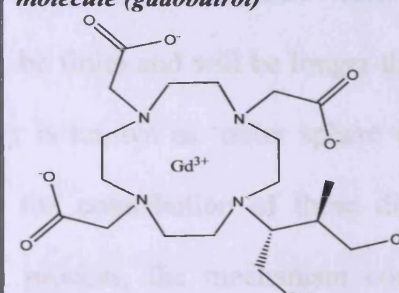
Gadolinium-based contrast agents				
Organ Specific/ Blood pool	Extracellular			
Linear ionic		Linear non-ionic	Macrocylic	
0.25M	0.5 M		1.0 M	
Gadoxetic acid (Primovist®)	Gadopentetate dimeglumine (Magnevist®)	Gadoversetamide (OptiMARK®)	Gadoteridol (ProHance®)	Gadobutrol (Gadovist®)
Gadofosveset	Gadobenate dimeglumine	Gadodiamide (Omniscan®)	Gadoterate meglumine (Dotarem®)	
<i>Example of a linear molecule (gadopentetate dimeglumine)</i> 			<i>Example of a macrocyclic molecule (gadobutrol)</i> 	

Figure 1:- Depicting the variety of commercial contrast agents currently in use

Therefore, with the advancement of NMR imaging, two major approaches have been undertaken to enhance relaxivities. Firstly, through the optimisation of parameters those are governing the relaxivity of the water protons (such as water exchange rate, rotational correlation time) and secondly, through linking the gadolinium complexes. For instance, gadolinium chelates appended to a polyamide dendrimer (giving rise to Gadomer), reported to possess high relaxivities ($16.5 \text{ mM}^{-1}\text{s}^{-1}$ at 40°C , 0.47 tesla per Gd). To optimise rotational correlation times, macromolecules are employed. These macromolecules employed in the covalent or non-covalent binding could be ranging from natural molecules like DNA³, proteins⁴, lipids,⁵ and have been widely reported in many reviews.

Defining 'Relaxivity'

In mathematical terms relaxivity could be defined, as the degree of change in the relaxation rate of the water protons, after the administration of the contrast agent, normalized to the concentration of the paramagnetic chelate (see Eq-1).

$$r_1 = \frac{\Delta(1/T_1)}{[M]} \quad (1)$$

Potential Multimodal Imaging Agents

'Relaxivity of the solvent water protons is a complex, multifaceted phenomenon. In typical *in-vitro* or *in-vivo* studies, initially, the water protons situated in close proximity to the paramagnetic metal ion are relaxed. This relaxation effect is then translated rapidly to bulk water in the vicinity. T_1 relaxation of water protons induced by the Gd (III) ion takes place mainly through a dipolar mechanism. To explain this mechanism, water could be divided in to three categories. Firstly as 'inner sphere water', where oxygen atom of the water molecule is directly coordinated to the paramagnetic centre. The water molecules involved in the hydration of the complex belongs to the second category, 'second sphere water'. The residence time of the second sphere water molecule will be finite and will be longer than the translational diffusion of the bulk water. Third category is known as 'outer sphere water'. This is the bulk water in the vicinity. According to the contribution of these different categories of water protons to the overall relaxation process, the mechanism could be classified in to three major categories. Firstly, as 'Inner sphere mechanism' and secondly as 'Outer sphere mechanism' finally as 'Second coordination sphere mechanism'.

Inner sphere mechanism

This is most significant and widely studied contribution to the relaxivity. Gd (III) has a high magnetic moment (7.9 BM) due to seven unpaired electrons. Therefore high relaxivity is produced by the fluctuating dipole created by the interaction of the electron spin of the paramagnetic centre with that of the nuclear spins of the water protons. This fluctuating dipole could facilitate the spin transitions and spin relaxation.

To understand this dipole, it could be characterised in terms of a time constant, known as the correlation time ($1/\tau_c$). There are four different correlation times that have been identified and named according to their origin of contribution. Firstly, rotational diffusion of the complex contributes to the fluctuating dipole, this is known as the rotational correlation time ($1/\tau_R$) and secondly, residence time of the water proton in the inner coordination sphere ($1/\tau_m$) (residence time is also referred to as water exchange rate between the inner or 2nd coordination sphere and the outer coordination sphere).

The rest of the contribution arises from electronic longitudinal relaxation rate ($1/T_{1e}$) and the transverse relaxation rate ($1/T_{2e}$) (also see Eq-4).

The parameters influencing Inner sphere Mechanism

To understand the complex process, Peter Caravan proposed the following diagram⁷ (see Fig- 2).

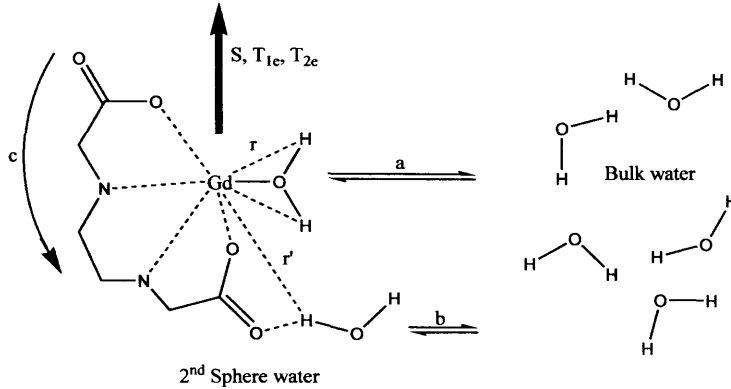


Figure 2:- Diagrammatic representation of the parameters influencing inner sphere mechanism.⁷

According to the figure, there are q water molecules in the inner coordination sphere with Gd-H distance of r , residency time τ_m . Further gadolinium ion is denoted by a large vector due to its high magnetic dipole, which is indicated by spin S . These spins undergo longitudinal and transverse relaxation, described in terms of T_{1e} and T_{2e} , respectively. Moreover, assuming the complex tumbles isotropically, the rotational diffusion could be attributed towards rotational correlation time. This is denoted by τ_R . Also we must take in to consideration the second sphere water with a distance of r'_{Gd-H} , its residence time could be denoted by τ_m' . It is evident that the influence of these parameters to each other could not be ascertained by measuring the relaxivity alone. Through the relaxivity measurement, however, some of the parameters could be determined individually, and thereby other parameters could be simulated. The contribution of the inner sphere water, to the relaxivity could be described by the following equation

$$r_1^{IS} = \frac{q/[H_2O]}{(T_{1m} - \tau_m)} \quad (2)$$

T_{1m} is the proton relaxation time of water protons in the inner coordination sphere. Clearly, to optimise relaxivity, one must lower the T_{1m} and τ_m , while increasing the q . It is obvious that the concentration of the water can not be altered.

Hydration Number (q)

Although the concentration of the water molecules could not be altered, it was discovered that it is possible to adjust the number of water molecules in the inner sphere. So as to say, the hydration number could be altered. This could be achieved by creating more vacant sites for the oxygen atom of the water molecules. There is, however, an inherent risk involved in carrying out this exercise. When the coordination sites around the metal ions get reduced, it compromises thermodynamic stability of the complex. This will result in increased toxicity. The second trade-off in increasing the q is the possibility of coordination with other ligands (such as phosphate and carbonate which are endogenous anions). This will in turn, displace the water molecules and lead on to reduction in relaxivity.

The estimation of hydration number could be carried out through X-ray crystallography and luminescence life time measurements (on isostructural Eu complexes). ENDOR⁸ spectroscopy is also employed presently to determine the hydration number. This technique basically correlates the difference in the intensity of the ENDOR spectrum taken in both D₂O and H₂O of the complex. The hydroxy pyridinone compounds reported by Raymond *et al.*⁹ stand in testimony of a successful optimisation of hydration number.

They have determined the q value as 2 and the complex was found to be thermodynamically stable, coupled with the resistance to anion coordination.⁹

The water proton relaxation rate (T_{1m})

From Eq-2 it is clear, water proton relaxation time of the bound water should be short as possible. T_{1m} is greater than τ_m with regard to first generation contrast agents. Further, T_{1m} is the limiting factor for relaxivity of these contrast agents.

Therefore an understanding of the factors influences T_{1m} , will be helpful to comprehend the role of other parameters affecting the relaxivity of a contrast agent. Following equations will provide the necessary foundation (see Eq-3 and Eq-4).

$$\frac{1}{T_{1m}} = \frac{2}{15} \frac{\gamma_H^2 g_e^2 \mu_B^2 S(S-1)}{r_{GdH}^6} \left[\frac{7\tau_{c2}}{1 - \omega_S^2 \tau_{c2}^2} - \frac{3\tau_{c1}}{1 - \omega_H^2 \tau_{c1}^2} \right] \quad (3)$$

$$\frac{1}{\tau_{ci}} = \frac{1}{\tau_m} + \frac{1}{\tau_R} + \frac{1}{T_{ic}}; i = 1, 2 \quad (4)$$

The terms in the equation are:

The distance between the bound water and that of Gd (III), r_{GdH} , the electron Larmor frequency ω_s ($\omega_s = 658\text{vH}$), proton Larmor frequency ω_H and correlation times of τ_{c1} and τ_{c2} related to longitudinal relaxation and transverse relaxation respectively.

As from the above equations, it is evident that the factors affecting correlation times related to longitudinal and transverse relaxation influences the inner sphere water proton relaxation.

Gadolinium –water distance

Literature values ranging 2.7-3.1 Å have been obtained indirectly from fitting of NMRD data. It is possible to directly measure this parameter through ENDOR spectroscopy. It will be of paramount importance if it could be reduced some how; it will lead to significant enhancement in relaxivity (see Eq-3). It is, however, virtually impossible to alter this parameter.

Rotational correlation time

As aforementioned, the contribution to the correlation time arises through the three factors, namely rotational diffusion, electronic relaxation and water residence time.

The commercially available MRI scans, however, operate at 1.5 Tesla. At this field, the correlation time is predominantly attributed to rotational diffusion. A simple monomeric Gd complex will have τ_R of 0.1ns on average. The attachment of proteins, however, will increase the tumbling time resulting in enhanced relaxivity.¹⁰

Rotational diffusion could be determined by number of techniques, such as EPR, fluorescence and NMR spectroscopy. A huge amount of work has been undertaken to optimise the rotational correlation time¹¹ there by increasing the relaxivity.

Electronic relaxation time

This is a complex phenomenon and depends on the field strength of the magnetic field. Similar to the rotational correlation time, 'electronic relaxation time' also needs optimisation. This is because at low fields (0.1 Tesla), electronic relaxation time is very high and predominantly contributed to correlation time. At high fields, however, electronic relaxation will be declining to an extent where at some point it becomes slower than the rotational motion

$$1/T_{1e}, 1/T_{2e} \gg 1/\tau_R; T_{1e} \approx \tau_{e1}, T_{2e} \approx \tau_{e2}$$

at low field ($B_0 < 0.1$ T)

$$1/T_{1e}, 1/T_{2e} \ll 1/\tau_R; \tau_R \approx \tau_{e1} \approx \tau_{e2}$$

at high field ($B_0 > 1.5$ T)

Water residence time or Water exchange rate

The relaxation effect experienced by the bound water molecule in the inner coordination sphere is transmitted to the bulk solvent through the exchange of water molecules. This is characterised in terms of water residency time or sometimes called water exchange rate. Water exchange is an inevitable factor which determines the relaxivity. This parameter influences the relaxivity directly as well as through the influence exerted on the proton relaxation time (sees Eq-2 and Eq-4).

There is an intense need, however, to optimise the water exchange rate. The relaxivity of a Gd based contrast agent could be limited; if the water exchange rate is too slow as the relaxation effect is transferred poorly to the bulk.

On the other hand, if the water exchange rate is very high, relaxivity will be reduced as the water molecule does not remain coordinated to the Gd (III), long enough for it to be relaxed. The water exchange rate could be directly measured through ^{17}O NMR transverse relaxation rate measurements.

A.4.1.2 Influence of Temperature and Field strength in the measurement of Relaxivity

Given that temperature influences the rate of water exchange and rotational diffusion, it is evident that temperature changes will have profound effect on relaxivities. Therefore it is a must to report relaxivity data with the appropriate temperature used. The appreciable temperature could be 37 °C due to the fact, it is the physiological temperature. Field strength also equally influences the relaxivity data. The high field strengths are increasingly used in today's clinical practice. This in turn increases the tissue relaxation times. Therefore long tissue relaxation time and high resolution scans lead on to long acquisition times. The use of a contrast agent, however, significantly reduces the acquisition time.

To estimate the efficacy of the contrast agent, prior to the *in-vivo* imaging studies, a detailed investigation will be carried out *in-vitro*. In this respect, the investigations carried out with Fast field reflexometry are of paramount importance. Therefore following section will give a brief introduction to this very important technique.

A.4.1.3 Principles of NMR spectroscopy underlying the Magnetic Resonance Imaging

The subatomic particles, electron, proton and neutron all possess spin of a half by nature. This spin could be positive or negative. Within an atom any of their arrangement will ensure a combined value of zero or multiples of $\frac{1}{2}$. In an applied magnetic field, bearing field strength of B_1 , a particle with a net spin can absorb a photon of frequency ν .

This ν is dependent on the gyro magnetic ratio, which is a characteristic constant for a particular nucleus. For instance $\gamma_H = 42.58 \text{ MHz / T}$.

$$\nu = \gamma B \quad (5)$$

A proton, because of its inherent spinning, generates a magnetic field, thus has a magnetic moment vector. When the proton is subjected to an applied magnetic field, the spin vector of the particle gets aligned with the applied magnetic field. This alignment could be parallel or anti-parallel. Hence, the spins with a high energy configuration will be aligned along the

direction of the magnetic field, while the spins belong to the lower energy configuration will be aligned in the opposite direction of applied magnetic field. If the system is subjected to radio frequency (RF) radiation at this stage, it may lead on to transition of the low energy proton to the high energy spin state. This transition is possible only if the energy of the photon absorbed by the proton overcomes the energy barrier of the two spin states (i.e energy difference between low and high energy spin states). The frequency in relation to the energy of the photon responsible for this transition is known as 'resonance' or 'lamor frequency'. This is influenced by another factor, planks constant ($h = 6.626 \times 10^{-34}$ Js). See Eq-6.

$$E = h\nu \quad (6)$$

Combing equations (5) and (6) leads to the expression:

$$E = h\gamma B \quad (7)$$

The slight excess of spins in the lower energy level, N^* , compared to the higher energy level, N , is reflected in expression (4):

$$N/N^* = e^{-E/kT} \quad (8)$$

Where E is energy difference of the high and low energy spin states; k is Boltzmann's constant (1.3805×10^{-23} J/Kelvin); and T is the temperature in Kelvin. The ratio N/N^* will decrease as the temperature decreases. As the temperature increases, the ratio of the difference in population between energy states will eventually become zero. That is to say ratio N/N^* achieves unity.

The observed signal intensity in MRI arises due to the difference in energy absorbed by nuclei which undergoes transition from low to high energy spin state and that of the energy released by the nuclei due to their simultaneous transition taking place from high to low energy spin states. In other words, signal intensity is proportional to the population difference between the high and low energy spin states.

In short, sensitivity of MRI is a consequence of the energy exchange taking place between the spectrometer and that of the spins at a particular frequency. 'Targeting' proton is justified by its natural abundance (i.e. 99.985%) and also because of its biological abundance (a typical biological tissue contains more than 60% of water).

T₁ 'Longitudinal/Spin-Lattice' Relaxation

The net magnetisation vector arises from the population difference in the two spin states, aligned parallel to the externally applied magnetic field B₁. This vector is known as equilibrium magnetisation (denoted by M₁). The vector solely composed of longitudinal magnetisation component (M_Z) and there are no transverse components (M_X and M_Y) involved.

When this nuclear spin system is subjected to RF radiation of a frequency equal to that of the energy barrier between the two spin states, net magnetisation vector will be altered and it will acquire a transverse component.

At the same time, clearly, nuclei will be rotating around the z axis at a frequency equal to that of the frequency of the photon that induces transition between the two energy states. If the magnitude of the RF radiation is of sufficient intensity, then the spin system will be saturated. Therefore the net magnetisation vector comprises entirely the transverse component, inducing the M_Z to become zero.

When the applied radiation is removed, however, the spin system relaxes back to the initial equilibrium state. This induces the recovery of the longitudinal magnetisation to its initial equilibrium value. This process is illustrated by a time constant. This time constant is known as spin-lattice relaxation time, denoted by T₁. The variation of M_Z as a function of time t (after initial displacement) could be depicted through the following equation.

$$M_Z = M_1 (1 - e^{-t/T_1}) \quad (9)$$

Therefore, after time T₁, the longitudinal magnetisation will have returned to 63% of its initial value (see Fig-3).

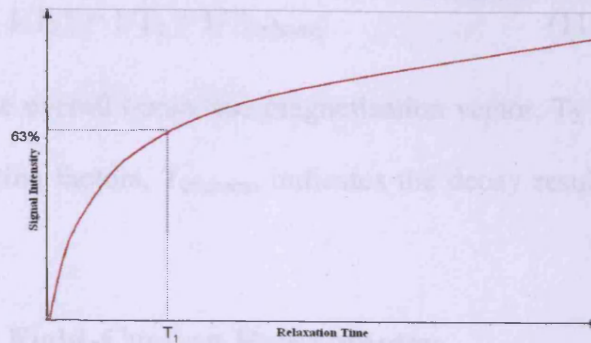


Figure 3:- A graphical representation of equation 9, showing how the recovery of the longitudinal magnetisation follows an exponential process.

T_2 'Transverse/Spin-Spin' Relaxation

The transverse component of the net magnetisation vector is designated as M_{xy} and is perpendicular to B_0 . The pattern of growth of T_2 is a complex phenomenon. The explanation, however, could be attempted as follows.

The rotation around B_0 by the nuclei together, creates interaction of the local magnetic fields produced by the spinning protons. This will lead on to the cumulative loss in phase with time. The process of the recovery of transverse magnetisation vector to its equilibrium state is best described by a time constant. This time constant is known as the spin-spin relaxation time, T_2 and could be illustrated by the following equation. Also see Fig-4.

$$M_{XY}(t) = M_{XY}(0) e^{-t/T_2} \quad (10)$$

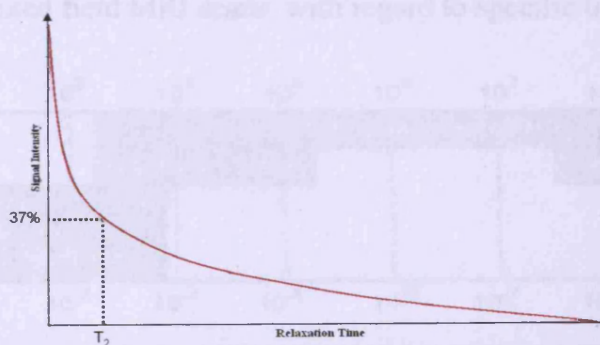


Figure 4:- A graphical representation of equation 10, showing how the recovery of the transverse magnetisation follows an exponential process.

The spin-spin relaxation is also caused by the magnetic field inhomogeneity experienced by the nuclei, *in-vivo*. Further, the various chemical environments in which protons are located also causes the dephasing of the transverse magnetisation vector. Therefore, the overall decay of the transverse magnetisation could be attributed to both these factors. This is illustrated by the following equation.

$$1/T_2^* = 1/T_2 + 1/T_{2\text{inhomo}}$$

Where T_2^* indicates the overall transverse magnetisation vector. T_2 indicates spin-spin decay without these contributing factors, $T_{2\text{inhomo}}$ indicates the decay resulting from magnetic field inhomogeneity.

A.4.1.4 Fast Field-Cycling Relaxometry

Significance and Applications

Field cycling relaxometry is an exclusive technique among the various NMR techniques (see Fig-5) available. Field cycling relaxometry allows one to cover several decades of frequency by utilising the same instrument.

There are various applications of the field cycling relaxometry in the literature that could be discussed; bio polymers, investigations regard to biological tissues, liquid crystals and lipid bilayer investigations¹² to name a few.

Due to its versatility to determine T_1 decay over a range of field strengths, however, it has emerged as the powerful tool for characterisation of molecular dynamics, especially in complex media.

More precisely it has provided the basis for Fast field cycling MRI and has provided advantage an over the fixed field MRI scans, with regard to specific tissue imaging.¹³

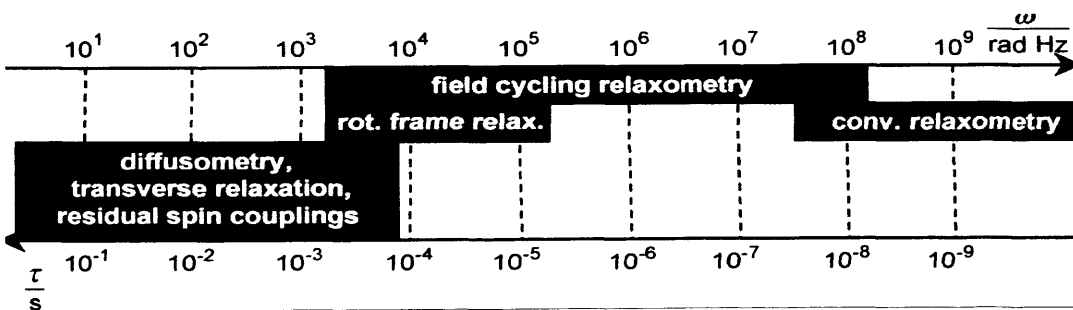


Figure 5:- Depicting the variety of NMR techniques available over a range of angular frequencies and time

A.4.1.4.1 General Aspects of Practical Application of FFC

During a fast field-cycling relaxometry (FFC) experiment carried out in a relaxometer, one measures the spin lattice relaxation time of a sample as a function of external magnetic field.

This external magnetic field is cycled through a range of discrete field strengths.

Although, spin-lattice relaxation time is the most commonly measured parameter, spin-spin relaxation times are also measured by FFC, to obtain further information occasionally.

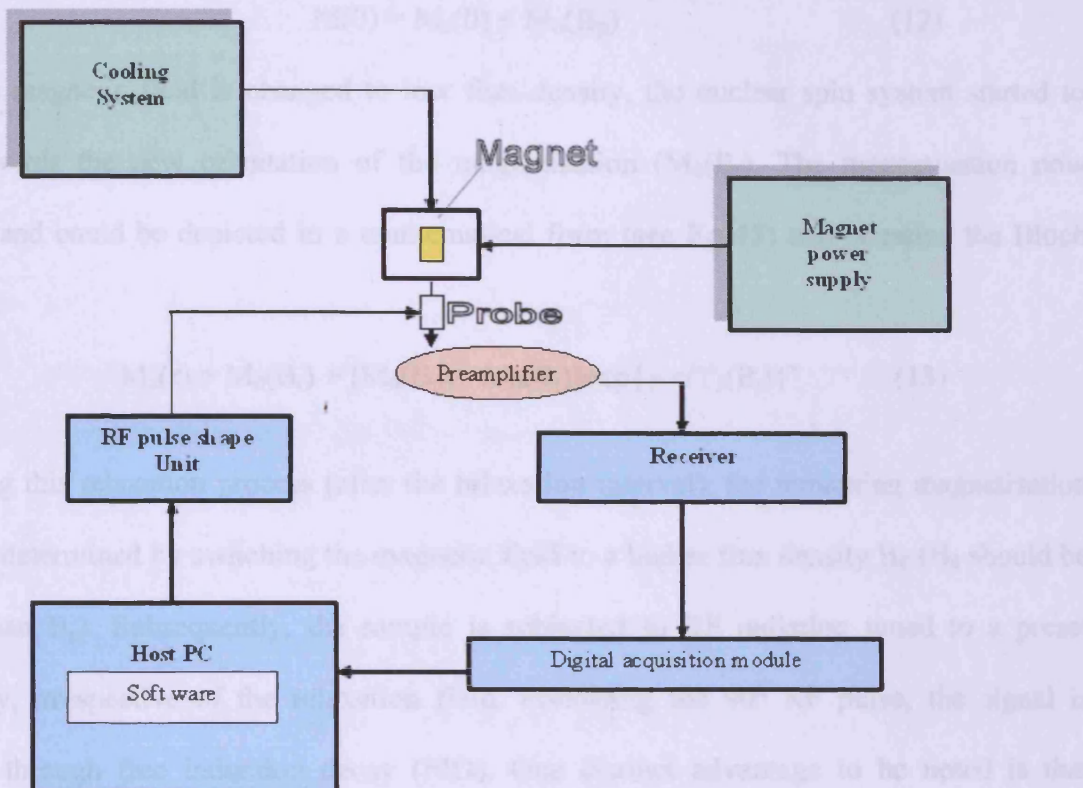


Figure 6:- Schematic representation of the typical field cycling relaxometer

A.4.1.4.2 Basic principles of FFC

As aforementioned, FFC is used to obtain, nuclear magnetic relaxation profiles. This is possible by employing two different methods, namely pre-polarised sequence (PPS) and non-polarised sequence (NPS).

Pre- Polarised Sequence used in low fields (When $B_r \ll B_p$)

When compiling NMRD profile, during the PPS phase, initially a strong magnetic field is established, B_p . This will polarise the nuclear spin system as in a typical NMR experiment. Thereafter, the instrument switches the magnetic field of the higher flux density, B_p towards lower flux density, B_r . The magnetic field will remain in this low flux density for a known period of time, τ (as far as, Stellar Spin master FFC-2000 relaxometer is concerned, switching on to high flux to low flux density is achieved, by modifying the current in the magnetic coil. There are instances, however, where mechanically the sample will be shifted onto different field strengths, for eg;-sample shuttling technique). At this stage, the magnetisation lies

parallel to the externally applied magnetic field and its value initially equal to the equilibrium magnetisation of the polarisation field (see Eq-12).

$$M(0) = M_z(0) = M_0(B_p) \quad (12)$$

Once the magnetic field is changed to low flux density, the nuclear spin system started to relax towards the new orientation of the magnetisation ($M_0(B_r)$). The magnetisation now evolves, and could be depicted in a mathematical form (see Eq-13) and is called the Bloch equation.

$$M_z(\tau) = M_0(B_r) + [M_0(B_p) - M_0(B_r)]\exp\{-\tau/T_1(B_r)\} \quad (13)$$

Following this relaxation process (after the relaxation interval), the remaining magnetisation could be determined by switching the magnetic field to a higher flux density B_d (B_d should be higher than B_p). Subsequently, the sample is subjected to RF radiation tuned to a preset frequency, irrespective of the relaxation field. Following the 90° RF pulse, the signal is detected through free induction decay (FID). One distinct advantage to be noted is that acquisition time for FID will be in milliseconds. This brings the possibility to keep the detection field period (time remaining in B_d) to be kept as short as possible. This will in turn improve the duty cycle.

In order to switch back the net magnetisation vector to $M_0(B_p)$, the field is now reverted to polarisation field, bearing flux density B_p . The field will remain at this flux density for an extended period of time, after which the process will be repeated. So as to say, the second cycle begins. This could be illustrated in Fig-3.

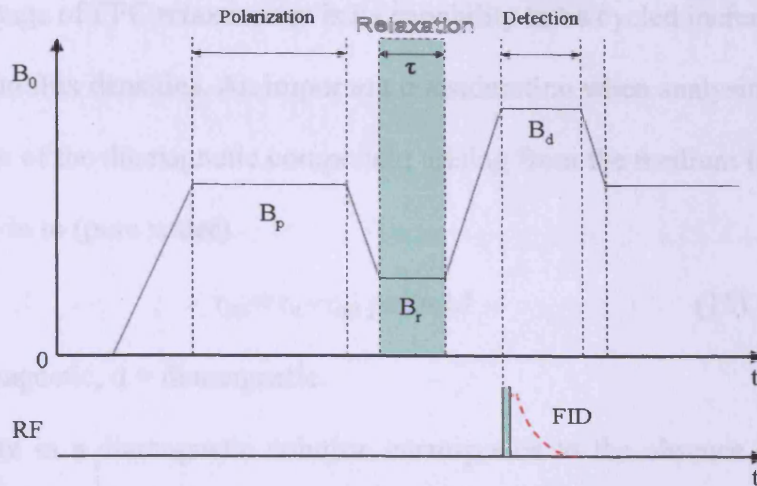


Figure 3:- Graphical representation of the variation of magnetic field strength during a pre-polarised sequence

Non-Polarised sequence used in high fields: where $B_r \rightarrow B_d$

A pre-polarised sequence is suitable in experiments where the relaxation flux density B_r , is considerably lower than the polarisation field B_p . The accuracy of the data, however, is compromised when the difference in magnetisation vector, ΔM_z^{eff} of the high and low flux densities becomes sufficiently small. This has brought up the essential need for a non-polarised sequence, especially where B_r becomes high that it approaches B_p .

Non polarised sequence begins, without the initial polarisation phase of the nuclear spin system. Thus the relaxation curve is produced through a typical inversion recovery method. An 180° pulse rotates the net magnetisation vector down to the $-z$ axis, thereafter the net magnetisation undergoes spin lattice relaxation, which returns the net magnetisation vector to its equilibrium value along the $+Z$ axis. The resulting relaxation curve will be starting from zero or quite close to zero. The relaxation curve is then of the type:

$$M_z^{detected}(\tau) = M_z^\infty - \Delta M_z^{eff} \cdot e^{-\tau/T1} \quad (14)$$

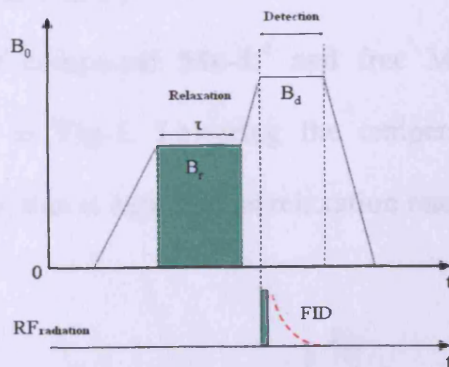


Figure 4:- Graphical representation of a non-polarised sequence, indicating the absence of polarisation field B_p ,

The major advantage of FFC relaxometry is its capability to be cycled incrementally over a range of relaxation flux densities. An important consideration when analysing relaxivity data is the contribution of the diamagnetic component arising from the medium in which the sample dissolved in to (pure water).

$$r_{ap} \equiv r_a - r_{ad} \text{ per mM} \quad (15)$$

Where p = paramagnetic, d = diamagnetic.

The reference rate in a diamagnetic solution corresponds to the absence of a paramagnetic Gd-L complex and is denoted by:

$$r_{ad} \equiv 1/T_{ad} (\alpha = 1, 2) \quad (16)$$

The relaxivity, r_a ($s^{-1} \text{ mM}^{-1}$), of a paramagnetic compound such as a contrast agent is thus defined as a paramagnetic relaxation enhancement (PRE) of added Gd-L complex:

$$r_a \equiv r_{ap} / [\text{GdL}] \quad (17)$$

Due to the large magnetic moment of the Gd^{III} centre resulting from its electronic spin $S=7/2$, the observed relaxation rates R_a increase markedly with the concentration $[\text{GdL}]$ (mM) of the Gd-L complexes added to the solution.

A.4.2 Results and Discussion

A.4.2.1 Manganese and Copper complexes of EDTA bis amino methyl pyridine (Mn-L^4 and Cu-L^4)

An Overview of Manganese Complex (Mn-L^4)

The ^1H NMRD profiles of compound Mn-L^4 and free Mn-(II) each at two different temperatures are illustrated in **Fig-1**. Lowering the temperature of the sample induces enhancement in the relaxivity, this is expected as relaxation rates are inversely proportional to the diffusion coefficient.¹⁴

At 30 MHz, the relaxivity of Mn-L^4 (at 37 °C) is $3.52 \text{ mM}^{-1}\text{s}^{-1}$, which is comparable to the performance of commercially available, gadolinium based contrast agents Magnevist[®] and Dotarem[®].

At the same time it is still markedly higher in comparison to Teslascan[®] (the only clinically approved manganese based contrast agent at present) $1.88 \text{ mM}^{-1}\text{s}^{-1}$ (at 20 MHz, 37 °C).

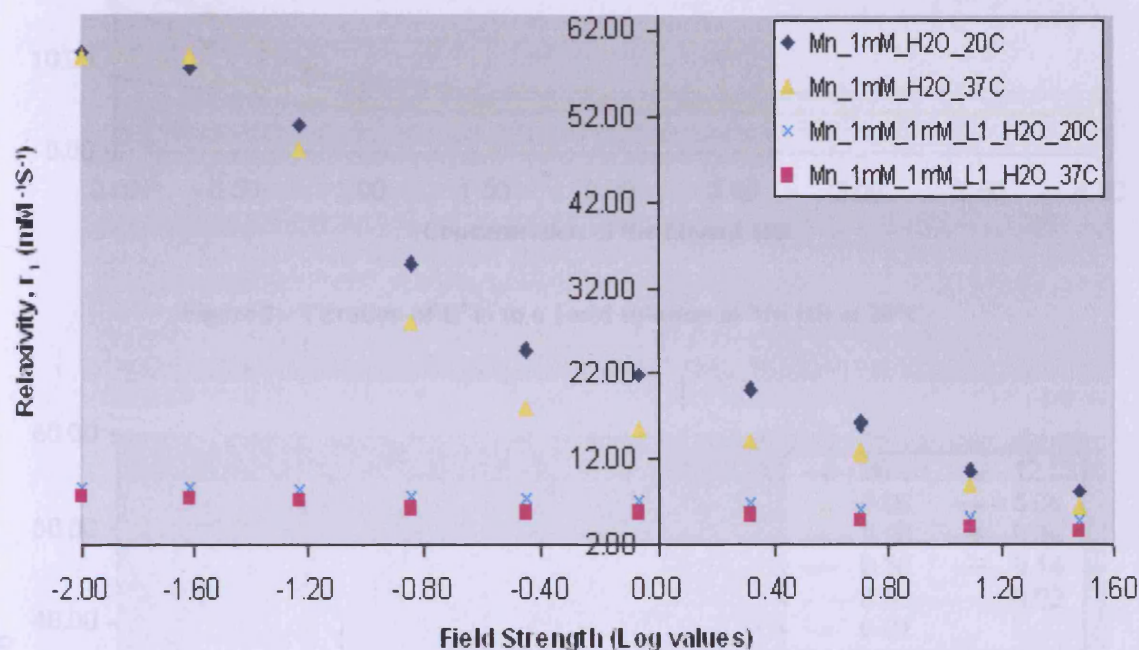


Figure 1:-The ¹H NMRD profiles of compound Mn-L^4 and Free Manganese in 20 °C and 37 °C. Figure reveals the effects of changes in temperature.

Fig-2 and Fig-3 depict the representative titration results, in this case L^4 added to 1mM solution of Mn (II) at 20 °C and 37 °C respectively. The sharp break in the L^4 titration indicates that the association constant is relatively high.

Further, high relaxivities observed before the sharp breaking point at 1 mM concentration of the ligand is due to the free Mn (II) ions, which has higher number of coordination sites for the inner sphere water molecules. The complex stability is reflected by the consistency in the relaxivity, even in higher ligand concentrations and. also clearly, a 1:1 complex is formed.

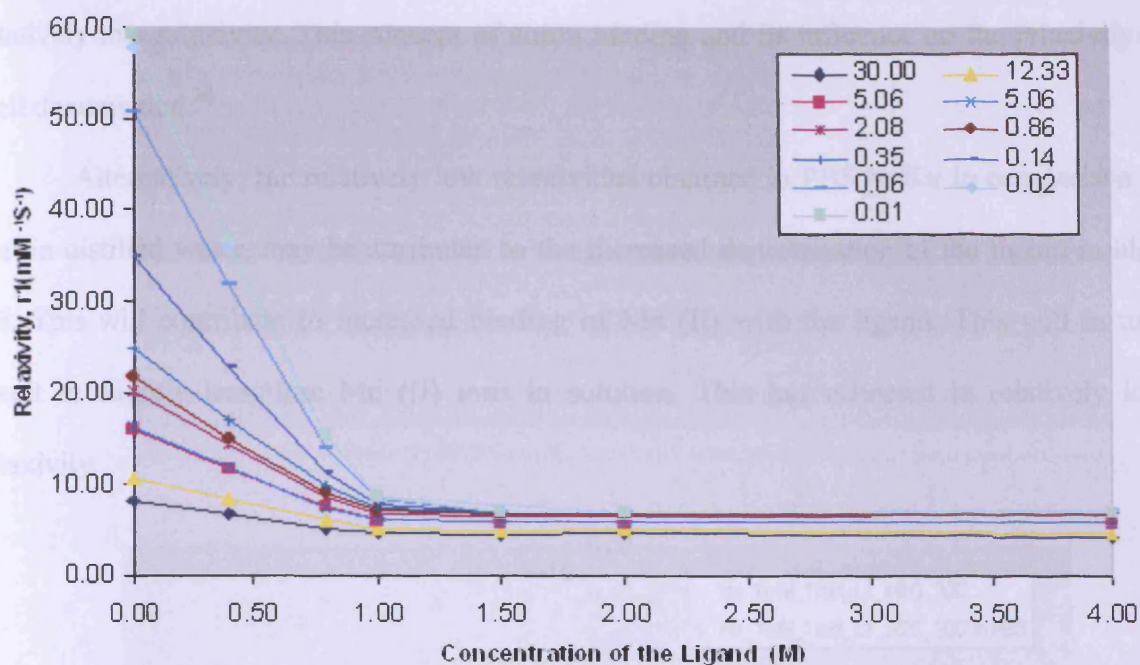


Figure 2:- Titration of L^4 in to a 1mM solution of Mn (II) at 20°C

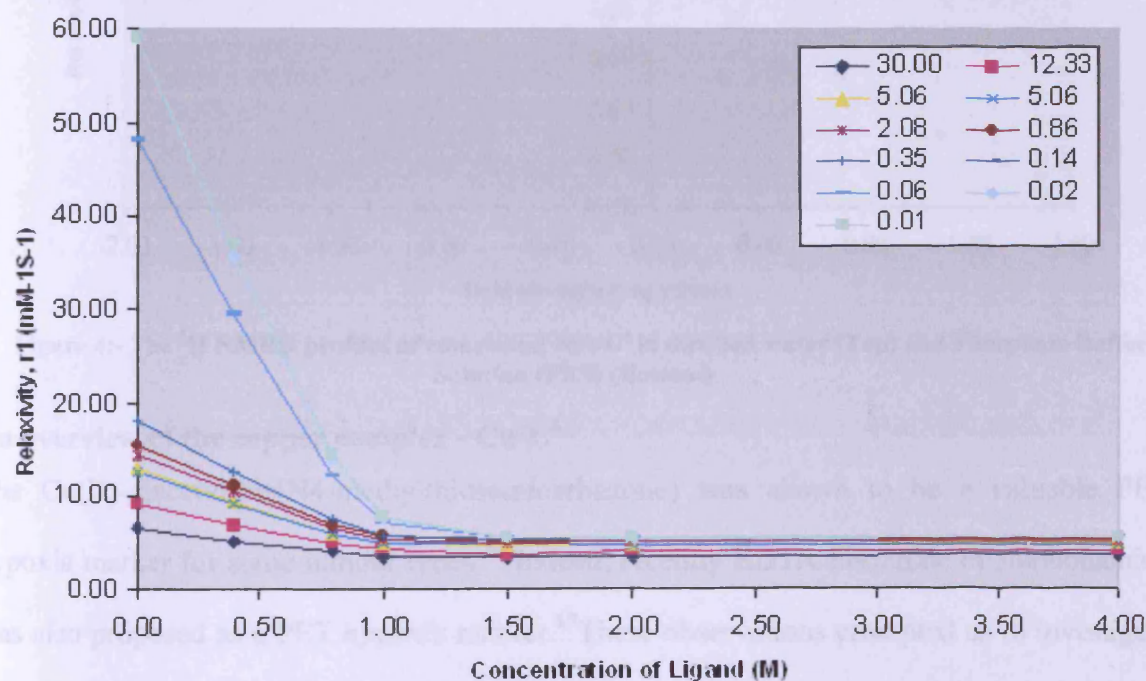


Figure 3:- Titration of L^4 in to a 1mM solution of Mn (II) at 37 °C

The 1H NMRD profile obtained upon addition of 1mM of L^4 in to 1 mM of Mn (II) in PBS and distilled water are depicted in **Fig-4**. The relatively low relaxivities obtained in PBS buffer in comparison to that in distilled water, may be attributed to phosphate ions binding to the complex, thus displacing the inner sphere water molecules.

Therefore the decrease in number of inner sphere water molecules could have resulted in relatively low relaxivity. This concept of anion binding and its influence on the relaxivity is well documented.¹⁵

Alternatively, the relatively low relaxivities obtained in PBS buffer in comparison to that in distilled water, may be attributed to the increased deprotonation of the ligand in high pH. This will contribute to increased binding of Mn (II) with the ligand. This will in turn result in slightly less, free Mn (II) ions in solution. This has reflected in relatively low relaxivity.

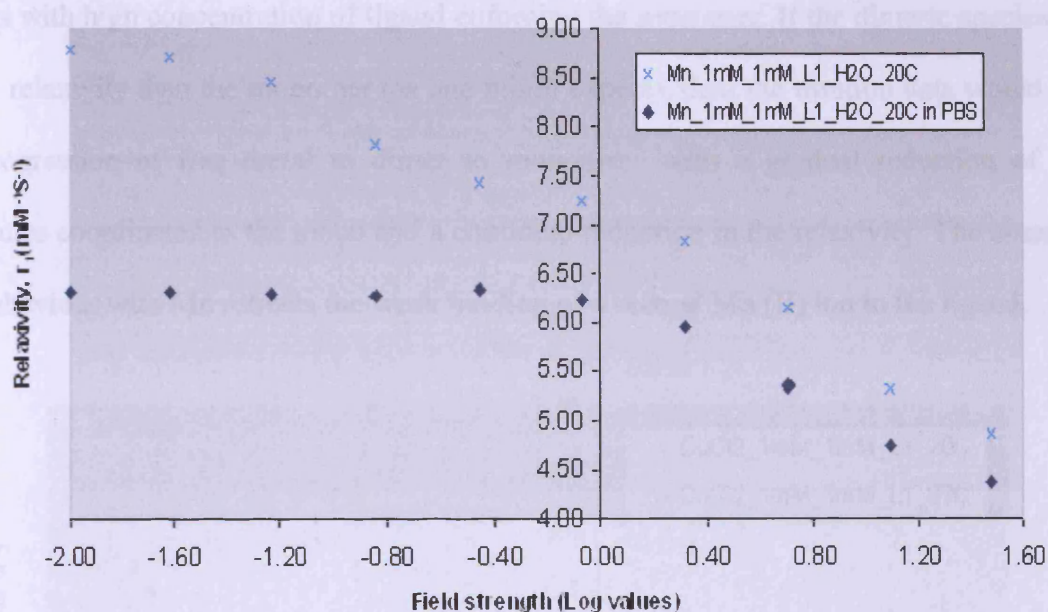


Figure 4:- The ¹H NMRD profiles of compound Mn-L⁴ in distilled water (Top) and Phosphate Buffer Solution (PBS) (Bottom)

An overview of the copper complex - Cu-L⁴

The Cu(II)-diacetyl-bis(N4-methylthiosemicarbazone) was shown to be a valuable PET hypoxia marker for some tumour types.¹⁶ Indeed, recently EDTA bis amide of sulphonamide was also proposed as a PET hypoxia marker.¹⁷ These observations prompted us to investigate the complex formation of Cu (II) with L⁴ as to estimate its potential to be used as PET imaging agent. The ¹H NMRD profile of compound Cu-L⁴ in two different temperatures (20 °C and 37 °C) is illustrated in Fig-5. Lowering the temperature of the sample induces enhancement in the relaxivity as observed and reasoned for Mn-L⁴.

The notable feature, however, is the relatively low relaxivities experienced by **Cu-L⁴** (see **Fig-6** and **Fig-7**), when compared to **Mn-L⁴** under similar conditions. In fact relaxivity of naked Cu (II) in water is $8.14 \text{ mM}^{-1}\text{S}^{-1}$ as against $0.90 \text{ mM}^{-1}\text{S}^{-1}$ enjoyed by naked Mn (II) in water.¹⁸ The observation is mainly attributed to the relatively long electronic relaxation time experienced by Cu (II) ions in comparison to its Mn (II) counterparts. Interestingly, the titration of the metal with ligand does not display the clear inflexion point at the 1:1 ratio as displayed by the Mn species. This is surprising as copper binds to ligand more strongly than Mn (II). Thus this is perhaps suggestive of equilibrium of a dimeric species and a monomeric species with high concentration of ligand enforcing the monomer. If the dimeric species has a higher relaxivity than the monomer (as one might expect), then the titration data would effect the progression of free metal to dimer to monomer with a gradual reduction of water molecules coordinated to the metal and a continual reduction in the relaxivity. The absence of this behaviour with Mn reflects the weak binding of a second Mn (II) ion to the ligand.

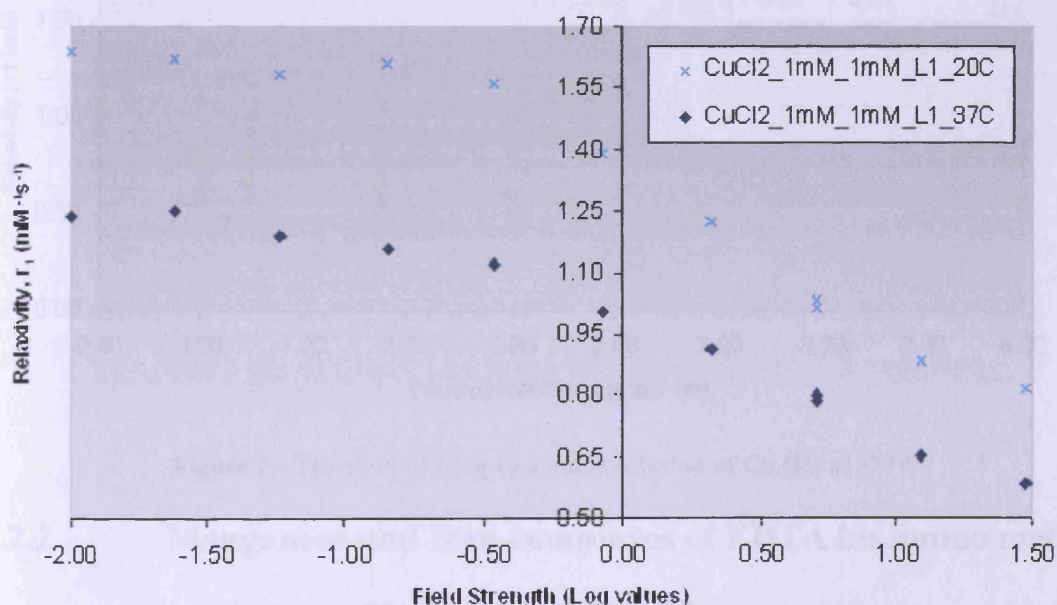


Figure 5:- The ¹H NMRD profiles of compound Cu-L⁴ in 20 °C and 37 °C, revealing the effects of changes in temperature.

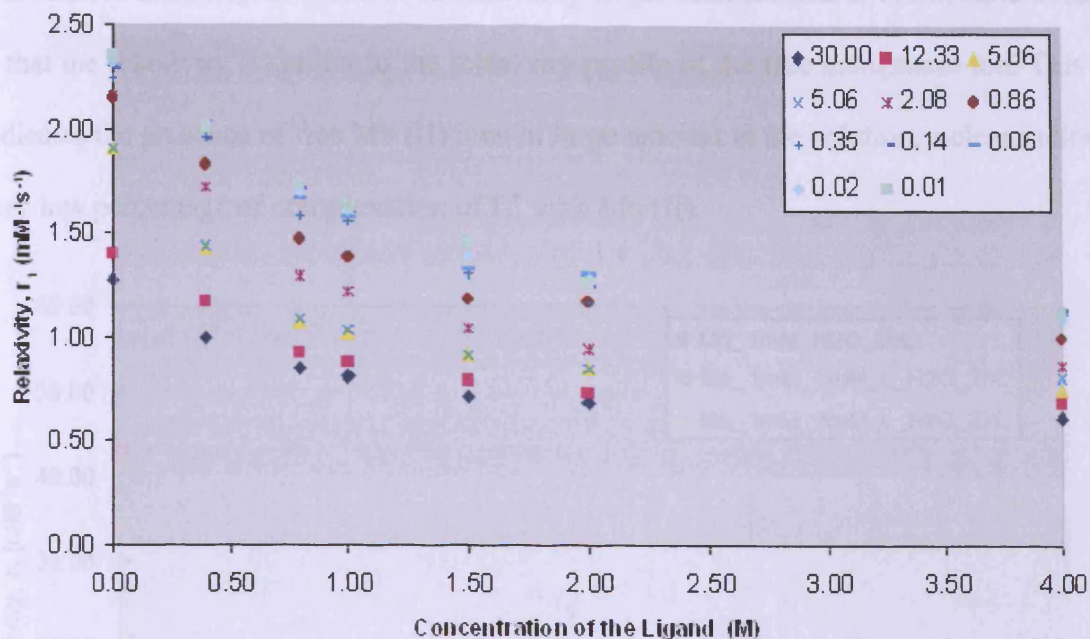


Figure 6:- Titration of L^4 in to a 1mM solution of Cu (II) at 20 °C

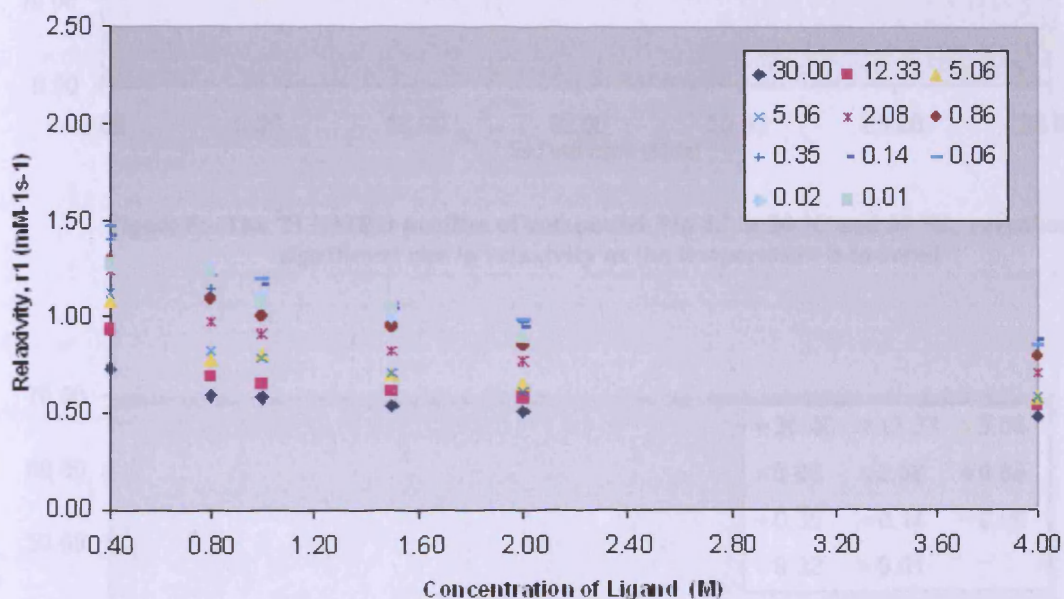


Figure 7:- Titration of L^4 in to a 1mM solution of Cu (II) at 37 °C

A.4.2.2 Manganese and Iron complexes of EDTA bis amino methyl sulphonic acid ($Mn-L^6$ and $Fe-L^6$)

An Overview of the Manganese Complex – $Mn-L^6$

The 1H NMRD profile of compound $Mn-L^6$ at two different temperatures is illustrated in Fig-8. Lowering the temperature of the sample induces enhancement in the relaxivity, as observed and reasoned for $Mn-L^6$ and $Cu-L^6$.

The relative increase, however, is considerably larger than for Mn-L^4 . A notable observation is that the relaxivity is similar to the relaxivity profile of the free manganese ion. This clearly indicates the presence of free Mn (II) ions in large amount in the solution, a clear indication of very low percentage of complexation of L^6 with Mn (II).

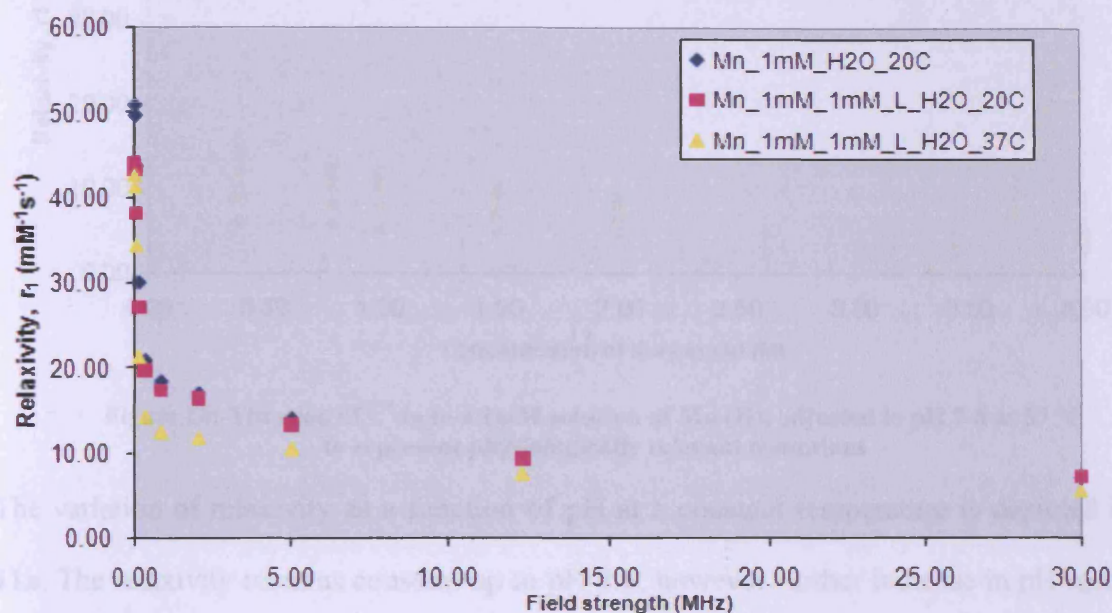


Figure 8:- The ^1H NMRD profiles of compound Mn-L^6 in 20 °C and 37 °C, revealing the significant rise in relaxivity as the temperature is lowered

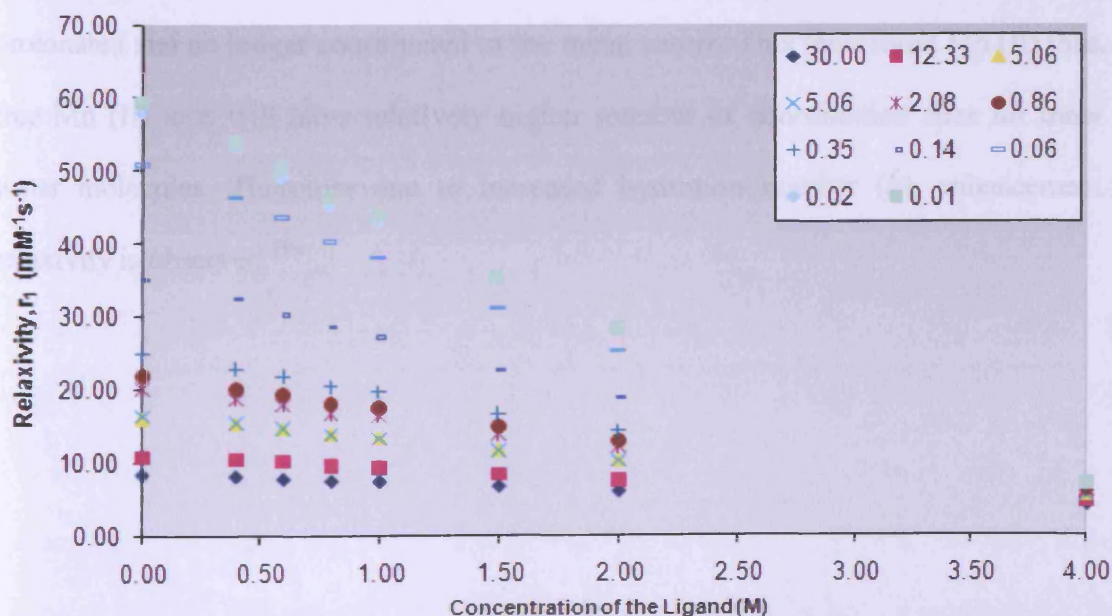


Figure 9:-Titration of L^6 in to a 1mM solution of Mn (II) adjusted to pH 7-8 at 20 °C

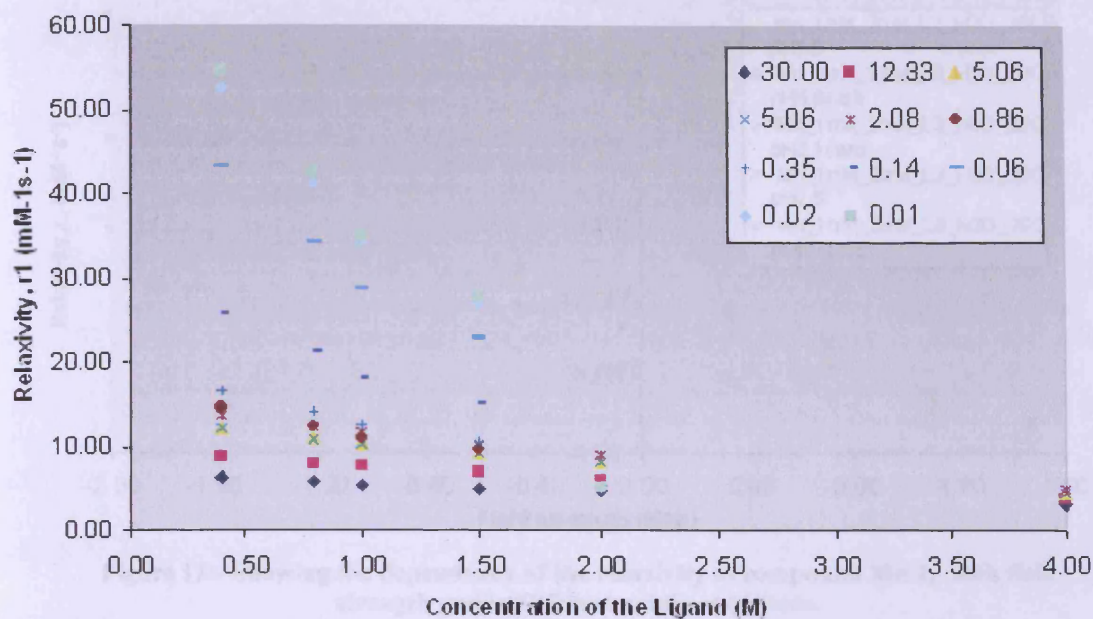


Figure 10:-Titration of L^6 in to a 1mM solution of Mn (II), adjusted to pH 7-8 at 37 °C to represent physiologically relevant conditions

The variation of relaxivity as a function of pH at a constant temperature is depicted in Fig-11a. The relaxivity remains constant up to pH 7.1, however further increase in pH resulted in enhanced relaxivity. As the solution is made increasingly acidic, the relaxivity is considerably enhanced due to progressive dissociation of the complex. The relaxivity of free Mn (II) ions is *ca.* $8.0 \pm 0.1 \text{ mM}^{-1}\text{s}^{-1}$ (20 MHz, 37 °C). Further when the pH is lowered, carboxylates gets protonated and no longer coordinated to the metal centre. This frees more Mn (II) ions. These, free Mn (II) ions will have relatively higher number of coordination sites for inner sphere water molecules. Therefore due to increased hydration number (q), enhancement in the relaxivity is observed.^{19a}

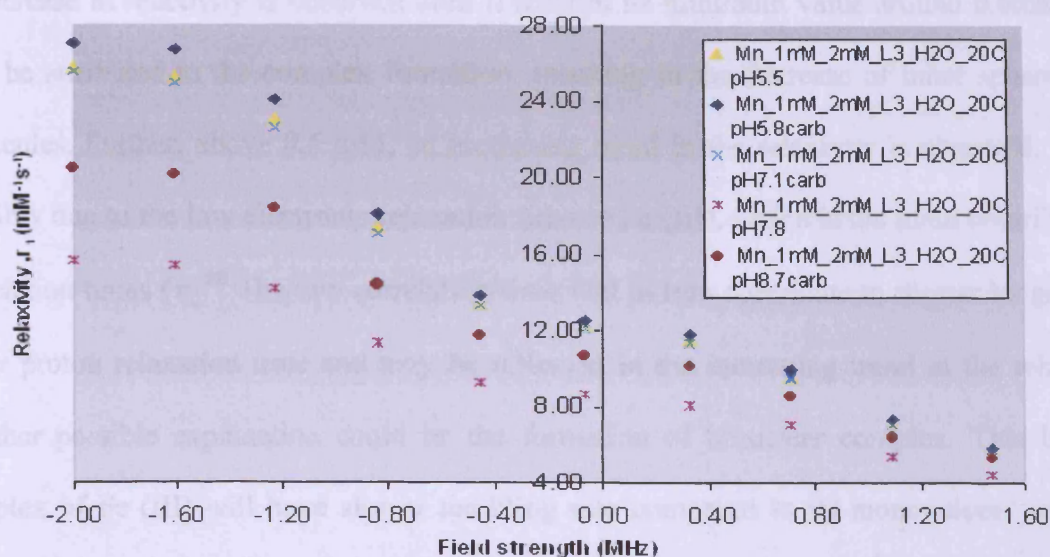


Figure 11:- Showing the dependency of the relaxivity of compound Mn-L^6 with field strength under different acidic conditions.

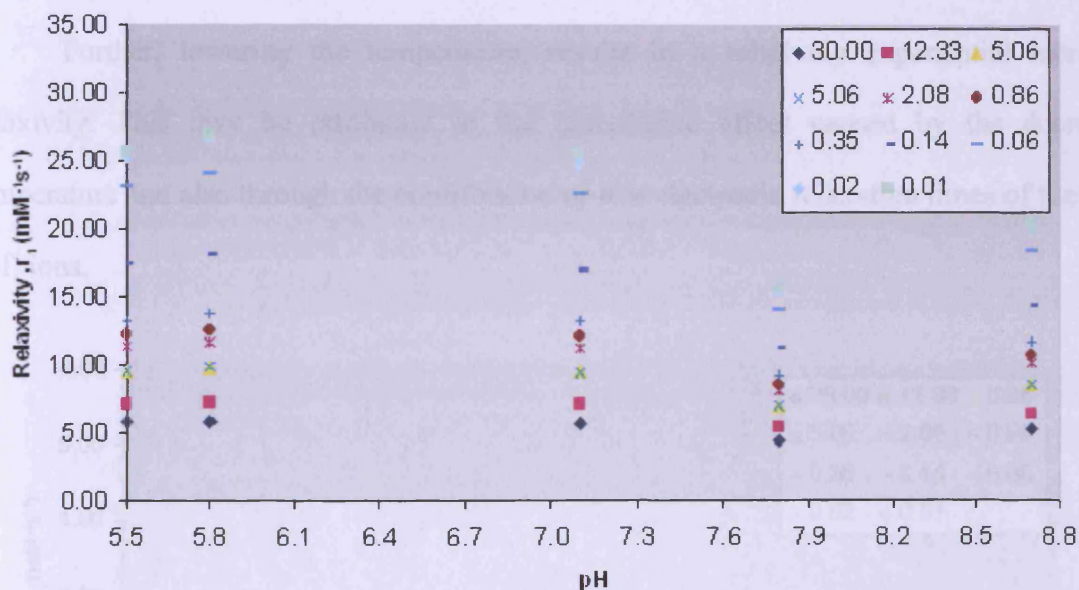


Fig 11a :- Showing the dependency of the relaxivity of Mn-L^6 on pH (at 20 °C)

An Overview on the Iron complex (Fe-L^6)

^1H NMRD profile of compound Fe-L^6 in two different temperatures (20 °C and 37 °C) has been illustrated in Fig-12 and Fig-13. Initially, relaxivity is high due to free Fe (III) ions. These free Fe (III) ions have relatively higher number of coordination sites for the inner sphere water molecules but not as high as Mn (II). It is worthy to note that the r_1 relaxivity of the coordinatively saturated $\text{Fe}(\text{EHPG})^-$ was found to be $\sim 1 \text{ mM}^{-1} \text{ S}^{-1}$. It was also reported that the water proton relaxation occurs only via outer sphere mechanism in this complex.^{19b}

A decrease in relaxivity is observed until it reaches its minimum value around 0.6mM. This may be attributed to the complex formation, resulting in the decrease of inner sphere water molecules. Further, above 0.6 mM, an increasing trend in the relaxivity is observed. This is possibly due to the low electronic relaxation time of Fe (III), which is the main contributor to correlation times (τ_c).²⁰ The low correlation time will in turn contribute to shorter longitudinal water proton relaxation time and may be reflected in the increasing trend in the relaxivity. Another possible explanation could be the formation of binuclear complex. This binuclear complex of Fe (III) will have slower tumbling rate compared to its mononuclear complex. Reduction in tumbling rate at low field strengths (less than 1.5 Tesla) leads to increase in relaxivities.

Further, lowering the temperature, results in a relatively exponential increase in relaxivity. This may be attributed to the cumulative effect caused by the decrease in temperature and also through the contribution of low electronic relaxation times of the free Fe (III) ions.

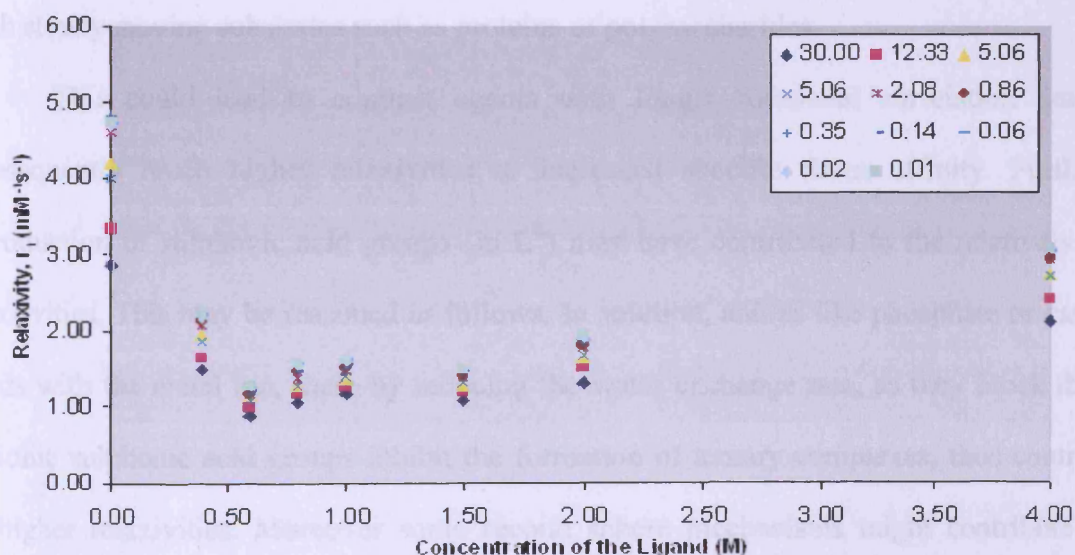


Figure12 :-Titration of L^6 in to a 1mM solution of Fe (III) adjusted to pH 7-8 at 20 °C

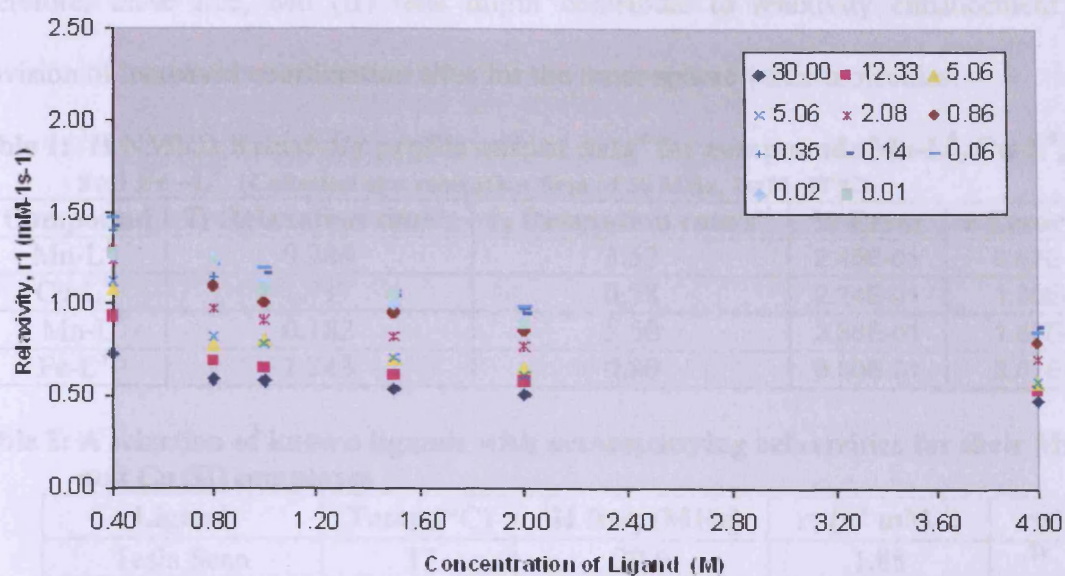


Figure 13:-Titration of L^6 in to a 1mM solution of Fe (III) adjusted to pH 7- 8 at 37 °C

A.4.2.3 Collective overview

Compounds $Mn L^4$ and $Mn L^6$: Overview

While the comparative relaxivities of compounds $Mn-L^4$ and $Mn-L^6$ are only slightly higher (see Table-1), the introduction of substituents on the pyridine ring (in L^4) allows us to envisage ligands bearing functional groups capable of noncovalent or covalent interactions with slowly moving substrates such as proteins or polysaccharides.

This could lead to contrast agents with longer rotational correlation times and consequently much higher relaxivities or increased specific tissue affinity. Further, the introduction of sulphonic acid groups (in L^6) may have contributed to the relatively higher relaxivities. This may be reasoned as follows. In solution, anions like phosphate or carbonate binds with the metal ion, there by reducing the water exchange rate, as they block the area. Anionic sulphonic acid groups inhibit the formation of ternary complexes, thus contributing to higher relaxivities. Moreover some second sphere mechanisms might contribute to the higher relaxivities, resulting from sulphonic acid moieties. On the other hand, the sulphonic acid moieties are acid groups. They may not allow the complexation. This will in turn free more Mn (II) ions.

Therefore, these free, Mn (II) ions might contribute to relaxivity enhancement by the provision of increased coordination sites for the inner sphere water molecules.

Table 1: ^1H NMRD Relaxivity profile output data^a for compounds Mn-L⁴, Cu-L⁴, Mn-L⁶ and Fe-L⁶ (Collected at a relaxation field of 30 MHz, 1mM, 37°C)

Compound	T_1 Relaxation time/s	r_1 Relaxation rate/ s^{-1}	% Error	\pm Error (R1)
Mn-L ¹	0.284	3.52	2.45E-01	8.62E-03
Cu-L ¹	1.717	0.58	2.24E-01	1.30E-03
Mn-L ³	0.182	5.50	3.38E-01	1.86E-02
Fe-L ³	1.243	0.80	3.50E-01	2.82E-03

Table 2: A selection of known ligands with accompanying relaxivities for their Mn (II) and Cu (II) complexes

Ligand	Temp (°C)	^1H freq (MHz)	r_1 ($\text{s}^{-1} \text{mM}^{-1}$)	ref
Tesla Scan	37	20.0	1.88	21
Lumenhance	37	10.0	20.90	22
FerriSeltz	-	16.0	1.60	23

Another important observation is related to the reduced significance of temperature change on relaxivity. As aforementioned, relaxation rates are inversely proportional to the diffusion coefficient and while this is clearly still a feature of the ^1H NMRD profile of the nitrate-free compound, the reduced temperature effect could be a consequence of enhanced water exchange rates.

Impact on Water Exchange Rate

It has been reported, water residence time is being dominated mainly by four factors. They are as follows: The charge on the complex, solvent accessibility, steric constraints at the binding of the water molecules and the mechanism of water exchange. Out of these four factors, solvent accessibility and steric constraints may be attributed to the relaxivity enhancement of the ligands in question.

The presence of hydrophilic groups is known to change the access of bulk water molecules towards the coordinated inner sphere water molecules (through affecting the water accessibility surface) and thereby contribute to the change in water exchange rate. This will have a pronounced affect in the relaxivity.²⁴

The relatively high relaxivities observed in the case of Mn-L⁶ may be partially attributed to the presence of sulphonic acid groups as the hydrophilic group.

On the other hand, relaxivity enhancement observed in Mn-L^4 could be attributed to the presence of pyridine moieties, which has contributed to the steric constraints. The steric constraints are also known to contribute to relaxivity enhancement through fast water exchange rate. It has been found that introduction of pyridine-N-oxide pendant arm induces rapid water exchange rate.²⁵

Further, it was reported that the polyamino carboxylates undergo water exchange through dissociative process. The steric compression around the bound water site is crucial for such dissociative processes as it facilitates leaving of the inner sphere water molecules.

This will result in increased water exchange rate. Therefore it could reasonably concluded that the increased steric compression due to the presence of pyridines induces relaxivity enhancement through the increased water exchange rate.^{26,27}

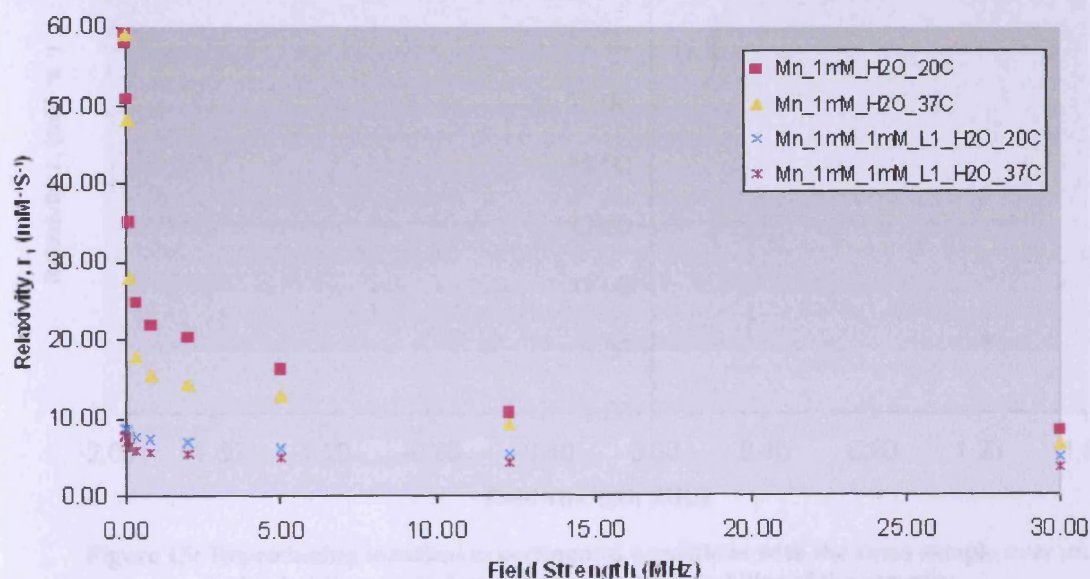


Figure 14: The ^1H NMRD profiles of compound Mn-L^1 and Mn-L^3 , revealing the effects of changes in temperature. pH of the samples was adjusted to 7-8 to represent physiologically relevant conditions.

A.4.2.4 Symmetric naphtha derivative of N-(2-Aminoethyl)-1,8-naphthalimide (L^{11})

Fig-15 depicts the ^1H NMRD profile of Gd complex of the symmetric naphtha derivative (see Fig-15). As is seen, the relaxivity of the 1mM concentration of the complex is significantly high (i.e. $8.8 \text{ mM}^{-1}\text{S}^{-1}$ at 30 MHz, 25 °C).

Reproducibility of the results were ensured by repeating the whole synthesis and repeating the measurements under the same conditions ($8.5 \text{ mM}^{-1}\text{s}^{-1}$ at 30 MHz, 25 °C). Furthermore, the Free Gd (III) was not detected in the sample, by means of xylenol orange as indicator.

Most of the polyamino polycarboxylate scaffolds used as commercial contrast agents have relaxivities in the range of $4\text{-}5 \text{ mM}^{-1}\text{s}^{-1}$ (at 30 MHz, 25 °C). Acyclic DTPA analogues reported to date also have comparable relaxivities to those of commercially available contrast agents based on polyamino polycarboxylates. Exceptionally higher relaxivities were reported by Raymond *et al.*²⁸ for their HOPO based contrast agents. ($7\text{-}13 \text{ mM}^{-1}\text{s}^{-1}$). As such, to the best of our knowledge, this is the highest value reported for a ligand of this nature.

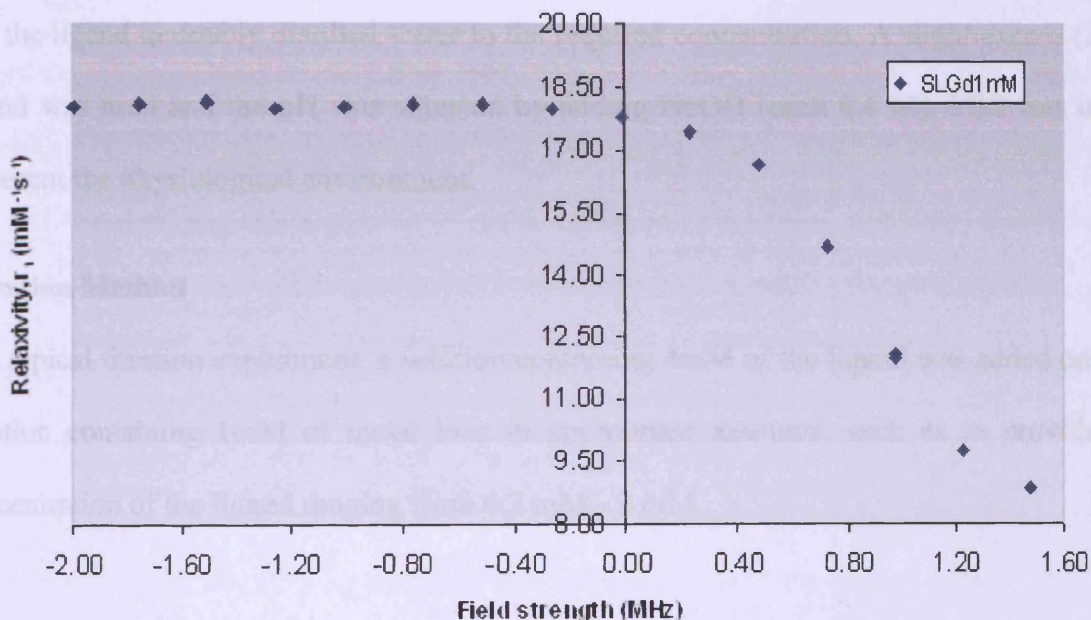


Figure 15: Reproducing identical experimental conditions with the same sample over an extended time period confirmed the high stability of the complex.

Experimental

^1H NMRD acquisition:

The $1/T_1$ NMRD profiles were obtained on a Stellar Spin master* FFC-2000 relaxometer, typically covering a continuum of magnetic fields from 2.4×10^{-4} to 0.72 T (corresponding to a proton larmor frequency range 0.01-30 MHz). Technical details are available in the reference manual available upon request from Stellar*.

* www.stelar.it

Potential Multimodal Imaging Agents

A Spin master Variable Temperature Controller (VCT) allowed the setting and monitoring of the sample temperature at two different temperatures, 20°C and 37°C with a resolution up to 0.01°C. The temperature gradient over the sample region was dependent on the air (nitrogen) flow and the installed temperature. The temperature in the probe head was measured with a Fluke 52 k/j digital thermometer with an uncertainty of 0.5 K. The temperature inside the probe was controlled by circulation of perfluoroalkanes. Each sample was allowed to acclimatise to the desired temperature for 15 minutes prior to data collection. The reproducibility in T_1 measurements was within less than 1%.

The Mn (II), Cu (II) complexes complexes were prepared in a sample tube by mixing equimolar amounts of either $\text{MnCl}_2 \cdot 6\text{H}_2\text{O}$ (99.99%; Aldrich) or $\text{CuCl}_2 \cdot \text{H}_2\text{O}$ (99.99%; Aldrich) and the ligand in doubly distilled water to the required concentration. A slight excess (5%) of ligand was used and the pH was adjusted by adding NaOH (each 0.1 M). PBS was used to represent the physiological environment.

Titration Method

In a typical titration experiment, a solution containing 4mM of the ligand was added on to the solution containing 1mM of metal ions in appropriate amounts, such as to provide final concentration of the ligand ranging from 0.2 mM - 2 mM.

Chapter 4: Part B

Potentiometric Measurements

B.4.1 Evaluation of Potential Contrast Agents

B.4.1.1 Need for evaluation of contrast agents

As aforementioned in “Chapter 1”, the potential contrast agent must meet the criteria of maintaining high stability, while improving the relaxivity enhancement to appreciably higher standards. In short, successful preparation of a potential contrast agent means incorporating both these properties to their optimum values.

Tolerance to Toxicity

Safety/Toxicity has been evaluated by acute toxicity (LD₅₀), sub chronic toxicity, local tissue tolerance, cardiovascular pharmacology, mutagenic potential, absorption, distribution, and metabolism and excretion studies.²⁹ As aforementioned, these synthetic complexes are composed of relatively toxic components (i.e., metal ion and ligand, loosely bonded together) and subject to dissociation. The future development of radio or magneto pharmaceuticals inevitably relies on *in-vivo* affinity of these components for each other. The *in vitro* measurements of stability of these synthetic complexes have been considered as a step in the right direction. The stability constant measurement is one such parameter, among the number of parameters that are being used for this purpose. As such, a brief account on stability constants will not be out of place.

B.4.1.2 Protonation Constants and Stability Constants

The development of the theory of stability constants throughout the ages

Throughout history, the estimation of stability constants has provided means for, understanding the degree of association of a ligand towards metal ion in solution. The initial interest in stability constants dates back to the early nineteenth century. This was initiated by Von Euler³⁰ and Bodlander.³¹

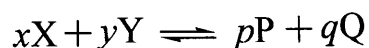
Their efforts, however, could not precede beyond the empirical formulae and overall stability constants. N. Bjerrum³² and J. Bjerrum³³ later made significant advances in this field that serves as a basis for the present day, more detailed analysis of the complex systems. This also paved way for the introduction of stepwise hydrolysis constants and step wise stability constants. The numerous reports published in this field follow the same principles or basic criteria. They are, constant ionic medium, high degree of accuracy (both during the measurements as well as during interpretation), broad range of mass balance equations utilising very complex algebraic manipulations. The theoretical background for these complex calculations was initially provided by Rossotti and Rossotti.³⁴

It was only two decades ago, however, significant advancements took place in this field and eventually they have lead on to advantageous implications. A notable advancement is the advent of tailor made computer programs. These programs, comprising computational methods, accelerated the processing of equilibrium data and thereby gave rise to more precise stability constants. One such program, known as “Hyper Quad” designed by Peter Gans *et al.*³⁵, was of tremendous significance with regard to this project.

Furthermore, the arrival of two stability constant databases³⁶ has added lustre to this field. The significant aspect of these databases is the provision of a comprehensive selection of stability constants from literature, coupled with more detailed information on experiments. This information is crucial for drawing conclusions from the reported data as well as for comparative purposes.

B.4.1.2.1 What is meant by ‘Stability Constants’?

The constant corresponding to stability constant arises from the ratio between the products of the activities of product species to that of the product of the activities of the reacting species in solution, at the point of equilibrium. This could be interpreted in mathematical terms by the following equation (see Eq-1)



$$K_{eq} = \frac{a_P^p \cdot a_Q^q}{a_X^x \cdot a_Y^y} \quad (1)$$

The species in the equilibrium either concerned with product or reactant will have their individual Gibbs free energies. This will pave the way for a quantitative description of the reactivities of all the species involved. The difference in these Gibbs free energies could be directly measured in terms of stability constant measurements.

Ionic strength and Stability Constants

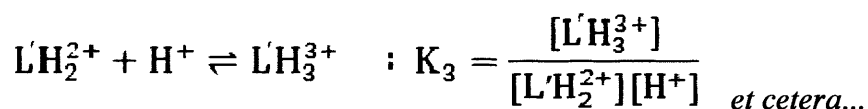
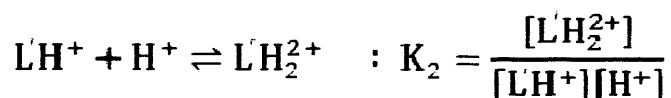
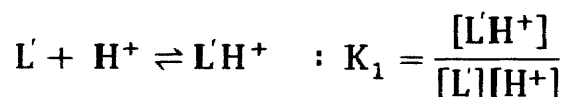
A significant factor that needs to be considered when estimating stability constants is the ionic strength of the solution in consideration. It is quite impossible to measure the ionic activities of the complex ionic species while the reaction proceeds. Therefore in order to eliminate the problem, a non reacting electrolyte could be introduced far in excess of the reacting ionic species in consideration. This will in turn facilitate the control of ionic strength and thereby equate the activities of the ionic solutes to that of concentrations. This procedure used to determine stability constants, while maintaining constant ionic strength through the supporting electrolyte, has been adapted as standard practice. Clearly, it brings practicality. So as to say, the activity terms in Eq-1 could now be replaced with molar concentrations (see Eq-2).

$$K_c = \frac{[P]^p \cdot [Q]^q}{[X]^x \cdot [Y]^y} \quad (2)$$

It also has an added advantage in that any concentrations obtained from the potentiometric measurements could be correlated with that of the measurements obtained by other means (eg:-absorbance techniques). Moreover, the results could be directly applied to mass balance equations used for the estimation of stability constants and protonation constants.

Importance of measuring Protonation Constants

In the solution, there is a competition between the metal ions and protons for the ligand sites. Therefore it is imperative that the measurements for protonation constant should precede the measurements for stability constants. The protonation constants for the potential ligands could be defined as follows.³⁷



The expected number of protonation constants depended upon two factors, namely the nature of the ligand and the number of potential sites available for protonation. With the subsequent addition of base (as aliquots) to the reaction solution, the ligand in consideration will become increasingly deprotonated. As a result, the dynamic equilibrium will be reverted to its original forms.

The significance of Stability Constants

All of the usages of stability constants lie on a common platform. This may be further explained by taking into consideration a system having species which are held together by weak bonding interactions. Through the variation of concentration or by variation in pH, it is possible for a reactive species to exist in many various forms. The knowledge of stability constants is useful to understand these vital dynamic equilibria in solution. The knowledge obtained of these equilibria (through stability constants) is found to be of immense use in various fields as wide as analytical, biological, industrial and coordination chemistry research itself.³⁸ In addition to the role of evaluating MR image enhancement agents, there are other practical applications that could be discovered in the literature.

The field of 'Molecular Recognition'³⁹ extensively uses stability constants to determine the extent of host-guest interaction (see Fig-1). For example, Liu *et al.*⁴⁰ have utilised stability constants to assess the stability of anions (oxalate, fumarate, sulphate etc) to determine the extent of host-guest interactions. The usage of stability constants is inevitable in the development of chemo sensors and luminescent probes.⁴¹ M.A. Santos *et al.*⁴² have used stability constants measured through potentiometry, to evaluate Al-decaporating agents used in the treatment of Parkinson diseases. Attracted by the role of arylazo derivatives of benzimidazole and barbituric acid in biochemistry, Amrallah *et al.*⁴³ have evaluated formation constants of binary systems (where, selected amino acids acted as primary ligands and aryl benzo derivatives acted as secondary ligands with regard to Cu (II), Zn (II) and Cd (II)). Furthermore stability constants for complexes of haemoglobin and myoglobin with dioxygen, CO, CN⁻, facilitate the treatment of early stages of CO poisoning.⁴⁴ The determination of stability constants are useful in the preparation of silver cleaning solutions (as the silver cleaning solution contains ligand with a higher affinity for Ag (I) than the tarnish) and also in various Fe (III) complexing agents in rust removers.

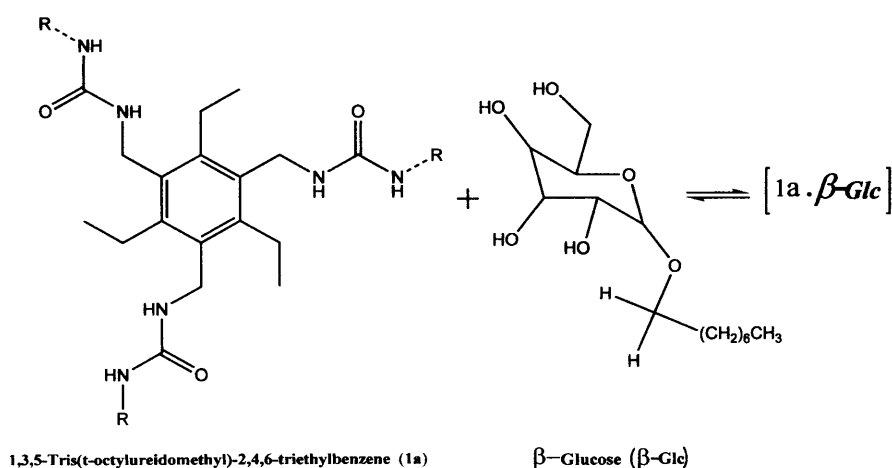


Figure 1:- 'Molecular Recognition' is a rapidly developing field, where the role of stability constant determination is inevitable.

There are many other areas, where usage of stability constants is of great importance.

Environmental science⁴⁵, waste management⁴⁵, agriculture⁴⁶, behaviour of radiopharmaceuticals in blood plasma⁴⁷ are such areas to name a few.

B.4.1.3 Complex formation and Chelate Effect

A metal ion does not exist as isolated ion in solution; rather it would exist in combination with ligands (either solvent molecules or ions) or chelating groups. This leads to the formation of complex ions or coordination compounds. The Latin word '*Chela*', meaning great claw, give rise to the term 'Chelate'. In Coordination Chemistry, the term is used to refer to a molecule or ion containing two or more donor atoms. Linking two or more donor atoms with metal ions will result in greatly enhanced stability constants, as compared to their individual donor groups. Various investigations have been made in various perspectives to reason out this effect.

The conventional thermodynamic explanation has attributed the chelate effect to increase in entropy associated with chelate binding in relation to binding of the separate monodentate donors. The increase in disorderliness has been related to increase in total number of particles generated upon displacement. The effect could be studied effectively with a suitable coordinating ligand along with its dimer. Schwarzenbach⁴⁸ has studied EDTA complexes along with IDA complexes. He has reported the favourable entropy change that has resulted upon stabilization of the chelated species.

In addition to the thermodynamic explanation, the chelate effect could be explained in terms of kinetics. According to this theory there is a formation of the second M-L' (where L' indicate any donor atom) with respect to an unlinked second donor atom. Donor atoms constructing the flexible chelate are known to dissociate as rapidly as analogous unidentate ligands. As such in order to prevent this chelate dissociating in a similar rate to donor atoms, it could be assumed that rapid re-association also takes place. This fact supports the enhanced stability through associative S_N2 mechanism. Carter and Beattie have reported the kinetic chelate effect observed during the complexation of ethylene diamine with Pt (II) along with the monodentate ethylene diamine. They have confirmed the observed chelate effect as of kinetic origin by means of comparison with analogous substitution of ammonia.

B.4.1.3.1 Hard-Soft Acid-Base Classification (HSAB)

In 1941, Sidgwick delivered a lecture to the Chemical Society, which was later on published and titled as 'Complex Formation', where he has recognized the similarities in the affinities of some common ligands (such as cyanide and nitro) for a variety of acceptor ions and molecules. In 1958, Ahrlund *et al.*⁴⁹ expanded the theory and proposed two well defined types of metal ions and ligands: class 'a' and class 'b' categories on the basis of trends observed in stability constants.

Class A consisted of fluoride, oxygen and nitrogen donor ligands while class 'b' consisted of other halides, sulphur and phosphorus donor ligands. The guiding principle was 'like ion-like ligand pairs' ('a'+ 'a', or 'b'+ 'b') gave stable complexes, while the unlike pairs ('a'+ 'b') gave complexes of lower stability. This was further modified and described by Pearson⁵⁰ as the HSAB principle (see Table 1). In his own words: 'Hard acids bind strongly to hard bases and soft acids bind strongly to soft bases'. Pearson has explained the phenomena in terms of various degrees of ionic and covalent interactions, electron correlation and solvation effects.

Table 1: A selection of metal ions and ligands classified into hard and soft categories

	Hard	Intermediate	Soft
Metal Ions	Mn ²⁺ , Sc ³⁺ , Cr ³⁺ , Fe ³⁺	Fe ²⁺ , Co ²⁺ , Ni ²⁺ , Cu ²⁺	Ag ⁺ , Pd ²⁺ , Pt ²⁺ , Rh ⁺
Ligands	R ₂ O, ROH, OH ⁻ , SO ₄ ²⁻ , Cl ⁻	Br ⁻ , py	R ₂ S, R ₃ P, CO, CN ⁻ , I ⁻

The Irving-Williams Order

In 1948, H.Irving and R.J.P.Williams⁵¹ in a preliminary communication to 'Nature', reported an order of stability of complexes for a series of bivalent, first row transition metal ions. The order Mn < Fe < Co < Ni < Cu > Zn has been discovered to hold for the stability of nearly all such complexes irrespective of the nature of the co-ordinated ligand or of the number of ligands involved in coordination. They have provided theoretical justification in 1953⁵² for the phenomena observed (see Fig-2).

Potential Multimodal Imaging Agents

The order of stability has been attributed to two factors, namely reciprocal of ionic radii and the second ionisation potential of the metals involved in the investigation. Furthermore, these two factors increase monotonically across the series (from manganese to copper). This is to say that, replacing a water molecule with a ligand of higher electron donating power will increase the stability with the simultaneous increase in second ionisation potential. On the other hand, replacement of a water molecule by a ligand bearing formal negative charge will also result in enhanced stability due to increase in electrostatic interactions, which ultimately decrease the cationic radius .

Irving and Williams also pointed out that entropy factors and stereochemistry might also have an impact in such stability order. They also noted the very high stability observed for Fe (III). Unusual, high stability was attributed to the changes that take place in the bonding orbitals due to the changes in the nature of ligand. In fact, stability constants are anomalously higher for copper complexes. This is now attributed to the Jahn–Teller effect (namely distortion from the, for example, octahedral geometries).

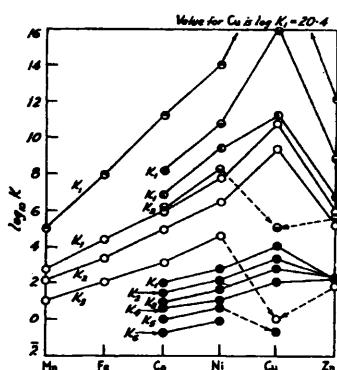


Figure 2: - Taken from Irving and Williams, J.Chem.Soc, 1953

B.4.1.4 Methods available for determining stability constants

B.4.1.4.1 Potentiometry

This is far the most convenient method for the determination of stability constants. For reasons of clarity, the theory behind the potentiometry will not be dealt in this chapter, except for highlighting the inevitable aspects. The method, however, could be briefed as follows:

It is based on the measurement of pH utilising a cell composed of two half cells. One of the two half cells is reversible to hydrogen ions, in that its potential changes as the hydrogen ion

concentration is changed. The other half cell (known as reference electrode) will have a constant potential throughout the experiment and it is used to complete the circuit. The difference in the potential between the two electrodes will indicate the hydrogen ion concentration. The most commonly employed electrode system will have a glass electrode in combination with saturated calomel electrode as reference electrode.

B.4.1.4.2 Spectrophotometry

This is commonly used to directly observe (in the UV region or visible region) the mixtures of ionic species and molecular species at a known pH. Although relatively time consuming, it is useful for sparingly soluble substances. The method is active at very low pH and very high pH, unattainable by glass electrode. One important aspect is that the molecular species and ionic species should be able to absorb UV or visible light and must have their specific spectra.

B.4.1.4.3 NMR spectroscopy

This may be employed in circumstances where the substance could not be measured by UV spectroscopy (if UV spectra of the substance, does not change upon ionisation) and potentiometry (if the substance is too weak an acid or base or poorly soluble). A series of solutions of known pH will be prepared and the chemical shift results from the non-exchanging proton (closer to the ionizing group) will be plotted against the pH. The requirement of high concentrations at which the NMR values are determined, imposes limitation on this method. Nevertheless, it is useful to define the region where the accurate pKa value lies.

B.4.1.4.4 Conductimetry

This is also relatively time consuming when compared to potentiometry and can not be considered as a versatile method. The method is based on the change in conductivity resulting from successive dilution with water to an aqueous solution of a moderately weak acid. 'Catalysis of Hydrolysis' and 'Thermometric titration' are some other ancient methods which have been used with little success.

B.4.1.5 Some Theoretical Aspects relevant to Potentiometric

Measurements

Electrode Calibration Theory

The concentration of hydrogen ions in an aqueous solution under acid/base equilibria could be measured through the usage of hydrogen electrode or glass electrode. The hydrogen electrode, however, is rarely being used for this purpose, as it easily gets poisoned and often chemically alters the substance in question. Therefore glass electrode is considered ideal for the measurement of ionization constants. Clearly, essential requirement is therefore to calibrate the electrode response with respect to hydrogen ion concentration. Ideally the potential, E , of a glass electrode obeys the Nernst equation:

$$E = E^0 + \frac{RT}{nF} \log_e \{H\} \quad (3)$$

where E^0 is the standard electrode potential, R is the gas constant, T is the temperature in Kelvin, F is the Faraday constant, and $n = 1$ in the case of the glass electrode.

From the above equation, it follows that the electrode response is proportional to the activity of the hydrogen ion. As aforementioned, the usage of a supporting electrolyte maintains the ionic strength constant with higher magnitude. This in turn prevents the obstacles encountered with the fluctuating activity coefficients. Thus the following equation will result thereof.

$$E = E^0 + s \log_e [H] \quad (4)$$

Where the slope, s , ideally should have a value of around $T/5.0399$ mV. It further follows that, for a series of data points, E^0 and the slope factor could be estimated from the slope and intersect of the E vs $\log_e [H^+]$ plot respectively, if the hydrogen ion concentrations are known.

The titration is carried out using strong acid and strong base of known concentrations in a supporting electrolyte of high ionic strength. The titration vessel is filled with 2 mL of acid (HNO_3 , 0.10 M) and 50 mL of the supporting electrolyte solution ($NaNO_3$, 0.1 M).

After addition of 0.05 mL of base (NaOH, 0.1021 M), the mineral acid concentration, T_H , is given by the following equation:

$$T_H = \frac{a_H \cdot v_0 + y \cdot b_H \cdot v}{v_0 + v_1 + v_2} \quad (5)$$

where a_H is the concentration (mol dm^{-3}) of acid of which v_0 mL were added to the titration vessel, b_H is the concentration (mol dm^{-3}) of base in the burette (by convention given a negative sign), v_1 is the volume (mL) of background electrolyte solution added to the titration vessel, and v (mL) is the volume of base added from the burette. The uncertainty in the concentration of the base is treated with a coefficient gamma, γ .

As conventionally, base concentration given a negative sign (as it is being added from burette), T_H is positive at low pH, zero at the equivalence point and negative at high pH. Thus it is possible to estimate T_H by knowing all the relevant parameters and substituting the same in Eq-5. This in turn will facilitate the calculation of hydrogen ion concentration.

The hydrogen ion concentration can be determined from the mineral acid concentration, T_H , while taking in to consideration of the self-dissociation of water, K_w . A reasonable agreement within the literature was noted for the value of -13.78 for $\log(K_w)$ under the specified conditions of 25°C, 0.1 M KCl.

$$[H_2O] = K_w \cdot [H] \cdot [OH]; \quad pK_w = -\ln(K_w) \quad (6)$$

$$T_H = [H] - K_w \cdot [H]^{-1} \quad (7)$$

(i) At pH values lower than 5, the second term in equation 7 is minute compared to the initial term and hence can be regarded as negligible; $[H] = T_H$.

(ii) At pH values higher than 9, the initial term in equation 7 is minute compared to the second and can be regarded as negligible; $[H] = K_w / (-T_H)$.

One inevitable concern is that the base solution may be contaminated with a slight amount of carbonate. The extent of impurity is determined as a percentage, *via* a Gran's plot²⁸ and this will be used to amend the alkali concentration.

The parameters E^0 , s , γ and pK_w are determined by least-squares fitting of the observed electrode potentials to the values calculated by equation 5.

Common Sources of Errors and their minimisation: Ensuring Precision and Accuracy

By nature, there is an inevitable need to maintain high degree of precision and accuracy, throughout this technique. This brings the inevitable need to eliminate errors. These errors have the potential to invoke adverse effects on the quality of results obtained. This in turn justifies the need to eliminate any scope for error, throughout the entire experiment.

Upward Trend & Purity of the Sample

One of the most common errors could be observed is the *upward trend* of the pK_a values (in titrating with alkali) during the progress of titration. This is usually due to impurity in the sample undergoing determination. Hence, that not so much of it is present as has been supposed. The impurity could be mainly due to water. In order to avoid this problem, it is imperative to dry under the same conditions preceded its determination. Analytical purity of the sample also needs to be ensured. 'Upward trend' has two other causes. It could be due to very fast nitrogen flow, which will be expelling some solution. Although accurate amount of material is present throughout the experiment, not all of it would have dissolved in solution. Needless to say, the presence of undissolved material can not yield any reliable pK_a value.

Standardisation of Reagents

One of the possible causes of error is due to inaccurate standardisation of reagents. Any kind of uncertainty in initial protonated ligand concentration would result in a marked error in the available hydrogen ion concentration. Very conveniently, Hyper Quad, however, has the feature to establish the true initial concentrations of both the ligand and hydrogen ions, through a lengthy refinement process. This will in turn minimise any possible errors due to inaccuracy in standardisation of reagents.

Maintenance and Storage of Glass Electrode

Another major source of error could arise from glass electrode itself. It is a must to ensure that the electrode is stored properly during and after the experiments, in line with the manufacturer's specifications. When the electrode is not in use, it should be immersed in the supporting electrolyte containing roughly 0.001 M H⁺.

Unpredictable behaviour of the electrode may be experienced, if it comes in to contact with a heavy metal. Touching the metal temperature probe may give rise to considerable leaps in pH. This can be restored, however, by immersing the electrode in 0.1M HCl.

Time required for the system to reach Equilibrium

It is necessary to allow adequate time for the system to reach equilibrium, before any kind of data points can be recorded. In order to ensure this, two factors must be taken into consideration.

Firstly, there should be enough time for the system to physically adjust itself, to new conditions. Secondly, time also needs to be allowed for the varying reaction rates of different species undergoing dissociation. Equilibrium is assumed to be reached, if the pH has remained stable for 30 seconds, however, near the end-point of a titration, where the leap in pH value is observed, it may be necessary to wait for periods of ten minutes or more for the system to achieve the complete equilibrium. Further, achievement of equilibrium could also be noted from the first aliquot of base being added to the titration vessel.

B.4.2 Results and Discussion

Potentiometric titrations were carried out for EDTA based bisamides and DTPA based bisamides as well as for symmetric naphtha Ligand (synthetic analogue of DTPA) (See Fig-1). The protonation constants for all the water soluble bisamides were obtained. Specifically, EDTA based bisamides of sulphanilamide (L²), amino methyl pyridine (L⁴), and amino methyl sulphonic acid (L⁶) have been selected for potentiometric titration, due to their solubility in water.

Potential Multimodal Imaging Agents

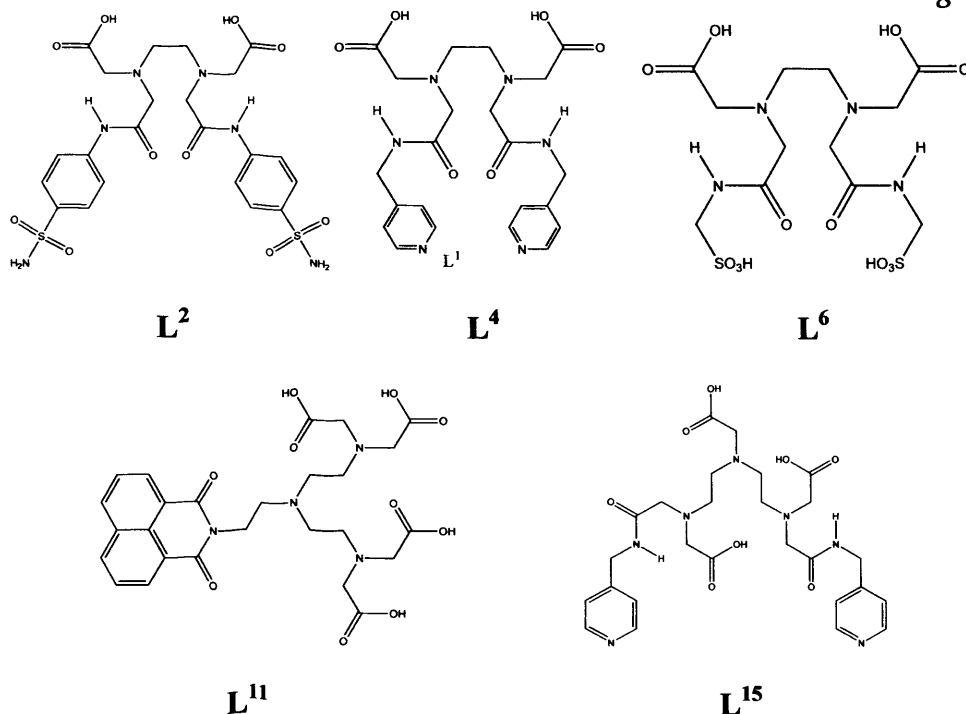


Figure 1:-Depicting the water soluble candidates of EDTA and DTPA based bisamides along with DTPA analogue selected for potentiometric evaluation

EDTA based bisamides of N-(2-Aminoethyl)-1, 8-naphthalimide (L¹), para amino phenol (L³), 2-amino anthraquinone (L⁵), however, was found to be insoluble in water. Therefore titrations were not carried out for these ligands.

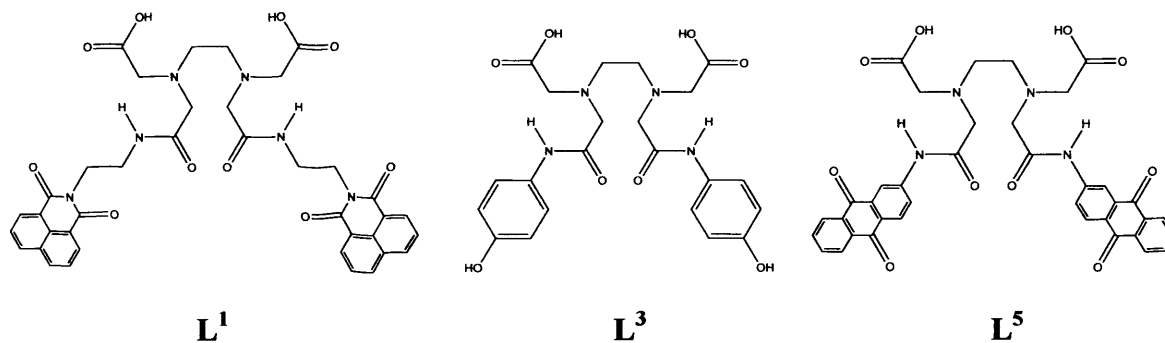


Figure 2:-Depicting the insoluble EDTA based bisamides

B.4.2.1 Evaluation of EDTA based Ligands

B.4.2.1.1 Protonation Constants and Deprotonation Curves of EDTA bisamides

Among the EDTA based bisamides evaluated by potentiometric titration, EDTA bis amino methyl pyridine (L⁴) and EDTA bis sulphonamide (L²) gave good protonation constants.

These values agreed with the literature values related to similar ligands.⁶²⁻⁶⁴ Best fits of the models between the measured and calculated titration data along with their protonation constants for L⁴, L² and L⁶ are reported in Fig 3-4 and Table 1.

The protonation constants obtained by potentiometric titration of the EDTA bisamides, specifically for L^4 , L^2 , and L^6 (see Fig-1) are depicted in Table 1. Depicted here are 6, 3, 2 stepwise protonation constants respectively and these number of protonation constants corresponding to number of donor atoms actively involved in each ligand.

All constants were determined at 25°C and 0.1 M NaNO₃.

Table 1: Thermodynamic Properties for the Ligands L^4 , L^2 and L^6

Quotient	Constant	L^4	L^2	L^6
$[HL]/[L][H]$	$\log K_{HL}$	7.30	9.75	6.84
$[H_2L]/[HL][H]$	$\log K_{H_2L}$	6.20	6.62	0.74
$[H_3L]/[H_2L][H]$	$\log K_{H_3L}$	5.40	5.25	-
$[H_4L]/[H_3L][H]$	$\log K_{H_4L}$	4.80	-	-
$[H_5L]/[H_4L][H]$	$\log K_{H_5L}$	4.00	-	-
$[H_6L]/[H_5L][H]$	$\log K_{H_6L}$	2.40	-	-
ΣpK_a		30.10	21.62	6.84

B.4.2.1.1.1 Assignment of Protonation Constants

A review of the literature carried out with the aid of a stability constant database⁵³ revealed many examples of protonation constants for fragments of an ethylene diamine backbone and carboxylate fragments. Further utilising such examples (see Table-2) meaningful comparisons can be drawn. EDTA bisamides of amino methyl pyridine (L^4) and sulphonamide (L^2) both have eight potential protonation sites. Only six and three maxima, however, were observed in the titration curves for L^4 and L^2 respectively.

Attributing Sequence to L^4

The pKa of the carboxylic acid groups are too acidic to be determined with this technique.⁵⁴ Among the remaining basic groups, the nitrogen sites of the ethylene diamine backbone are considered to be most vulnerable for protonation, due to their highest basic strength, pKa values reported from the literature also stand in testimony (see Table-2). Therefore, it is a reasonable assumption that the first two protonation constants for L^4 are attributable to the protonation of the nitrogen sites of the ethylene diamine backbone.⁵⁵

Further, noted the marked difference in the K_1 and K_2 values of L^4 . The sequence of K_n values is $K_1 > K_2$ which relates to the build up of positive charge as the nitrogens are successively protonated.

Statistical contribution to K_n should be favourable for initial protonation. So as to say, the statistical contribution for a reaction $LH_{n-1} + H \rightarrow LH_n$ is dependent on the relative number of sites available for a new proton to attach.

Moreover, compared to EDTA, the replacement of two of the carboxylate arms in the parent EDTA structure with amide containing fragments (amino methyl pyridine) could have caused the decrease in $\log K_1$ values (i.e. 2.87 units). This may partially be due to the reduced inductive effect of the amide group in relation to that of carboxylate.⁵⁶ Although, this is valid for the reduction of pK_{a1} , it does not hold for the significant reduction in pK_{a2} values, which may be rationalized by the electrostatic effect due to the presence of two carboxylate groups instead of four in EDTA.

The first two protonation constants of L^4 range from 7.3-6.2 (log units). Which is expected, considering the backbone nitrogen atoms of a structurally similar ligand, EDTA bisamide of 2-aminopyridine, displays a protonation constants ranging 6.82-3.49, depending on the experimental conditions involved. The third and fourth protonation constants could be attributed to either pyridine nitrogens or to the amide oxygens. Most likely target for protonation however, could be the nitrogen atoms of pyridine moieties than the amide oxygens. This is partly justified, by the comparable range obtained for third and fourth protonation constants for L^4 with that of pyridine nitrogens, i.e. range from 5.4-4.8 for L^4 in comparison to 5.42-4.89 for pyridines, depending on the experimental conditions.

Further, a pyridinium cation is usually less acidic when compared to carboxylic acids. This is partly due to the resonance stabilisation of a carboxylate group, in contrast to a pyridine-N atom in which the lone pair on the N atom is not part of the aromatic π -system. Increased nucleophilicity of the amide oxygen in relation to pyridine nitrogen is well known.

This has enabled the protonation of the amide oxygen relatively easy and has resulted in comparatively low protonation constants 4.0 and 2.4.

Attributable protonation sequence for L²

In the case of L², pK_{a1}, however, has to be attributed to the protonation of sulphonamide-N, rather than for the protonation of the ethylene nitrogens. This has been justified partly by pK_{a1} of 4-aminobenzene sulfamide, which is 0.73 units higher than that of the backbone nitrogen atoms of EDTA partly by the fact that the basicity of sulphonamide-N is considerably affected by the two highly electronegative oxygen atoms, rendering it less vulnerable for protonation. The observed value for pK_{a1}, 9.75 of sulphonamide-N stands in close testimony with the literature values and the aforementioned explanation.⁵⁷

Consequently pK_{a2} attributable to the protonation of one of the nitrogen sites of the ethylene diamine backbone. Thus pK_{a3} is attributable to one of the oxygen of the peptide bond and the explanation given for L⁴ could hold for L² as well. Further, the relative increase in pK_{a3} from 4.80-5.4 to 5.25 may be attributed to the electron withdrawing affect of sulphonyl moiety in contrast to the electron inductive effect of a methyl group in pyridine moiety. The summation of pK_a values for individual ligands (ΣpK_a) provides us with a valuable insight in to the parameter called as overall basicity. While basicity is not the sole determining factor to be considered, when designing thermodynamically more stable complexes (since, for instance, electrostatic hard-soft interactions also plays a vital role), some of the scientists have succeeded in optimising the basicity of similar ligands, which facilitates the stability enhancement.

Table -2: Tabulated data for the possible fragments obtained from stability constant data base

Fragment or Moiety	Binding Species	Method	Medium (Ionic concentration)	Temp/°C	Log K Value(s)	Ref
	H ⁺	G	KCl (1M)	25	10.98	58
	H ⁺	G	No electrolyte	25	4.76	59
	H ⁺	G	KNO ₃ (1M)	25	10.17	60
	H ⁺	G	KNO ₃ (0.15M)	25	9.62	61
	H ⁺	cal	NaCl (0.15M)	25	8.65	62
	H ⁺	G	NaNO ₃ (1M)	25	9.53	63
	H ⁺	G	NaNO ₃ (1M)	25	10.93	64
	H ⁺	G	NaNO ₃ (1M)	25	9.99	65
	Cu ²⁺	G	NaNO ₃ (1M)	25	22.46	65
	Mn ²⁺	G	KNO ₃ (0.1M)	25	14.05	66
	Zn ²⁺	G	KNO ₃ (0.1M)	25	16.24	66
	H ⁺	G	NaNO ₃ (1M)	25	9.16	67
	H ⁺	g	NaCl (0.15M)	25	8.47	68

B.4.2.1.1.2 Analysis of Deprotonation Curves

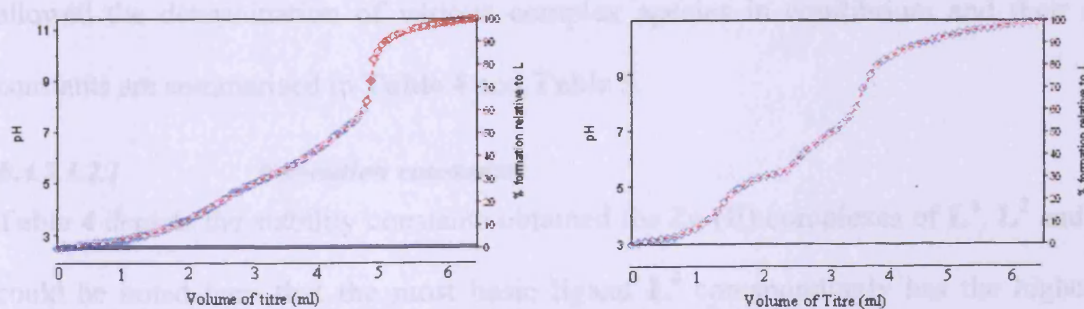


Figure 3:- Depicting the titration curves in the absence of metal ions for L⁴ (Left) and L² (Right)

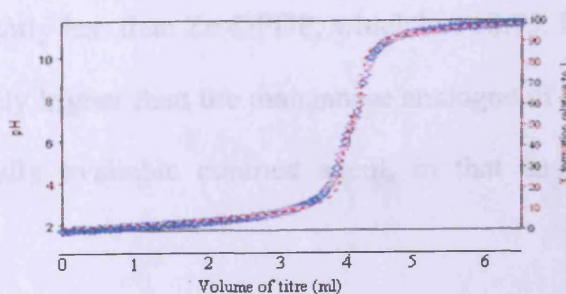


Figure 4:- Depicting the titration curves in the absence of metal ions for L⁶

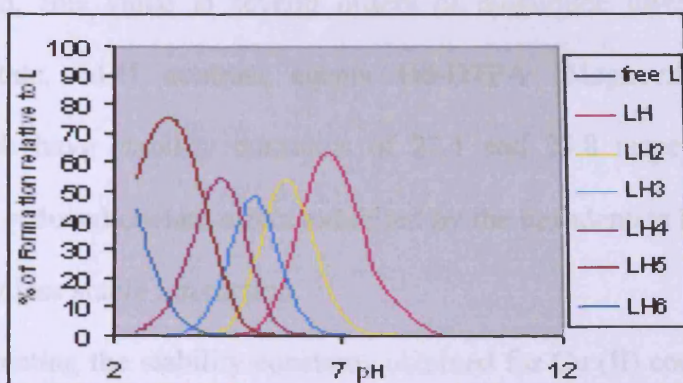


Figure 5:- Speciation diagram for L^4 in the absence of metal ion

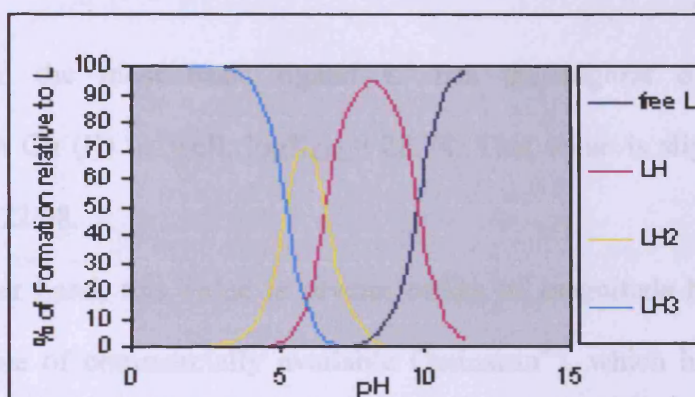


Figure 6:- Speciation diagram for L^2 in the absence of metal ion

B.4.2.1.2 Formation constants and Complexation Curves

Analysis of potentiometric curves (Fig 7, 8 and 9) by the software program Hyperquad 2006 allowed the determination of various complex species in equilibrium and their formation constants are summarised in Table 4 and Table 5.

B.4.2.1.2.1 Formation constants

Table 4 depicts the stability constants obtained for Zn (II) complexes of L^4 , L^2 and L^6 and it could be noted here that the most basic ligand L^4 correspondingly has the highest overall stability upon complexation, $\log K_{ZnL} = 16.03$.

This value is slightly less than Zn-DPDP, which has 18.95. It should also be mentioned here, this value is slightly higher than the manganese analogue of DPDP, namely Mn-DPDP (Teslascan®); commercially available contrast agent, in that an overall stability has been reported as 15.1.²¹

On the other hand, this value is several orders of magnitude lower than commercially available octadentate, MRI contrast agents Gd-DTPA (Magnevist®) and Gd-DOTA (Dotarem®), which have stability constants of 22.1 and 25.8 respectively. This may be rationalized by the reduced chelate effect exhibited by the hexadentate ligand, leading on to a thermodynamically less stable interaction.

Table 5 depicting the stability constants obtained for Cu (II) complexes of L^4 , L^2 and L^6 . The overall stability constant obtained for Cu (II) complex of L^6 is significantly lower than that of L^2 .

Once again the most basic ligand L^4 has the highest overall stability upon complexation with Cu (II) as well, $\log K_{CuL} = 28.74$. This value is slightly higher than Cu-DPDP, which has 22.08.

On the other hand, this value is several orders of magnitude higher than Zn-DTPA BMA (Zn analogue of commercially available Ominscan®), which has 12.04.⁶⁹ It will be interesting to note that the Gd (III) complex formed with EDTA-PA₂ and EDTA-IPA₂ has been reported to possess 10.3 and 12.79 respectively.

Table 4: Stability constants of ligands L^4 , L^2 and L^6 with Zn^{II}

Quotient	Constant	L^4	L^2	L^6
$[ZnL]/[Zn][L]$	$\log K_{ZnL}$	16.03	9.69	-
$[ZnLH]/[ZnL][H]$	$\log K_{ZnLH}$	5.94	8.23	11.43
$[ZnLH_2]/[ZnLH][L]$	$\log K_{ZnLH_2}$	-	-	-
$[ZnH_{.1}]/[Zn][H_{.1}]$	$\log K_{ZnH_{.1}}$	-7.89	-7.89	-7.89

Table 5: Stability constants of ligands L^4 , L^2 and L^6 with Cu^{II}

Quotient	Constant	L^4	L^2	L^6
$[CuL]/[Cu][L]$	$\log K_{CuL}$	28.74	Unsteady refinement	12.55
$[CuLH]/[CuL][H]$	$\log K_{CuLH}$	3.67	-	-
$[CuLH_2]/[CuLH][L]$	$\log K_{CuL_2}$	1.35	-	-
$[CuH_{.1}]/[Cu][H_{.1}]$	$\log K_{CuH_{.1}}$	-6.29	-	-6.29

B.4.2.1.2.2

The best-fit models obtained from Hyperquad included ML and MLH for Zn (II) and Cu (II) of L^4 and ML, MLH and MH_{-1} for Zn (II) complex of L^2 . Inclusion of other species worsened the fit or was rejected during the refinement process.

Attempted modelling with Hyper Quad yielded no success with Cu (II) complex of L^2 . Modelling with 1:1 ratio led to unstable refinement and resulted in large χ^2 -squared values conveyed a poor correlation between the calculated and experimental titration curves.

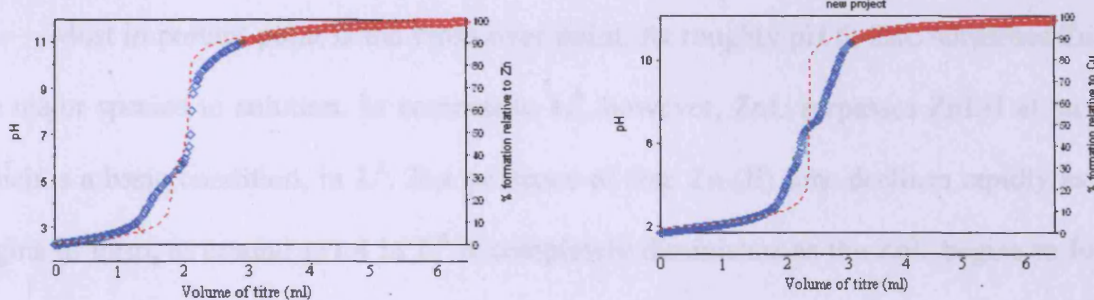


Figure 7:- Depicting the titration curves of L^4 in the presence of Zn^{II} (Left) and Cu^{II} (Right)

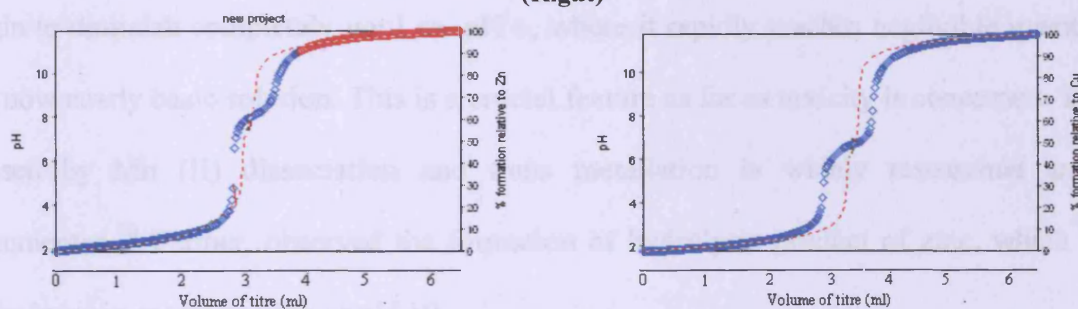


Figure 8:- Depicting the titration curves of L^2 in the presence of Zn^{II} (Left) and Cu^{II} (Right)

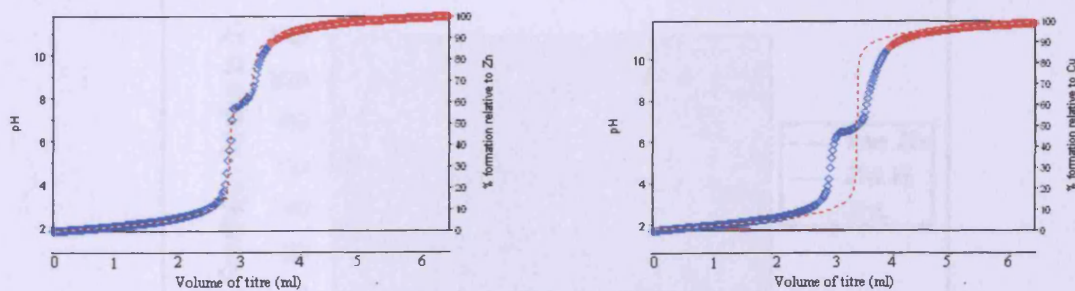


Figure 9:- Depicting the titration curves of L^6 in the presence of Zn^{II} (Left) and Cu^{II} (Right)

Speciation Plots

The speciation diagrams of each ligand have been displayed below in **Figures 10-11**. These diagrams are in a form which represents the percentage of species in solution relative to the transition metal ion (for eg: - Zn (II)) across the entire experimental pH range.

The speciation plot of L^4 (Fig-10) reveals that the species ZnL begins to be formed at approximately pH 4 unlike in the case of L^2 (Fig-11), where it begins at pH 6. In contrast, this species rapidly rises until pH 6, however, after which it gradually increases further to reach a maximum around pH 10, at which point it has started to decline gradually.

The species ZnLH is formed at *ca.* pH 2 and gradually increases, in precise contrast to the species ZnL, until pH 4, whereupon it undergoes a sharp decline until *ca.* pH 6.5, after which it gradually declines.

Most important point is the cross over point. At roughly pH 6, ZnL surpasses ZnLH as the major species in solution. In contrast to L^4 , however, ZnL surpasses ZnLH at *ca.* pH 8, which is a basic condition, in L^2 . The presence of free Zn (II) ions declines rapidly as ZnLH begins to form, at around pH 4 in L^4 it completely diminishes as the ZnL begins to form. In contrast, in L^2 , the presence of free Zn (II) ions sharply declines until pH 4, but does not begin to diminish completely until *ca.* pH 6, where it rapidly reaches negligible quantities in the now nearly basic solution. This is a crucial feature as far as toxicity is concerned. Toxicity caused by Mn (II) dissociation and trans metallation is widely researched and well documented.⁷⁰ Further, observed the formation of hydrolysis product of zinc, which can be hydrolysed in media as high as pH 10.

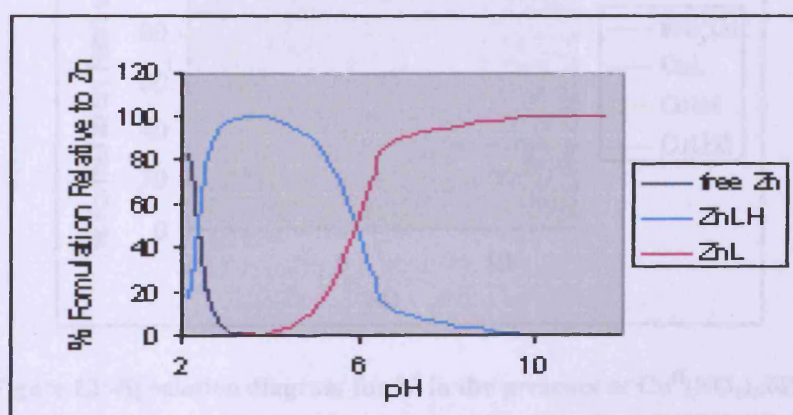


Figure 10:- Speciation diagram for L^4 in the presence of $Zn^{II}(NO_3)_2 \cdot 6H_2O$

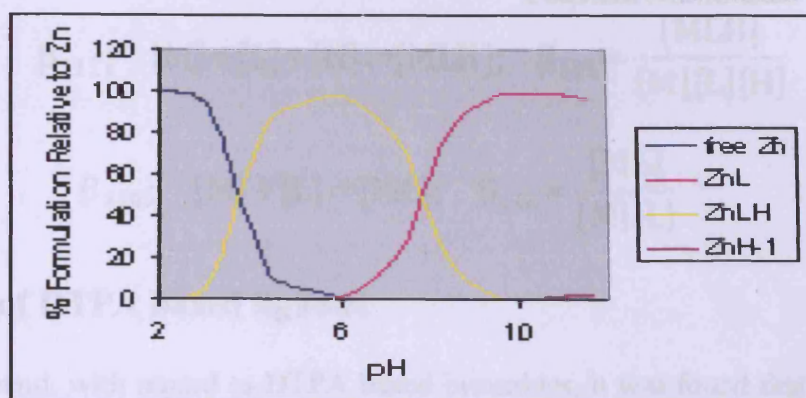


Figure 11:- Speciation diagram for L^2 in the presence of $Zn^{II}(NO_3)_2 \cdot 6H_2O$

The speciation plot of L^4 with Cu is presented in **Fig-12**. The species CuL begins to form at *ca.* pH 2 and rapidly rises until around pH 5, at which point it gradually increases to reach *ca.* pH 10, similar to ZnL in L^4 after which it decreases gradually. On the other hand, the species $CuLH$ gradually increases until pH 3 and sharply declines until pH 4, whereupon it gradually declines.

The point of cross over also to be noted here. At around pH 4, CuL surpasses $CuLH$ as the major species in solution, which is a more acidic condition, in comparison to the zinc complex of L^4 .

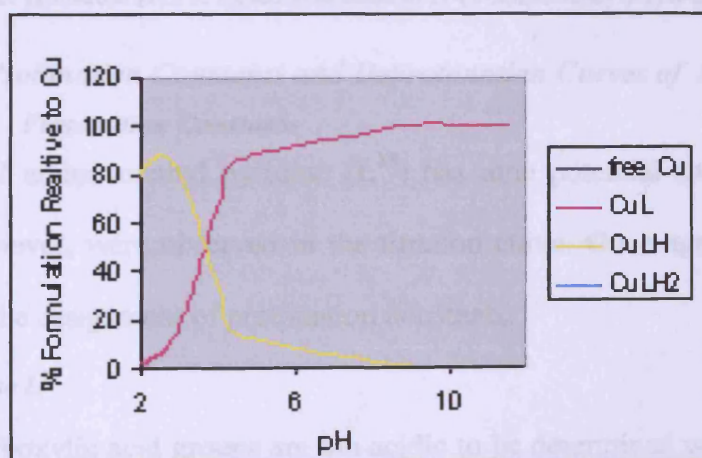


Figure 12:-Speciation diagram for L^4 in the presence of $Cu^{II}(NO_3)_2 \cdot 6H_2O$

In the case of L^4 (**Fig-10** and **Fig 12**) and L^2 (**Fig-11**) there are two major species formed during the course of the titration tending towards higher pH. These are successively MLH and ML , which could be represented by following equations.

$$\beta_{111}; [M] + [L] + [H] \rightleftharpoons [MLH]; \quad \beta_{111} = \frac{[MLH]}{[M][L][H]} \quad (1)$$

$$\beta_{110}; [M] + [L] \rightleftharpoons [ML]; \quad \beta_{110} = \frac{[ML]}{[M][L]} \quad (2)$$

Evaluation of DTPA based ligands

On the other hand, with regard to DTPA based bisamides, it was found that DTPA bisamide of 4-aminomethylpyridine (L^{15}) was readily soluble in water. The DTPA bisamide of N-(2-Aminoethyl)-1,8-naphthalimide (L^{14}), however, was found to be insoluble in water.

Potentiometric titration was not carried out for this ligand.

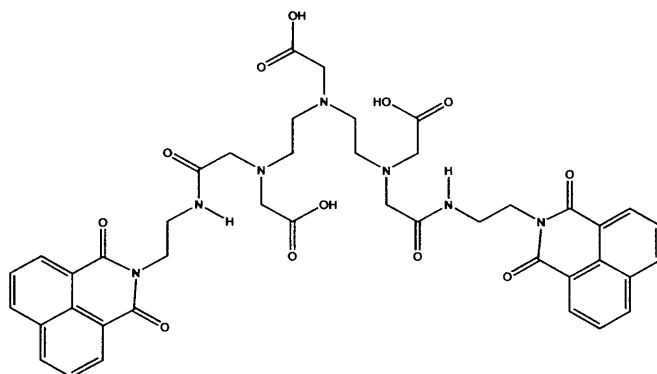


Figure 13:- Water insoluble DTPA based bisamide of N-(2-Aminoethyl)-1, 8-naphthalimide (L^{14})

B.4.2.2.1 Protonation Constants and Deprotonation Curves of L^{15} and L^{11}

B.4.2.2.1.1 Protonation Constants

DTPA bisamide of amino methyl pyridine (L^{15}) has nine potential sites. There were only three maxima, however, were observed in the titration curve. Once again the review of the literature aided in the assignment of protonation constants.

Attributing Sequence to L^{15}

The pKa of the carboxylic acid groups are too acidic to be determined with this technique, as in the case of EDTA bisamides. Among the remaining sites, out of the three nitrogen atoms, the central nitrogen atom is often the primary target for protonation. It has been reported that the unprotonated form of the ligand will be capable of producing hydrogen bond rings inclusive of the amide hydrogens, the terminal hydrogens and the terminal carboxylate ions.

Therefore addition of protons to the basic sites could only be possible through the destruction of these hydrogen bond rings, which in turn justifies the marked preference for the first protonation at the central nitrogen atom. This has been reflected in the $\log K_1$ of 10.03 and the value tallies to a good extent with literature value. Further, it was also pointed out that the formation of amide linkages leads to the reduction of $\log K_1$ from 0.8-1.1 units and $\log K_2$ value by 4.0-4.2 as far as DTPA bisamides based on alky amines is concerned. While the observation supports the first protonation constant observed in the experiment, it does not justify the slight reduction in $\log K_2$.

The second protonation occurs at one of the terminal nitrogen sites, simultaneously causing the proton attached to central nitrogen to migrate to terminal nitrogen. This happens in order to reduce the positive charge repulsion. This is possible through the destruction of hydrogen bond network.

Table 6: Thermodynamic Properties for the Ligands L¹⁵ and L¹¹

Quotient	Constant	L ¹⁵	L ¹¹
$[HL]/[L][H]$	$\log K_{HL}$	10.03	7.73
$[H_2L]/[HL][H]$	$\log K_{H_2L}$	9.24	5.12
$[H_3L]/[H_2L][H]$	$\log K_{H_3L}$	-	-
$[H_4L]/[H_3L][H]$	$\log K_{H_4L}$	9.16	-
ΣpK_a		28.43	12.85

B.4.2.2.1.2 Analysis of Deprotonation Curves

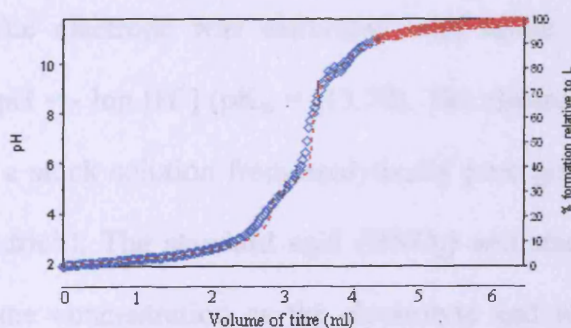


Figure 14:- Depicting the titration curve of L¹⁵ in the absence of metal ions

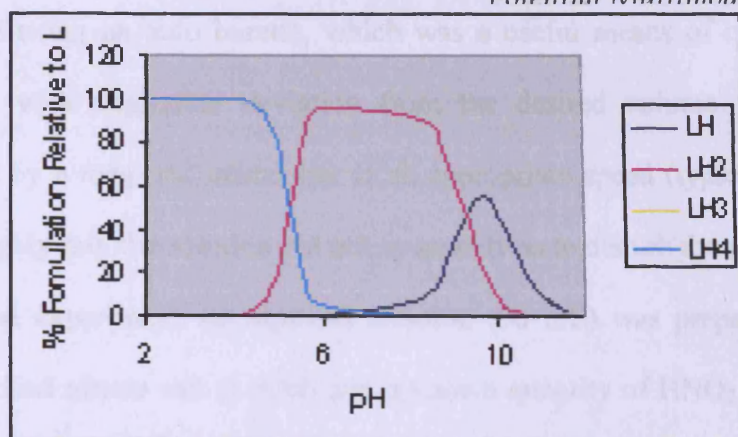


Figure 15:- Speciation diagram for L^{15} in the absence of metal ions

Deprotonation Curve of Symmetric Naphtha Derivative (L^{11})

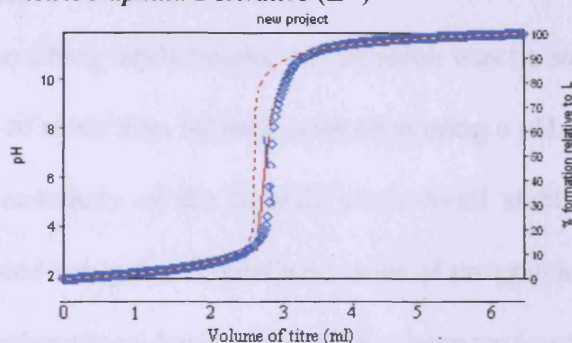


Figure 16:- Depicting the titration curve of L^{11} in the absence of metal ions

B.4.3 Experimental Section

The potentiometric studies were carried out with a TIM840 autotitrator (Radiometer Analytical). A Metrohm combined pH glass electrode (Ag/AgCl) with 3M KCl internal filling solution was used. Solutions were prepared using doubly deionised freshly distilled water ('Boiled out water'). The electrode was calibrated with dilute standard acid and alkali solutions, thus defining $\text{pH} = -\log [\text{H}^+]$ ($\text{pK}_w = -13.78$). The electrolyte, NaNO_3 (0.1 M), was prepared in the form of a stock solution from analytically pure grade NaNO_3 obtained from commercial sources (Aldrich). The standard acid (HNO_3) and standard base (NaOH) were also prepared to the same concentration as the electrolyte and were again obtained from commercial sources (Aldrich) free from any carbonate contamination which would have had the adverse effect of buffering the reaction mixture. The temperature of the reaction mixture was controlled by a thermostat which maintained a flow of water in a water-tight layer encapsulating the reaction cell at a constant 25°C (298K). The standard base was delivered in

Potential Multimodal Imaging Agents

0.05 mL aliquots using an auto burette, which was a useful means of measuring identical amounts quickly with negligible deviation from the desired volume. The solution was constantly mixed by a magnetic stirrer bar at an appropriate speed (typically 200 rpm), fast enough to thoroughly mix the solution but not so quickly as to disturb the electrode.

In a typical experiment, an aqueous solution (50 mL) was prepared containing the ligand (1 mM), metal nitrate salt (1 mM) and a known quantity of HNO₃ (0.1 M). The ionic strength (*I*) of this solution was adjusted to 0.1 with 1M NaNO₃. The temperature of solutions (25 °C) in the covered, water-jacketed cell was kept constant by a Fischer Scientific BC10 circulating bath. Upon reaching equilibrium, this solution was titrated with NaOH (0.1021 N). Each titration consisted of more than 80 data points spanning a pH range of 2–10.

The protonation constants of the ligands and overall stability constants of the metal complexes were calculated using the HyperQuad suite of programs, namely HyperQuad 2006 and HySS 2006. The mathematical basis of which has been reviewed in the literature.⁷¹ HyperQuad 2006, software's selection of equilibrium models was dominated by critical evaluation of the least squares fitting results. This could be explained in terms of analysis of the weighted residuals and statistical parameters (χ^2 and σ). The reported equilibrium constants are the mean average of two separate measurements. Immediately prior to this investigation, a trial experiment involving the known ligand tris(2-aminoethyl)amine (TREN, Fig. 4) was used as a control. The data matched, within statistical error, the comprehensive set of data from the literature.⁷²

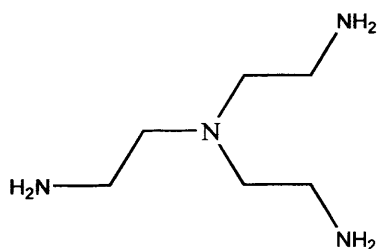


Figure 21: The ligand TREN. Literature protonation constants: 10.42, 9.88, 8.90. This work: 10.48, 9.70, 8.40.

References

1. (a) N. Bloembergen, E. M. Purcell and R.V. Pound, *Phys. Rev.*, 1948, **73**, 678
(b) I. Solomon, *Phys. Rev.*, 1955, **99**, 559.
2. H. Lammers, F. Maton, D. Pubanz, W. V. Laren, H. V. Bekkum, A. E. Merbach, R.N. Muller and J.A. Peters, *Inorg. Chem.*, **97**, **36**, 2527.
3. J. Eisinger, R. G. Shulman and W.E. Blumberg, *New Biol.*, 1961, **192**, 963.
4. E. J. Werner, A. Datta, C. J. Jocher and K. N. Raymond, *Angew. Chem. Int. Ed.*, 2008, **47**, 8568.
5. F. Kielar, L. Tei, E. Terreno and M. Botta, *J. Am. Chem. Soc.*, 2010, **132**, 7836.
6. R. K. Tekade, P.V. Kumar and N. K. Jain, *Chem. Rev.*, 2009, **109**, 49.
7. P. Caravan, *Chem. Soc. Rev.* 2006, **35**, 512.
8. S. G. Zech, W. C. Sun, V. Jacques, P. Caravan, A. V. Astashkin and A. M. Raitsimring, *ChemPhysChem.*, 2005, **6**, 2570.
9. A. Datta, K. N. Raymond, *Acc. Chem. Res.*, 2009, **42**, 938
10. (a) S. G. Zech, H. B. Eldredge, M. P. Lowe and P. Caravan, *Inorg. Chem.*, 2007, **46**, 3576. (b) G. Bodlander and O. Storbeck, *Z. Inorg. Chem.*, 1902, **31**, 458.
11. G. Lipar and A. Szabo, *J. Am. Chem. Soc.*, 1982, **104**, 4546.
12. R. Kimmich and E. Anoardo, *Prog. Nucl. Magn. Reson. Spectrosc.*, 2004, **44**, 257.
13. (a) D. J. Lurie, S. Aime, S. Baroni, N. A. Boothd, L. M. Broche, C. H. Choi, G. R. Davies, S. Ismail, D. Ohogaina and K. J. Pine, *C. R. Physique.*, 2010, **11**, 136. (b) R. D. Boer, *Medical Imaging.*, 2006, 43.
14. P. Vallet, Y. V. Haverbeke, P. A. Bonnet, G. Subra, J. P. Chapat and R. N. Muller, *Magn. Reson. Med.*, 2005, **32**, 11.
15. R. M. Supkowski and W. D. Horrocks, *Inorg. Chem.*, 1999, **38**, 5616.
16. H. Yuan, T. Schroeder, J. E. Bowsher, L. W. Hedlund, T. Wong and M. W. Dewhirst, *J. Nucl. Med.*, 2006, **47**, 989.
17. M. Rami, J. Y. Winum, A. Innocenti, J. L. Montero, A. Scozzafava, C. T. Supuran, *Bioorg. Med. Chem. Lett.*, 2008, **18**, 836.
18. M. Z. Koylu, S. Asubay and A. Yilmaz, *Molecules.*, 2009, **14**, 1537.
19. (a) B. J. Blacompt, A. Carpenteran and L. D. Hall, *J. Chem.*, 1992, **70**, 2693;
(b) R. B. Lauffer, *US Pat.*, 4,899,755, 1990.
20. S. Aime, M. Botta, M. Fasanoa and E. Terrenoa, *Spectrochim. Acta Part A: Molecular Spectroscop.*, 1993, **49**, 1315.

21. S. M. Rocklage, W. P. Cacheris, S. C. Quay, F. E. Hahn and K. N. Raymond, *Inorg. Chem.*, 1989, **28**, 477.
22. M. E. Bernardino, J. C. Weinreb, D. G. Mitchell, W. C. Small and M. Morris, *J. Magn. Reson. Imaging.*, 1994, **4**, 872.
23. D. L. Rubin, H. Mullera and S. W. Young, *Magn. Reson. Med.*, 1992, **23**, 154.
24. A. L. Thompson, D. Parker, D. A. Fulton, A. K. Howard, S. U. Pandya, H. Puschmann, K. Senanayake, P. A. Stenson, A. Badari, M. Botta, S. Avedano and S. Aime, *Dalton Trans.*, 2006, 5605.
25. M. Polasek, J. Rudovsky, P. Hermann, I. Lukes, L. V. Elst and R. N. Muller, *Chem. Commun.*, 2004, 2602.
26. (a) S. Aime, A. Barge, A. Borel, M. Botta, S. Chemerisov, A. E. Merbach, U. Muller, and D. Pubanz, *Inorg. Chem.*, 1997, **36**, 5104. (b) E. Balogh, M. M. Iglesias, C. P. Iglesias, E. Toth, K. Djanashvili, J. A. Peters, A. de Blas and T. R. Blas, *Inorg. Chem.*, 2006, **45**, 8719.
27. R. J. Dimelow, N. A. Burton and I. H. Hillier, *Phys. Chem. Chem. Phys.*, 2007, **9**, 1318.
28. A. Datta and K. N. Raymond, *Acc. Chem. Res.*, 2009, **42**, 938.
29. W. P. Cacheris, S. C. Quay and S. M. Rocklage, *Magn. Reson. Imaging.*, 1990, **8**, 467.
30. H. Von Euler, *Ber.*, 1903, **86**, 1854.
31. G. Bodlander and O. Storbeck, *Z. anorg. Chem.*, 1902, **31**, 458.
32. (a) N. Bjerrum, Ph.D. Thesis, Technical University of Denmark, 1908. (b) N. Bjerrum, *Z. physik. Chem.*, 1910, **73**, 724.
33. (a) J. Bjerrum, in *Metal Ammine Formation in Aqueous Solutions*, P. Haase and Sons, Copenhagen, 1941. (b) J. Bjerrum, *Chem. Rev.*, 1950, **46**, 381.
34. F. J. C. Rossotti, H. Rossotti, in *The Determination of Stability Constants*, McGraw-Hill, New York, 1961.
35. P. Gans, A. Sabatini and A. Vacca, *Talanta.*, 1996, **43**, 1739.
36. IUPAC Stability Constant Database: *A comprehensive database of published data on equilibrium constants of metal complexes and ligands. Version 5.7.* Academic Software.
37. A. E. Martell, R. J. Motekaitis, in *Determination and Use of Stability Constants*, Wiley-VCH, 2nd Edition, 1992.
38. J. Burgess, in *Ions In Solution: Basic Principles of Chemical Interactions*, Ellis Horwood Limited, Chichester, 1987.

39. A. Vacca, C. Nativi, M. Cacciarini, R. Pergoli and S. Roelens, *J. Am. Chem. Soc.*, 2004, **126**, 16456.
40. J. C. Hsu, W. H. Chen, C.Y. Liu, *Analyst.*, 1997, **122**, 1393.
41. Y. Engel, A. Dahan, E. R. Kemelmakher and M. Gozin, *J. Org. Chem.*, 2007, **72**, 2318.
42. M. A. Santos, S. Gama, L. Gano and E. Farkas, *J. Inorg. Biochem.*, 2005, **99**, 1845.
43. A. H. Amrallah, N. A. Abdalla and E. Y. El-Haty, *Talanta.*, 1998, **46**, 491.
44. H. Sakai, H. Horinouchi, E. Tsuchida and K. Kobayashi, *SHOCK.*, 2009, **31**, 507.
45. R. M. Martell and A. E. Smith, *Sci. Total. Environ.*, 1987, 64.
46. H. E. Allen, C. P. Huang, G. W. Bailey, A. R. Bowers (Eds.) and B. Raton in *Metal Speciation and Contamination of Soil*, Lewis Publishers, 1995.
47. J. R. Duffield, P. M. May and D. R. Williams, *J. Inorg. Biochem.*, 1984, **20**, 199.
48. Schwarzenbach, *Anal. Chem.*, 1960, **32**, 6.
49. S. Ahrland, J. Chatt and N. R. Davies, *Q. Rev. Chem. Soc.*, 1958, **12**, 265.
50. R.G. Pearson, *J. Am. Chem. Soc.*, 1963, **20**, 3533.
51. H. Irving and J. P. Williams, *Nature.*, 1948, **162**, 746.
52. H. Irving and J. P. Williams, *J. Chem. Soc.*, 1953, 3192.
53. K. J. Powell and L. D. Petti, IUPAC Stability Constant Database, 1989-1993.
54. A. E. Martell and R. Smith in *Critical Stability Constants*, Plenum Press, New York, 1989.
55. A. F. D. de Namor and A. P. Tanaka, *J. Chem. Soc., Faraday Trans.*, 1998, **94**, 31105.
56. G. R. Choppin and K. M. Schaab, *Inorg. Chim. Acta.*, 1996, **252**, 299.
57. (a) T. K. Jankowska, H. Kozłowski, L. D. Pettit, K. Pawelczak and M. Makowski, *J. Inorg. Biochem.*, 1995, **57**, 183; (b) C. S. Correa, R. O. Esquivel and R. P. Sagar, *International Journal of Quantum Chemistry.*, 2003, **94**, 165.
58. L. Asso, M. Asso and G. Carpeni, *Rev. Chim. Minerale.*, 1972, **9**, 647.
59. R. Goldberg, N. Kishore and R. Lennen, *J. Phys. Chem.*, 2002, **31**, 231.
60. I. Poulsen and J. Bjerrum, *Acta Chem. Scand.*, 1955, **9**, 1407.
61. J. Ambrose, A. Covington and H. Thriskn, *Trans. Faraday Soc.*, 1984, **65**, 1897.
62. E. G. Espana, F. Nuzzi, A. Sabatini and A. Vacca, *Gazz. Chim. Ital.*, 1987, **117**, 275

Potential Multimodal Imaging Agents

63. Y. Couturier, C. Petitfaux, *Compt. Rend.*, 1972, **275C**, 953.
64. P. Amico, R. Bonomo and R. Cali, *Inorg. Chem.*, 1978, **28**, 3555.
65. J. Ambrose, A. Covington and H. Thirsk, *Trans. Faraday Soc.*, 1969, **65**, 1897.
66. A. Brunetti, G. Nancollas and P. Smit, *J. Am. Chem. Soc.*, 1969, **91**, 4680.
67. S. Musso, G. Anderegg, J. Ruegger, C. W. Schlapfer and V. Gramlich, *Inorg. Chem.*, 1995, **34**, 3329.
68. S. H. Laurie and E. S. Mohammed, *J. Chem. Soc., Dalton Trans.*, 1995, 129.
69. J. F. Carvalho, S. H. Kim and C. A. Chang, *Inorg. Chem.*, 1992, **31**, 4065.
70. B. Gallez, C. Baudalet, J. Adline, M. Geurts and N. Delzenne, *Chem. Res. Toxicol.*, 1997, **10**, 360.
71. P. Gar, A. Sabatini and A. Vacca, *Talanta.*, 1996, **43**, 1739.
72. K. Adam and A. D. Baldwin, *Dalton Trans.*, 1985, 1869.

CHAPTER 5

Luminescence

Measurements

Chapter 5

Luminescence Measurements

5.1 Luminescence: An Introduction

The phenomenon of luminescence has dramatically expanded its horizon in the past two decades. It was initially considered as an important tool in biochemistry and biophysics. This emphasis, however, widens its scope. Presently this methodology (especially fluoroscopy and time dependence fluorescence) is dominating in the areas of DNA sequencing,¹ medical diagnostics,² flow cytometry,³ biotechnology to name a few. Particularly, it has dramatically advanced in the area of cellular and fluorescence imaging, to the extent of single cell detection and imaging.⁴

To appreciate the importance of luminescence measurements with regard to new multidentate ligands, it is important to have an understanding of the phenomenon. The proceeding section is devoted to the principles underlying the phenomenon of luminescence.

5.1.1 What is luminescence?

In very simple terms, it could be defined as “Emission of light from a substance”. This is possible because an electron that goes from ground state to the excited state upon excitation loses its excess energy in the form of photon, when the electron returns to the ground state. According to the type of excited state and the mode of excitation, it can be classified into three types of behaviour:

- a. Fluorescence
- b. Phosphorescence
- c. Chemiluminescence

Fluorescence

This type of emission takes place as result of a three step process, that occurs within molecules (usually poly aromatic hydrocarbons or heterocyclic molecules), which are known as chromophores (more specifically fluorophores).

These are also known as fluorescent dyes. Then the question arises, how do we relate fluorophores to the fluorescent probes? A Fluorescent probe is a fluorophore designed to respond to a specific stimulus or be localized within the specific site of a biological specimen. The process of fluorescence could be further explained by means of a simple electronic state diagram, known as Jablonski diagram (see Fig-1).

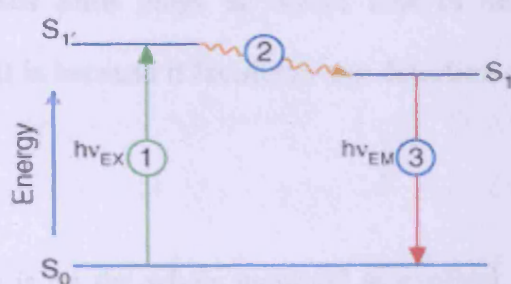


Figure:- 1 Jablonski Diagram explaining the process of fluorescence

Step 1: Excitation

The light energy, supplied in terms of photons ($h\nu_{EX}$) by an external source (incandescent lamp or a laser) will be absorbed by the fluorophore. This will result in the formation of excited singlet electronic state (S_1'). This stage of luminescence distinguishes fluorescence from chemiluminescence, as the excited state is created by the chemical reaction in the latter.

Step 2 Excited-State Lifetime

The excited state could last for a specific period (1-10 nano seconds), within this period the fluorophore undergoes many conformational changes and may also interact with the environment in many ways.

These interactions have two different impacts on the excited state. Firstly, energy of the S_1' is partially dissipated, while yielding a relaxed singlet state, through which fluorescence emission originates. Secondly, not all the molecules initially excited by absorption (Step 1)

return to the ground state (S_0) by fluorescence emission. Other processes help to relax the molecule and involve fluorescence resonance energy transfer (FRET) and intersystem crossing. Further, 'fluorescence quantum yield' should also be defined. It is the ratio of the number of photons emitted through fluorescence to the number of photons absorbed.

Step 3: Fluorescence Emission

When the fluorophore returns to its ground state (S_0), a photon is emitted. Obviously, the energy of this photon is lower due to the partial dissipation of energy. Thus it has a longer wavelength than the excitation photon. The very difference in energy or wavelength could be represented by $(h\nu_{EX}-h\nu_{EM})$. This gives rise to another interesting phenomenon, called the 'Stokes shift'. This Stokes Shift plays an active role in determining the sensitivity of fluorescence techniques. It is because it facilitates the detection of emission photons against a low background.

Fluorescence Spectra

The fluorescence process is on the whole assumed as cyclical. Except in the case of Photo bleaching or similar cases, where the fluorophore is destroyed in the excited state, the same fluorophore can be repeatedly excited and its emission detected. So many thousands of detectable photons may be generated by a single fluorophore. This fact, contributes towards the high sensitivity of fluorescence detection techniques.

When considering polyatomic molecules in solution, the discrete electronic transitions ($h\nu_{EX}$ and $h\nu_{EM}$) are replaced by very broad energy spectra called the fluorescence excitation spectrum and fluorescence emission spectrum, respectively. When in the case of simultaneously detecting two or more different fluorophores, spectral bandwidths have to be considered. It could be generalised, excluding few exceptions that absorption spectra of single fluorophore species is identical to its fluorescence excitation spectrum. Moreover, the intensity of emission is proportional to the amplitude of the fluorescence excitation spectrum at the excitation wavelength (see Fig-2).

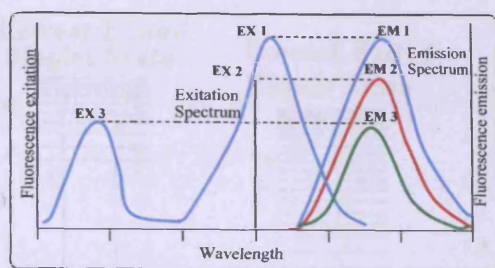


Figure 2:- Excitation of a fluorophore at three different wavelengths (EX 1, EX 2, EX 3) does not change the emission profile but does produce variations in fluorescence emission intensity (EM 1, EM 2 EM 3) that correspond to the amplitude of the excitation spectrum.

Phosphorescence

In order to understand this phenomena, it is imperative to know about “Intersystem crossing”. Intersystem crossing occurs when the spin of an excited electron is reversed. This is possible because the energy of the excited triplet state is lower than that of the energy of the excited singlet state. If the vibrational levels of these two different states overlap, the chances are more likely for this phenomenon to take place. For instance, the lowest singlet vibrational level may overlap with one of the highest triplet excited state vibrational levels.

Under such circumstances, a molecule in high triplet state vibrational level can collide with solvent molecules and lose energy. As a result it will relax to the lowest vibrational level of the excited triplet state. Then it may undergo a second intersystem crossing to the high excited singlet state vibrational level and eventually lose energy to come back to the lowest vibrational level of the ground state via vibrational relaxation (see Fig-3).

On the other hand, a molecule in the excited triplet state may not always be utilise intersystem crossing to return to the electronic ground state, instead it might lose energy by emission of a photon. An important fact to remember here is that triplet/singlet transition is much less probable than singlet/singlet transition. The lifetime of an excited triplet state could be up to 10s, whereas the lifetime of the excited singlet state ranges from 10^{-5} to 10^{-8} s. Typically, for most fluorophores, phosphorescence is not observed, with fluorescence dominating the room temperature spectra. This is because, other radiationless transfers compete with phosphorescence, but it does become prominent at low temperatures or in high viscous media.

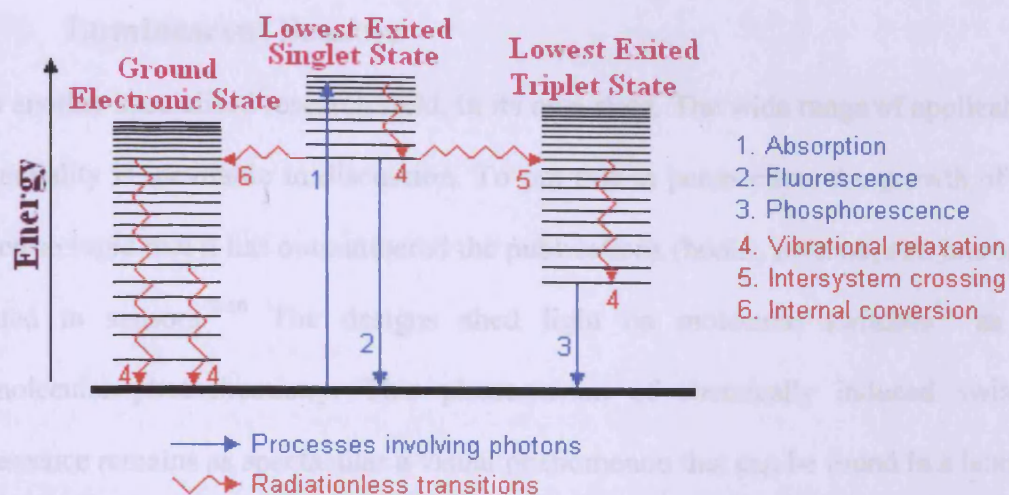
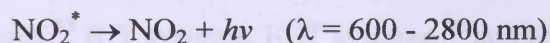
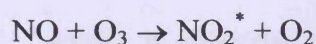


Figure 3:- Depicting the possible physical processes, following absorption of a photon by a molecule

Chemiluminescence

Contrary to fluorescence, this is produced by the emission of the electronically excited species, created by a chemical reaction. This kind of luminescence could be encountered in biological systems, where it is termed as bioluminescence. Chemiluminescence, however, is not produced by many chemical reactions although it has some environmental significance.

One appropriate example is the determination of nitric oxide:



5.1.2 Lifetime (of luminescence)

The time required for the luminescence intensity to decay from some initial value to $1/e$ of that value ($e = 2.718$). Lifetimes can be measured by phase fluorimetry (phosphorimetry) where the phase shift between the sinusoidally modulated exciting light and the emitted light is measured.

The aforementioned, brief introduction to the basic principles underlying luminescence has positioned us to know about its application. One such application is its usage in luminescent sensors.

5.1.3 Luminescent Sensors

This is another specialised research field, in its own right. The wide range of applicability and its potentiality is inevitable in discussion. To put this in perspective, the growth of the field has been so rapid that it has outnumbered the publications (books, reviews, and journal issues) dedicated to sensors.⁵⁻¹⁰ The designs shed light on molecular switches¹¹ as well as supramolecular photochemistry. This phenomenon of chemically induced switching of luminescence remains as spectacular a visual phenomenon that can be found in a laboratory.

Moreover, with the advancement of science there is a need to quantify chemical species of various kinds; especially in biological studies (systems responding to biologically relevant targets). This could be effectively achieved by the use of sensors. The active role enacted by coordination chemistry, from the stages of designing the luminescent sensors to the stage of characterisation is second to none.

Types of Luminescent Sensors

According to the various mechanisms applicable to this switching behaviour (as it could be switched between “on” and “off” states), it gives rise to various types of sensors, such as PET systems,¹² PCT systems,¹³ ICT systems, EET systems,¹⁴ and Eximer-Exiplex systems.¹⁵

Reporter–target interactions caused by the ion coordination could be of great help to cause this required switching behaviour. This could, however, be possible only if an appropriate photochemical process is brought in to action. Aforementioned quenching mechanisms (except PET) are considered to be not so ‘smart’ enough to respond to binding of the target species. Though there has been a great amount of effort exerted in the past to overcome this short coming, (such as the development achieved in EET), there is still much work to be done in this area.

Photo Induced Electron Transfer (PET)

The luminescent sensors based on PET mechanism (PET systems) are widely studied and thoroughly reviewed.¹⁶⁻¹⁸ The large, significant change in fluorescence intensity, which is commonly observed upon cation binding, is a unique advantage for PET sensors.

The other important characteristic is the absence of shift in the fluorescence or excitation spectra, which could prevent the possibility of intensity–ratio measurements at two different wave lengths. This kind of sensor could be quantitatively designed and the observable parameters could be predicted. These are prominent features of this PET mechanism.

5.1.3.1 Understanding PET

It is a well known fact that when molecules absorb light they transfer an electron to another system (exception–dye sensitized solar cell). Since the electron is getting transferred upon the absorption of light, it is known as Photo induced Electron transfer abbreviated as ‘PET’.

Mechanism of PET

In spite of its broad usage and wide range of applications, the mechanism could be explained in simple terms. This could be approached in two ways. One is to utilise fluorophore-spacer-receptor archetype and the other is making use of molecular orbital energy diagrams. Let us first consider the typical model introduced by A. P. de Silva *et al.*¹² As it could be seen (see Fig-4) this model comprises three components.

- a. Fluorophore/luminophore - Chromophore part of the system
- b. Spacer – bridge(non conjugated)
- C. Receptor- Docking area for the analyte

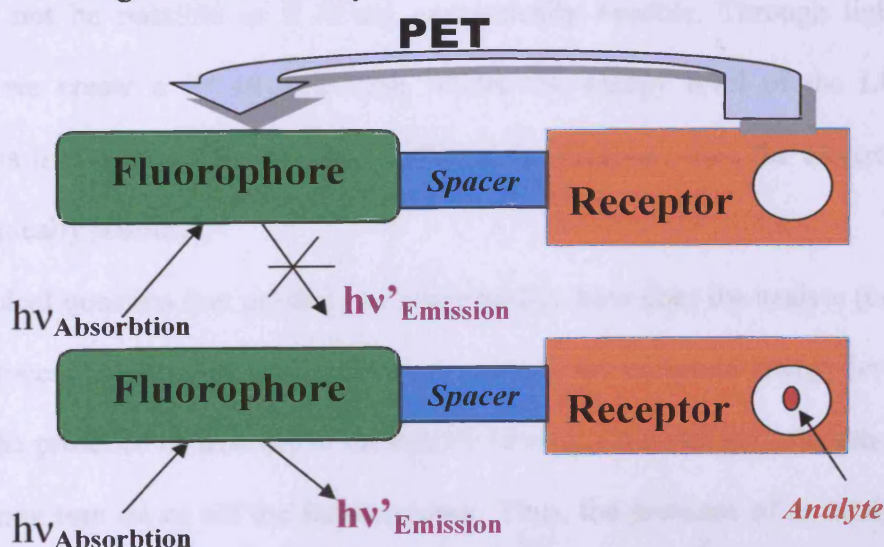


Figure 4:-Depicting the fluorophore-spacer-receptor model suggested by A.P.Silva *et al.* For an Off- On- type sensor, figure depicts the ‘switch-on’ of fluoresce binding of the analyte, which inhibits PET from the receptor to the fluorophore.

Here, one could consider the fluorophore and receptor as analogous to a donor and acceptor system. The switching behaviour could be interpreted in terms of 'On' and 'Off' states of the sensor.

Background understanding

Before we try to understand the model in detail, let us focus our attention on each component of the model. Here the fluorophore is the component which absorbs light; this could either donate the electron from the excited state to the receptor or accept an electron from the receptor in its ground state to fill the vacancy. Thus it is obvious, that the receptor could accept/donate electron from/to the luminophore (fluorophore).

The last one is the spacer that connects these two together. This could be a virtual component or may be absent altogether. Further, the transfer of electrons becomes viable only if it is energetically feasible, a thermodynamical condition discovered by Weller.¹⁹

Further, it is a known fact that excited states of the fluorophore (which arises upon excitation by the light source) are better oxidising agents/reducing agents than their ground state counterparts. Consider a situation where the fluorophore is a reducing agent and the receptor is an oxidising agent. Also consider the fact that, the energy level of the HOMO of the fluorophore, lies below the energy level of the LUMO of the receptor. Then electron transfer will not be possible as it is not energetically feasible. Through light excitation, however, if we create a F* excited state, where the energy level of the LUMO of the fluorophore is higher than that of the LUMO of the receptor, then the electron transfer is thermodynamically feasible.

The typical question that needs to be addressed is, how does the analyte (target species) affect this process? It is quite straightforward now. If the receptors energy levels could be tweaked in the presence or absence of an analyte (for eg: - a metal ion), then the presence of the analyte may turn on or off the luminescence. Thus, the presence of an analyte enhances the luminescence or quenches the luminescence. This forms the basis for all the PET sensors.

Potential Multimodal Imaging Agents

In the “on” state of the sensor, the excitation of the fluorophore gives emission. It is because the PET is inactive upon the arrival of the analyte. For instance, if we assume the analyte is H^+ , then the hydrogen ion draws the electron towards itself on the basis of electrostatic interaction. As a result, the oxidation potential of the target species bound receptor will increase to an extent that the thermodynamic conditions become unfavourable for PET to take place. The excess energy is released in the form of luminescence.²⁰

In the “off” state of the sensor, in the absence of an analyte, thermodynamics favour the electron transfer from the receptor to the fluorophore or in some cases from fluorophore to the receptor. This concept forms the basis for “*Off-On-type*” PET sensors.

In contrast, reversed, “*On-Off-type*” PET sensors have also been designed and developed. In that, the “off” state of the sensor is attributed to the activation of PET due to favourable thermodynamic conditions arise upon complexation.

5.1.3.2 *Kinds of PET sensors on the basis of modulating factor*

A review of the literature revealed that there are many sensors available or in the process of development for main group elements, transition metal cations, lanthanides and actinides. There are PET sensors that have developed to target a range of anions, such as acetates, phosphates, some halides, and amino acids.^{21, 22} Organic compounds as target species, also have drawn attention from PET sensor designers.²³ Further, some physical properties were also the target for PET sensor development. For instance, in the early 21st century, pH sensor development based on PET mechanism started receiving significance.^{24, 25}

This project is, however, concerned on developing cation sensors. Therefore we shall now focus our attention towards cation sensors.

Cation Recognition: A PET perspective

Why is it necessary?

Cation recognition is of utmost importance to many scientists (including chemists, biologists, clinical biochemists, environmentalists and especially among the PET Sensor designers). Some of the main group elements (e.g. sodium, potassium, magnesium, calcium) are of great biological importance. As they tend to regulate many biological processes. Conduction of nerve impulses, regulating muscle contraction, regulation of cellular activities, is just to name a few of these processes.

Further, there are some enzymes containing metal ions, along with proteins as part of their constituents (metallo enzymes). There are various metal ions influencing the regulation of these metallo enzymes. In medicine, in the treatment of psychological diseases, for instance manic depression, it is important to regulate serum levels of lithium.²⁶ Furthermore, regulating the level of potassium in the serum, is very important in the treatment of high blood pressure. To elaborate further, one could consider the adverse impact of heavy elements (e.g. mercury) and the toxicity caused by these elements to living organisms. As prevention is better than cure, their early detection will help to save many lives.

The nature of the cation-controlled, photo induced processes brings variety in to the type of cation sensors available for this purpose. They could be based on photo induced electron transfer, photo induced charge transfer, excimer formation or disappearance and so on. The classification gets subtle with the type of complexing moiety (podands, crown ethers, cryptands, calixarenes etc), which has been used in each type of mechanism.

So vast and potent are the cations in day to day life, it is no surprise that there were many methods introduced to recognize and monitor these cations. Flame photometry, Atomic absorption spectrometry, ion sensitive electrodes, electron microprobe analysis, and neutron activation analysis, are a selected few examples, out of the many analytical methods introduced so far to serve the purpose. They, however, are expensive and often require samples of large size. Further none of these techniques allow continuous monitoring.

Contrary to the above, fluorescent sensors are well known for their selectivity, sensitivity, response time, local observation (this is possible via fluorescence imaging). Moreover, the remote sensing is also possible.

These facts together, establish the great importance given by the scientists all over the world, to develop selective cation sensors, more specifically, based on PET mechanism.

5.1.3.3 Cation sensors; Targeting main group Elements

Na (I)

Most of the animal cells preserve large differential in their intracellular and extracellular concentration of the Na (I) ions. Therefore knowledge of concentration of the Na (I) ions is necessary to understand the physiological processes at the cellular level. Consequently, anthracene and naphthalene based PET sensors (1-3) have been developed by Gunnlaugsson *et al.*²⁷, Geu *et al.*²⁸ and Huarui He *et al.*²⁹ to detect mainly Na (I) ions (See Fig 5).

Geu *et al* also examined the degree of variation of PET quenching the fluorescence upon complexation with Li (I), Na (I), K (I) and Rb (I).

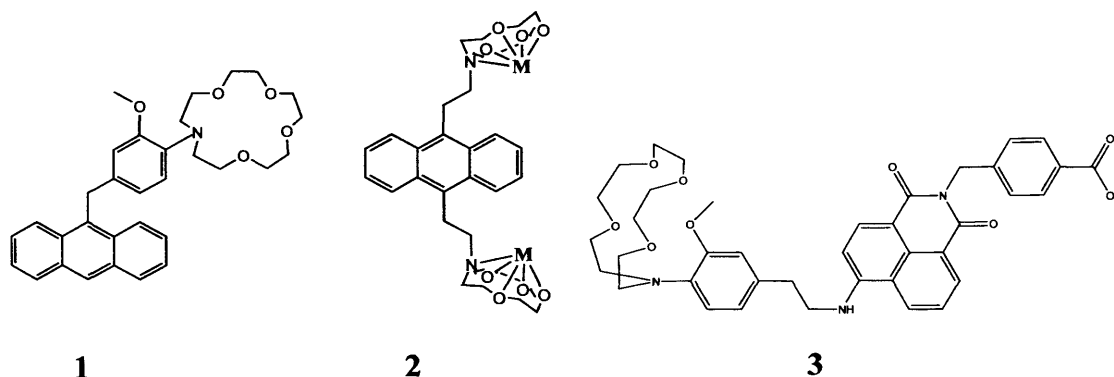


Figure 5:- Depicting 'Off-On-type' PET sensors developed by Gunnlaugsson *et al.* and He *et al.*, comprising crown ether 1 and aza-crown ether 3 as receptor moieties. PET sensor designed by Geu *et al* based on azacoronand system 2.

K (I)

The determination of extracellular concentrations of K (I) ions is also necessary to monitor biological processes, similar to Na (I) ions. Therefore Huarui He *et al.*²⁹ developed another highly selective PET sensor 4, targeted for K (I) ions. 4-aminonaphthalimide acted as the fluorophore, while the diaza-18-crown-6 acted the role of an ionophore (see Fig-6). When the

K (I) selectively binds the aza crown ether, it prevented PET from the anisidine donor, resulting in emission enhancement. Kaur *et al.*³⁰ also prepared naphthalene based, tripodal multifunctional probe 5. The results of their investigation suggested that Na (I) initially binds with tripod before K (I) is permitted to do so. The sensing was attributed to AND type molecular gates. Also it was noted that through excited state intermolecular proton transfer (ESIPT) there is keto and enol forms of 3 forms which facilitates the ratiometric fluorescence determination of Mg (II).

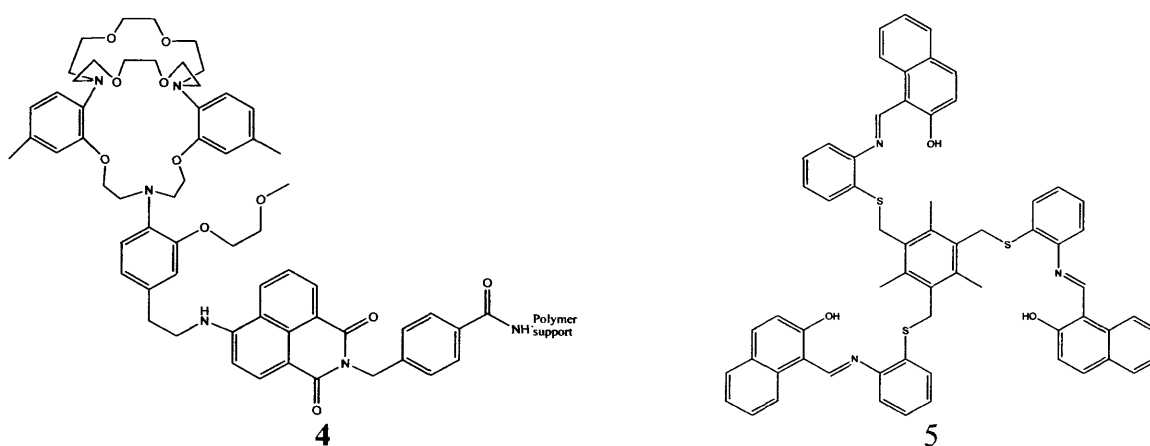


Figure 6:- Depicting the PET sensor for K (I) by Huari *et al.* (Left) and Tripodal multifunctional probe designed by Kaur *et al.* for Na (I), K (I) and Mg (II) based on PET (Right)

Li (I)

Detection of Li (I) in the biological samples is of great interest, in terms of treatment for manic depressive psychosis and other related illnesses. Presently this is being carried out with Li (I) selective electrodes. Owing to its small size and high charge density, selective determination of Li (I) in the presence of Na (I) has become a challenging task. Gunnlaugsson *et al.*³¹ have developed another PET sensor 6, selective to Li (I) ions. Here the naphthalene group acts as a fluorophore while the amine crown ether accepts the metal ion and serves as a receptor. This was found to be an 'Off-On-type' PET sensor as upon the addition of Li (I) in acetonitrile to 6, resulted in emission enhancement. Further, there were no significant changes in emission upon addition of group I and II cations. This indicates the PET sensor is selective to Li (I). The selectivity was attributed to size discrimination by the crown ether.

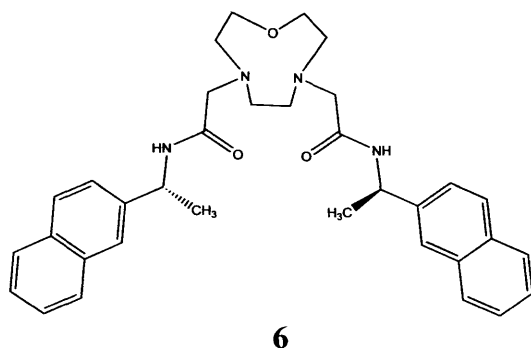


Figure 10:- An *Off-On-type* PET sensor for Li (I), developed by Gunnalaugson *et al.*

5.1.3.4 Targeting Alkaline Earth metal ions as analytes

Ca (II)

The measurement of concentration of cytosolic free Ca (II) is an inevitable requirement to evaluate the role of calcium as an intracellular messenger. This is important to compare the stimuli and responses which are varying continuously. Currently, the concentration of calcium ions is monitored via an indicator. This is known as “Quin 2”, however this is suffering from severe limitations in terms of too short, excitation wavelength (339 nm). This causes auto fluorescence in the cells, thus resulting in biological side effects. Further it penetrates poorly into microscope-optics, resulting in inefficiency.³²

In 1990 A. P. de Silva and Nimal³³ designed a PET sensor for submicromolar Ca(II). In their model they used bis(2-aminophenoxy)ethane-N,N,N,N'-tetraacetic acid(BAPTA) as the receptor and anthracene was incorporated as the fluorophore to yield **7** (see Fig-13).

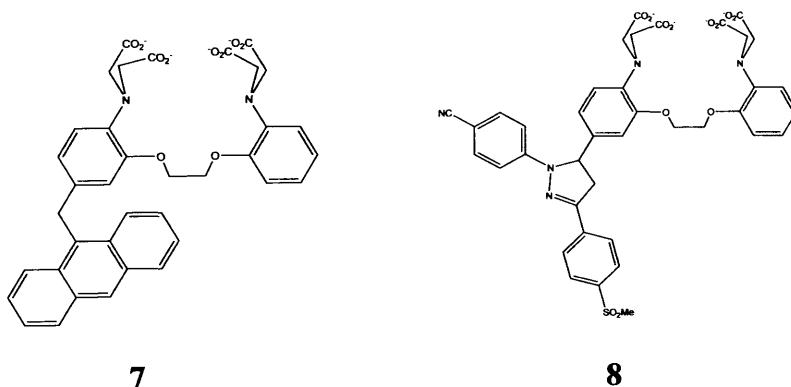


Figure 13:- The PET sensors **8-QCa1** (Left) and **9-QCa2** (Right) designed and developed to detect micromolar calcium

The development of sensors for calcium ion, however, seems to be still in its infancy.

5.1.3.5 Targeting Transition Metal ions

Zn (II)

To understand the importance of Zn (II) recognition, we shall have an idea on its significance exhibited in many cellular roles. This is released from nerve terminals through excitatory signals and then binds to N-methyl-D-aspartate receptor (NMDA). Further Zn (II) is co-stored with insulin in secretory vesicles of pancreatic cells. Zn (II) is an essential constituent of many protein scaffolds (eg:- Carbonic anhydrase and Zinc finger proteins). Zn (II) suppresses apoptosis.

Its role has been recognized in DNA and RNA synthesis. Although many significant cellular roles have come to light, Zn (II) regulation within the cells still needs to be understood, when compared to aforementioned alkali and alkaline earth metals. As such several chemical tools were developed to detect magnetically as well as spectroscopically silent, Zn (II) ions. One such tool is the fluorescent sensors based on PET.

The fluorophores were selected from a wide range of organic molecules, such as amino fluorescein, 1,8 naphthalimide, anthracene, pyrene and quinoline to name a few. Amino fluorescein based Zn (II) sensors (10-11) were developed by Hirano *et al.*³⁴, Burdette *et al.*^{35,36} and Nolan *et al.*³⁷ (see Fig 14-15). Hirano has reported that carboxylic acid group was the main cause for selectivity. It is because the ionic radius of Cd (II) is larger than that of Zn (II), hence carboxylate coordinates instead of nitrogen adjacent to the benzene ring. They have tested and proved that this hypothesis was correct indeed. Burdette *et al.*^{35,36}, on the other hand, initially integrated aniline nitrogen in between the receptor and fluorophore to enhance the quantum yield of the fluorescence. Later on, they synthesized a bi-substituted ligand on a fluorescein platform (12-13). Fluorescent enhancement is observed corresponding to the binding of Zn (II), which inhibits the PET quenching pathway (from benzilic amines to fluorescein).

The sensor design for Zn (II), often lies in overcoming the challenge to retain the delicate balance between the pH and the binding affinity of Zn (II). The design was further improved

Potential Multimodal Imaging Agents

by Nolan, who incorporated a mono substituted fluorescein platform for their sensor. Fabbrizzi and co-workers have appended anthracene to dioxocyclam to produce ‘Off-On-type’ PET sensors (14-17). The design was based on the special affinity exhibited by transition metal ions towards amines and amide groups (see Fig-15).

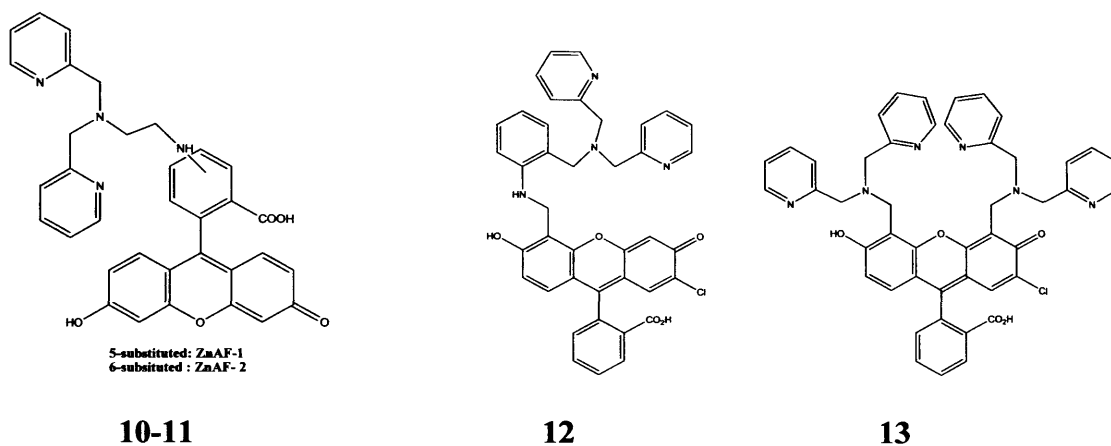


Figure 14:- The amino fluorescein derivatized PET sensor developed by Hirano *et al.* The PET sensor with Aniline spacer from the Zn-Pyridine family for Zn (II)

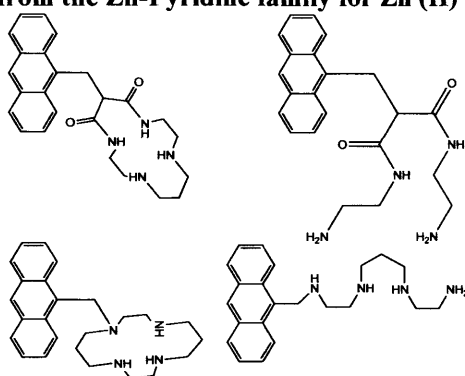


Figure 15:- The PET sensors developed by Fabbrizzi *et al.* for Zn (II) and Cd (II)

Apart from amino fluorescein and anthracene, naphthalene based PET sensors were also developed for Zn (II). Moro *et al.*³⁸, Tamanini *et al.*³⁹, Wang *et al.*⁴⁰ and Salman *et al.*⁴¹ used naphthalimide as fluorophores, while Kubo *et al.*⁴² utilised naphthyl pendants (see Figure 16-18). The di(2-picolylamine), cyclic crown ether and bis imidazole were employed as receptors respectively. Moro incorporated naphthalimide to di(2-picolylamine) and produced a ‘Off-On-type’ PET sensor 18 to evaluate ATP levels. When the receptor binds with the Zn (II), a modest enhancement in the emission intensity was observed. This was attributed to two factors competing with each other. Firstly, binding of Zn (II) by the DPA inhibits PET between DPA and naphthalimide. This has resulted in emission

enhancement. On the other hand, there is a de-excitation channel caused by the interaction between NH group and that of Zn (II), which moderates the emission. When the Zinc complex is brought into contact with ATP, however, it has decreased this interaction, which in turn results in considerable emission enhancement.

The first cyclam based PET sensor **19** for Zn (II) ions were developed by Tamanini *et al.*³⁹ The selectivity of the sensor in the presence Cd (II) was also established. Kubo and co-workers developed both 'Off-On' and 'On-Off' systems (**20-24**). The emission enhancement observed upon cation binding with the crown ether was attributed to the inhibition of PET occurring from nitrogen atoms of the receptor to the fluorophore.

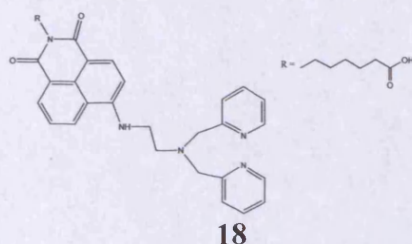


Figure 16:- The PET sensor developed by Moro *et al.* for detecting ATP levels

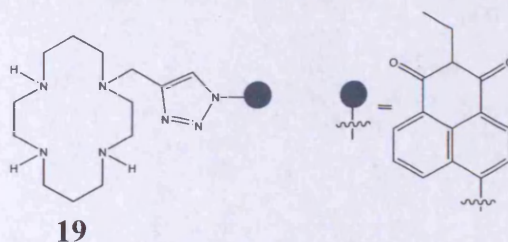


Figure 17:-The first Cyclam derivatized PET sensor developed by Emiliano *et al.* selective to Zn (II)

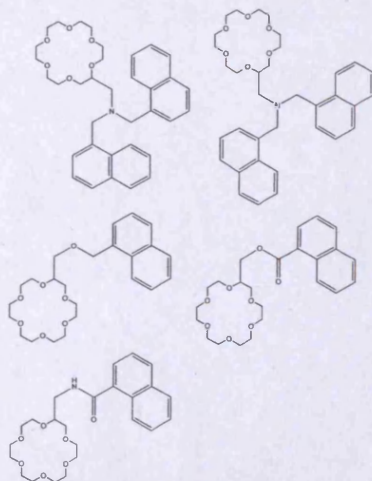


Figure 18: -The PET sensor developed by Kubo *et .al*, which could detect Zn (II) and SCN⁻

Wang *et al.*⁴⁰ selected N,N-bis(2-pyridylmethyl)ethylenediamine as the receptor segment for their PET sensor **25** (see Fig 19) Their selection was based on two advantages. Firstly, the receptor has a great deal of affinity for Zn (II) and secondly it was based on its high potential for cell permeance. A benzene ring was used as a spacer, based on “virtually” decoupled fluorophore-receptor strategy.

The PET process is attributed to the aniline nitrogen, where the lone pair of electrons was transferred to fluorophore. Upon metal binding, however, this lone pair was utilised in forming a coordinate bond. This has led to emission enhancement. In 2006, Salman *et al.* have reported a PET sensor **26** that is selective to Zn (II), in that bisimidazole acted the role as a receptor unit (see Fig-19). The complexing moiety, however, was electronically decoupled from its fluorophore, namely the naphthaleneimide moiety. Upon binding of Zn (II) to the bisimidazole moiety, the emission enhancement was observed. This could be attributed to prevention of the PET process that take place from the lone pair nitrogen atoms of the imidazole to the fluorophore, as the lone pair is now involved in forming the coordinate bond.

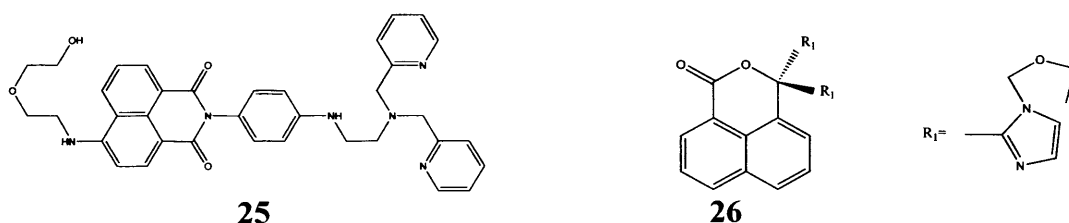
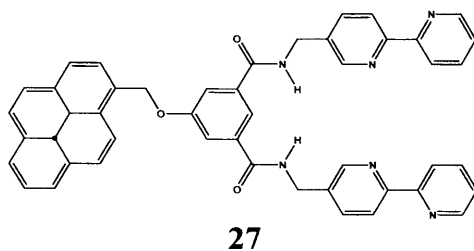


Figure 19:-The PET sensor developed by Wang *et al.* based on virtually decoupled strategy (Left), and PET sensor designed by Salman *et al.* (Right)

The 2,2'-bipyridine ligand is a widely studied bidentate ligand in coordination chemistry. It has, however, hardly been used for the synthesis of a sensor. Fages *et al.*⁴³ noted this and have synthesized a pyrene labelled bipyridine ligand **27** (see Fig-20). This comprises the pyrene as the fluorophore while the bipy acted as the ion-receptor. Contrary to the usual enhancement of fluorescence upon binding to Zn (II), a dramatic fluorescence quenching was observed. This infers, that there is significant PET taking place between the excited pyrene nucleus and the Zn bound receptor moiety. The complexation of the hard Lewis acid Zn (II) has increased the reduction potential of the bipy fragments. Hence, the bipy acts as an acceptor of electrons,

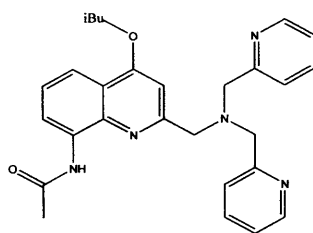
whereas the excited pyrene is the donor. This makes this sensor belong to the category of 'On-Off-type' PET sensor.



27

Figure 20:-The PET sensor based on bi pyridine ligand acting as fluorescence quencher upon binding with Zn (II)

Very recently, Xue *et al.*⁴⁴ have developed an interesting sensor **28** (see Fig-21) which could detect both Cd (II) through PET and Zn (II) through ICT. Since the Cd (II) and Zn (II) belong to the same group (with a d^{10} configuration), the biggest challenge in developing Cd(II) sensors lies in overcoming the interference (in terms of giving similar spectral changes) by Zn(II), when coordinated in fluorescent sensors. As expected, the operation of PET mechanism between the receptor moiety (amine N atom of DPA) and the fluorophore (quinoline) is severely inhibited upon metal binding. This has resulted in very high fluorescence enhancement (40 fold). A negligible emission shift was also observed. On the other hand ICT mechanism provided a red shift coupled with negligible emission enhancement. This has resulted in very distinct colour changes; to an extent it was visible to the 'naked eye'.



28

Figure 21:- A dual modality sensor acts on PET as well as through ICT

Cd (II)

As a d^{10} second row transition metal element, cadmium also has attracted the attention of PET sensor designers. This is mainly because of the health risk and environmental risk induced by the excessive usage of Cd (II) (in batteries, fertilisers etc.). Cadmium is found to be the cause

of profound biological effects (renal dysfunction, reduced lung capacity, while the tendency for accumulation in kidneys, thyroids, and spleen results in adverse physiological conditions).⁴⁵ It was found recently that demineralisation of bones is caused by Cd (II) activating the osteoclast bone cells.⁴⁶ Gunnlaugsson *et al.*⁴⁵ have reported two sensors 29-30. The sensor contains anthracene as the fluorophore and the simple iminodiacetate group as the receptor moiety (see Fig-22). The reason for their selection is two-fold. Firstly, anthracene is well known for its photophysical properties and secondly the aniline based receptor would undergo protonation, only in very high acidic conditions. Furthermore, they have used two receptor units in the single system. This has facilitated the effective PET rate quenching from the receptor to fluorophore, resulting in luminescent switching.

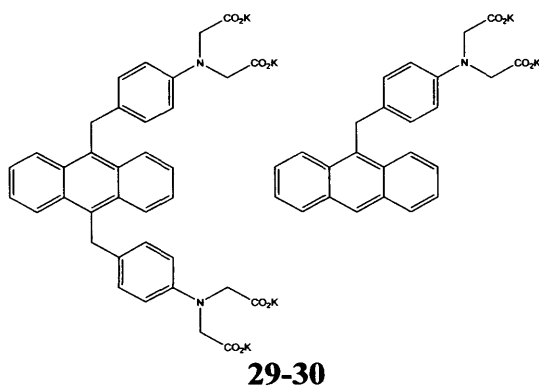


Figure 22:-The PET sensor based upon iminodiacetate on athracene platform

Hg (II)

Heavy metal contamination and its toxicological effects have been widely studied. Hg (II) is used largely in the industrial processes, which eventually causes harm and health risks. Similar to Cd (II), Hg (II) adverse impacts had lead to several neurological diseases (methyl mercury is a potent neurotoxin.⁴⁷). Therefore the considerable interest shown in developing sensors for Hg (II) is no surprise.

Boron dipyrromethene (BODIPY) and anthracene have been widely employed as fluorophores. Very recently Lu *et al* coupled two aniline units to BODIPY to produce a water soluble PET sensor 31 (see Fig-23). The sensor displayed high fluorescence emission enhancement upon binding with Hg (II). This was attributed to the inhibition of PET, upon

metal binding. Further, they have tried the metal binding with Zn (II) and Cd (II), where no significant change was observed. The emission enhancement is expected due to inhibition of reductive PET occurring from the receptor to the fluorophore. Since, oxidative PET from the fluorophore to the receptor (which quenches the fluorescence) also occurs simultaneously, the enhancement is not significant. In contrast, Wang *et al.*⁴⁸ have appended anthracene to cholic acid moiety to produce a sensor **32** (see Fig-23) for methyl mercury (I). In the unbound state, PET occurred from preorganized dithiocarbamate pending groups (which are part of the cholic acid moiety) to the fluorophore. This was retarded by the binding of Hg (II) with dithiocarbamate upon metal binding. This has lead to fluorescence enhancement. Therefore contribute to 'Off-On-type' PET sensor for Hg (II). Selectivity of the sensor was also studied in detail.

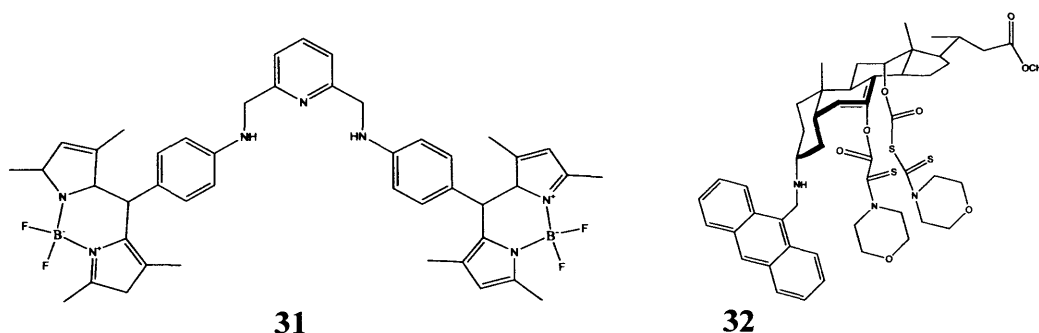


Figure 23:-THE PET sensor developed for Hg (II) based on BODIPY cholic acid derivatized PET sensor, capable of detecting Hg (II) and MeHg (II).

There were two-in-one PET sensors also have been developed. For instance, Sung *et al.*⁴⁹ have designed and developed a sensor **33** to detect Fe (III) and Hg (II). In this system, it comprises anthracene as fluorophore and the amide/ β -amino alcohol-a tridentate ionophore as the receptor moiety (see Fig-24).

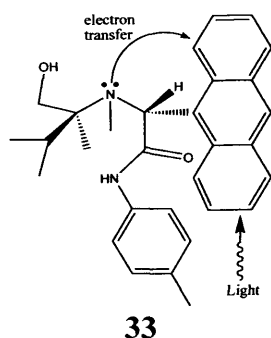
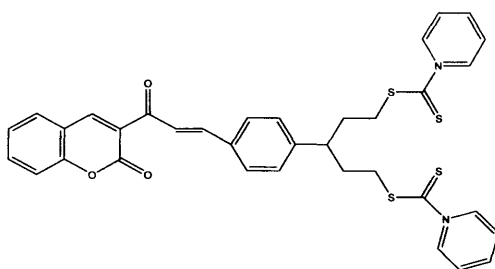


Figure 24:-The PET sensor prepared by Sung *et al.* based on Tridentate ionophore

Ag (I)

Their presence in various commercial sectors and their presence in augmented industrial sludge, environmental contamination and similar reasons have raised awareness in detecting Ag (I) in the respective fields. Not much interest, however, has been shown by the PET sensor designers in the recent past. Wang *et al.*⁵⁰ have decided to address this niche area of research. They have developed a coumarin based PET sensor **34** (see Fig-25). Upon binding with Ag (I), PET was retarded thus resulted in fluorescence enhancement.

**34****Figure 25:- The preparative pathway for CS1 – PET sensor for Ag (I)****5. 1. 3. 5. 1 Ratiometric Sensors for Ag (I)**

The distinct advantage of the ratiometric measurement is its ability to minimise or nullified the possible variability due to differences in the instrumental efficiency and composition of the sensor. Yang *et al.*⁵¹ have reported a ratiometric fluorescent sensor for Ag (I) with high selectivity and sensitivity. The selection of pyrene is justified by its extreme sensitivity to the polarity of local environment. The binding of Ag (I), with pyrene-tethered receptor resulted in self assembled complex. This has lead to dramatic increase in the fluorescence intensities of the excimer and a simultaneous, dramatic reduction of the monomer's fluorescence intensity.

Cu (II)

Copper takes part in many fundamental biological processes in all currently known life forms. On the other hand fluctuations in its role in homeostasis will lead to neurodegenerative diseases. Thus it is an inevitable requirement to have fluorescent sensors which could detect copper at the molecular level at sub-cellular resolution. Contrary to Zn (II) ions, the available literature on Cu (II) sensing is sparse. The challenge, however, lies, in increasing the emission enhancement, as usually upon metal binding emission enhancement is negligible due

to its intrinsic quenching behaviour. anthracenes, naphthalimides are some of the fluorophores employed in producing both 'Off-On' and 'On-Off' type sensors. Guangjie He *et al.*⁵⁵ employed coumarin and appended to dibenzyl hydrozone **36**, while, Kamila *et al.*⁵² incorporated naphthalene into β -aminobisphosphonate **37** and developed PET sensors (see Fig 26-27). Guangjie He attributed the emission enhancement upon binding of Cu (II) to the inhibition of PET occurring between lone pair of N atoms and the fluorophore. This was made possible by carefully tuning the redox potential of the fluorophore. Further, the selectivity of the sensor with a range of transition elements (Mn (II), Cr (III), Co (II), Ni (II), Cd (II), Hg (II), Pb (II) and Ag (I)) also was established. The 'On-Off-type' sensor developed by Kamila and co-workers exhibited a clear fluorescence quenching.

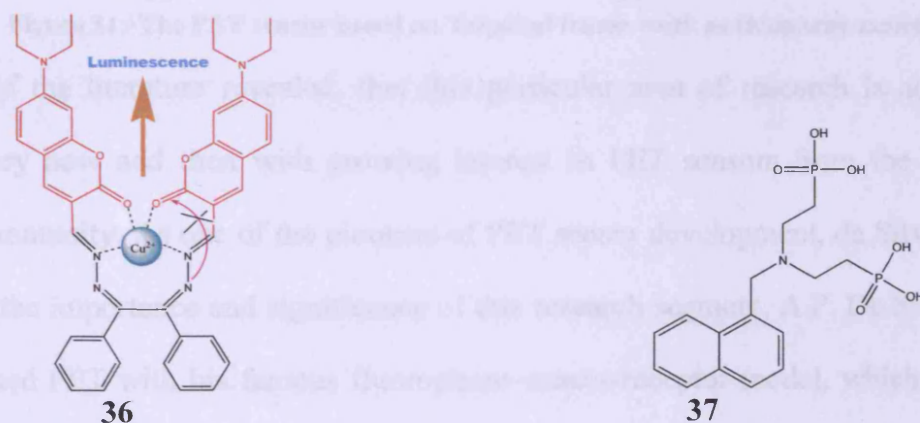


Figure 29:-The PET sensors for Cu (II) developed by He *et al.* and Kamila *et al.* based on dibenzyl hydrazone (Left) and β -amino bisphosphonate acting as receptor moieties respectively.

5.1.3.6 Targeting Lanthanide Ions

Ce (III) & Y (III)

Sensors were developed using fluorophores such as anthracene and quinine. In 2002, Ghosh *et al.*⁵³ appended anthracene to thiophene derivatized TREN in a tripodal frame work to develop a PET sensor **38**. This is believed to be the first PET sensor for Ce (III). Fluorescence quenching in the unbound state was attributed to PET, from lone pair of strong tertiary amines and also from the weak sulphur donors of thiophene moiety towards the fluorophore.

Okamoto *et.al*⁵⁴ devised a relatively more complex PET sensor **39**, in that quinone was tethered to a Zn-Porphyrin derivative (ZnP). A dramatic emission enhancement was observed upon metal binding (strong coordination of Y (III) with a quinone receptor moiety), due to the inhibition of PET from ZnP to the quinone based receptor.

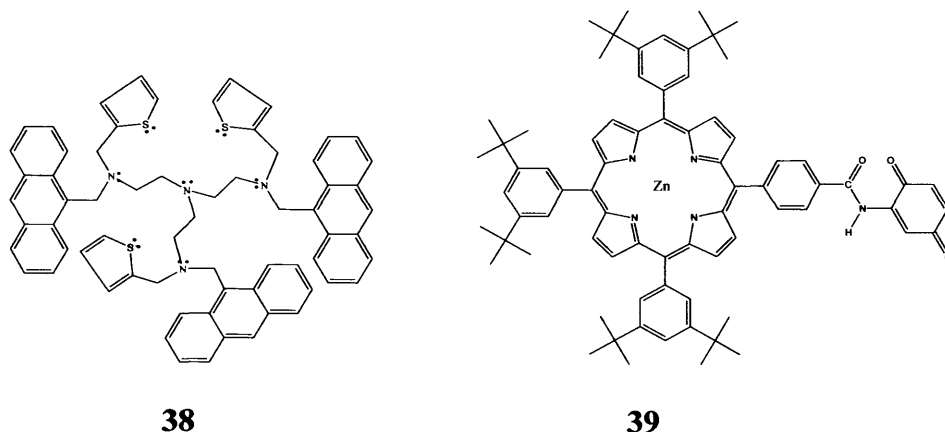


Figure 31:-The PET sensor based on Tripodal frame work as thiophene moiety

A review of the literature revealed, that this particular area of research is achieving new heights every now and then with growing interest in PET sensors from the bio-chemical research community. As one of the pioneers of PET sensor development, de Silva uses words to describe the importance and significance of this research segment. A.P. De Silva is the one who perfected PET with his famous fluorophore–spacer–receptor model, which was initially proposed by Weller *et al.*¹⁹ In de Silva's words;

"Hardly a week goes by without a PET Sensor being introduced"

Therefore interested readers are referred to these publications published elsewhere⁵⁵⁻⁵⁷

5.2 Results and Discussion

5.2.1 Importance of Fluorimetric Evaluation

The development of chemo sensors for a specific target, especially in aqueous systems will be confronted with two major difficulties. Firstly, the development of a suitable binding site⁵⁸ for the target molecule and secondly manipulating the receptor with a signal read-out device. Of these two difficulties, development of a precise binding motif towards the target molecule is of paramount importance. In order to realise this objective, the selection of a suitable

chromophore and the evaluation of its capability to act as luminescent sensor is a must (as there are instances, where the chromophore was inefficient upon binding with the ligand). However, although some of the synthetic steps required for a designed ligand may be long and low yielding, the synthesis of even relatively low quantities (few milligrams) of a fluorescent chemo sensor may be good enough for thousands of analyses.

It can be seen from the previous chapters that the ligands for these potential sensors, however, were prepared in good yield. The next objective will be to measure the efficacy of these ligands in terms of changes in luminescence upon binding with the desired analytes (in this case, cations, such as Cu (II), Zn (II), Mn (II), etc).

As such, the newly synthesized multidentate ligands were dissolved in appropriate solvents and the changes in luminescence were observed upon the addition of a large excess of the metal perchlorates ($\text{Zn}(\text{ClO}_4)_2$, $\text{Cu}(\text{ClO}_4)_2$, $\text{Mn}(\text{ClO}_4)_2$, $\text{Gd}(\text{ClO}_4)_3$ and $\text{Ca}(\text{ClO}_4)_2$). The spectroscopic behaviour of EDTA bisamides of N-(2-Aminoethyl)-1,8-naphthalimide (L^1) and 2-amino anthraquinone (L^5) (see Fig-1), in the presence of the transition metal ions (Zn (II), Cu (II) and Mn (II)) in solution was studied. DTPA analogues (see Fig- 2-3) in their protected, deprotected and complexed forms (with lanthanides Gd (III), Eu (III), and Yb (III)) were studied in detail. DTPA based bisamide of N-(2-Aminoethyl)-1,8-naphthalimide (L^{14}) (see Fig-4), in the presence of transition (Zn (II), Cu (II), Mn (II), lanthanide (Gd (III)) and alkaline earth (Ca (II)) metal ions were assessed. Water insoluble ligands (L^1 , L^5 and L^{14}) were dissolved in dimethylformamide and dimethyl sulphoxide and L^{10} and L^{12} were dissolved in dichloromethane. Water-soluble ligands (L^{11} , L^{13} and L^{15}) and complexes of DTPA analogues were dissolved in distilled water.

Potential Multimodal Imaging Agents

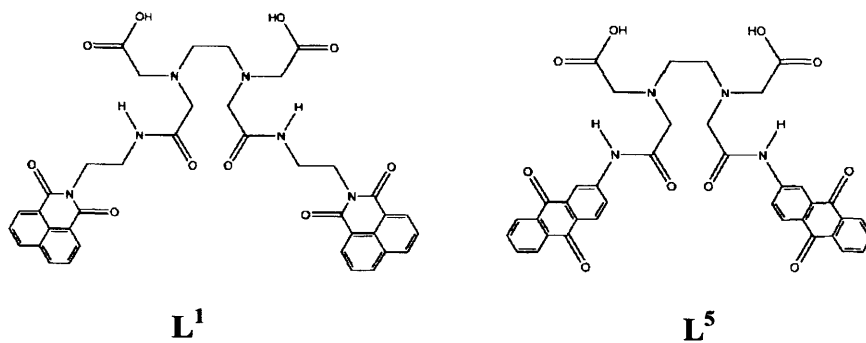


Figure 1:- EDTA bisamides of N-(2-Aminoethyl)-1, 8-naphthalimide (L¹), 2-Aminoanthraquinone (L⁵)

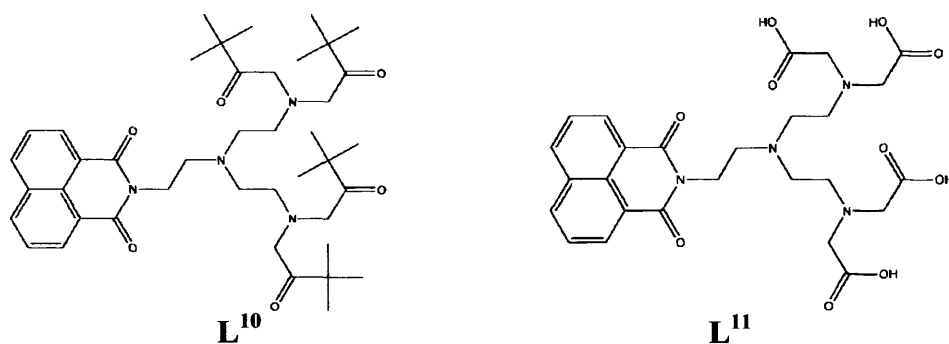


Figure 2:- Depicting the Protected (L¹⁰) Deprotected (L¹¹) forms of symmetric naphtha derivative

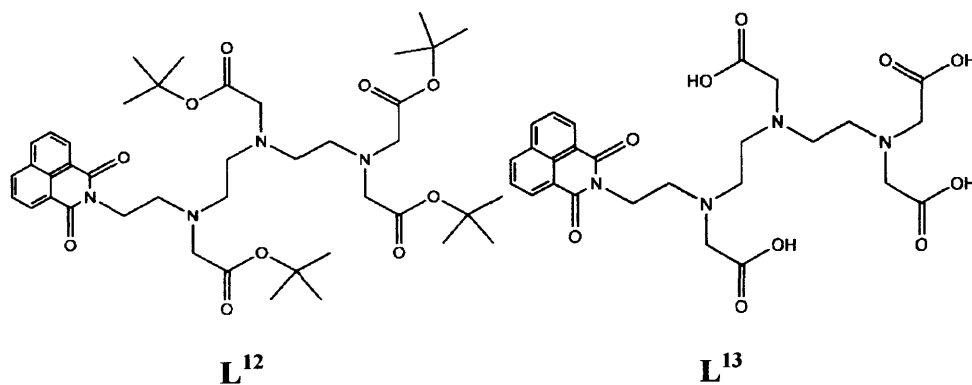


Figure 3:- Depicting the Protected (L¹²) Deprotected (L¹³) forms of Asymmetric naphtha derivative

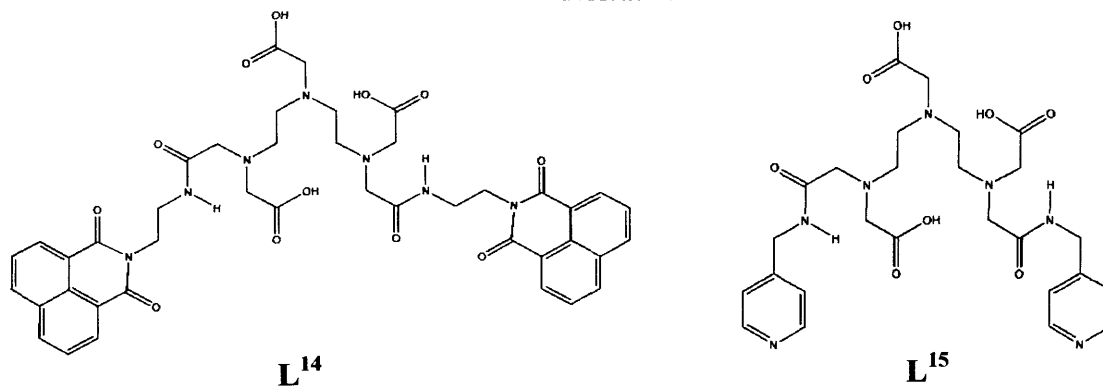


Figure 4:- DTPA bisamides of N-(2-Aminoethyl)-1, 8- naphthalimide (L¹⁴) and 4-Aminomethyl pyridine (L¹⁵)

5.2.1.1 Spectrofluorimetric Evaluation of the EDTA Bisamides

Evaluation of EDTA bisamide of *N*-(2-Aminoethyl)-1, 8-naphthalimide (L^1) and 2-Amino Anthraquinone (L^5)

Spectrofluorimetric measurements allow us to evaluate the impact caused on the emission properties of the ligands due to coordination of the transition metal cations. Excitation of the ligand at 370 nm resulted in an emission maximum at 450 nm. It could be seen from the emission spectra of L^1 (see Fig-5), that while addition of a large excess of Zn (II) to the ligand solution causes emission enhancement (by a factor of 2.0), addition of Cu (II) in large excess, causes quenching of fluorescence (by a factor of 1.5), on the respective ligand. It could also be observed, that addition of Mn (II) hardly causes any change (by a factor 1.0) on the emission properties of L^1 . Similar observations were noted for L^5 , though emission enhancement (by a factor of 1.0) by the addition of Zn (II) was not so significant (see Fig-6).

To explain these observations, a number of factors that modulate the photophysical properties of a fluorophore come to mind. Electron and energy transfer processes, changes of electronic density and the destabilisation of a non-emissive $n-\pi^*$ excited state need consideration. Among these factors photo induced electron transfer mechanism could be considered as the major influencing factor. Further, this argument is supported by the fact that the greatest effect on the emission enhancement was caused by Zn (II). Zn (II), having a d^{10} electronic configuration, does not usually contribute to EET mechanisms for the deactivation of the excited state.⁶⁰ Further it could be reasonably suggested, the considerable fluorescence enhancement is due to the inhibition of PET process, which becomes thermodynamically less favourable upon coordination with a metal ion.⁶¹

In L^5 , however, the lone pairs of tertiary nitrogens, carboxylate oxygens and amide oxygens do not quench the luminescence very much. This results in a moderate emission enhancement upon binding of Zn (II).

Intensity modulation by PET

On the other hand, quenching of fluorescence by Cu (II) could be reasonably explained by the PET mechanism. A possible explanation is that Cu (II) induced PET occurs from fluorophores in **L**¹ and **L**⁵ (naphthalimide moiety and anthraquinone moiety respectively) to their respective receptor moieties. While **L**¹ and **L**⁵ act as ‘*On-off-type*’ sensor for Cu (II), **L**¹ could also act as an ‘*Off-On-type*’ PET sensor with regard to Zn (II). The insignificant fluorescence intensity modulation exhibited by Mn (II) in **L**¹ also could be reasonably accounted for by the oxidative PET occurring from the fluorophore to the receptor moiety upon metal binding.

Stokes shift

The Stokes shift ($\nu_A - \nu_F$) is an important characteristic of fluorescent compounds. The Stokes shift is a parameter which indicates the difference in the properties and structure of the fluorophores between the ground (**S**₀) and first singlet excited state (**S**₁). It is calculated by the following equation.

$$(\nu_A - \nu_F) = (1/\lambda_A - 1/\lambda_F) \times 10^7 \text{ cm}^{-1}$$

The values of Stokes shift are in the range from 4038- 4804 cm^{-1} for **L**⁵. On the other hand, values of Stokes shift are in the range from 6140- 6594 cm^{-1} for **L**¹. The relatively large Stokes shift displayed by **L**¹ indicates a high potential for bio-imaging. Once again the aforementioned values are in good agreement with an analogous compound reported by Chovelon *et al.*⁶²

When the UV–Vis spectrum was recorded for **L**¹ a broad absorption was observed between 250 and 400 nm. Within the spectrum an internal charge transfer (ICT) state arises from the $\pi - \pi^*$ electron transfer occurring with λ_A maximum at 345 nm. The observation is in good agreement with those values reported in the literature.⁶²

The molar extinction coefficient ϵ at the absorption maxima is $21,197 \text{ M}^{-1}\text{cm}^{-1}$ for L^1 .

The observed value is in close agreement with the expected value, as it is two-fold larger than those of analogous monomeric *N*-methyl-1,8-naphthalimide.^{15a}

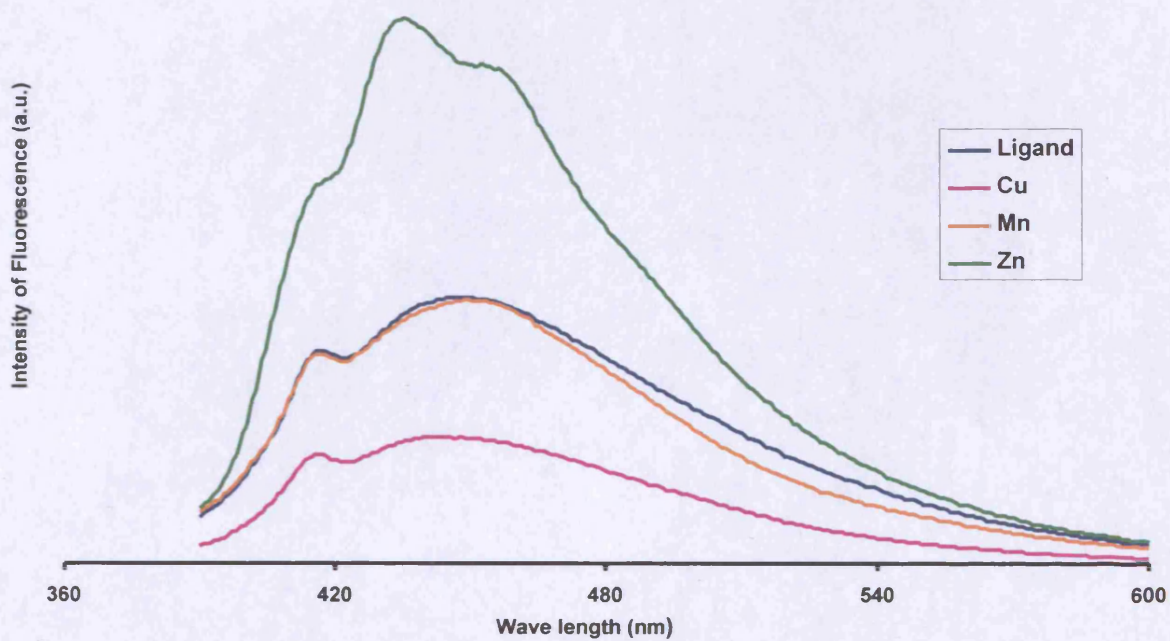


Figure 5:- Emission spectra of EDTA bisamide of N-(2-Aminoethyl)-1, 8-naphthalimide (L^1) (Excitation at 370nm)

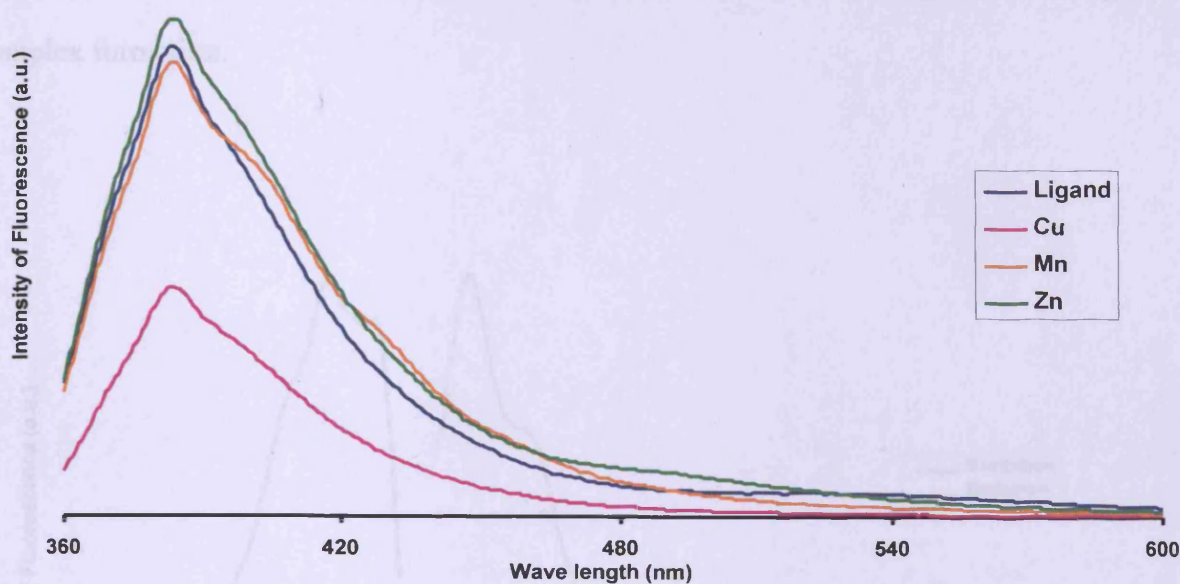


Figure 6:- Emission spectra of EDTA bisamide of 2-Aminoanthraquinone (L^5) (Excitation at 345nm)

5.2.1.2 Spectrofluorometric Evaluation of DTPA Analogues

Fluorescence on binding with Lanthanides

Unfortunately, the background fluorescence of biological samples, can at times, limit the use of luminescent probes in imaging. The usage of luminescent complexes based on lanthanides, brings elegant solution to this problem. This is possible due to the long lived luminescence of the lanthanide complexes in comparison to relatively negligible life time of the background emission, from the biological samples.

However, in the following experiments we have not concerned ourselves with the lanthanide phosphorescence spectrum. Instead, we are interested by changes in the fluorescence spectrum on lanthanide binding.

The emission profiles of protected symmetric ligand L^{10} and deprotected symmetric ligand exhibited marked difference. Furthermore, the relative emission intensities of the free ligand L^{11} exhibited marked difference, when compared to L^{11} -Gd, L^{11} -Eu, L^{11} -Yb and observed in the following order: $L^{11} < L^{11}$ -Yb $^{3+} < L^{11}$ -Eu $^{3+} < L^{11}$ -Gd $^{3+}$. This indicates the

successful formation of the respective complexes (see Fig 7-13). A similar behaviour was observed in the case of L^{13} and its gadolinium complex (L^{13} -Gd), once again, indicating the complex formation.

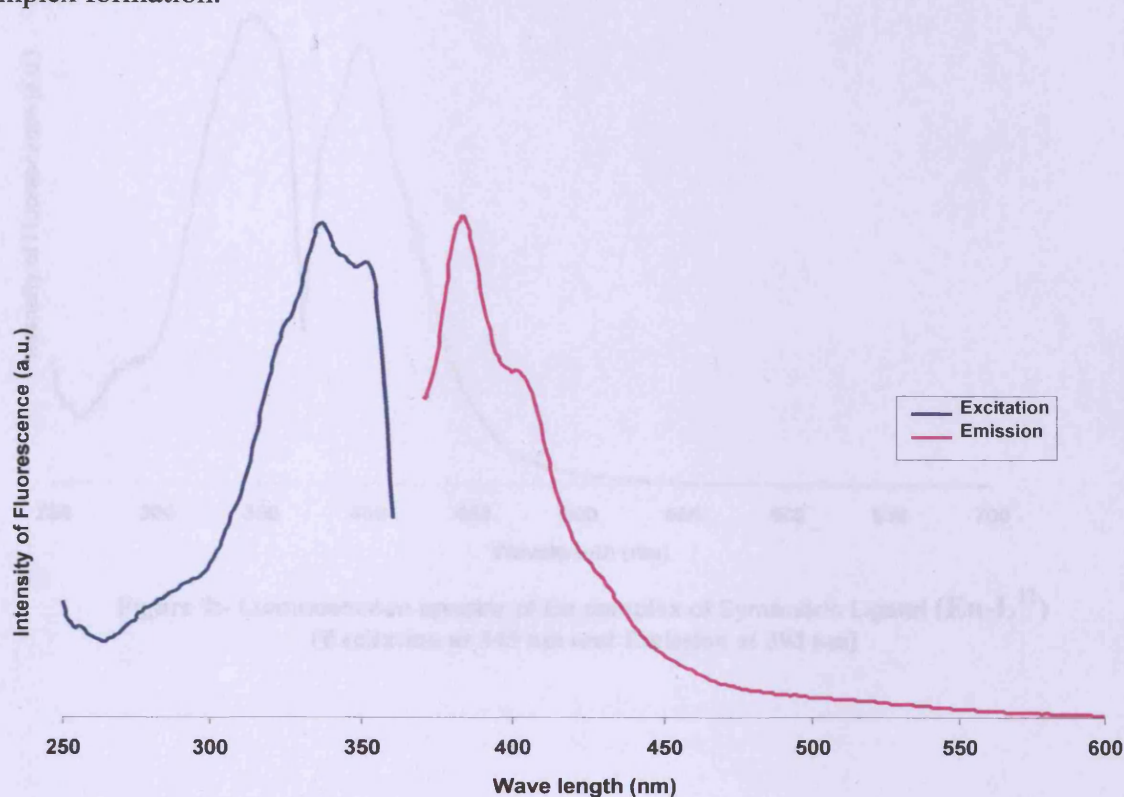


Figure 7:- Luminescence spectra of Symmetric Ligand-Protected (L^{10}) (Excitation at 336 nm and Emission at 383 nm)

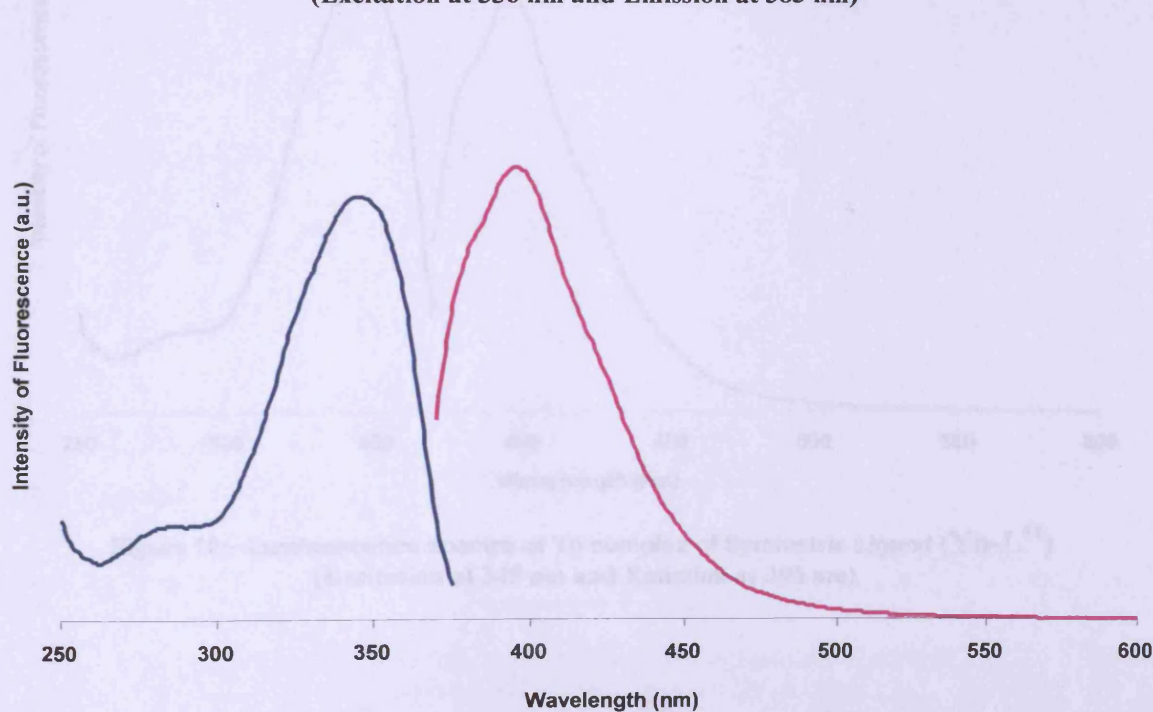


Figure 8:- Luminescence Spectra of Gd complex of Symmetric Ligand ($Gd-L^{11}$) (Excitation at 345 nm and Emission at 390 nm)

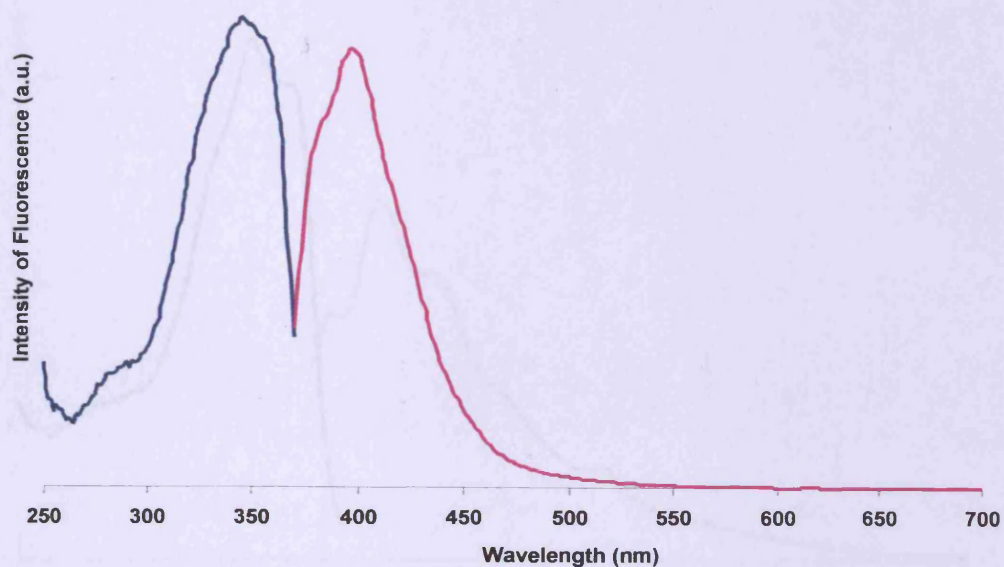


Figure 9:- Luminescence spectra of Eu complex of Symmetric Ligand (**Eu-L¹¹**)
(Excitation at 345 nm and Emission at 393 nm)

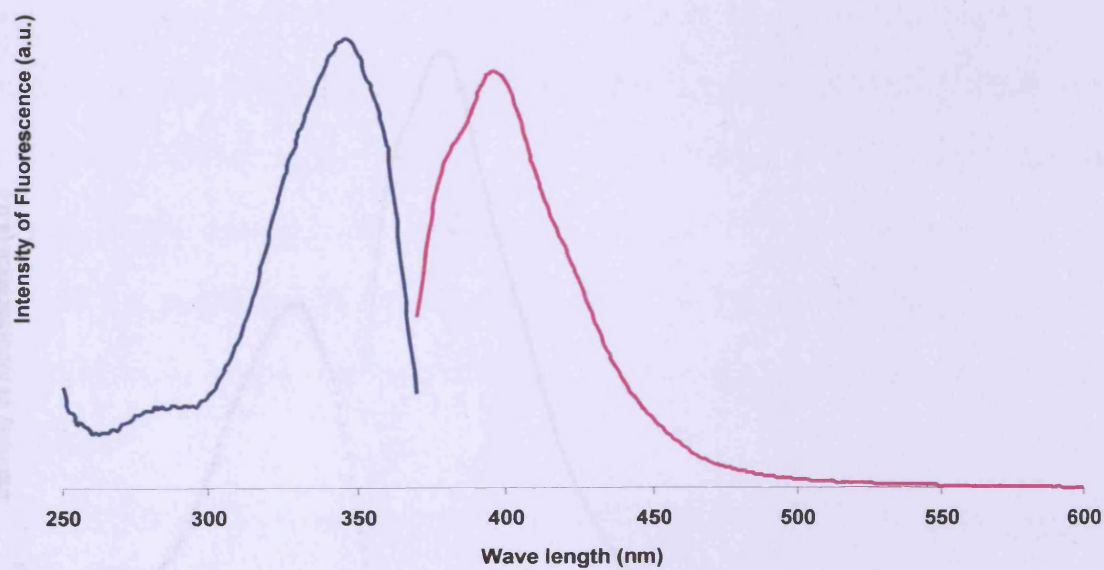


Figure 10:- Luminescence spectra of Yb complex of Symmetric Ligand (**Yb-L¹¹**)
(Excitation at 345 nm and Emission at 396 nm)

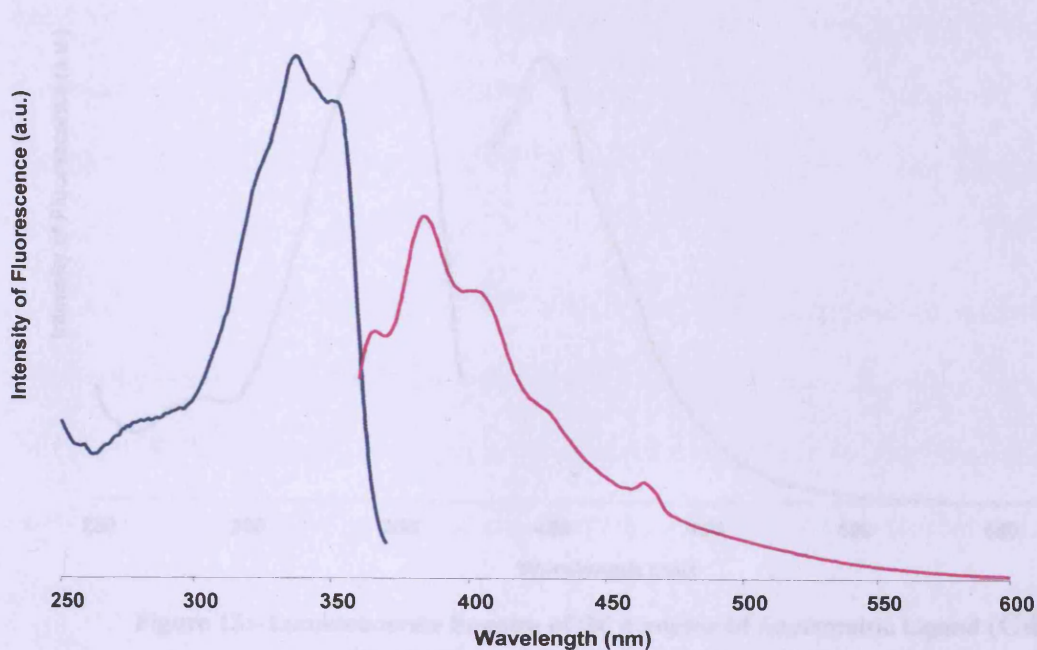


Figure 11:- Emission Spectra of Asymmetric Ligand-Protected (L^{12}) (Excitation at 335 nm and Emission at 383 nm)

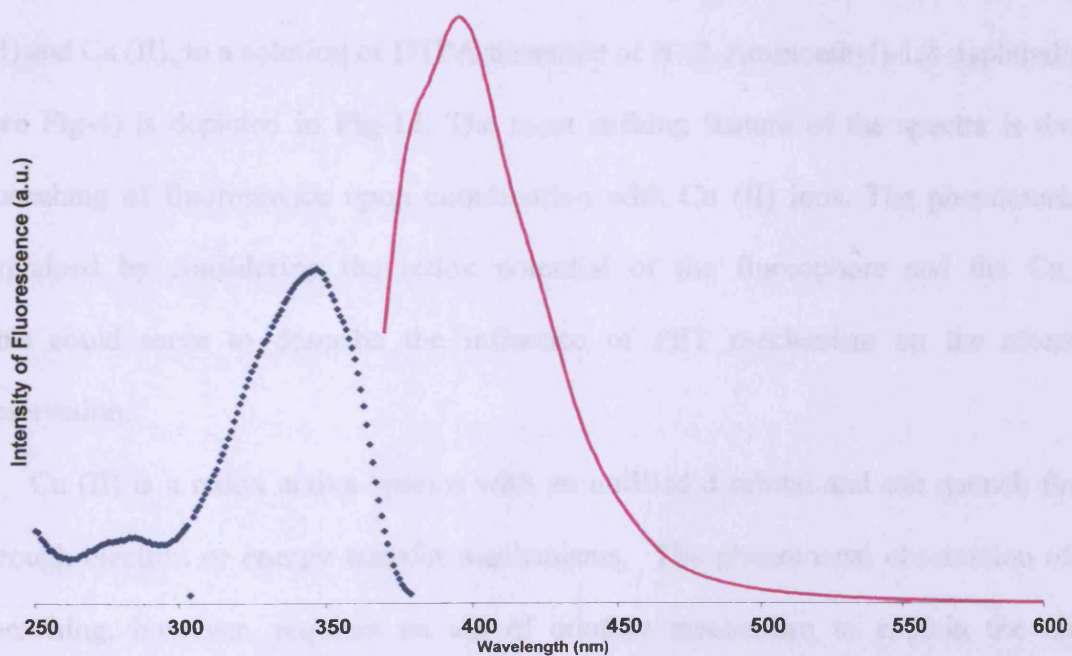


Figure 12:- Emission Spectra of Asymmetric Ligand-Deprotected (L^{13}) (Excitation at 346 nm and Emission at 396 nm)

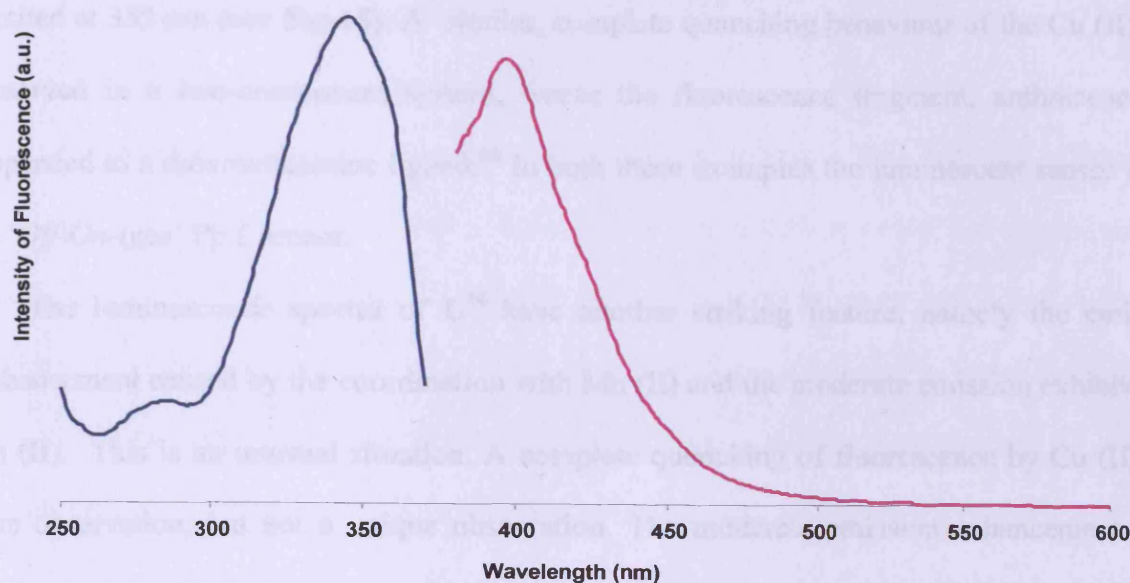


Figure 13:- Luminescence Spectra of Gd complex of Asymmetric Ligand (Gd-L¹³)
(Excitation at 345 nm and Emission at 396 nm)

5.2.1.3 Spectrofluorometric Evaluation of DTPA based bisamides

Evaluation of DTPA bisamide of N-(2-Aminoethyl)-1, 8-naphthalimide

Luminescence spectra obtained upon addition of large excess of Gd (III), Zn (II), Cu (II), Mn (II) and Ca (II), to a solution of DTPA bisamide of N-(2-Aminoethyl)-1,8-naphthalimide (L¹⁴) (see Fig-4) is depicted in Fig-14. The most striking feature of the spectra is the complete quenching of fluorescence upon coordination with Cu (II) ions. The phenomena could be explained by considering the redox potential of the fluorophore and the Cu (II) ions. This could serve to describe the influence of PET mechanism on the aforementioned observation.

Cu (II) is a redox active species with an unfilled d orbital and can quench fluorescence through electron or energy transfer mechanisms. The phenomenal observation of complete quenching, however, requires an aid of another mechanism to explain the observation. Further, for the PET mechanism to be activated it requires, the oxidation potential of the fluorophore should be higher than that of the receptor.

The complete quenching was observed upon addition of Cu (II), when excited at 314 nm. Furthermore, luminescence could be observed upon addition of Cu (II), provided L¹⁴ is excited at 353 nm (see Fig-15). A similar, complete quenching behaviour of the Cu (II) was observed in a two-component system, where the fluorescence fragment, anthracene was appended to a dioxotetraamine ligand.⁶⁶ In both these examples the luminescent sensor to act as 'Off-On-type' PET sensor.

The luminescence spectra of L¹⁴ have another striking feature, namely the emission enhancement caused by the coordination with Mn (II) and the moderate emission exhibited by Zn (II). This is an unusual situation. A complete quenching of fluorescence by Cu (II) is a rare observation, but not a unique observation. The moderate emission enhancement upon addition of Zn (II) is also not an unusual observation. What is, however, really unusual is the strong emission enhancement caused by Mn (II) when Zn (II) does not.

The observation is very difficult to explain in terms of the known theories. A possible explanation, however, may be given in terms of conformational changes of the chromophore with respect to the metal centre or indeed the other chromophore on binding to the Mn (II) centre; hence due to the different conformations, quenching may be more prominent in the Zn (II) complex than in the Mn (II) complex.

It could be seen from the above arguments that a plausible explanation for unusual observation is not forthcoming, given that we have limited knowledge of the coordination modes of L¹⁴ and the relative positioning of the chromophore.

Another notable feature of the spectra is the variation of the emission intensity of the secondary peak. Unlike the spectra of L¹, L¹⁴ clearly depicts a shoulder like peak (i.e. secondary peak) at 455 nm, apart from the primary peak which appears at 392 nm. Moreover, the ratio of emission intensity ($I_{392\text{ nm}}/I_{455\text{ nm}}$) was observed descending in the following order, upon addition of various metal ions: Mn (II) > Ca (II) > Gd (II) > Zn (II) (1.55>1.16>1.35>1.31). Furthermore, the secondary peak which appears around 455 nm

could be attributed to an excimeric species. The observation is in good agreement with the previous findings, reported by Barros *et al.*^{15b} for 1,8-alkyldinaphthalimides, in that the excimer emission was observed at 470 nm.

A comparison with emission spectra of L¹ and L¹⁴

While the emission spectra of L¹ exhibited intense structureless band with the vibronically structured features, L¹⁴ exhibited a broad band characteristic with the fine structure. Furthermore it has been reported that EDTA derivative of a pyrene, give rise to a static excimer. In contrast, emission spectra of the DTPA analogue of pyrene indicated the presence of dynamic excimer. Therefore, it is most likely to have a similar situation with L¹ and L¹⁴. In order to arrive at an unambiguous solution, density functional theory may be utilised.⁶⁷

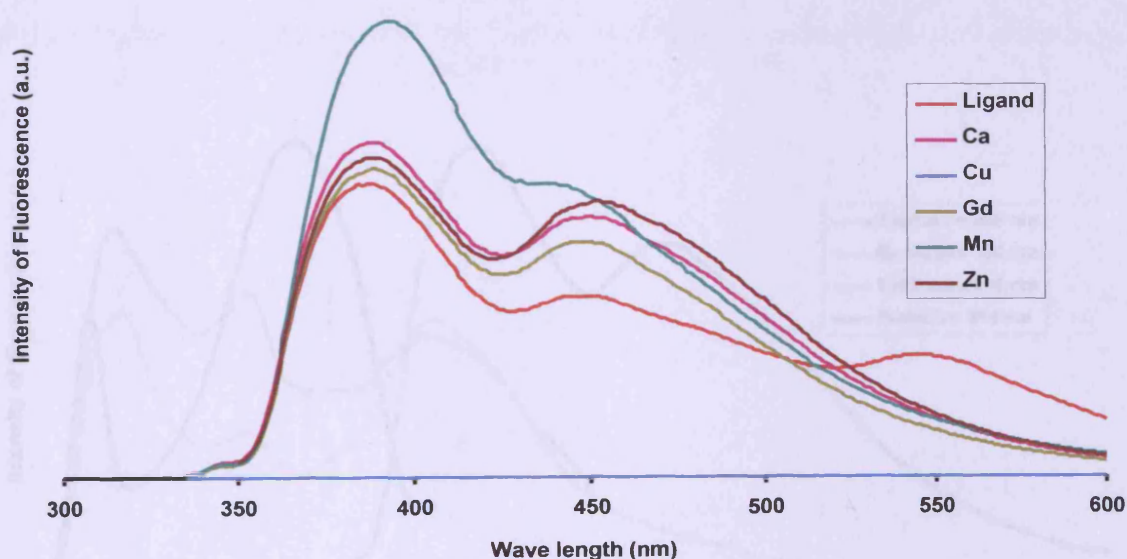


Figure 14:- Luminescence spectra of DTPA bisamide of N-(2-Aminoethyl)-1, 8-naphthalimide (L¹⁴) (In the presence of various metal ions, Excitation at 314 nm)

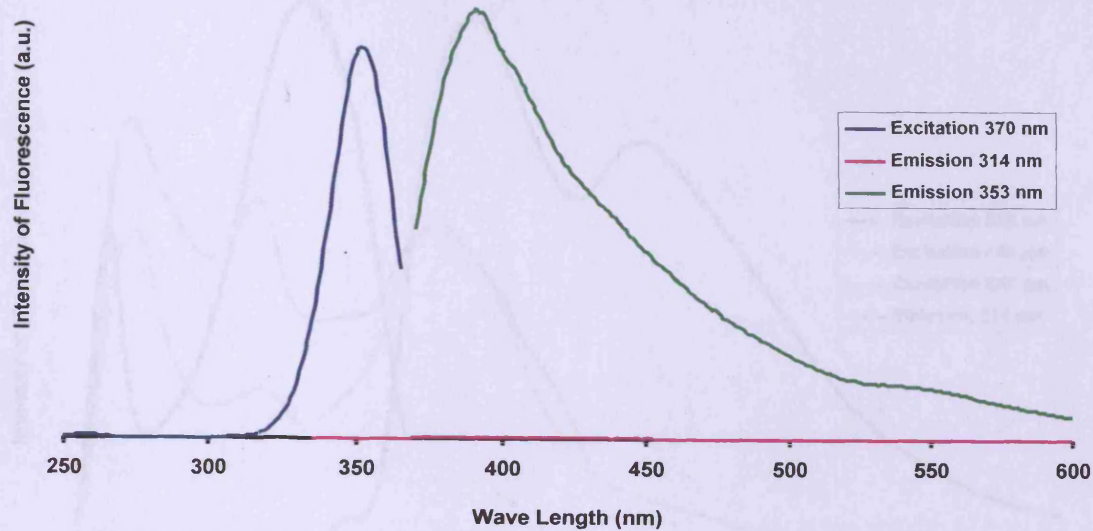


Figure 15:- Luminescence spectra of DTPA bisamide of N-(2-Aminoethyl)-1, 8-naphthalimide (L^{14}) (in the presence of excess $Cu(II)$)

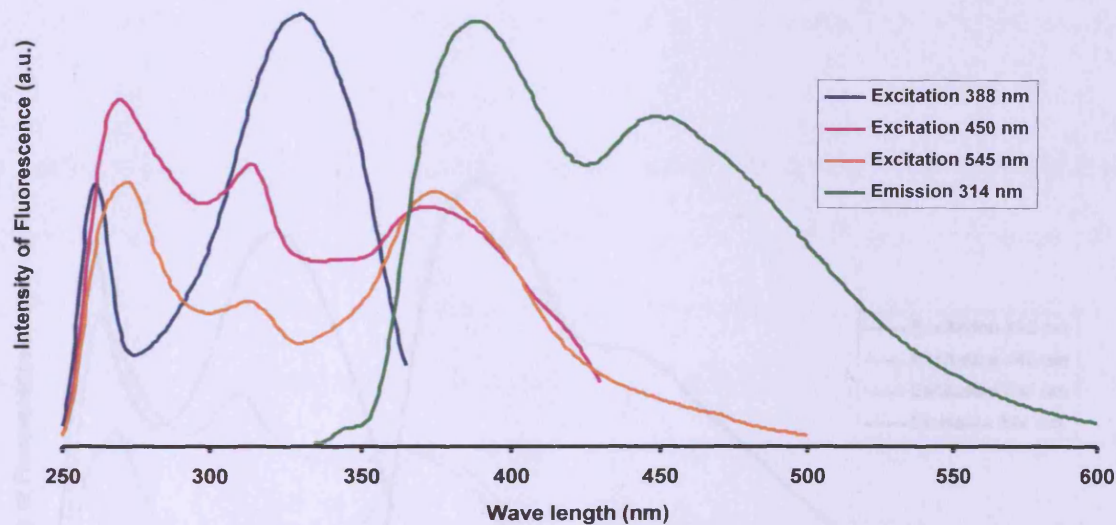


Figure 16:- Luminescence spectra of DTPA bisamide of N-(2-Aminoethyl)-1, 8-Naphthalimide (L^{14}) (in the presence of excess $Ca(II)$)

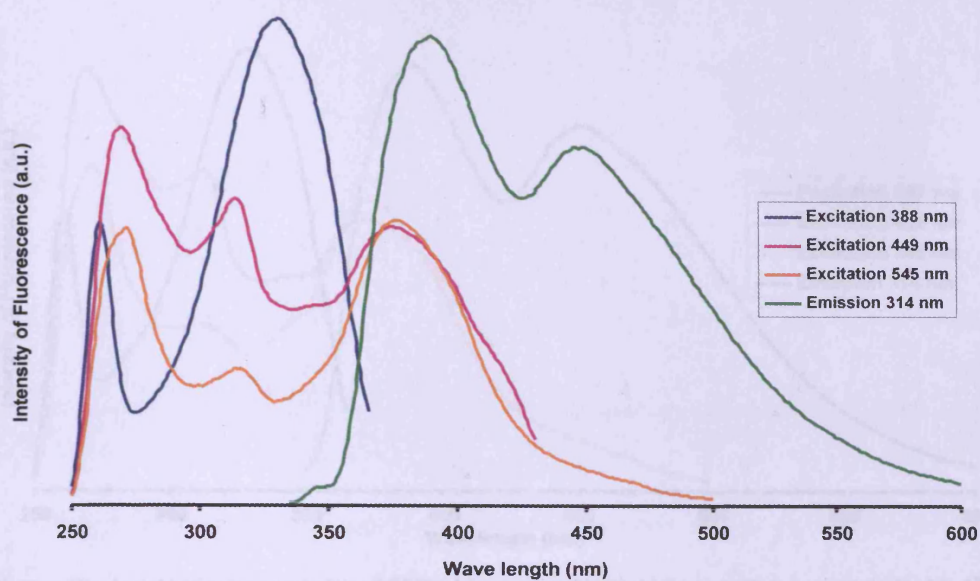


Figure 17:- Luminescence spectra of DTPA bisamide of N-(2-Aminoethyl)-1, 8-naphthalimide (L^{14}) (in the presence of excess Gd (III))

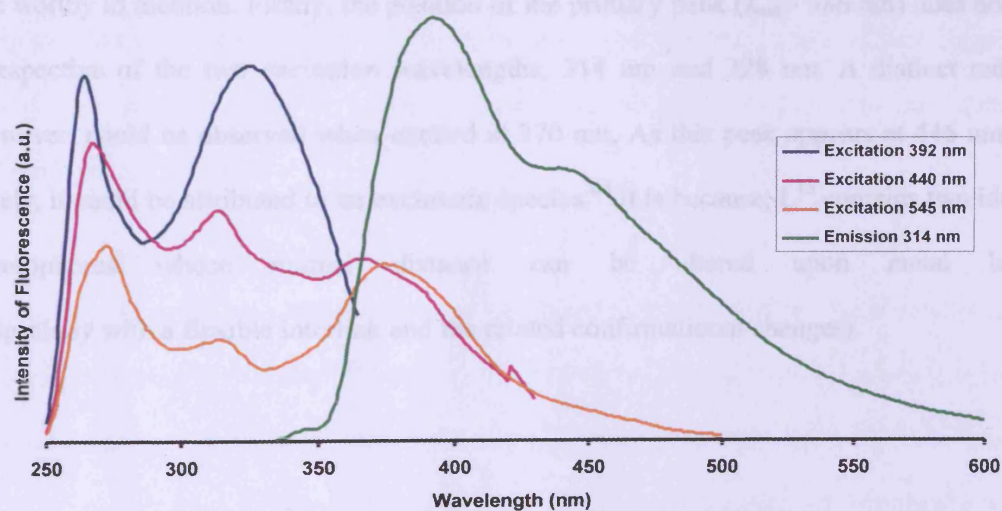


Figure 18:- Luminescence spectra of DTPA bisamide of N-(2-Aminoethyl)-1, 8-naphthalimide (L^{14}) (in the presence of excess Mn (II))

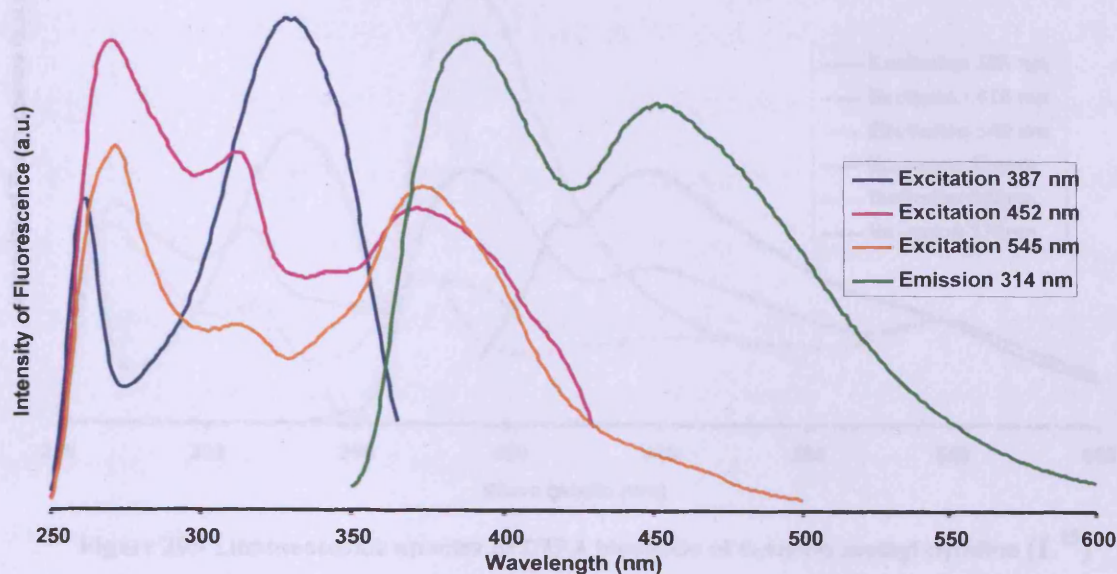


Figure 19:- Luminescence spectra of DTPA bisamide of N-(2-Aminoethyl)-1, 8-naphthalimide (L^{14}) (in the presence of excess Zn (II))

Evaluation of DTPA bisamide of 4-Aminomethyl pyridine

The luminescence spectra of L^{15} depicted in Fig-20. L^{15} was excited at different wavelengths and the variation in the emission wavelengths observed. There are two observations, which are worthy to mention. Firstly, the position of the primary peak (λ_{em} - 386 nm) does not vary, irrespective of the two excitation wavelengths, 314 nm and 328 nm. A distinct red shift, however, could be observed when excited at 370 nm. As this peak appears at 446 nm, most likely, it could be attributed to an excimeric species.⁶⁸ It is because, L^{15} contains two identical fluorophores whose mutual distance can be altered upon metal binding (especially with a flexible interlink and the related conformational changes).

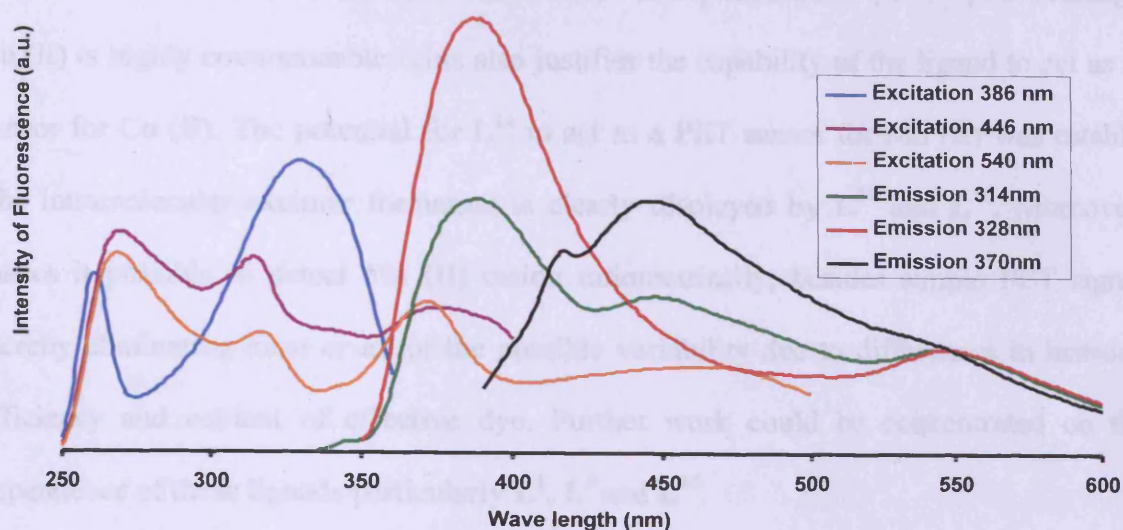


Figure 20:- Luminescence spectra of DTPA bisamide of 4-Amino methyl pyridine (L^{15})

5.3 Experimental Section

The photophysical data for luminescence were obtained on a JobinYvon-Horiba Fluorolog spectrometer fitted with a JYTBX picosecond photo detection module. Water-soluble EDTA bisamides were dissolved in water. Water insoluble bisamides and complexes were dissolved in chloroform and DMSO as required. Although all of the new ligands and complexes prepared were air stable both in the solid state and solution, some of the ligands and complexes were found to be mildly hygroscopic, when left in the open atmosphere for prolonged periods of time.

5.4 Conclusion

As the project seeks to develop Multimodal Imaging Agents, bearing good relaxivities and optical properties, it's crucial to evaluate the optical properties. With this objective in mind, luminescence measurements were carried out with series of ligands (L^1 , L^5 , L^{10} - L^{13} , and L^{14} - L^{15}). A comparison of luminescence spectra of DTPA analogues of Symmetric naphtha derivative (L^{10} - L^{11}) indicated the success of complexation with Gd (III) and/or Eu (III).

Luminescent measurements of EDTA bisamides (L^1) yielded good results; two fold enhancement of emission upon binding with Zn (II) is commendable, positioning them as

potential Zn (II) sensors. On the other hand, complete quenching of fluorescence observed with DTPA bisamide of N,N-(2-Aminoethyl)-1,8-naphthalimide (**L**¹⁵) upon binding with Cu (II) is highly commendable. This also justifies the capability of the ligand to act as a PET sensor for Cu (II). The potential for **L**¹⁴ to act as a PET sensor for Mn (II) was established. The intramolecular excimer formation is clearly displayed by **L**¹⁴ and **L**¹⁵. Moreover, **L**¹⁴ makes it possible to detect Mn (II) cation ratiometrically, besides simple PET signalling, thereby eliminating most or all of the possible variability due to differences in instrumental efficiency and content of effective dye. Further work could be concentrated on the pH dependence of these ligands particularly **L**¹, **L**⁵ and **L**¹⁴.

Acknowledgement

The contribution from Dr. Andy Harlett, towards obtaining luminescence measurements is acknowledged.

References

1. A. E. Karger, J. M. Harris and R. F. Gesteland, *Nucleic Acids Res.*, 1991, **19**, 4955.
2. H. Kobayashi, M. Ogawa, R. Alford, P. L. Choyke and Y. Urano, *Chem. Rev.*, 2010, **110**, 2621.
3. D. Cohen, J. A. Dickerson, C. D. Whitmore, E. H. Turner, M. M. Palcic, O. Hindsgaul and N. J. Dovichi, *Annual rew. analytical chem.*, 2008, **1**, 165.
4. N. Blow, *Nature*, 2008, **456**, 825.
5. R. A. Bissell, A. P. de Silva, Q. N. Gunaratne, L. M. Lynch, E. M. Maguire and A. S. Sandanayake, *Chem. Soc. Rev.*, 1992, **21**, 187.
6. R. F. Chen and H. Edelhoich, *Biochemical Fluorescent Concepts*, Dekker, New York, 1976.
7. D. Parker, *Analyst*, 1996, **121**, 1749.
8. A. J. Bryan, A. P. de Silva, S. A. de Silva, D. D. Rupasinghe and A. S. Sandanayake, *Biosens.*, 1989, **4**, 169.
9. T. D. James, A. S. Sandanayake and S. Shikai, *Angew. Chem. Int. Ed.*, 1996, **35**, 1911.

10. V. Balzani, M. Venturi and A. Credi, *Molecular Devices and Machines*, Wiley-VCH, Weinheim, 2003.
11. J. Otsuki, T. Akasaka and K. Araki, *Coord. Chem. Rev.*, 2008, **252**, 32.
12. A. P. de Silva, T. S. Moody and G. D. Wright, *Analyst*, 2009, **134**, 2385.
13. M. Kadarkaraisamy and A. G. Sykes, *Polyhedron*, 2007, **26**, 1323.
14. J. Otsuki, A. Yasuda and T. Takido, *Chem. Commun.*, 2003, 608.
15. (a) M. Licchelli, A. O. Biroli, A. Poggi, D. Sacchi, C. Sangermania and M. Zema, *Dalton Trans.*, 2003, 4537; (b) T. C. Barros, B. Filho, V.G. Toscano and M. J. Politi, *J. Photochem. Photobiol., A*, 1995, **89**, 141.
16. R. A. Bissell, A. P. de Silva, Q. N. Gunaratne, L. M. Lynch, E. M. Magurie, C. P. McCoy and A. S. Sandanayake, *Top. Curr. Chem.*, 1993, **168**, 223.
17. A. P. de Silva, B. McCaughan, O. F. McKinney and M. Querol, *Dalton Trans.*, 2003, 1902.
18. T. Gunnlaugsson, D. P. Ali, M. Glynn, P. E. Kruger, G. M. Hussey, F. M. Pfeffer, M.G. dos Santos and J. Tierney, *J. Fluorescence.*, 2005, **15**, 287.
19. A. Weller, *Pure Appl. Chem.*, 1968, **16**, 115.
20. J. F. Callan, A. P. de Silva and D. C. Magria, *Tetrahedron*, 2005, **61**, 8551.
21. C. Lakshmi, R. G. Hanshaw and B. D. Smith, *Tetrahedron*, 2004, **60**, 11307.
22. P. D. Beer, *Chem. Commun.*, 1996, 689.
23. A. P. de Silva, Q. N. Gunaratne and T. Gunnlaugsson, *Tetrahedron Lett.*, 1998, **39**, 5077.
24. N. Saleh, Y. A. Al-Soud and W. M. Nau, *Spectrochim. Acta, Part A.*, 2008, **71**, 818.
25. W. F. Jager, T. S. Hammink, O. Van den Berg and F. C. Grozema, *J. Org. Chem.*, 2010, **75**, 2169.
26. T. Gunnlaugsson, B. Bichella and C. Nolana, *Tetrahedron Lett.*, 2002, **43**, 4989.
27. T. Gunnlaugsson, M. Nieuwenhuyzen, L. Richarda and V. Thoss, *J. Chem. Soc., Perkin Trans.*, 2002, **2**, 141.
28. A. P. de Silva, B. McCaughan, O. F. McKinney and M. Querol, *Dalton Trans.*, 2003, 1902.
29. M. A. M. Huarui He, Marc J. P. Leiner, Robert J. Fraatz and James K. Tusa, *J. Am. Chem. Soc.*, 2003, **125**, 1468.
30. N. Kaur, N. Singh, D. Cairns and J. F. Callan, *Org. Lett.*, 2009, **11**, 2229.

31. T. Gunnlaugsson, B. Bichella and C. Nolana, *Tetrahedron Lett.*, 2002, **43**, 4989.
32. G. Grynkiewicz, M. Poenie and R. Y. Tsien, *J. Biol. Chem.*, 1985, **260**, 3440.
33. A. P. de Silva and Q. N. Gunaratne, *J. Chem.Soc., Chem. Commun.*, 1990, 186.
34. T. Hirano, K. Kikuchi, Y. Urano, T. Higuchi and T. Nagano, *J. Am. Chem. Soc.*, 2000, **122**, 12399.
35. S. C. Burdette, G. K. Walkup, B. Spingler, R. Y. Tsien and S. J. Lippard, *J. Am. Chem. Soc.*, 2001, **123**, 7831.
36. S. C. Burdette, C. J. Frederickson, W. Bu and S. J. Lippard, *J. Am. Chem. Soc.*, 2003, **125**, 1778.
37. E. M. Nolan, S. C. Burdette, J. H. Harvey, S. A. Hilderbrand and S. J. Lippard, *Inorg. Chem.*, 2004, **43**, 2624.
38. A. J. Moro, P. J. Cywinski, S. Korstena and G. J. Mohr, *Chem. Commun.*, 2010, **46**, 1085.
39. K. E. Tamanini, L. M. Sedger, M. H. Todd and M. Watkinson, *Inorg. Chem.*, 2009, **48**, 319.
40. X. J. Wang, Z. Zhang, X. Qian, Y. Yanga and Q. Xua, *J. Mater. Chem.*, 2005, **15**, 2836.
41. T. H. Salman, Y. Chuvilov, O. Solovey, Y. Abraham, M. Kapon, K. Suwinska and Y. Eichen, *Inorg. Chem.*, 2006, **45**, 5315.
42. S. K. Kubo and T. Sakurai, *Talanta*, 1999, **49**, 735.
43. E S.Sohna, P. Jaumier and F. Fages, *J. Chem. Research.*, 1999, 134.
44. L. Xue, C. Liu and H. Jiang, *Org. Lett.*, 2009, **11**, 1655.
45. T. Gunnlaugsson, T. C. Leeb and R. Parkesha, *Tetrahedron*, 2004, **60**, 11239.
46. A. Åkesson, P. Bjellerup, T. Lundh, J. Lidfeldt, C. Nerbrand, G. Samsioe, S. Skerfving and M. Vahter, *Environ. Health Perspect.*, 2006, **114**, 830.
47. T. W. Clarkson, L. Magos and G. J. Myers, *The New Eng. J. Me.*, 2003, **349**, 1731.
48. H. Wang and W. H. Chan, *Tetrahedron*, 2007, **63**, 8825.
49. K. Sung, H.K. Fu and S. H. Hong, *J Fluoresc.*, 2007, **17**, 383.
50. M. X. Wang, X. M. Meng, M. Z. Zhu and Q. X. Guo, *Chin.Chem. Lett.*, 2008, **19**, 977.
51. R. H. Yang, W. H. Chan, W. M. Lee, P. F. Xia, H. K. Zhang and K. Li, *J.Am.Chem.Soc.*, 2003, **125**, 2884.

52. S. Kamila, J. F. Callan, R. C. Mulrooney and M. Middleton, *Tetrahedron Lett.*, 2007, **48**, 7756.
53. P. Ghosh, A. D. Shukla and A. Das, *Tetrahedron Lett.*, 2002, **43**, 7419.
54. K. Okamoto and S. Fukuzumi, *J. Am. Chem. Soc.*, 2004, **126**, 13922.
55. A. P. de Silva, D. B. Fox, T. S. Moody and S. M. Weir, *Pure Appl. Chem.*, 2001, **73**, 503.
56. S. A. De Silva, M. L. Kasner, M. A. Whitener and S. L. Pathirana, *Int. J. Quantum Chem.*, 2004, **100**, 753.
57. R. Ludwig and T. K. Dzung, *Sensors*, 2002, **2**, 397.
58. T. C. Barros, P. B. Filho, V. G. Toscano and M. J. Politi, *J. Photochem. Photobiol. A.*, 1995, **89**, 141.
59. A. P. de Silva, Q. N. Gunaratne, T. Gunnlaugsson, J. M. Huxley, P. McCoy, J. T. Rademacher and T. E. Rice, *Chem. Rev.*, 1997, **97**, 1515.
60. T. Cao and S. E. Webber, *Macromolecules*, 1991, **24**, 79.
61. B. Valeur and I. Leray, *Coord. Chem. Rev.*, 2000, **205**, 3.
62. J. M. Chovelon and I. Grabchev, *Spectrochim. Acta, Part A.*, 2007, **67**, 87.
63. T. Gunnlaugsson and J. P. Leonard, *Dalton Trans.*, 2005, 3204.
64. D. Parker and A. G. Williams, *J. Chem. Soc., Dalton Trans.*, 1996, 3613.
65. D. Parker and A. G. Williams, *J. Chem. Soc. Perkin Trans.*, 1995, **2**, 1305.
66. G. d. Santis, L. Fabbrizzi, M. Licchelli, C. Mangano, D. Sacchi and N. Sardone, *Inorg. Chim. Acta.*, 1997, **257**, 69.
67. L. Machia, I. C. Munoz, R. P. Gonzalez, M. Sanchez and M. Inoue, *Supramol. Chem.*, 2009, **21**, 665.
68. T. Handa, Y. Utena, H. Yajima, R. Katayama, T. Ishii and T. Yamauchi, *J. Phys. Chem.*, 1986, **90**, 6324.

